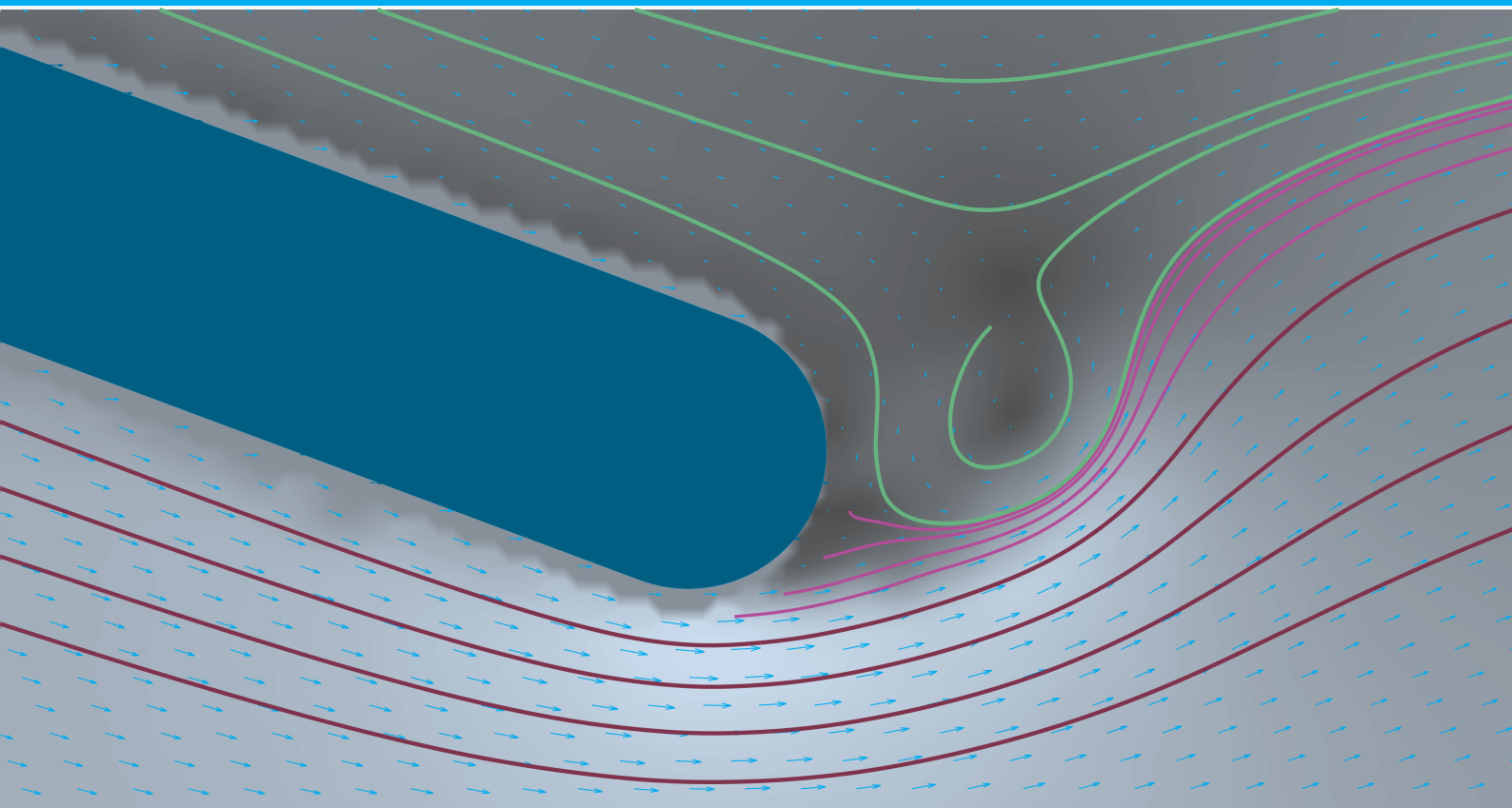


Genesis of the Kutta condition

An empirical study of the transient flow which produces the Kutta condition flow-field

Pieter van Pelt



Genesis of the Kutta condition

An empirical study of the transient flow which produces the Kutta condition flow-field

by

Pieter van Pelt

to obtain the degree of Master of Science

at the Delft University of Technology,

to be defended publicly on Friday September 27, 2019 at 14:00 h.

Student number:	4168712
Project duration:	March 2018 – September 2019
Thesis committee:	Prof. dr. ir. L.L.M. Veldhuis, TU Delft, principal supervisor
	dr. M.I. Gerritsma, TU Delft, supervisor
	Prof. dr. F. Scarano, TU Delft
	Prof. dr. ing. G. Eitelberg, TU Delft

An electronic version of this thesis is available at <http://repository.tudelft.nl/>.

Abstract

The purpose of this report is to present an empirical study of the transient flow which produces the Kutta-condition flow-field. The Kutta condition refers to the flow at the trailing edge of a wing. This phenomenon is of special importance for the production of fluid-dynamic lift. One specific property is the smooth flow-off of streamlines above and below the trailing edge. A study of literature concerning the Kutta condition makes clear that two perspectives on the Kutta condition can be distinguished. The mathematical perspective regards the Kutta condition as a boundary condition which is needed to obtain a unique solution in the problem of calculating the magnitude of lift by a wing. The empirical perspective, taken in this report, regards the Kutta condition as a flow-field which is produced by a transient flow. Regarding this transient flow, a synthesis of a number of descriptions of it found in literature is given. This informs the hypothesis of the present research: *When a wing is put in motion from rest, fluid moves from the pressure side towards the suction side, past the trailing edge (TE). A boundary layer is produced, in which shear stresses cause momentum loss, which results in a shift of the stagnation point (which is initially on the suction side) and separation of flow from the wing. Finally, the stagnation point is at the very edge and flow leaves the trailing edge smoothly.* A small number of numerical studies of this process have been done in the past, however they remained without empirical confirmation. Thus, the present research aims to answer the following main question using empirical means: *“How is the Kutta condition flow-field created at the trailing edge of a wing which is accelerated from rest?”*.

An experimental setup is produced to this end. It consists of a wing model which is oriented vertically in a bucket of water (0.9x0.9 m). The wing is oriented perpendicular to the bottom, with ≈ 0.5 mm tip clearance, to produce 2-dimensional flow at the measurement plane. The wing section is a rounded flat plate: a rectangle with rounded leading and trailing edges, where the radius of curvature R is 0.5% of the chord length c , which is 200 mm. The wing is uniformly accelerated at 2.50 m/s^2 using a weight. A high-speed camera is used to record flow-field images which are processed into velocity vectors fields using Particle Image Velocimetry (PIV) techniques.

The main results of the empirical work are: 1) a time-series of instantaneous streamline pictures in the wing reference frame, 2) velocity profiles which clearly show boundary-layer-like patterns, 3) a detailed textual description of the transformative transient process, 4) a graph of the development of regions of separated flow, 5) a graph of the development of the radius of curvature of streamlines directly above and below the trailing edge. The results confirm the hypothesis regarding the development of the flow-field.

Next to the experimental part of the present research, some analyses of the surface velocity distributions of TE flows are done using a panel method. Linearly distributed vortex panels are used with a boundary condition of zero total circulation. Comparison of a NACA-0012 airfoil with a rounded flat plate using the panel method reveals that the overall airfoil shape has no significant effect on the velocities in the TE region, nor does the value of R/c . The surface velocity distribution in the trailing edge region calculated using the panel code and that obtained from the PIV data agree in qualitative sense.

Comparison of the empirical results with that of other works concerning transient trailing-edge flows reveals that the most important difference is that other works generally consider bodies with a strictly sharp (i.e. pointed) trailing edge while the present research considers a rounded trailing edge having finite thickness. Therefore the present results show the presence of two points of flow separation (upper and lower) and a wake in between them, which is not the case for the classical sketches which informed the hypothesis for this research. A similarity is found with results of numerical simulation in literature, where flow separation initially occurs in two separate regions on the suction side, one starting at the initial potential-flow stagnation point location, and the other starting at the trailing edge. They grow in size over time until they merge, after which a single point of flow separation remains. Regarding the hypothesis, the important role of viscosity in the creation of the Kutta condition flow-field is confirmed.

Special attention is paid to the qualitative properties of the case which was selected for empirical study such that the results can be generalised. Consequentially, the theory under consideration may be regarded as generally valid for cases in which a smooth airfoil having a rounded trailing edge of R/c of $O(0.001)$ at non-zero angle of attack is accelerated uniformly from rest towards a final chord-based Reynolds number of at least $O(1k)$ while the wing section is completely immersed in viscous inertial flow.

Preface

L.S.,

This report presents my MSc thesis work. The subject of the work is the Kutta condition: a particular phenomenon which occurs in the flow of fluid over a wing.

My interest in the Kutta condition started when studying aerodynamics for my BSc's degree. I read Anderson's statement in his book *Fundamentals of aerodynamics* that a wing cannot produce lift in a non-viscous fluid. I thought that was really remarkable because viscosity is usually regarded as having exclusively negative effects (i.e. drag), but here somebody states that it is a crucial thing. Actually I thought it could not be true; it was contrary to my own intuitive understanding of the Kutta condition, and it seemed too general and discriminating. Furthermore, the statement was made without proof, so I was determined to falsify it; that was the motivation for the investigation described in this report. If you want to know the outcome, you should read it.

The working of the trailing edge flow in cases of a real wing in real flow attracts relatively little attention although its occurrence is crucial for the working of a wing. It is so important for the functioning of an aircraft that one expects it to have been studied elaborately almost 100 years ago. This is however not the case; not at all. I assume that the delay is partly due to the absence of adequate performance of measurement equipment in earlier times. It is remarkable that such an important piece has not yet been laid in the puzzle of understanding flight. However, at the same time it has been exciting for me to try to understand the puzzle and to add my piece. I might have overlooked some pieces of research so perhaps my work has been predated by someone else's. But if not, I am glad to present my considerations.

The content of this report has mainly a fluid-dynamic character, but in some places its character tends towards philosophy. It is evident that the Kutta condition is a curious phenomenon. Increasing understanding of it requires not only using the toolbox of physics to describe its properties and discover relations, but also thinking about the interrelations between reality and the perspectives of physics and mathematics. Reading the very interesting book *The enigma of the aerofoil* by David Bloor was helpful to get started with a philosophical understanding of the difficulties which are present 'under the surface'.

This work was performed in the period of March 2018 to September 2019 at Delft University of Technology in The Netherlands, at the faculty of Aerospace Engineering. I thankfully acknowledge the help of some particular people: Tomas Sinnige for assisting with using the PIV equipment, Frits Donker-Duyvis for assisting with practicalities in the production of the wings and setting up the PIV equipment, Nico van Beek for assistance with IT-related issues, Item Systems BV for assistance with designing the frame of the experiment setup, Kimberley Graauw for the speedy handling of administrative tasks and the purchasing of items, Leo Veldhuis and Marc Gerritsma for critical questions and helpful suggestions, Rijk van Manen and Teunis van Manen for interesting discussions and useful suggestions and friendship. Last but not least, the present author acknowledges the Present Author of this awesome universe for creating the opportunity to be amazed by fantastic fluid flows.

Pieter van Pelt

Delft, September 2019

Contents

	Page
Abstract	iii
Preface	v
1 Introduction	1
1.1 Introduction to the Kutta condition	2
1.2 Perspectives on the Kutta condition	4
1.3 Description of the Kutta condition flow-field	7
1.4 The transient flow-field that results in the Kutta condition	9
1.5 The role of viscosity	19
1.6 Conclusions of the literature study	21
1.7 Research definition	22
2 Methods	29
2.1 Methodology for theory verification	30
2.2 Parameterisation	35
2.3 Dimensional analysis	39
2.4 Potential flow analysis	43
2.5 Experiment	47
2.6 PIV processing methods and tools	59

	Page
3 Results	71
3.1 Panel method results	72
3.2 Experimental results	74
3.3 Comparison of experimental and panel method results	83
4 Discussion	85
4.1 Discussion of results from panel method	86
4.2 Discussion of results from experiment	87
4.3 Answers to research questions and hypotheses	93
4.4 Notes on the cruciality of viscosity	97
4.5 An alternative mechanism for production of the Kutta condition	100
5 Conclusions and Recommendations	103
5.1 Conclusions.	103
5.2 Recommendations	107
Bibliography	109
 Appendices	
A Determination of stagnation point location by streamfunction method	113
B Performance analysis of the “direction and speed method”	115
B.1 Comparison with streamfunction method	115
B.2 Sensitivity analysis	116
B.3 Validation	116
B.4 Conclusions.	116
C Photos of the flow-field around an airfoil starting from rest	123
D Images of the transient trailing edge flow around an airfoil started from rest from numerical simulation	125

1

Introduction

The purpose of this report is to present an empirical study of the transient flow which produces the Kutta-condition flow-field. This research is located in the field of aircraft aerodynamics. It is assumed that the reader is familiar with basic aerodynamic theory. The problem is introduced in Chapter 1, which starts with an overview and ends with a research definition. Chapter 2 explains the methods used to achieve the research objective. The main method is Particle-Image Velocimetry combined with an experimental setup. This is supported by potential flow calculations which serve to generalise the results. Chapter 3 presents the observations from both methods. Chapter 4 discusses the results; for both methods separately, and discusses the implications of the combined results. Conclusions and recommendations are given in Chapter 5.

A roadmap of Chapter 1 is presented in Figure 1.1. The aim of this chapter is to introduce the reader to the phenomenon of interest (Section 1.1), to sketch the meaning of the term “Kutta condition” while introducing a mathematical and a physical perspective (Section 1.2) and give a detailed description of the Kutta condition flow-field based on literature (Section 1.3). Then the origin of the Kutta condition flow-field is discussed, mainly by synthesising a number of descriptions from authoritative authors (Section 1.4). A separate section (1.5) is devoted to the role of viscosity because this supposedly has a major role in the creation of the Kutta condition flow-field. After that, an overview of available knowledge regarding the Kutta condition has been obtained. This is concluded in Section 1.6, and research for filling a particular knowledge gap is defined in Section 1.7.

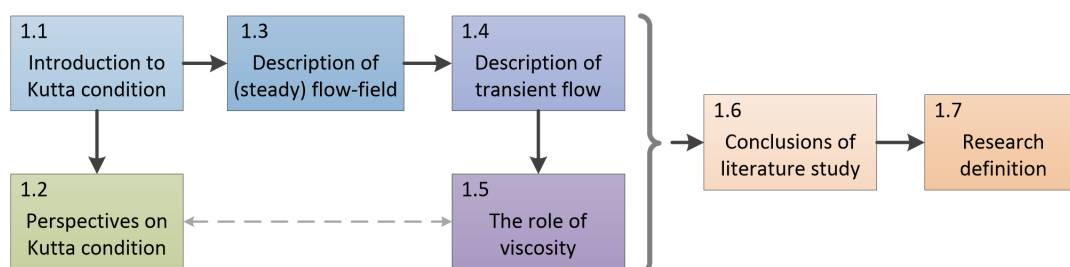


Figure 1.1: Roadmap of this chapter. Each block indicates one section, including the section number. The arrows indicate how each section follows logically from a prior section. (The colours have no meaning but serve for contrast.)

1.1. Introduction to the Kutta condition

We start with ‘the bigger picture’. The research presented in this report deals with a phenomenon which occurs in the flow of air (or another fluid medium) around a wing. An example is illustrated in Figure 1.2. When the wing of an aircraft (be it one of the main wings, or one of the tail surfaces, as in Figure 1.2a) is cut through, the cross-sectional shape can be observed, as indicated by Figures 1.2b and 1.2c. Figure 1.2c shows a generic situation of an airfoil moving relative to a fluid in a two-dimensional view. The frame in Figure 1.2c indicates the region of interest for this research: the most rearward part of the airfoil, where the air separates from the body.

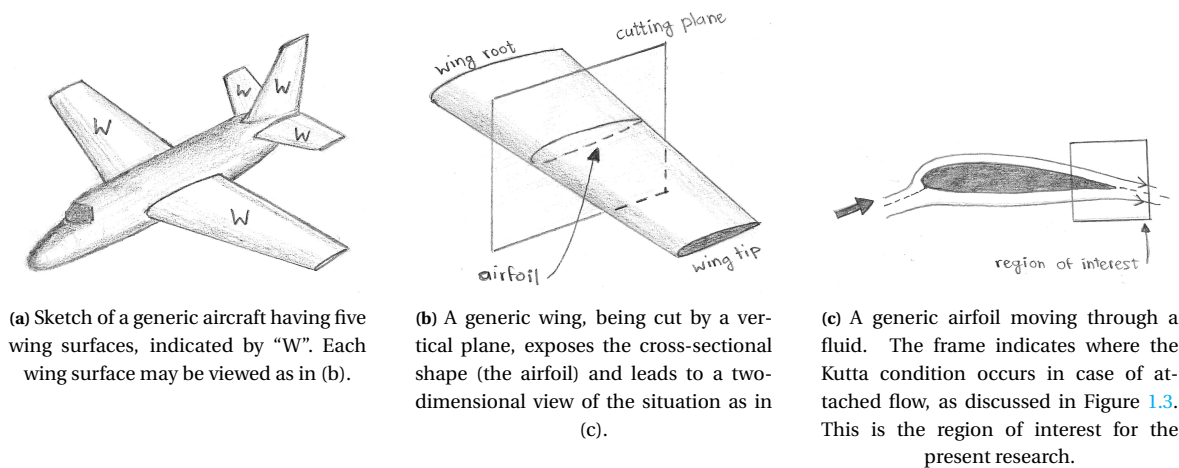


Figure 1.2: Illustration of the context of the “Kutta condition” phenomenon.

Figure 1.3 illustrates some possible ways in which flow might separate from the trailing edge by depicting the streamlines over the upper- and lower surfaces. The case of Figure 1.3a is called the “Kutta condition”, but the cases of Figures 1.3b to 1.3d are not.

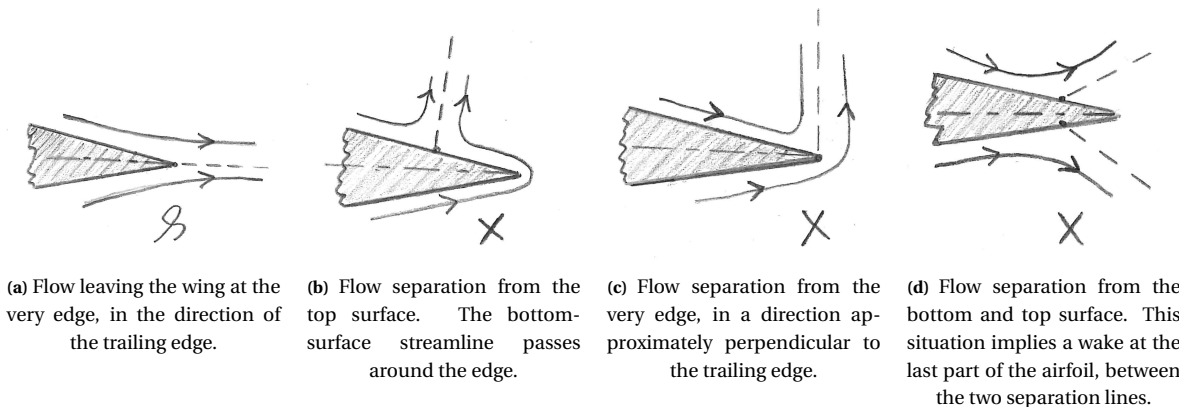


Figure 1.3: Some imaginary cases of flow separation from the trailing edge of an airfoil. Only the most rearward part of the airfoil is shown, corresponding to the dashed frame in Figure 1.2c. The case of (a) resembles the Kutta condition. All other cases may occur more-or-less in reality but do not correspond to the definition of the Kutta condition and are in general undesirable. The dots indicate locations of flow separation; the dashed lines indicate the direction of separation.

Historical background of the term “Kutta condition”

The term “Kutta condition” is almost as old as the modern science of aerodynamics. According to Anderson, the “Kutta condition” refers to a particular phenomenon which was first described by Martin Wilhelm Kutta in 1902 (Anderson, 2011, p. 404). The names of *Joukowski* (sometimes spelled as *Zhukovski*) and *Chaplygin* are also sometimes mentioned for their similar but independent research. This phenomenon is mentioned in practically all books in the field of aerodynamics, often in the section which discusses how a wing produces lift force. Its definition differs per author, and is often somewhat vague. Ackroyd et al. (2001) describe the flow field around an airfoil as follows, in their study of *Early developments in modern aerodynamics*:

“(...) the value of the vortex circulation is determined by the condition of finite velocity at the sharp trailing edge. This condition results in smooth flow there, in the sense that the flow departs tangentially to the edge’s cusped contour. This condition is now usually referred to as the Kutta-Zhukovskii condition. In Russian literature, in contrast, reference is often to the Zhukovskii-Chaplygin condition, thereby commemorating Chaplygin’s involvement in its discovery.”

About the reference to either Kutta or Joukowski or a combination of them, Crighton (1985) remarks:

“(...) the name “Kutta condition” (no doubt largely for brevity) has come to be used to connote the removal of a velocity singularity at some distinguished point on a body in unsteady flow.”¹

¹ Tani (1979) argues convincingly for the attribution of the trailing-edge condition to Kutta alone (...)

Gostelow (1975) discusses the variation in definition of the Kutta condition. Concerning the scope of the term, Gostelow argues that Kutta and Joukowski themselves only considered the cases of a cusped trailing edge in steady, incompressible flow, and concludes that the term “Kutta condition” should not be used in other cases. Actually, it does not seem that there has ever been consensus about the precise definition of the Kutta condition. We will look at this in more detail in Section 1.3.

Relevance of studying the Kutta condition

It can be argued in several ways that the occurrence of the Kutta condition is a crucial factor for the production of lift force by an airfoil. For example, according to the description of lift which refers to a zone of relatively high pressure existing on one side of the airfoil and a lower-pressure zone on the other side, the airfoil will develop lift more effectively when the high- and low-pressure zones are separated and maintained strictly at the lower and upper sides of the airfoil, respectively. The sharp trailing edge of an airfoil contributes to this because (without referring to any detailed explanation of the underlying mechanism) this edge prevents the ‘leaking’ of fluid from the high-pressure zone to the low-pressure zone.

Alternatively, from potential flow theory and the circulation theory of lift it is known that the amount of lift produced by an airfoil is related to the position of the rear separation point. A larger lift force corresponds to the position of the separation point being more on the pressure side of the airfoil (see for example Figure 1.4 on p. 4). Based on experience (again without referring to any detailed explanation of the underlying mechanism) it is noted that the airfoil’s sharp trailing edge somehow fixes the position of the stagnation point at the edge and thereby determines the amount of lift that is produced, as discussed in Section 1.2.

The Kutta condition has been roughly sketched in this section. Before we can proceed with giving a more comprehensive description of the properties of the Kutta condition, we first have to consider two different perspectives on the Kutta condition, and define what our philosophical approach to investigating this remarkable phenomenon will be. We will look at this in the next section.

1.2. Perspectives on the Kutta condition

The word ‘condition’ can be used with the meaning ‘requirement’ as well as ‘state’. A study of literature concerning the Kutta condition makes clear that roughly two perspectives on the Kutta condition can be distinguished: the mathematical and the physical/empirical perspective. Both perspectives have significantly different appreciation for the Kutta condition. Some authors are seemingly not aware of this, which results in confusion. We will look at both perspectives, discuss their correspondence, and define what perspective will be taken in the present study.

The mathematical perspective

In many pieces of literature¹ the Kutta condition is treated as a boundary condition which is necessary in the problem of calculating the magnitude of lift by a wing in order to obtain a unique solution. Introductory textbooks on aerodynamics usually state that the lift force produced by an airfoil can be modelled by (1.1), the so-called Kutta-Joukowski equation, in which ρ is the fluid density, V is the velocity of the wing w.r.t. the bulk of fluid, and Γ is the circulation. Each value of Γ corresponds to a specific flow-field picture, see Figure 1.4. This is similar to the potential flow analysis of lifting flow over a cylinder (Anderson, 2011, p. 267), which can be modelled by a combination of a uniform free stream, a source-sink doublet, and a vortex with circulation Γ . Anderson (2011, p. 270) writes: “ Γ is clearly a parameter that can be chosen freely. There is no single value of Γ that “solves” the flow over a circular cylinder; rather, the circulation can be any value. Therefore, for the incompressible flow over a circular cylinder, there are an infinite number of possible flow solutions, corresponding to the infinite choices for values of Γ . This statement is not limited to flow over circular cylinders, but rather, it is a general statement that holds for the incompressible flow over all smooth two-dimensional bodies.” “(...) we need an additional condition that fixes the magnitude of the circulation for a given airfoil at a given angle of attack.” (Anderson, 2011, p. 331)

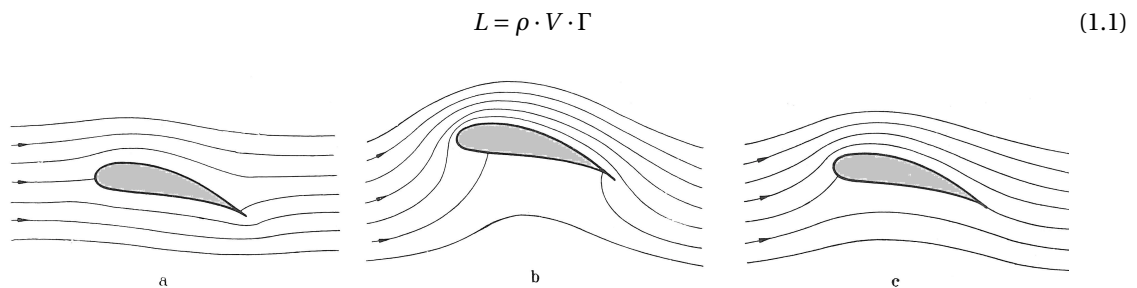


Figure 1.4: Illustration of different pictures of the flow-field around an airfoil, each having a different stagnation point position and a different magnitude of circulation and lift: a) zero circulation, rear stagnation point on suction side; b) very large circulation, rear stagnation point on pressure side; c) circulation of such magnitude that the stagnation point is on the trailing edge, smooth flow off; the Kutta condition is satisfied. This figure is copied and modified with translated caption from (Schlichting and Truckenbrodt, 1967, p. 393).

The ‘options’ for the flow-field around an airfoil suggested by Figure 1.4 look similar but are distinguished by the flow in the vicinity of the trailing edge. Mathematically oriented aerodynamicists argue that option (c) is the only viable option because the others would have a so-called “singularity” at the trailing edge, which effectively means that the flow velocity would be infinitely large. Options (a) and (b) would have an infinitely large velocity at the trailing edge, which is problematic. Why exactly the occurrence of such a velocity singularity is problematic is difficult to determine from literature, but many authors seem to be satisfied by the assumption that infinitely large velocities cannot occur in nature, so such behaviour should be avoided in mathematical results. From that perspective the Kutta condition is regarded as the application of a universal principle to the case of flow about a sharp edge. Crighton (1985) writes: “the name “Kutta condition” (...)

¹A number of references are given in the following text. For more references and a more nuanced picture of perspectives on the Kutta condition see (van Pelt, 2018).

has come to be used to connote the removal of a velocity singularity at some distinguished point on a body in unsteady flow” and Bassanini et al. (1999) refer to the Kutta condition by calling it a ‘singularity removal principle’.

From another angle of attack, Morino (1986) argues that a trailing-edge condition is required in order for the solutions of the Euler equations to be the limit of the solutions of the Navier-Stokes equations for inviscid flow. Similarly, Craig (1959, p. 42) writes:

“The fundamental equation of hydrodynamics is the Navier-Stokes equation for a viscous fluid: $\rho \frac{d\vec{V}}{dt} = -\nabla p + \eta \nabla^2 \vec{V}$ where p is the pressure and η is the viscosity. The boundary conditions to be used with this equation are the vanishing of the normal and tangential components of velocity at any surface. However, for zero viscosity the equation reduces to $\rho \frac{d\vec{V}}{dt} = -\nabla p$ which is of lower order. Thus a perfect fluid cannot be expected to obey all the boundary conditions of a real fluid. The boundary condition of zero tangential velocity is lost, and the fluid may slide along the walls. The flow pattern in the limit as $\eta \rightarrow 0$ may be completely different from that obtained if $\eta \equiv 0$.”

This implies that an additional boundary condition is required, which effectively replaces the condition of zero-slip between the surface and the fluid. This again determines a unique solution. Craig continues with an explanation of how this condition is determined:

“For an arbitrary shape the problem cannot be solved theoretically. However, Kutta and Joukowski pointed out independently that for a wing with a sharp trailing edge, dissipation effects must be maximal where the local velocities are highest and the shear forces therefore maximum, and that this will occur at the trailing edge. The boundary condition in such a case then requires that the local velocity at the trailing edge vanish. This condition, usually known as the Kutta condition, does not depend in any way the magnitude of the viscosity, but only upon its existence.”

In summary, from the mathematical perspective the Kutta condition is regarded as a mathematical condition based on a physical or theoretical consideration. It determines which flow-fields that are mathematical solutions are actually possible in a real flow, which constrains the solution space to just one possible flow-field, which corresponds to one unique value of the circulation. From this perspective we may regard the Kutta condition as a boundary condition which defines the magnitude of circulation and lift produced by an airfoil. The trailing edge of the airfoil has a crucial role here. A practical example of the application of these considerations is the implementation of the Kutta condition as a boundary condition in a panel code for the purpose of calculating the flow-field around an airfoil which moves through a fluid. See for example Drela (1989) and Katz and Plotkin (2001).

The physical perspective

The mathematical analysis of a lifting airfoil leads to the recognition of the trailing-edge flow-field as an important part of the study of lifting wings. Now, the mathematician can happily continue his calculations once he has his trailing-edge boundary condition. However, the mathematician’s appreciation of the Kutta condition as a ‘singularity removal principle’ or a ‘boundary condition’ leaves open the question what the properties of the flow-field in the vicinity of a trailing edge in a real flow are.² And it certainly does not explain how such a flow-field is produced in reality and what mechanisms are responsible for this. The physicist is interested in these questions. But the physicist or empiricist has a different appreciation of the Kutta condition compared to that of the mathematician.

²Here a ‘real’ flow, with its full richness of phenomena, is contrasted with the model of potential flow which takes only certain aspects of the real flow into account. There are also models which approximate real flows to a larger degree than potential flow, such as the Navier-Stokes equations.

The mathematician asks: *‘what trailing-edge flow-field is required for solving the mathematical problem such that the lift of an airfoil can be calculated?’* or *‘what trailing-edge flow-field is required such that my mathematical problem has a unique solution?’*, but the empiricist asks: *‘given a lifting airfoil, what are the properties of the trailing-edge flow-field?’* and *‘how was that flow-field produced in the first place?’*

A curiosity arises when it is realised that the mathematical idealisation of a pointed trailing-edge, with its associated theoretical problem of infinitely large velocity at the very edge if no Kutta condition is present, does not have a strict counterpart in reality. Nevertheless, it appears that, due to some obscure mechanism, the flow-field picture of Figure 1.4c is produced in real situations, even when the trailing-edge is not very sharp. From the empirical perspective this is observed and taken as a (fortunate) fact, not as a required condition. Once this observation is noted, we can start searching for detailed descriptions and explanations.

The perspective taken in this report

In this report, the physical perspective is taken. The term “Kutta condition” is used in the sense that refers to a physical phenomenon, or in other words: an ‘observed fact’ or a ‘phenomenon’ or a ‘set of properties’ of a flow-field. It is something that is created by the processes which naturally act in fluid flow.

The next sections address the properties of the Kutta-condition flow-field as given in literature. They result from a mix of mathematical and empirical work. Actually, these perspectives cannot be strictly separated from each-other. Nevertheless, the reader may find the distinction useful to understand literature about the Kutta condition.

1.3. Description of the Kutta condition flow-field

Various definitions and descriptions of the Kutta condition exist in literature, each one being slightly different from others. Most authors mention multiple flow-field properties and the emphasis which is put on one or the other property differs per author. A relatively clear description of the properties of a flow-field at the trailing edge of a lifting airfoil is given by [Anderson \(2011, p. 333\)](#); he sums up his conclusions as follows:

- “For a given airfoil at a given angle of attack, the value of Γ [the circulation] around the airfoil is such that the flow leaves the trailing edge smoothly.
- If the trailing-edge angle is finite, then the trailing edge is a stagnation point
- If the trailing edge is cusped, then the velocities leaving the top and bottom surfaces are finite and equal in magnitude and direction.”

Anderson continues by remarking that, from the last two bullet points, it follows theoretically that the vorticity at the trailing edge is zero in either case, described mathematically as $\gamma(TE) = 0$. This means that the vortex sheets on the airfoil's upper- and lower surfaces have equal magnitude and opposite direction at the trailing edge. In general, the following flow-field properties are mentioned in literature.³

- The flow leaves the trailing edge smoothly
- Equality of pressures at both sides of the trailing edge
- Equal tangential velocity magnitude at both sides of the trailing edge
- Zero net vorticity flux into the wake
- The velocity is finite everywhere in the fluid domain
- The Kutta condition is a stable phenomenon

Two properties (smooth flow-off and stability) will be discussed in more detail hereafter; the former because it is the only property which is directly visible on a streamline picture and the latter because it points us to important considerations for understanding the cause of the Kutta condition. Please note that all these properties are applicable only to *steady* flows. For more elaborate discussion of the other properties the reader is referred to ([van Pelt, 2018](#)).

Property: The flow leaves the trailing edge smoothly. This property is mentioned by many authors, for example by [Tietjens and Prandtl \(1931, p. 182\)](#), [Karamcheti \(1966, p. 393\)](#), [Schlichting and Truckenbrodt \(1967, p. 392\)](#), and [Anderson \(2011, p. 331\)](#). It is however often not clear what the author means by the word “smooth”. Two questions can be raised here: 1) what exactly is the thing that has the quality of being smooth, and 2) what does “being smooth” amount to? [Goldstein \(1965\)](#) is slightly more clear by mentioning that the *streamlines* are smooth. Concerning smooth streamlines, the most intuitive interpretation (according to the present author) is that the streamlines show no kinks or sharp bends. So the streamlines are more-or-less straight in the vicinity of the trailing edge and do not abruptly change direction, as sketched in [Figure 1.5](#). This implies that the direction of the streamlines is approximately parallel to the airfoil surface for the part where the streamline is between the leading edge and the trailing edge, at the suction side as well as at the pressure side of the airfoil. It also implies that behind the trailing edge the direction of the streamlines is approximately equal to the direction in which the trailing edge points. This direction may be defined in different ways if the trailing edge has a finite angle. This ambiguity is illustrated in [Figure 1.6](#). Perhaps the most intuitive definition is the direction of the bisecting line of the trailing edge. The dividing streamline should at least be in the sector formed by the slopes of the upper and lower surfaces.

³This list summarises the descriptions of [Anderson \(2011\)](#), [Batchelor \(1967\)](#), [Kuethe and Chow \(1998\)](#), [Goldstein \(1965\)](#), [Schlichting and Truckenbrodt \(1967\)](#), [Glauert \(1947\)](#), and [Robinson and Laurmann \(1956\)](#). A literature overview is given in [Radwan \(1981\)](#).

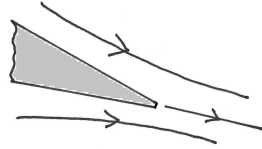


Figure 1.5: Interpretation of the property that ‘the flow leaves the trailing edge smoothly’. The upper- and lower streams join while their direction changes gradually.

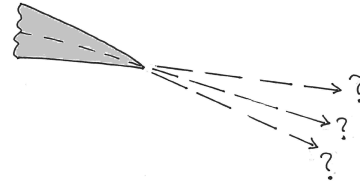


Figure 1.6: Ambiguity of the direction of the dividing streamline. It is reasonable to expect that the dividing streamline is in the sector formed by the slopes of the upper and lower surfaces of the airfoil.

Property: The Kutta condition is a stable phenomenon. The Kutta condition might be a stable phenomenon, in the sense that when any deviation from the flow situation occurs due to some disturbance, some transient effect will be produced which restores the original situation. Regarding this, [von Kármán and Burgers \(1935\)](#) remark:

“Every change in velocity and likewise every change in the angle of incidence of the airfoil is accompanied by the formation of a new starting vortex, of the same sign as the original one when the velocity or the angle of incidence is increased (supposing that the latter does not surpass its critical value) and of opposite sign in the contrary case.”

[Karamcheti \(1966, p. 393\)](#) writes:

“Whenever the condition of smooth flow at the trailing edge is disturbed, say by a change in the speed of the airfoil or in its angle of attack, a new starting vortex is formed, and a new value of the circulation is established such as to restore smooth flow at the trailing edge.”

[Batchelor \(1967, p. 440\)](#), after presenting his description of a certain transient process, remarks:

“... we can argue that any steady value of the circulation other than that which places the rear stagnation point right at the sharp trailing edge would immediately set the above sequence of changes in train and cause further adjustment of the circulation, always of such a kind as to make the rear stagnation point move towards the trailing edge.”

These remarks are important, because if they are correct, they imply that an understanding of the *causes* of the Kutta condition should be obtained by investigating the transient flow which precedes the existence of the Kutta condition, focusing on the working principles, and studying how the flow-field develops in time towards its equilibrium. If an explanation can be given of why a certain transient phenomenon occurs and why it develops towards a certain equilibrium, and if it can be shown that the equilibrium - or steady state - situation is stable, then an explanation for the existence of that steady-state situation has been given as well. It has then been explained why the steady-state situation is as it is. Regarding this, [McLean \(2013, p. 268\)](#) writes:

“One might wrongly infer (...) that the final steady-state lift depends on the details of the initial time history. But the final steady state is nearly always a unique “stable attractor” that is the end point of any one of an infinity of time histories (impulsive starts, gradual starts, varying angle of attack, etc.) Thus the final steady state is in a sense more fundamental than any of the possible starting sequences, and a more satisfying explanation would deal directly with it and show us why it does what it does. And this would require establishing more details than just the circulation.”

This section presented some properties of the steady-state flow-field. We agree with McLean that we should find-out what causes this flow-field to be so persistent. In the following section we make a start, by looking at descriptions from literature of the transient flow which produces the steady-state flow-field.

1.4. The transient flow-field that results in the Kutta condition

In the usual definitions the term ‘Kutta condition’ refers to a steady-state flow-field. However, we are not only interested in the steady-state flow-field but also in the transient process that leads to the establishment of that steady-state flow-field, because hopefully knowledge of this transient process will be helpful to understand the properties of the Kutta condition. We would like to have not only a ‘factual’ description of the transient process but also an explanation in which different parameters corresponding to the flow development are linked to each other via causal mechanisms.

This section presents some views on the problem, found in literature. In the first half of this section, we will first look at descriptions by some authoritative authors and synthesise them into a single description which covers all properties and mechanisms. This will have a theoretical and hypothetical character. Then we will treat some investigations that were done specifically to study the transient flow-field. To that end we will temporarily widen our scope to separation of flow from sharp edges. This will lead us to a particularly difficult problem, namely the definition and detection of flow separation.

1.4.1. Theoretical descriptions of the transient flow

The writings of early authors indicate that no theory concerning the working principles of the Kutta condition was present before 1930, or at least not widely known and accepted. (Witoszyński and Thompson, 1934, p. 10) write that *“at the trailing edge the fluid in some way tears itself loose from the surface of the profile, producing the same effect as is obtained by the outflow from a vessel of fluid under pressure.”* The words ‘in some way’ indicate a certain amount of incomprehension. In the following text a number of citations are presented which show how the transient flow which precedes the Kutta condition is described by a number of various authoritative authors. The citations are copied entirely such that the reader obtains an impression of the qualitative character of those descriptions.

Tietjens and Prandtl (1931, p. 181) describe the process more completely but do not give a detailed explanation of what occurs in the region where the starting vortex is formed (accompanying photographs can be found in Appendix C):

“As observation shows, the fluid performs in the first instant actually a potential flow without circulation (...) in which it flows around the rear edge with very large velocity. For explanation of the creation of the circulation we will assume that the rear side is a sharp edge; the viscosity may be regarded as very small, such that (...) infinitely large velocities are created at the trailing edge. But these lead due to the action of however small viscosity to a separation plane. This separation plane, progressing from the trailing edge, winds itself up to a vortex, a so-called starting vortex.”

“The [circulation] grows as long as the flow from both sides of the wing at the trailing edge joins together smoothly. From the moment that this situation is reached (taking a displacement in the order of magnitude of the wing chord) the starting vortex also does not grow anymore. When one increases the velocity of the flow or the angle of attack, a further vortex delivery in the direction of rotation of the starting vortex takes place.”

(Translated from the original in German by the present author)

Although **Witoszyński and Thompson** did not present an explanation of the “bubbling” at the trailing edge (as they called it), in the same book series an explanation is given by **von Kármán and Burgers (1935, p. 11)**:

“It has been deduced both from experimental observation and from theoretical reasoning, that when a body starts moving in a fluid originally at rest, the motion first generated is an irrotational flow (...) This initial motion nowhere presents a circulation around the airfoil. The general course of the lines of flow around a particular section of the airfoil at this stage is given in Fig. 10 [the figure given in the original text is very similar to Figure 1.7a in this report], from which it will be seen that

there are two stagnation points (...) It must be observed that in consequence of the very small radius of curvature of the profile at the trailing edge (in theoretical investigations the radius of curvature is usually taken equal to zero here, giving a sharp trailing edge), the velocity of the fluid moving around the trailing edge will be very high; hence the pressure will be low at [the trailing edge].

In the case of an ideal fluid, experiencing no frictional forces, the kinetic energy of the motion at [the trailing edge] is just sufficient to drive the fluid to the stagnation point, where the pressure is equal to the impact pressure. In any actual cause, however, viscous forces are present; they give an additional retardation to the fluid on the way from [the trailing edge] to [the stagnation point], and this retardation proves to be so effective, that in the immediate neighborhood of the surface of the airfoil the fluid does not reach [the stagnation point], but stops somewhere on the way. In consequence of this a backflow appears, caused by the pressure gradient acting from [the stagnation point] towards [the trailing edge], which separates the original flow from the surface of the airfoil, and produces a vortex as indicated (...)

This vortex, which is formed along the whole trailing edge of the airfoil and is called the starting vortex, appears to be unstable: it separates from the trailing edge and is carried along by the general motion. (...)

While the starting vortex is moving away, the two trailing vortices are formed from the fluid particles which are driven from the lower (high pressure) surface of the airfoil around the end edges to the upper (low pressure) surface. They make the connection between the ends of the airfoil and the ends of the starting vortex.

Simultaneously with this process the motion around the airfoil itself is changed; the line of stagnation points is displaced, until it approximately coincides with the trailing edge. The fluid then no longer moves around the trailing edge, but flows off tangentially at both sides with a velocity differing only slightly from the original velocity V , as pictured already in Fig. 6." [the figure given in the original text corresponds to Figure 1.7g in this report]

(The symbols 'A' and 'B' in the original text are replaced by 'the trailing edge' and 'the stagnation point', respectively.)

Batchelor (1967, p. 438), in a paragraph under the heading "The generation of circulation round an aerofoil and the basis for Joukowski's hypothesis" gives the following account:

"The circulation round an aerofoil with a rounded leading edge and a sharp trailing edge in steady translational motion is observed to be independent of the past history of the flow, and for purposes of explanation we may suppose that the motion has been set up from rest and that the aerofoil has been brought rapidly to its ultimate steady velocity without change of the direction of its motion. Immediately after the aerofoil begins to move, the motion of the fluid is irrotational everywhere, because the transport of vorticity away from the aerofoil surface (which is where it is generated) by viscous diffusion, and subsequently also by convection, takes place at a finite rate. This initial irrotational motion is characterized by zero circulation (...), and there is an associated definite position of the rear stagnation point which depends on the given orientation of the aerofoil relative to the direction of its motion. The initial position of the rear stagnation point does not coincide with the sharp trailing edge, in general, and as a consequence there is flow around the trailing edge with a high peak in the velocity at the edge (...) The extremely strong deceleration of the fluid flowing from the trailing edge towards the rear stagnation point leads almost immediately to the development of back-flow in the boundary layer there and to separation of the boundary layer (which at this stage is still very thin) at the sharp trailing edge."

"The shed vorticity is carried away from the edge by the fluid, and so needs continual reinforcement by further vorticity shed from the edge in order to be able to induce a velocity near the edge which exactly cancels the velocity round the edge due to the background irrotational flow."

Similar descriptions are given by (Glauert, 1947, p. 119), (Karamcheti, 1966, p. 393), and (Truckenbrodt, 1998, p. 218).

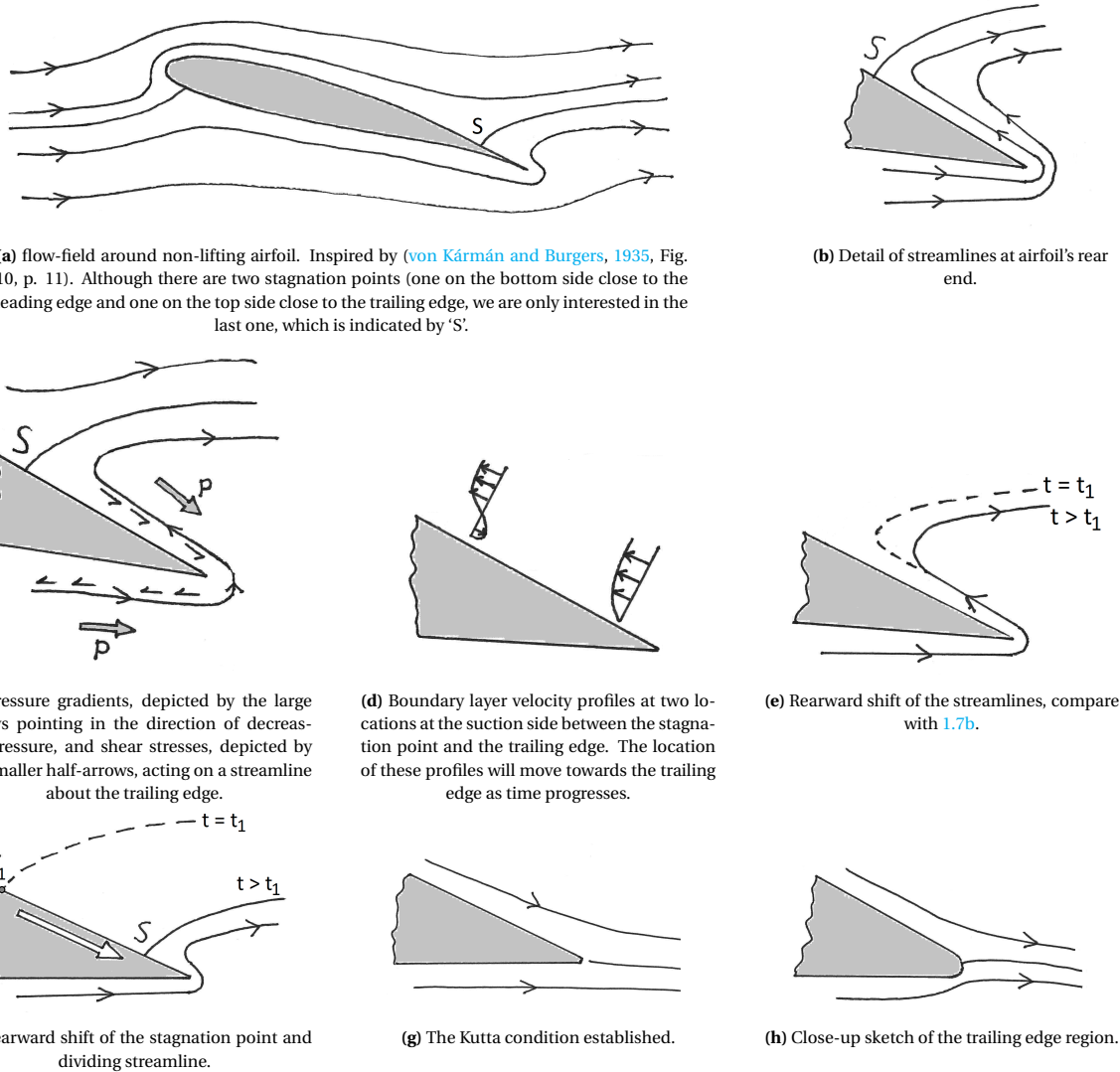


Figure 1.7: Illustration of the working principle of the creation of the Kutta condition, sketched by the present author on the basis of descriptions found in literature. When the airfoil is set in motion from rest the flow-field will initially be like (a) and during a process in which the separation point moves towards the trailing edge it will transform to the eventual picture of (g). Figure h) corresponds to a hypothesis presented on p. 12.

1.4.2. The main theory: Synthesis of descriptions of the transient flow

The descriptions of the evolution of the flow-field cited or referred to in the foregoing paragraphs are quite similar. Their common idea is illustrated in Figure 1.7; an accompanying description of the process by the present author is given as follows. When an airfoil is accelerated from rest, the initial flow-field has streamlines like shown in Figure 1.7a. Fluid curves around the leading edge as well as around the trailing edge. At this moment there is no circulation around the airfoil. The streamlines turning around the trailing edge are shown in more detail in Figure 1.7b. The stresses acting on the fluid that is close to the airfoil surface are sketched in Figure 1.7c which shows the direction in which pressure and friction stresses act on the streamlines. The pressure at the very edge is small⁴ while the pressure closer to the airfoil's leading edge is larger,

⁴This can be expected from a consideration of the general pressure distribution in a vortex, see also Section 4.5.

both on the pressure- and the suction side.⁵ Thus the fluid is accelerated by a favourable pressure gradient at the pressure side when it is travelling towards the trailing edge, while it is opposed by an adverse pressure gradient at the suction side when it is travelling away from the trailing edge. Furthermore, the movement of fluid is opposed by friction stresses on both the pressure- and suction side. The fluid close to the surface is opposed most by friction (compared to fluid being further away from the airfoil) and a velocity profile like shown in Figure 1.7d will develop. Due to loss of total pressure (we may also say loss of total mechanical energy) the fluid which comes from the trailing edge towards the stagnation point does not reach the original stagnation point anymore, but it will stagnate at a location closer to the trailing edge. This will result in a pressure gradient normal to the surface (since fluid cannot accumulate at the stagnation point) which causes the fluid to separate and move away from the surface at a position closer to the trailing edge compared to the initial situation, as illustrated in Figure 1.7e. The stagnation pressure of the fluid coming around the trailing edge is smaller than that of the fluid coming from the leading edge: the stagnation pressures at both sides of the original stagnation point location are not equal anymore which corresponds to a pressure gradient tangential to the surface at that location causing a rearward movement of the stagnation point, as illustrated in Figure 1.7f. This process occurs continuously until the point of separation reaches the trailing edge after which it remains there, as in Figure 1.7g. The Kutta condition is then established. During the process just mentioned the lift and drag forces acting on the airfoil vary. Both are present from the very moment the motion is started, even though circulation is absent or still very small. This can be expected (assuming that the fluid has inertia), because kinetic energy and momentum have to be supplied to the flow when the airfoil is accelerating.⁶

An hypothesis regarding the trailing-edge flow in microscopic view. The present author proposes the following hypothesis. On any lifting airfoil a pressure difference is present between the pressure side and the suction side (hence those identifiers) and this difference is in general also present in the vicinity of the trailing edge. This pressure difference will push the fluid around the trailing edge towards the suction side. The occurrence of the boundary layer separation mechanism described in the foregoing paragraph will result in some equilibrium position of the separation point. It is thus expected that the separation point will be slightly on the suction side of the trailing edge in the steady flow situation (in which the free-stream velocity and angle of attack are constant). Since it is in practice impossible to produce an ‘infinitely sharp trailing edge’ there will always be an edge of finite thickness which may be approximated by the rounding on Figure 1.7h. So on a macro-scale the streamlines at the trailing edge will look like in Figure 1.7g, however when zooming in on the region around the trailing edge, the micro-scale situation of Figure 1.7h might be observed.

In an early experiment, Albert Betz explained the deviation between the measured lift of an airfoil and the theoretically predicted lift by referring to the absence of a perfect Kutta condition, and mentioned that the flow did not separate at the trailing edge but on the suction side.⁷ This arguably occurs for every airfoil which does not have a perfectly sharp trailing edge, which, in practice, is every airfoil. The extent to which flow separation occurs on the suction side is arguably determined by the ‘sharpness’ of the trailing edge. McLean (2013, p. 264) remarks:

“Of course, an edge doesn’t have to be perfectly sharp to provoke viscous-flow separation, and in the real world separation will still anchor itself near the trailing edge of an airfoil even if there is a considerable degree of rounding. Thus even if the trailing edge is rounded, something like the Kutta condition still applies, albeit with some uncertainty as to where it applies.”

⁵We will refer to the upper side of the airfoil as the ‘suction side’ and to the lower side as the ‘pressure side’, corresponding to the pressure distribution over an airfoil at positive angle of attack.

⁶According to Wagner (1925) the lift force starts at approximately 50% of its steady-state value and increases to its asymptotic value. It is however not clear from Wagner’s paper whether he assumes an accelerating or an impulsive start. In potential flow a drag force is present from the beginning and goes to zero, which is discussed by Tietjens and Prandtl (1931, p. 183).

⁷This is mentioned in (Bloor, 2011, pp. 235-238).

1.4.3. The Kutta condition and the general case of vortex shedding from a sharp edge

The Kutta condition might be regarded as being a specific case in the category of “fluid flow past a sharp edge” It is well-known that a so-called ‘starting vortex’ is created when the relative motion between an airfoil and the surrounding fluid is (suddenly) changed, which was documented and shown photographically by [Tietjens and Prandtl \(1931\)](#), see Figure 1.8. In such a situation, the flow separates at the sharp edge (or very close to it) and a vortex is created which grows and moves away from the airfoil when the airfoil proceeds through the fluid. This is also mentioned in the discussion of the stability of the Kutta condition flow-field on p. 8. This event occurs independent of the angle of attack. An airfoil is usually inclined w.r.t. the main stream direction at a small angle ($\alpha < 20^\circ$) but very similar effects can be observed when a sharp-edged plate-like object is moved through a fluid at a much larger angle of attack, or even when a plate is oriented perpendicular to the flow. When a plate is perpendicular to a stream, a vortex might be produced at both edges. These fascinating phenomena can be easily produced and observed when moving a spoon through a cup of soup or a kitchen sink.⁸ The evolution of starting vortices has been studied empirically by several authors, for example [Tietjens and Prandtl \(1931\)](#). The development of circulation and lift after the start of motion of an airfoil was determined theoretically using potential flow theory by [Wagner \(1925\)](#). A similar study by [Anton \(1939\)](#) considers development of vortices from a plate which is moved perpendicularly in a flow. [Pullin and Perry \(1980\)](#) present time-sequenced close-up photographs of the creation of vortices in flows past sharp edges. A numerical study by [Evans and Bloor \(1977\)](#) shows that, when the Kutta condition is applied (in the mathematical sense) by specifying some boundary condition on the strength of shed vortices at the location of the sharp edge, the trajectory of the starting vortex can be predicted reasonably well, and theoretical estimations of roll-up rates can be made.

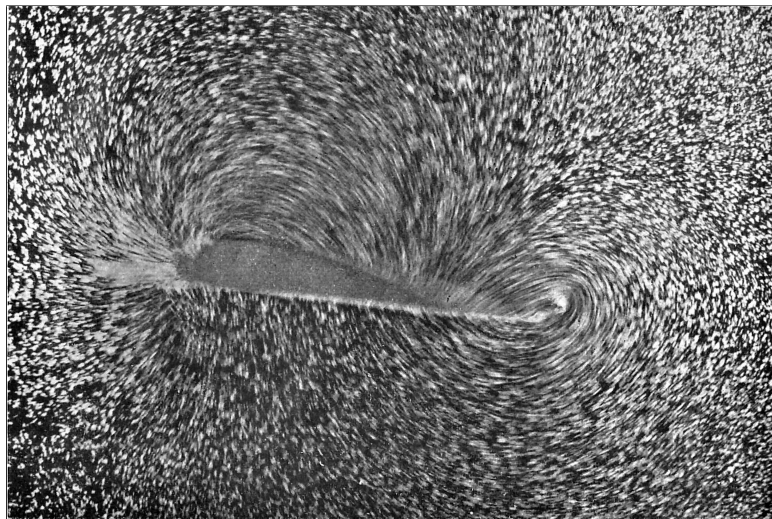


Figure 1.8: Photograph of an instantaneous flow-field about an airfoil which has been brought into motion (from right to left) from rest. The bound vortex and starting vortex can be observed on the left and right respectively. The camera was stationary w.r.t. the main stream. Copied from ([Tietjens and Prandtl, 1931](#), Fig. 52).

The present author noticed that people often relate the creation of the Kutta condition to the production of a starting vortex. That is the reason why this paragraph is included in this report. Certainly, the starting vortex is related to the existence of lift. The magnitude of vorticity in the starting vortex is related to the magnitude of circulation about the airfoil via Kelvin's theorem, and as such it is related to the steady-state lift ([Batchelor, 1967](#)). In that sense the starting vortex has an important role in a discussion of the creation of lift. However, for the present research we are interested in the transient flow which occurs even *before* a starting vortex is shed.

⁸In fact, Felix Klein wrote a ‘coffee-spoon paper’ about the creation of circulation in 1910, see reference list. This is discussed by [Bloor \(2011\)](#) in his great work about the development of aerodynamics in 1900-1930.

1.4.4. Studies of the transient flow-field

The development of the flow-field before the production of the starting vortex is considered by some works in the period around 1970. The work of [Mehta and Lavan \(1975\)](#) considers the flow-field development around an airfoil having a rounded trailing edge being impulsively set in motion. Similarly, the work of [Lugt and Haussling \(1974\)](#) considers the same situation but for an ellipse at incidence instead of an airfoil shape. More recently, the work of [Badr et al. \(2001\)](#) presents numerical study of unsteady flow about ellipses at several angles of incidence. The works just mentioned all employ Computational Fluid Dynamics (CFD). The empirical works of [Taneda \(1972\)](#) and [Honji \(1972\)](#) are cited often and serve as references for comparison of flow patterns. According to [Badr et al.](#): “one of the most comprehensive experimental works on unsteady separated flows around bodies is that of Taneda. He studied flow patterns around two-dimensional bodies like circular and elliptic cylinders, flat plates, and flexible plates. The unsteady motions studied were the impulsive start from rest, change of velocity, translational oscillation, change of angle of incidence, uniform rotation, rotational oscillation and swimming motion.” Unfortunately the present author could not obtain these works. However, it is clear that a detailed, quantitative, empirical study of the development of the flow-field behind an airfoil-like body brought in motion from rest is lacking. Table 1.1 shows the degree of realism of the works just mentioned. It is clear that no single work completely represents the real situation of a wing being put in motion in a viscous fluid. A real airfoil will not have a pointed trailing edge (i.e. perhaps in a practical sense but not in the strict mathematical sense) and will be accelerated w.r.t. the flow, not impulsively started.

Table 1.1: Several properties of works concerning unsteady flow separation behind bodies put in motion from rest. The right-most column indicates the present research. All other pieces of research are in one or more aspects not representative for the case of an airfoil which is accelerated from rest in viscous fluid in a practical situation. A green item indicates a realistic property, a red item indicates an un-realistic property. An orange-coloured item is approximately neutral regarding realism.

	Wagner (1925)	Lugt & Haussling (1974)	Mehta & Lavan (1975)	Zhu et. al. (2015)	present research (2019)
steady / transient	transient	transient	transient	transient	transient
pointed / rounded trailing edge	pointed	rounded	rounded	pointed	rounded
inviscid / viscous fluid	inviscid	viscous	viscous	viscous	viscous
impulsive / accelerated start		impulsive	impulsive	accelerated	accelerated
separation visualised yes / no	no	yes	yes	yes	yes
cylinder / airfoil plate	airfoil	cylinder	airfoil	airfoil	airfoil
theoretical / empirical	theoretical	CFD	CFD	CFD	empirical

1.4.5. The difficulty of defining and detecting flow separation

From reading the above mentioned works it becomes evident that it is difficult to define the phenomenon of ‘flow separation’ in case of unsteady flow. Although there is no dispute about whether such a thing as ‘flow separation’ exists (we may roughly describe it by “flow not following the contour of the body immersed in the fluid”), there is no universal consensus about its precise definition. It seems difficult to define what markers exist in the flow-field which signify that flow separation is going to occur or where it occurs precisely. This is a relevant problem because flow separation is an important aspect of the transient flow studied in this report. It results in the creation of the starting vortex with the associated convection of vorticity.

Concepts for defining flow separation

The following quote from [Mehta and Lavan \(1975\)](#) concerning unsteady flow separation mentions a number of relevant concepts:

“Stuart (1971), while discussing the flow-field around a circular cylinder started impulsively from rest, states that after a short time a separation bubble is produced at the rear of the cylinder “but still within the boundary layer”. He hesitates to label this phenomenon as separation since it does not involve a large-scale breakaway of fluid. Sears & Telionis (1971) maintain that the definition of unsteady flow separation must be based on physical phenomena such as the shedding of vorticity into the flow, but not flow reversal in general. They further state that when the vorticity of the boundary layer, or at least its outer part, is carried out into the flow (the shedding of vorticity), the flow ceases to be of boundary-layer character. Finally, Wang (1971) holds the view that the definition of unsteady separation from physical phenomena, such as the shedding of vorticity and actual flow reversal (on a fixed body), cannot be formulated by any of the existing theories. He concludes that “only a Lagrangian description of pathlines can characterize such unsteady phenomena.”

We see that the concepts of ‘boundary layer’, ‘separation bubble’, ‘break-away of fluid’, ‘vorticity’, ‘flow reversal’, and ‘pathlines’ are apparently relevant to the problem. The relation between a boundary layer and a region of separated flow is somewhat controversial. Since flow separation has its spatial origin close to the body, in the boundary layer, it is often indicated with the term “boundary layer separation”. But actually this term is not wholly applicable. Perhaps it can better be replaced by “boundary layer termination” if we want to refer to the boundary layer, because, as pointed out by [Sears and Telionis \(1975\)](#), where the flow separated from the wall, the velocity field does not show the pattern of a boundary layer anymore but the pattern of a circulation bubble or a wake. [Mehta and Lavan \(1975\)](#) use the following definitions when analysing the process of flow separation:

“a bubble is said to be open (or burst) if it is not completely enclosed by a zero streamline and there is a closed streamline loop within this region. A vortex is defined by closed equi-vorticity lines. Bubbles and vortices are separate entities that may have some region in common. The attached bubble is bounded by a streamline with a stream function value of zero. This is brought about at any instant by a bifurcation of the surface streamline and the recombination of the branches. (...) The bifurcation point is called here the separation point and the unification point is named the reattachment point of the bubble. (...) our definition of a separation point, as a location at which the instantaneous streamline bifurcates and downstream of which there is reverse flow, is based on the physical behaviour of the flow. (...) the streamline bifurcation point is very near (or at) the location where the vorticity (or skin friction) is zero”.

This offers some additional useful concepts: ‘streamlines’, ‘streamfunction value’, ‘reattachment point’, ‘skin friction’; and some topological properties of streamline behaviour: ‘bifurcation’, ‘recombination’, ‘unification point’. Note that the last couple of citations date from around 1975. The problem remains unsolved 40 years later. [Zhu et al. \(2015\)](#) write: “A fundamental fact of unsteady flow is that the patterns of streamlines, pathlines, and streaklines of the same flow can be very different. This simple fact makes local separation criteria and the triple-deck theory developed for steady separation, all in terms of the behaviour of streamlines or stream-

surfaces in the separation zone, no longer effective” and further they remark that attempts have been made, from different perspectives, to produce a generic theory of unsteady flow separation, however this has not yet lead to methods that can be conveniently applied in complex-flow diagnosis.

Detecting flow separation using material lines

Haller and coworkers developed methods for finding a stagnation point by analysing the curvatures of so-called “material lines” in a flow (Haller, 2004), (Serra et al., 2018). A material line is made by drawing an imaginary line through the boundary layer, tangential to the wall. The fluid parcels which lie on the line are kept in memory. At later times a line is drawn through these same fluid parcels. The deformation of a material line through time thus represents the flow behaviour in a certain way (in addition to concepts like streamlines and pathlines etc.). When a boundary layer approaches a separation bubble, fluid moves upward just in front of the bubble and when the material lines, which are initially parallel, are followed through time they will form a marked spike. Searching for the location of the smallest radius of curvature on a material line leads to the peak. The locus of peaks represents the path along which the flow separates from the surface. See Figure 1.9 for an illustration. However, this method requires knowledge of the velocity field close to the surface (i.e. data covering the whole boundary layer) and such data is not available in the present research. Furthermore, this method is quite mathematically involved so implementation is not feasible within the scope and time-frame of the present study.

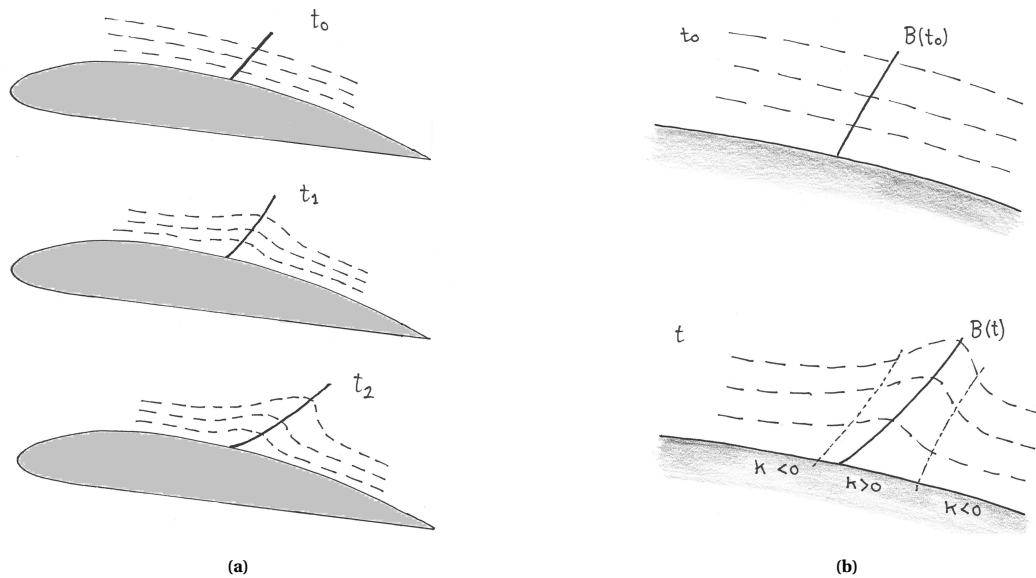


Figure 1.9: Illustration of defining a point of separation on a body in case of unsteady flow, based on material lines. The dashed horizontal lines represent material lines. Figure a) illustrates the time-wise evolution of material lines in the flow over an airfoil, starting at $t = t_0$. Figure b) depicts the same situation as Figure a) but zoomed-in on the region in the vicinity of the separation point. The top picture corresponds to the top picture of Figure a), which depicts the initial situation when separation has not yet occurred. The bottom picture corresponds to times larger than t_0 . The symbol κ indicates the direction of the curvature of the material lines. The vertical dotted lines indicate the regions where the radius of curvature is zero. The points of smallest radius of curvature of these lines are at their peaks. The locus of these points determines the so-called ‘backbone of separation’ which represents the path along which material separates from the surface. This line is depicted by the thick vertical line and indicated by the symbol B . This line is also shown in the top picture on the left, however in that case the black line indicates the pieces of material which will later form the ‘backbone of separation’. Inspired by (Serra et al., 2018).

Distinctions in terminology

A number of distinctions can be made to make the discussion of flow separation more clear. We will look at six distinctions.

1) Viscous vs non-viscous flow. The streamline picture of flow around an airfoil is different for viscous and non-viscous (inviscid) flows. In viscous flow, the airfoil's contour is a stagnation line. The flow region can be divided in two regions: the boundary layer, where viscous effects are significant, is located around the airfoil. This is illustrated in Figure 1.10a. The rest of the flow can be approximated as potential flow. The situation can be approximated by a replacing body in inviscid flow, where the 'replacing body' replaces the airfoil + boundary layer. In inviscid flow, the airfoil's contour is a streamline of the flow, as illustrated in Figure 1.10b.

2) Stagnation point vs separation point. In viscous flow, the airfoil's contour is a stagnation line. This is illustrated in Figure 1.10c. So, although every point on the airfoil's contour is a stagnation point, only one (or only few) of these points are separation points. When there is attached flow over the whole airfoil, only the trailing edge is a separation point, as illustrated in Figure 1.10d, so there is only one point which is both a stagnation point and separation point.

3) Unproblematic vs problematic separation. The term 'flow separation' is often used to indicate the occurrence of undesired behaviour, as illustrated by Figure 1.10f. However, at some points (i.e. the trailing edge) flow leaves the body although this is not at all undesirable, as illustrated in Figure 1.10e. McLean (2013, p. 170) admits that confusion exists regarding the terminology and remarks: *"In common parlance, the term 'separation' is often reserved for situations where the flow separates 'prematurely' (...) But this use of terminology ignores the fact that even if the flow doesn't separate prematurely, it must leave the body somewhere, and it seems logical to refer to that as 'separation' as well."*

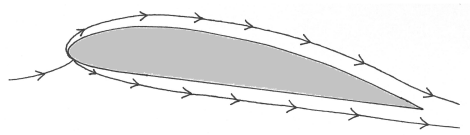
4) Full-pressure vs partial pressure stagnation points. In potential flow over a body there are two stagnation points: one on the front and one on the rear. At both points, the pressure coefficient (defined as $C_p = 1 - V^2/V_\infty^2$, where V is the local flow velocity and V_∞ is the flow velocity at a point infinitely far upstream) is equal to one. This is illustrated in Figure 1.10g, which shows a point (S) on the rear of a blunt body. Three properties correspond to this point: the point is a separation point, it is a stagnation point, and the pressure coefficient equals 1. However, in viscous flows, as illustrated in Figure 1.10h, it may occur that flow separation occurs at a sharp edge. In such a situation, the point of flow separation is also a point of flow stagnation. However, due to the loss of total pressure which occurs in the wake (which is related to friction stresses) the pressure coefficient is smaller than 1. So such a point is not a 'full pressure stagnation point' like the stagnation point in Figure 1.10g.

5) Separation on a body vs in a flow. Some discussions of flow separation use the bifurcation of the airfoil contour streamline as definition of the location where flow separation occurs on an airfoil, as illustrated in Figure 1.10i. However, we can also say about points which do not lie on the airfoil that they are in a region of separated flow, as illustrated in Figure 1.10j.

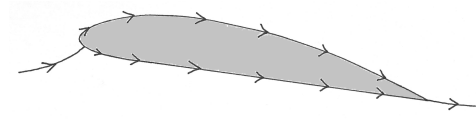
6) Separation detection in analytical or numerical vs experimental work. The methods for the detection of flow separation which have been mentioned in the foregoing paragraphs use properties which are related to the airfoil contour, such as friction stress, the bifurcation of a contour streamline, and velocities in the boundary layer. Such data may be available when flow analysis is done using analytical or numerical methods; however, this is usually not the case in experimental work.

Now these distinctions have been clarified, we can define what kind of method for detecting flow separation is lacking: *We would like to have a method that can detect the occurrence of undesired flow separation (in unsteady flow), at points that either lie on the body or in the flow, using data of the flow-field outside the boundary layer.*

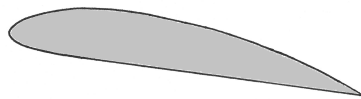
In the foregoing paragraphs we have discussed the geometrical properties of separating flow. However, in order to understand why a flow exhibits separation at all, it is necessary to study the associated causal mechanisms. The citations of Von Kármán and Burgers and others presented in the first part of this section give us a direction, because these authors agree unanimously that *viscosity* is a driving factor in the development of the flow-field. Therefore we will consider the role of viscosity in the next section.



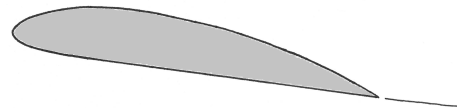
(a) An airfoil in viscous flow. Viscous effects are negligible outside the boundary layer, so in that part the flow is approximated as potential flow. The edge of the boundary layer is a streamline of the flow.



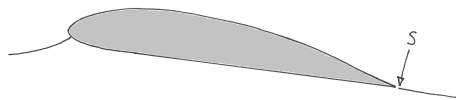
(b) An airfoil in inviscid flow. The flow is potential and the airfoil's contour is a streamline of the flow.



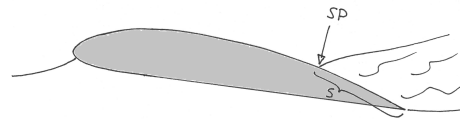
(c) An airfoil in viscous flow. A no-slip condition applies: at all points on the airfoil's contour the flow velocity is zero, so the contour line is a stagnation line. However, no flow separation occurs, except at the trailing edge.



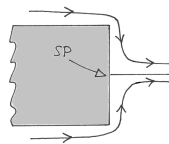
(d) The same situation as in the figure on the left. The trailing edge is a stagnation point and a separation point, whereas all other points on the contour are stagnation points without being separation points.



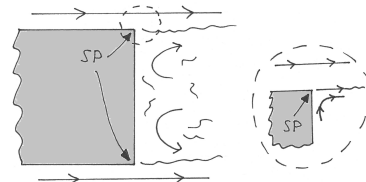
(e) An airfoil in attached flow. Flow separation occurs only at the trailing edge (S), which is not undesirable. The flow must leave the airfoil somewhere.



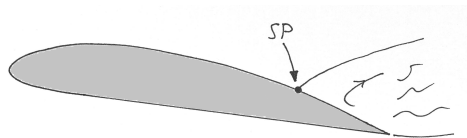
(f) An airfoil without completely attached flow. Undesirable flow separation occurs at the suction side in the vicinity of the trailing edge.



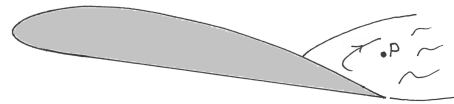
(g) A stagnation point (SP) at the back of a blunt body in potential flow. The pressure coefficient (C_p) at S equals 1.



(h) A blunt body in viscous flow, with a region of separated flow behind the body. The corners of the body are points where separation and stagnation occurs, however the pressure coefficient (C_p) is smaller than 1.



(i) A separation point (SP) on an airfoil's contour.



(j) A point (P) in a region of separated flow, at some distance from the airfoil.

Figure 1.10: Illustrations of several distinctions that can be regarding flow separation. The situations depicted in the left and right columns oppose each other.

1.5. The role of viscosity

There is general consensus about the importance of viscosity in the production of the Kutta condition in a real flow. This can be read in the citations and references given in Section 1.4. Due to its importance, this topic is treated in particular by this section. We will look at how the role of viscosity is appreciated in literature.

The role of viscosity relates the mathematical and physical perspectives on the Kutta condition which are introduced in Section 1.2 to each other. One could say that the “mathematical Kutta condition” determines, in an ideal description of flow about a wing, a flow-field that is qualitatively equal to the real flow-field about a real wing; the latter being due to viscosity, according to the physicist. McLean (2013) holds a similar view:

“Over the many years since Kutta introduced it, there has been much discussion of what the Kutta condition really means, physically speaking. Some critics have seen it as a mathematical artificiality and argued that the need for it demonstrates the physical inadequacy of potential-flow theory. The holders of this harsh view seem to be in a minority, however. The more prevalent view is that when a physical theory leaves out some physical effect, it is reasonable to adopt a rule or adjustment if it can be shown to effectively compensate for what was left out. In the case of potential-flow theory, what was left out is the combination of viscosity and the no-slip condition. It is often observed that viscous flow cannot generally negotiate a sharp corner (...) without separating (...) In this view, the Kutta condition is seen as a perfectly reasonable proxy for one of the major effects of viscosity; that is, that viscous flows tend to separate from sharp edges.”

The following statement by Batchelor (1967, p. 437) is also interesting:

“It is a remarkable fact that in practice a circulation is generated round an aerofoil, owing to the convection of a non-zero amount of vorticity from the rear edge of the aerofoil at an initial stage of the motion, and that when the aerofoil is in steady motion the circulation is established with just this special value. This fortunate circumstance, that the effect of viscosity acting in the boundary layer initially is to cause the establishment of precisely the value of the circulation that enables effects of viscosity to be ignored (since no separation of the boundary layer occurs) in the subsequent steady motion, is usually given the name Joukowski’s hypothesis.”

For the theorists it is indeed ‘fortunate’ that the effect of viscosity allows the use of ‘ideal fluid theory’ for the calculation of flow about an airfoil. Anderson (2011, p. 334) goes further by stating that viscosity is actually necessary:

“However, if we lived in a perfectly inviscid world, an airfoil could not produce lift. Indeed, the presence of friction is the very reason why we have lift. (...) What is going on here? The answer is that in real life, the way that nature insures that the flow will leave smoothly at the trailing edge, that is, the mechanism that nature uses (...) is that the viscous boundary layer remains attached to the surface all the way to the trailing edge. Nature enforces the Kutta condition by means of friction. If there were no boundary layer (i.e., no friction), there would be no physical mechanism in the real world to achieve the Kutta condition.”

This is one of the most bold statements that the present author has read about the working principles of the Kutta condition. In a similar fashion Ackroyd et al. (2001) write:

“(...) it must be emphasized at the outset, that, without viscosity, all flight, even in nature, would be impossible since wings would produce no lift. From this it follows that both marine and aircraft propellers - essentially rotating wings - would be useless (...) Moreover, without viscosity we would all be in severe danger of asphyxiating in our own exhalations. Thus an understanding of the role of viscosity emerges as not only vital to any explanation of flight but also vital, quite literally, to life itself.”

It is strange that viscosity would be a requirement for the production of lift, because usually we regard viscos-

ity as being detrimental for the performance of a flight vehicle: its effects result in the production of drag and reduction of the quality of energy. If Anderson is right, then why is a proper explanation of the cruciality of viscosity lacking in so many writings?

Put abstractly, the reasoning put forward in the last citations is that, when mechanism M has a crucial role in the production of phenomenon F in situation S_A , phenomenon F cannot be expected to occur in a different situation S_B when mechanism M is not present in S_B .⁹ But this argumentation is only valid in the case that mechanism M is the only mechanism that is able to produce F . But in different situations with different qualitative properties there might be different mechanisms producing the same result. It will be quite challenging to prove that viscosity is the only mechanism that can lead to the Kutta condition. At least the present author does not know of any rigorous proof or comprehensive argumentation. Unfortunately, Anderson gives no explanation for his statement that “there would be no physical mechanism in the real world to achieve the Kutta condition”. Indeed, such a substantiation would be very difficult to give, since it is very difficult to prove in general that “something does not exist” for the simple reason that it is very difficult to prove that our knowledge is complete.

Concerning the empirical side of the present discussion, one particular work that stands out due to its methods and relevance is *Observations of perfect potential flow and critical velocities in superfluid helium II* by [Craig \(1959\)](#). This Phd-thesis discusses how a small propeller (having a diameter in the order of centimeters) was put in a can of liquid helium. The helium was cooled down to such a low temperature that its viscosity vanished. The propeller was set in rotating motion and the torque on the propeller axis was measured. From the absence of torque the absence of lift on the propeller blades was inferred, and from the absence of lift the absence of the Kutta condition was inferred. Craig states:

“In fact, in the absence of dissipative forces the circulation cannot change, for no mechanism exists to change the system energy. Should a nondissipative system possess no circulation at a particular instant the circulation must remain zero at any succeeding time, and therefore the system can never show lift.”

The validity of this statement depends on whether it is correctly assumed that dissipative forces are necessary to change the circulation. Craig does not give an elaborate argument for his statement. The conceptual design of Craig’s research is very interesting, however its practical implementation limits its persuasiveness. The thickness-to-chord ratios and the angles of attack of the blades that were used were mostly not representative of (aircraft) propeller blades. Also, McLean remarks about this research: “*I don’t know how definitive this result is. Given the small scale of the experiment, it’s unlikely that the trailing edges were very sharp on the scale of the blade chord*” ([McLean, 2013](#), p. 264). Regarding the absence of lift from which the absence of a Kutta condition was concluded, a lift force was absent only for velocities below some particular value, which might also occur in viscous flows where a ‘neat’ Kutta condition (flow separation at the very edge and no wake forming) is not created at very small Reynolds numbers.

Concluding: It is clear that some (authoritative) authors have the opinion that lift can only be produced in a viscous fluid. However, no proof for this statement is known. Thus it remains interesting to investigate the necessity of viscosity for the production of lift.

⁹A very similar reasoning is given by [Schlichting and Truckenbrodt \(1967, p. 395\)](#) and by [Glauert \(1947, p. 121\)](#) who also state that lift cannot be produced in inviscid fluid.

1.6. Conclusions of the literature study

This section concludes the literature study that was presented in the foregoing sections. The aim was to find the status of knowledge about the Kutta condition (to the extent in which this can be determined from literature). Regarding the whole of the body of knowledge of the Kutta condition in literature it must be said that it is not concentrated. No single work discusses all relevant aspects in detail. There are some works that specifically consider the Kutta condition, but more often the Kutta condition is mentioned as a side-issue. This makes it difficult to obtain a complete overview of the relevant literature.

Two principal perspectives exist from which scholars consider the Kutta condition, one having a mathematical character and the other having a physical or empirical character. Regarding the flow-field that is referred to by the term “Kutta condition” there is some variety in the discussions among authors, although a number of properties seem to be generally accepted, such as that the flow leaves the trailing edge along a smooth path.

It is important to distinguish between transient flow-field and steady state flow-field features. The assumed cause-effect relationship between these implies that the transient part should be studied in order to understand the properties of the steady state part. There are indications that the Kutta condition is a stable phenomenon: that it is the equilibrium state reached by a stable dynamic phenomenon of general nature, regardless of the starting conditions. Explanatory descriptions of it, dating from ≈ 1910 to ≈ 1970 , are all qualitative. A number of numerical studies concerning this phenomenon was found, dating from ≈ 1970 . No empirical research giving detailed evidence that the flow-field descriptions resulting from the theoretical and numerical investigations correspond to what occurs in the case of a real wing in real flow could be found. A study of the working principles of the transient flow-field, which is the creation of the Kutta condition, is necessary in order to understand the important role of viscosity in the production of lift by an airfoil by validating the theoretical descriptions which have been accepted for such a long time. The intriguing question of whether the presence of viscosity is required for the production of the Kutta condition - and thus for the production of lift - remains open.

Researchers who studied or recorded the evolution of the Kutta condition flow-field do not study their results in such a way that an increase in understanding of the working principles of the Kutta condition is produced. On the other hand, researchers who present descriptions of the same flow-field based on theoretical considerations do not relate their findings to empirical results.

It must be mentioned that this report lacks appreciation for the substantial effort made in the period 1970-1985 to understand the flow-field in the vicinity of the trailing edge using the theory of multi-structured boundary layers and asymptotic expansions. Such research is passed by in this report because the present author feels that it contributes little to the kind of understanding that is sought here.

Finally, it must be said that the status of knowledge and understanding (i.e. the lack of it) regarding the Kutta condition is very remarkable because the phenomenon is actually very relevant to the production of lift. The level of understanding and the thoroughness of descriptions that are given are not proportional to the importance of this phenomenon in the functioning of aircraft.

1.7. Research definition

As mentioned in the preface of this report, the original motivation for researching the Kutta condition was to answer the following question: is viscosity required for the production of lift? This question implies a lot of research, more than can be done in the time-frame of a MSc thesis project. So, instead of answering this big question completely, we will try to take a number of steps towards answering it. This section defines a research plan to that end.

The present research in its context

When introducing the Kutta condition, we looked at two perspectives on the Kutta condition: the mathematician's (which regards it as a boundary condition) and the physicist's perspective (which regards it as a certain flow-field). We took the physicist's perspective of the Kutta condition, which corresponds to questions like '*given a lifting airfoil, what are the properties of the trailing-edge flow-field?*' and '*how was that flow-field produced in the first place?*'; see Section 1.2. When studying the Kutta condition in more detail in Section 1.3 we noted that the Kutta condition's property of *stability* is important, and that in a real flow the Kutta condition flow-field is the result of a transient flow. This lead us to the phenomenon of interest for our research:

Research phenomenon: *The evolution of the flow of fluid in the region around the trailing edge of a wing when the wing is set in motion from rest.*

We shall call this “the research phenomenon” or just “the phenomenon” further on. In Section 1.4 we synthesised a number of theoretical descriptions from literature and found that an empirical investigation of the research phenomenon is necessary in order to verify the theoretical descriptions. Furthermore, we studied the role of viscosity in Section 1.5 and noted that it is generally assumed that the presence of viscosity in a flow is crucial for the occurrence of the research phenomenon, however this has not been proven.

Goals, approach, and objective

As said, an empirical investigation of the research phenomenon is necessary in order to verify theoretical descriptions of it, and also to obtain more detailed knowledge. The literature study learned that empirical studies which were done in the past¹⁰ lacked parameterisation; consequentially it is difficult to obtain quantitative or even qualitative correlation with results from theory or numerical experimentation. A parameterisation should be made that complies with the characteristic features of the Kutta condition as given in literature (e.g. position of the stagnation point); such that it enables validation of the theories and descriptions given in literature. Eventually we would like to see verification of the claims regarding working principles (especially regarding the effects of viscosity) but this is a highly complex business and therefore most probably unachievable in the time-frame of a MSc thesis.

Figure 1.11 depicts a ‘goal structure’ which visualises a research path which relates empirical measurement of trailing edge flows to the ultimate goal of determining the cruciality of viscosity. When synthesising the aforementioned considerations, we determine the aim of the present research, namely to achieve tasks 1-4 in Figure 1.11: to measure the development of a trailing edge flow, to describe that parametrically, to use the resulting knowledge to verify existing theories of the Kutta condition, and to offer some interpretations of the measured flow development. This research will not be able to prove that lift can be produced in an inviscid fluid, however it will be of value for understanding how lift is generated in the practical - and usual - case of a viscous fluid. Thus, when including some practical constraints, we arrive at the following research objective:

¹⁰The ones which were found are based on photography.

Objective: *To make a parametric description of the spatial and temporal development of the 2D flow-field in the trailing edge region of an airfoil which is accelerated from rest, by doing time-sequential PIV measurements in an experimental setup, and use this to verify existing theories regarding the creation of the Kutta condition flow-field.*

The choice of using the technique of Particle Image Velocimetry (PIV) is explained in Section 2.5.1. The constraints ‘2D flow-field’ and ‘acceleration from rest’ are explained in Section 2.5.

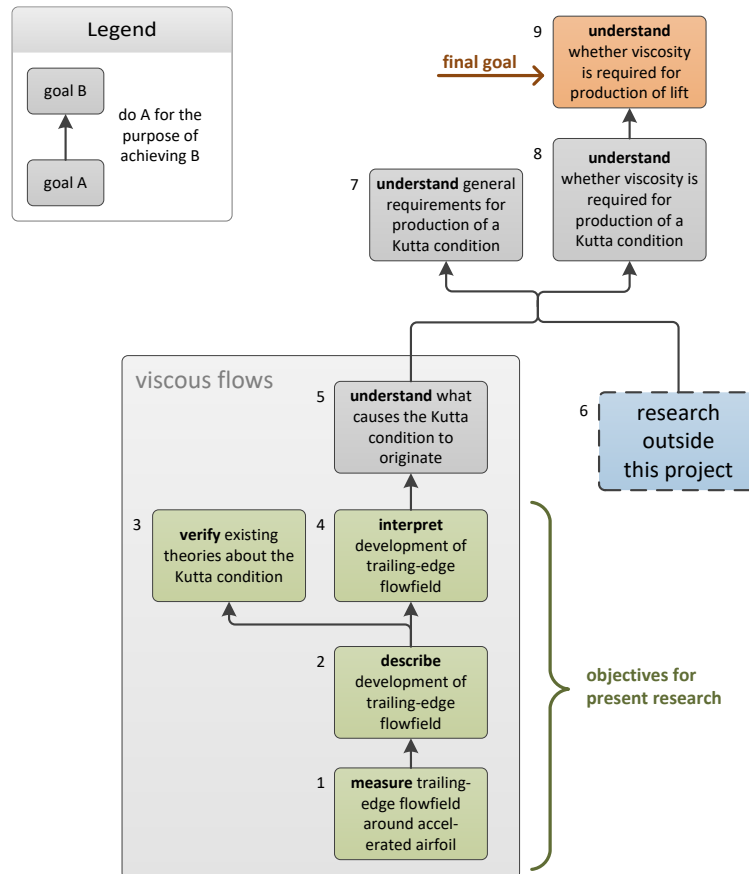


Figure 1.11: Goal structure of the research project defined in this section. The top-most goal corresponds to the original motivation for the author’s MSc thesis. The duration of the present research is too short for reaching this, but it is nevertheless included in the diagram because it informs the way in which ‘lower’ goals are approached. Goals 1,2,3,4 should be reached by the present research. The block ‘other research’ refers to general research in aerodynamics as well as other research specific about the Kutta condition.

Scope

Regarding project organisation, the scope is limited to somewhat more than the nominal timeframe for a MSc thesis, i.e. ≈ 1.5 years. Regarding methods, this project is limited to literature study, experimentation with PIV equipment, and theoretical analyses at the level of introductory aerodynamics textbooks.

Regarding flow and fluid properties, this research is limited to incompressible and adiabatic flow (corresponding to the Euler equations); so the only added complexity w.r.t. potential flow is the consideration of viscosity. This study assumes that the fluid is homogeneous and two-dimensional.

Deliverables

The research should produce the following items:

- A list of properties which characterise the flow-field
- A parameterisation of the phenomenon
- A factual description of the flow field resulting from empirical observation, according to aforementioned parameterisation
- A validation of the classical explanation of boundary layer separation by comparison of theoretical descriptions with aforementioned parametric description.

Research questions

A number of research (sub-) questions will assist in achieving the research objective. The main question for this research is: **How is the Kutta condition flow-field created at the trailing edge of a wing which is accelerated from rest?** This question is divided into sub-questions which are grouped in three moments/periods of time, as visualised in Figure 1.12. They are discussed hereafter. The first question addresses the initial flow-field, the second question addresses the transformation of the flow-field between the start of the wing motion and the end of the transient, and the third question addresses the final steady-state flow-field.

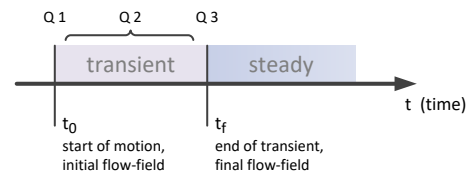


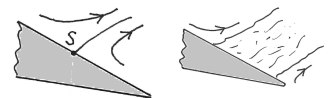
Figure 1.12: A timeline illustrating which research questions address which parts of the development of the experimentally produced flow-field.

Q 1. What is the topology of the flow-field immediately after the wing has been set in motion?

Rationale: This question serves to determine to what extent the flow corresponds to what is predicted by theory (see Section 1.4.2 and Figures 1.7a and 1.7b), and to describe the actual flow-field where there is no correspondence. With ‘immediately after the wing has been set in motion’ we mean that a quasi-steady flow-field has been created but no qualitative transformation such as is characteristic of the transient flow has occurred yet.

Q 1.1. Is there a single point or multiple points or a single zone or multiple zones of flow separation?

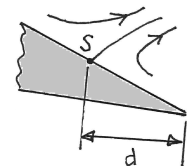
Rationale: The descriptions presented in the Section 1.4.2 consider potential flow for the initial flow-field, in which there is a single stagnation point somewhere on the rear of the body, but in real flow there might be multiple separation points and a separation bubble or a wake.



Q 1.2. What is/are the location(s) of the points/zones where flow separation occurs?

Q 1.3. Is that location coincident with what is predicted by potential flow theory? If not, what is the magnitude of the deviation?

Rationale for Q1.2 and Q1.3: answering these questions will provide a quantitative assessment of how much the observed real flow deviates from the ideal situation described by potential flow theory.

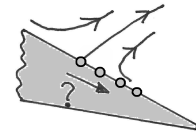


Q 2. How does the topology of the flow-field evolve during the transient flow?

Rationale: This question addresses the transformation of the flow-field between the moment when the wing is set in motion and the moment when the flow has become steady. The theory of Section 1.4.2 predicts that only a shift of the stagnation point occurs, but the work of [Zhu et al. \(2015\)](#) implies that a far more complex transformation occurs. We are interested to know what can actually be observed empirically.

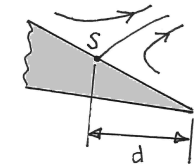
Q 2.1. What is/are the location(s) of the points/zones where flow separation occurs? and how does this evolve with time?

Rationale: This question addresses how the locations where flow separation occurs, which were identified in Q 1.2, evolve with time.



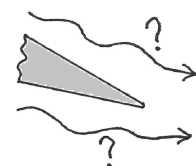
Q 2.2. How does the position of the stagnation/separation point (zone) on the suction side evolve as function of the displacement of the airfoil w.r.t. its initial location?

Rationale: An important part of the theory of Section 1.4.2 is that a stagnation point will be present on the suction side. This point will shift as the wing moves through the flow. If this actually occurs, answering this research question will provide a quantitative description of the flow-field development. A plot of this position might be useful to describe the 'status' of the trailing edge condition versus time.



Q 2.3. What is the evolution of the streamlines which come along the upper and lower surfaces and pass the trailing edge?

Rationale: Since streamlines are a useful visualisation of the flow, series of streamline plots will be helpful to understand the transforming flow-field. This will also show how the streamline picture evolves until the supposed "smooth flow-off" is attained.

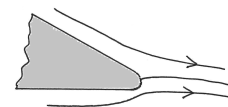


Q 3. What is the topology of the flow-field when the flow has become steady?

Rationale: This question serves to determine whether the final flow-field which is the result of the transient flow has the properties of the Kutta-condition flow-field described in Section 1.3. If this is the case, it is then known that the observed phenomenon is indeed the transient process which precedes the existence of the Kutta condition flow-field.

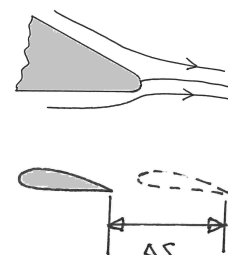
Q 3.1. What is the position of the separation point when the flow has reached equilibrium?

Rationale: This question serves to check hypothesis 3.2. It is especially interesting to check whether the separation point has moved all the way to the very edge, and, if that is not the case, how far its final position is away from the very edge. In the case of a 'not-so-sharp' trailing edge the separation point might be on the edge but its precise location on the edge can be regarded as a measure of the 'quality' of the trailing edge condition (compare (Gostelow, 1975)).



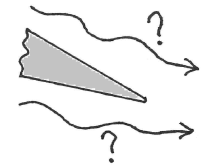
Q 3.2. When is the final position of the separation point reached in terms of the displacement of the airfoil?

Rationale: Perhaps the flow-field that is typical for the Kutta condition is reached qualitatively although the flow has not yet settled completely on to a steady state. Wagner (1925) predicted that the magnitude of the lift force has reached 90% of its steady-state value when the airfoil has travelled more than six times its chord length: $\Delta s > 6c$ where s is the airfoil displacement and c is the airfoil's chord length.



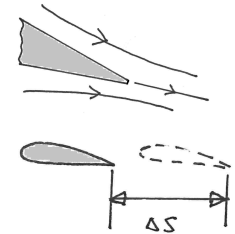
Q 3.3. What is the direction of the streamlines directly above and below the trailing edge?

Rationale: answering this question allows to verify the claims that fluid flows around the trailing edge and leaves the trailing edge smoothly. See also hypotheses 1.2 and 3.1.



Q 3.4. What travel distance/time is needed to obtain trailing edge confluence where the dividing streamline is in the direction of the trailing edge?

Rationale: This question is very similar to Q3.2. However, when the separation point has reached the trailing edge, this does not mean that the dividing streamline is in the direction of the trailing edge. Apart from this, the motivation for this question is the same as for Q3.2.



Hypotheses

The hypothesis for this research is based on the description of the Kutta condition and the flow-field evolution that leads to it as given in literature, presented in Section 1.4.2. In summary, the main hypothesis is: **When a wing is accelerated from rest, there will initially be a potential-flow-like flow-field with fluid moving from the pressure side along the trailing edge to the suction side, and a stagnation point on the suction side. As time progresses, this point will shift towards the trailing edge as result of friction stresses. Finally, fluid will leave the wing smoothly at the trailing edge.**

This hypothesis is divided in sub-hypotheses which are grouped in three moments/periods of time, as visualised in Figure 1.13. The first group of hypotheses addresses the initial flow-field, the second group of hypotheses addresses the transformation of the flow-field between the start of the wing motion and the end of the transient, and the third group of hypotheses addresses the final steady-state flow-field.

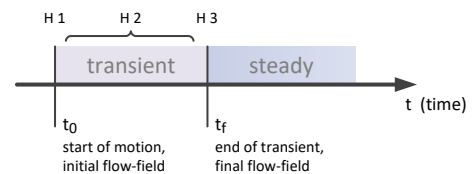
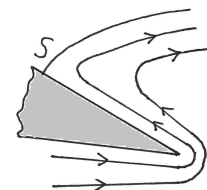


Figure 1.13: A timeline illustrating which hypotheses address which parts of the development of the experimentally produced flow-field.

H 1. Immediately after the wing has been set in motion the flow-field corresponds to potential flow.

Rationale: This hypothesis is paradigmatic, it originates from the descriptions of the evolution of the trailing edge flow discussed in Section 1.4.2.

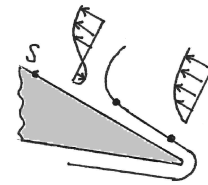


H 1.1. There will be a stagnation point on the suction side close to the trailing edge.

H 1.2. Fluid moves from the pressure side around the trailing edge to the suction side.

H 2. Flow separation at the suction side can be attributed to stagnation of the boundary layer.

Rationale: This hypothesis is paradigmatic, it originates from the descriptions of the evolution of the trailing edge flow discussed in Section 1.4.2.



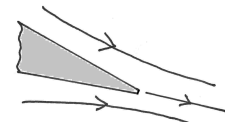
H 2.1. Flow stagnation in the boundary layer occurs.

H 2.2. Flow separates from the wing after flow in the boundary layer has stagnated.

H 3. Hypotheses regarding the steady-state flow-field.

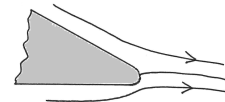
H 3.1. When steady flow is reached, the flow leaves the trailing edge in the direction where the trailing edge points. The dividing streamline as well as the neighbouring streamlines from the upper- and lower surfaces have no sudden changes in speed or direction.

Rationale: This hypothesis is paradigmatic, it originates from the descriptions of the steady-state trailing edge flow discussed in Section 1.3.



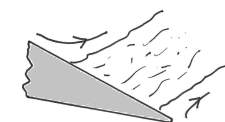
H 3.2. The separation point location is not on the most rearward point of the trailing edge but slightly upstream, on the suction side.

Rationale: See the hypothesis on p. 12. Presumably this effect can only be observed when looking at a small region around the trailing edge (smaller then required for observing the effects mentioned in the foregoing hypotheses) having a field of view in the order of 1% of the chord length.



H 3.3. A “dead-water region” or wake exists at the suction side close to the trailing edge just after the fluid has been set in motion.

Rationale: This flow pattern was observed by the present author in simple experiments at very low Reynolds numbers. Von Kármán and Burgers (1935) write about “the condition that, in the final flow, the rear stagnation point shall coincide with the trailing edge of the profile”: “Actually the condition is not quite rigorous; experimental investigations have shown that there remains at the upper side of the airfoil a region of irregular vortex motion which has a certain influence on the magnitude of the circulation, reducing its value somewhat as compared with that deduced from the supposition just mentioned. The extent of this region depends on various details of the form of the profile; for any given profile it extends gradually upstream farther and farther as the angle of incidence is increased; and when this angle exceeds a certain value, causes a breakdown of the whole type of motion as outlined.”



2

Methods

This chapter presents the methods that are used to reach the research objective which is defined in Section 1.7. Each section of this chapter describes a particular method or tool. Section 2.1 presents a strategy for verifying the theory discussed in Section 1.4.2 by measurements done for a specific case. Sections 2.2 and 2.3 describe parameterisation and dimensional analysis respectively, which support effective experimentation. Section 2.4 presents a theoretical/numerical method for analysis of the initial flow-field. Sections 2.5 and 2.6 present the main tools for this research: an experimental setup which uses Particle Image Velocimetry for flow-field measurement and a number of analysis methods for processing the PIV-data and extracting flow-field properties. This last section also presents a novel method for detection of separated flow.

The relations between the methods (and the sections of this chapter) are illustrated in Figure 2.1.

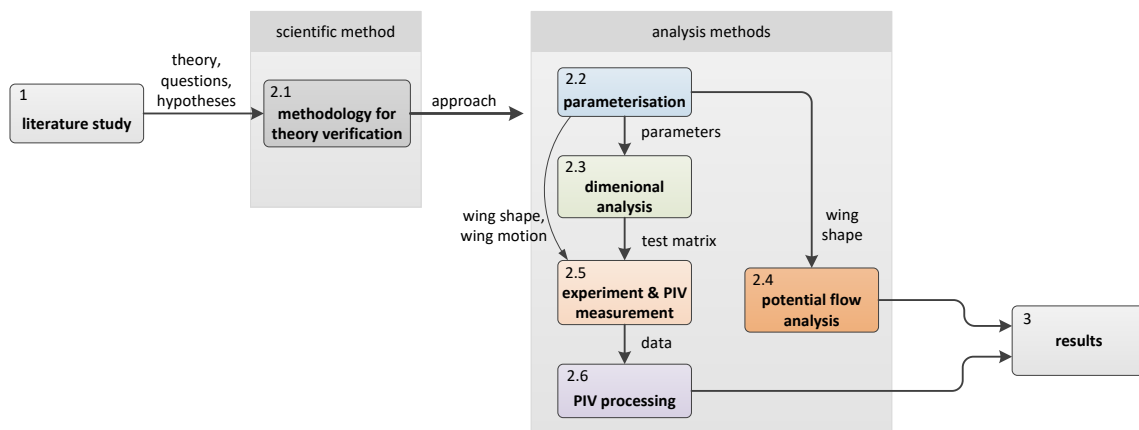


Figure 2.1: Roadmap for this chapter, showing how the methods applied in this research are synthesised. The numbers in the boxes indicate chapters/sections in this report.

2.1. Methodology for theory verification

The present research addresses a theory of quite general character by investigating the applicability of this theory to a specific case of a real wing in a real flow.¹ Only a small number of specific cases can be measured, so we would like to maximise the efficiency of our empirical work. How can we select the specific cases which we are going to study empirically such that the conclusions are valid for a large range of possible cases? This section presents a strategy to achieve that.

Let us denote the theory by T . Let us denote the events predicted by T by E and the relations described by T by R . Let us denote the set of cases for which the validity of T is claimed by C . Let us assume that we can determine a set of parameters P which identifies C . So P are a set of properties (which can also be called parameters or qualities) which is applicable to every single case c in C . It is necessary for c to have P in order to be in C . As long as any two cases c_A and c_B both have P , T is equally valid to both cases. Properties P are of qualitative character; they might be regarded as parameters and there might be differences in numerical parameter values between c_A and c_B .

So in order to determine a specific case c_S in order to validate T we should first determine what properties P are required, then select a case which has P with convenient parameter values. If E and R are observed in c_S , which has P , then T is valid for c_S and equally valid for all C which have P . So we regard T validated when E and R are observed in c_S . An example of this approach is given in the next sub-section.

Table 2.1: Nomenclature for this section.

T	theory	C	set of cases for which validity of T is claimed
E	events predicted by T	P	set of properties/qualities/parameters which identify C
R	relations described by T	c_S	specific case having P used for validating T

Example for illustration of methodology for theory verification

Suppose that it is unknown how houses are built. Somebody produces a theory (T) which is claimed to explain how houses are built. The theory goes like this:

“A citizen calls a housebuilder and asks to build him a house. The housebuilder then comes and takes a number of bricks with him. He will join the bricks together using a sticky substance, putting them on top of each other. In that way the walls of the house will be made from the ground up. When the walls are completed, windows will be put in and a roof will be put on. The final result of this process is a box-like building of bricks, windows, and a roof.”

The events (E) predicted by this theory are, for example:

- **E 1.** A citizen calls a housebuilder
- **E 2.** The housebuilder comes to the building site and brings some stuff with him
- **E 3.** Bricks are joined together
- etc.

The relations (R) predicted by the theory, are, for example:

- **R 1.** The arrival of the housebuilder is a result of the calling by the citizen
- **R 2.** The size of the final house depends on the number of bricks and their size, with a quantifiable relationship
- etc.

Now, the set of cases (C) for which the validity of T is claimed was not mentioned clearly by the creator of the theory, but we can determine it by looking at the properties of the general case described by the theory. We

¹Here ‘real’ is opposed to ‘modelled’ or ‘simulated’.

state that C consist of every case to which the properties P1, P2,... Pn apply. We assume that T explains every specific case in C equally well (because every case in C has all the properties P). Then it does not matter what specific case we pick for testing the theory on it. In order for this approach to work it is important that we do our best to be complete by identifying all properties. The properties (P) of the situation are, for example:

- **P 1.** Presence of a citizen
- **P 2.** Presence of a housebuilder
- **P 3.** Presence of bricks, which have certain size
- **P 4.** Presence of sticky stuff, which has a certain stickyness
- etc.

Now in order to verify the theory we seek a case of somebody who wants a house to be built and we make sure that all required properties are present. We watch and record the process, and we note whether the predicted events take place and whether the predicted relations are observed. So if all required properties are checked (i.e. there is a house builder, bricks are present, the final product has walls, windows, and a roof, etc.) and if the predicted events are observed (i.e. we see a housebuilder coming to the site, bricks are laid, etc.) and the predicted relations are observed (e.g. first the citizen calls the housebuilder, then the housebuilder comes to the site), we say that the theory is verified. We conclude that the theory is not only verified for this specific case, but we accept that the theory explains every specific case in C, because all cases in C are qualitatively equal. The number of bricks and other quantities that are specific to each case does not matter; it is the presence of qualitative properties that matters.

The theory to be verified in this research

The theory targeted in the present research is the synthesis of descriptions of the transient flow which results in the Kutta condition. This is presented in Section 1.4.2. The properties of the general case described by the theory, the range of validity of the theory, as well as the events and relations predicted by the theory will be listed in the following subsections.

The properties of cases described by the theory

We will deduce the properties (P) of the general case described by the theory by listing the properties of the phenomenon described in Section 1.4.2:

- **P 1.** A **wing** is present.
- **P 1.1.** The wing or airfoil has a **sharp trailing edge**. Note that all sketches corresponding to the theories depict cusped trailing edges which end in a point, but it is in principle not possible to produce in a real experiment. Therefore we describe this property by stating that the sharpness parameter R/c may not exceed a certain value. The order of magnitude should be $O(0.001)$ at most.²
- **P 2.** **Fluid** is present.
- **P 2.1.** The fluid is **viscous**: (dynamic viscosity $\mu > 0$).
- **P 2.2.** The fluid is **inertial** (density $\rho > 0$).
- **P 2.3.** The fluid is **initially at rest** w.r.t. the wing.
- **P 3.** The wing section is **completely immersed** in the fluid (no two-phase flow).
- **P 4** The wing is **accelerated from rest** (w.r.t. the inertial reference frame).

²Note that a value of $O(1)$ corresponds to a circle. One order of magnitude smaller (≈ 0.1) corresponds to an airfoil with blunt rear. Another order of magnitude smaller (≈ 0.01) corresponds to an airfoil with a thin but visibly rounded rear. Again an order of magnitude smaller (≈ 0.001) corresponds to a sharp rear that is almost indistinguishable from a pointed trailing edge when the airfoil is viewed as a whole.

- **P 5.** The wing has a positive **angle of attack** such that the wing would produce lift in potential flow when the Kutta condition applies.
- **P 6.** The final **Reynolds number**, Re , (corresponding to the steady-state which is reached after the transient) has a certain minimum value. Note that Re increases from zero to some final value Re_f because velocity starts from zero and increases to some final value. The Reynolds number of a real aircraft in flight is of $O(10^6)$ at least. The Reynolds number in the experiment should be such that flow separation such as is typical for high- Re flows can occur. This implies a Reynolds number as least as large as $O(10^3)$. At small Reynolds numbers flow separation might not even occur, see for example (Anderson, 2011, Sec. 3.18).

The events predicted by the theory

When reading Section 1.4.2 we extract the following predicted events (note all descriptions except for that of E 1 refer to the region in the vicinity of the trailing edge):

- **E 1.** Fluid moves once the wing is accelerated from rest.
- **E 2.** A potential-flow-like flow-field exists in the first phase of the process.
- **E 2.1.** A stagnation point exists on the suction side of the wing, close to the trailing edge.
- **E 2.2.** Fluid moves from the pressure side of the wing to the suction side, over the trailing edge.
- **E 2.3.** Circulation and lift force are zero.
- **E 3.** Pressure stresses occur in the flow, with decreasing static pressure towards the trailing edge on both sides of the airfoil.
- **E 4.** On the pressure side of the wing fluid accelerates towards the trailing edge, on the suction side it decelerates when moving away from the trailing edge.
- **E 5.** Friction stresses occur in the flow, mainly at points close to the wing surface.
- **E 6.** Fluid closer to the wing surface is decelerated w.r.t. fluid further away from the wing surface.
- **E 7.** A velocity profile like sketched in Figure 1.7d will exist.
- **E 8.** The position of the stagnation point on the suction side of the wing shifts towards the trailing edge as time progresses.
- **E 9.** Lift and drag forces acting on the wing vary with time.
- **E 10.** Eventually a steady flow-field is attained.
- **E 10.1.** The final location of the stagnation point is at the trailing edge, and it remains there.
- **E 10.2.** Eventually there is smooth flow-off of flow coming from the pressure side and the suction side, passing the trailing edge without sudden changes in direction.

The relations predicted by the theory

When reading Section 1.4.2 we extract the following predicted relations. Note that most of these properties can be mapped to the hypotheses presented on p. 26.

- **R 1.** The presence of the initial flow-field (see E 2) is caused by the acceleration of the wing from rest (P 1.2). This is a causal relation.

- **R 2.** The magnitude of pressure gradients (see E 3) are related to the magnitude of accelerations (see E 4) in the flow.
- **R 3.** The presence of friction stresses (E 5) causes events 6 to 10.

The range of validity of the theory

In Section 1.4.2 the range of validity of the theory was not clearly mentioned, but we will determine it from the properties of the general case described by the theory. These properties are identified in the last subsection. The range of validity of the theory equals the set of all specific cases which have all the properties listed in the last subsection.

Considerations for selection of specific research case

Quality vs quantity. Notice that the description of Section 1.4.2 has a qualitative and conceptual character. It concerns working principles, and quantities with their mutual relations. Numerical values are not mentioned so they do not have to be validated. This means that in our selection of a specific research case numerical values are important only where they are helpful for depicting the flow-field as clearly with minimal secondary effects.

Knowledge from velocity measurement. As shown on Figure 1.7 on p. 11, streamlines, stagnation points, and boundary layer velocity profiles play an important role in describing the flow-field. Notice that these properties can all be obtained from a measured velocity field. (In Figure 1.7 normal stresses and shear stresses are depicted. However, these cannot be measured. So we shall have to be satisfied with the other parameters, in which we will be able to see the effects of such stresses). Two ways to minimise the uncertainty of our empirical work immediately come to mind: first, it is better to make the velocities in the flow-field large w.r.t. the uncertainty of our velocity measurement, and secondly, by making sure that secondary flows (non-uniformities, turbulence) are relatively small.

Mechanisms which affect trailing-edge flow. We would like to observe the flow around the trailing edge of a wing as ‘purely’ as possible. This may be endangered by the practical fact that the trailing edge is - from the perspective of a fluid particle - the last part of a wing. In steady motion the flow which passes the trailing edge has washed the upper or lower surface of the wing. This makes it difficult to have undisturbed flow over the trailing edge. This difficulty is however lessened somewhat by the fact that we are concerned with starting flow instead of steady flow. Let us list some mechanisms through which the flow over the upstream part of the wing influences the flow in the trailing edge region:

1. **Vorticity transport by convection.** Vorticity implies the rotational motion of some amount of fluid. As this mass of fluid moves along the contour, the momentum, energy, and other properties that correspond to its rotational motion are transported with it. For example: vorticity created in the boundary layer upstream of the trailing edge region will move through the trailing edge region at some moment, provided that boundary layer stays attached to the wall. This vorticity, combined with the creation of new vorticity, might have important effects. This is discussed in more detail in [Zhu et al. \(2015\)](#).
2. **Vorticity transport by diffusion.** If the fluid is viscous and velocity gradients exist normal to the surface, any existing velocity will ‘smear out’ in the direction normal to local streamlines. It is expected that this mechanism does not have primary influence in the phenomenon studied here because its effect becomes profound only after relatively long time and relatively large displacements.
3. **Turbulence transport.** Turbulence means chaotic motion of fluid. It involves distributions of momentum and energy with a large range of length scales; however these scales are all orders of magnitude smaller than the airfoil.³

³Note that turbulence is related to vorticity, but then on a relatively small scale. So although it might be regarded as an instance of the mechanism of the transport of vorticity by convection mentioned above, it is mentioned apart here due to the difference in length scale.

4. **Pressure waves.** A (sudden) change in the flow topology will create pressure waves that move through the domain with the velocity of sound. However, this mechanism is relatively fast compared to the mechanisms mentioned above. Since we are concerned with motions that are orders of magnitude slower than the speed of sound, pressure equalises so quickly that we can regard the pressure field as being quasi-steady.

A phenomenon like flow separation at a point upstream of the trailing edge region influences the flow which is downstream of the separation point by the mechanisms just mentioned. Any vorticity and turbulence created in the separation process will be moved by convection to the trailing edge region, which will probably change the performance of the boundary layer there. If there is an ongoing process of separation and re-attachment this will be communicated through the whole domain by fast-moving unsteady pressure waves and also by convection. We see that in order to have an ‘as clean as possible’ flow-field in the trailing edge region we should be careful to select an airfoil shape and angle of attack that results in attached flow over the whole contour.

Effect of airfoil shape on TE flow-field. We are questioning whether, and how, the overall airfoil shape influences the properties of the fluid flow around the trailing edge. If the influence of the shape of the overall airfoil except the trailing edge part on the flow in the trailing edge region is only quantitative and not qualitative, for which support will be presented later in this report, we will be able to use an airfoil as simple as a flat plate with rounded leading and trailing edges to bring forth a trailing edge flow which is of such general kind that it is representative for the trailing edge flow of an airfoil in general (or perhaps even wider: for every geometry that has a sharp edge).

Practical constraints. Since this is an empirical work there are practicalities involved which constrain the selection of a specific research case. These are related to the choice of measurement equipment. This is discussed in detail in Section 2.5, which also states and discusses the final selection of the specific research case.

Selection of specific research case

In summary, the specific research case, as discussed more extensively in Section 2.5, is as follows. The fluid is water, which is incompressible, viscous, and inertial. The airfoil shape is a flat plate with rounded leading and trailing edges (see also Section 2.2). The wing model has a chord length of 200 mm and a thickness of 2 mm. The domain is square; the side length is 0.9 m. The fluid domain is oriented horizontally, with a height of ≈ 0.15 m. The wing is located in the middle of the domain at the start of the motion, with its tip-root axis being vertical. The distance between the wing tip and the domain bottom is ≈ 0.5 mm. The wing is accelerated from rest with a constant acceleration of magnitude $O(1 \text{ m/s}^2)$. A chord-based Reynolds number of $\approx 55k$ is reached after ≈ 0.1 s after start of the motion; the corresponding displacement is ≈ 10 mm. The angle of incidence is $\approx 20^\circ$. These properties comply to the set of properties listed on page 31.

We conclude that if we test the abovementioned case, record what happens, and observe the events and relations that are listed on page 32, then we have verified the theory in general.

2.2. Parameterisation

As remarked in the research definition (Section 1.7), the research phenomenon should be parameterised; otherwise it would be very difficult to compare results with those of other investigations. The parameterisation should preferably be simple, so it should have a minimum number of parameters. It should enable manufacturing of models and enable experimentation with minimal use of high-tech equipment. It should also be suitable for mathematical analysis, so it should have simple mathematical descriptions.

This section presents such a parameterisation. The problem is divided in four parts: the fluid, the airfoil shape, the motion of the wing through the fluid, and the flow-field; corresponding to the first four subsections of this section. The fifth subsection discusses the reference frames and coordinate systems that are used from now on in the report. A handy tabular overview and categorisation of all parameters used in this section is presented at the end of this section.

Parameterisation of the fluid

The fluid is homogeneous, isotropic, incompressible, viscous (Newtonian), and inertial. The viscosity is parameterised by the *dynamic viscosity* μ which is constant; its value is $1.15 \cdot 10^{-3}$ Pa·s. The inertia is represented by the *density* ρ which is constant; its value is 999 kg/m³. These values correspond to a temperature of 15 °C. Values are taken from (Kuethe and Chow, 1998, p. 532). The fluid is initially at rest w.r.t. the inertial frame, everywhere in the domain.

Parameterisation of the airfoil

Since we want to study the research phenomenon empirically, the trailing edge of the airfoil needs to have a certain thickness, whose minimum required value depends on the measurement equipment that is used. The trailing edge also should have a smooth contour. We would like to keep the design simple, which will have advantages for manufacturing of the airfoil models, for parameterisation, and also for mathematical/theoretical analysis. For these reasons a *rounded flat plate* is selected.

The airfoil is formed by rounding the front and rear edges of a flat rectangle such that these edges are semi-circles. The contour of the airfoil thus consists of two straight lines which tangentially join the semi-circles, as depicted in Figure 2.2. The airfoil is parameterised by the *thickness* t , which is equal to the half the *radius of curvature* of the edges R , and the *chord length* c .

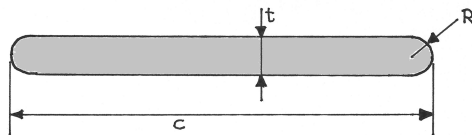


Figure 2.2: Parameterisation of the geometry of the airfoil used in the theoretical part (which is discussed in Section 2.4) and in the experimental part (which is discussed in Section 2.5) of this research.

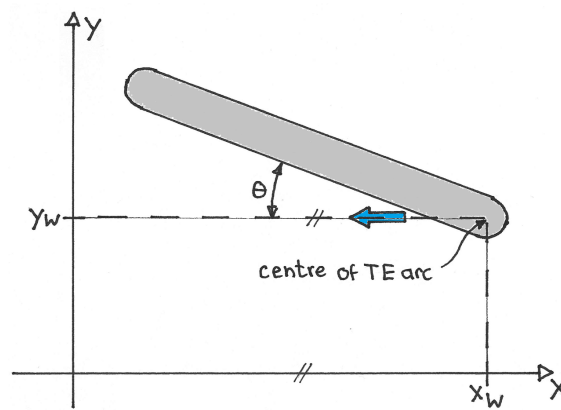


Figure 2.3: Parameterisation of the position and orientation of the wing w.r.t. the inertial reference system in the experimental part of this research. The X-axis is horizontal. The blue arrow indicates the direction of motion of the wing, which is horizontal. See also the discussion on p. 37.

Parameterisation of the wing motion

The airfoil is oriented at a constant *angle of incidence* θ w.r.t. the horizon (which is the X-axis of a Cartesian coordinate system, see Figure 2.3 and sub-section *Reference frames and coordinate systems*). The wing is initially at rest w.r.t. the inertial frame. At time t_0 the wing is put in motion with a constant *acceleration* a in horizontal direction. The wing thus moves in straight, horizontal line.⁴ The motion is parameterised by the *displacement* s and the *velocity* V . The parameters s, V, a are related to each-other via (2.1) and (2.2).

$$V = \int a dt = at \quad (2.1)$$

$$s = \int V dt = 1/2 at^2 \quad (2.2)$$

Parameterisation of the flow-field

The flow-field is described by a variation of parameters which are all related to the velocity field.⁵ The velocity field is a distribution of velocity vectors.⁶ **Streamlines** are everywhere tangential to the local flow direction and thus serve to show the direction of flow. Since the flow is unsteady, the streamlines depict the instantaneous velocity field. The **location of a stagnation/separation point** is representative for the location of (a region of) flow separation.⁷

Stagnation point location as status indicator. The position of the stagnation point (assuming that there is a single stagnation point) can be expressed by a single parameter, denoted s_s which describes the tangential location of the stagnation point on the contour of the wing in correspondence to the coordinate system shown in Figure 2.5. This parameter is assumed to be representative for the ‘status’ or ‘quality’ of the Kutta condition.⁸ The argument for this is as follows. It is generally assumed that in a potential flow the lift coefficient of a lifting airfoil (which is related to the circulation around the airfoil) corresponds to the flow-field around the trailing edge. This is discussed in Section 1.2. See also the sketches in (Schlichting and Truckenbrodt, 1967, p. 393). Let us assume that a unique map between the stagnation point position and the flow-field picture exists; which is implied by such illustrations. Then the single parameter s_s is representative for the whole flow-field. It is expected that in viscous flow no such unique map exists due to the possible presence of patterns like a recirculation bubble. However, before we have detailed knowledge about the flow topology, we assume that we can use the stagnation point location as an efficient means to represent the trailing-edge flow-field; and thus to represent the status of the evolution of the flow-field towards the Kutta condition. Note that in viscous flow all points on the body are actually stagnation points. But we mean here a point which is both a stagnation point and a separation point. In viscous flows there is still only one point (or perhaps a few more in case of circulation bubbles) to which the dividing streamline attaches.

⁴In the experiment performed for this research, the wing did not actually move in a straight line. This is discussed in Section 3.2.2 on p. 74. However, in this section the desired ‘ideal’ straight-line motion is presented, because it served as the basis for the dimensional analysis which is presented in Section 2.3.

⁵In the experiment (see Sections 2.5 and 2.6) the parameters which are used to visualise and understand the flow-field are all obtained from the measured velocity field.

⁶The result of PIV-measurements is a set of velocity vectors located at a discrete and uniform distribution of positions in a Cartesian coordinate system.

⁷The definition of a separation point is discussed in more detail in Section 2.6, *Detection of flow separation*, p. 65.

⁸With ‘Kutta condition’ I mean here a certain flow-field with properties as described in Section <Introduction>. The real flow-field in the vicinity of a starting wing can match this flow-field more or less.

Reference frames and coordinate systems

Two reference frames are used:

1. the **inertial reference frame**, which is fixed to the earth; and
2. the **wing reference frame**, which is fixed to the wing.

Three coordinate systems are used:

1. a **Cartesian (x,y) system** corresponding to the **inertial reference system** with the origin at an arbitrary location, depicted in Figure 2.3. This reference frame is used to measure the displacement of the wing during its motion. Since the absolute location of the wing is not important, it does not matter where the origin of the axis system is located.
2. a **Cartesian (x,y) system** corresponding to the **wing reference frame**, whose origin is at the centre of the trailing-edge arc, and whose orientation is equal to the former coordinate system, depicted in Figure 2.4.
3. the **wing (s,r) system**. This coordinate system is like a polar coordinate system, corresponding to the **wing reference frame**, depicted in Figure 2.5. This system has two coordinates, one being tangential to the wing contour and the other in the perpendicular direction. The distance *along* the contour is denoted by s and is measured from the point where the chord line intersects the trailing edge arc, and is measured positively towards the suction side. The distance *from* the contour is denoted by r . A grid of lines of constant s and r values has a horse-shoe shape. NOTE: in the remainder of this report all positions are normalised w.r.t. R ; see (2.3) and (2.4), and the tildes (\sim) will be omitted for the sake of clarity. So a point at $(s = 1, r = 1)$ will be at a distance of one wing-radius from the contour, at an angle of 1 radian from the wing chord, according to Figure 2.5.

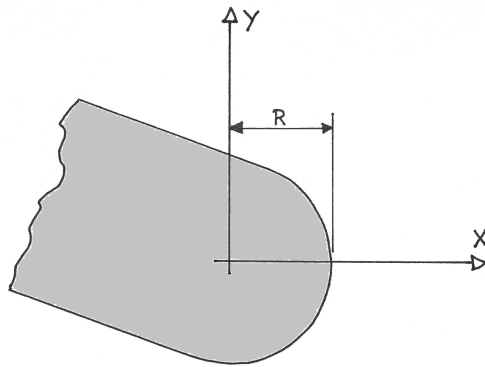


Figure 2.4: The wing-centered (x, y) coordinate system used for flow-field measurements in this research. The origin is located at the centre of the circular arc. The X and Y axis are parallel to those of the coordinate system presented in Figure 2.3.

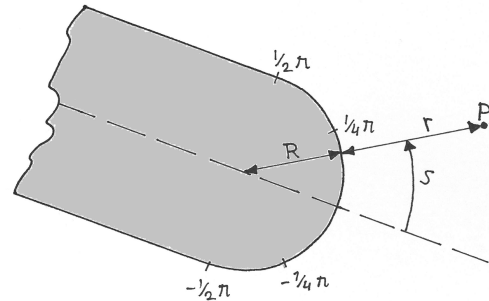


Figure 2.5: The wing-centered (s, r) coordinate system used for visualising flow-field features in this research. The parameter r indicates the distance from the wing to point P; it is measured perpendicular to the wing contour. The parameter s indicates the tangential location of the projection of P on the wing. Although the arrow is drawn a certain distance from the contour, s is measured *on* the contour, beginning from the chord line, positive in counter-clockwise direction.

$$\tilde{x} = x/R \quad \tilde{y} = y/R \quad (2.3)$$

$$\tilde{s} = s/R \quad \tilde{r} = r/R \quad (2.4)$$

Table 2.2: Categorisation of aspects mentioned in this sub-section. Within each cell of the table the parameters are grouped according to the number of dimensions they have. Since there are two spatial dimensions and one time dimension in this study the highest dimension that a parameter can have is three. 0-D means zero-dimensional, which is a constant value that is invariant with both space and time.

	Independent	Dependent
Airfoil	0-D parameters <ul style="list-style-type: none"> thickness t radius R chord length c 	
Wing motion	0-D parameters <ul style="list-style-type: none"> angle of incidence θ acceleration a time t 	1-D parameters <ul style="list-style-type: none"> displacement s velocity V Reynolds number Re
Fluid	0-D parameters <ul style="list-style-type: none"> viscosity μ density ρ 	
Flow field		1-D parameters <ul style="list-style-type: none"> location of separation point(s) s_s location of centre of starting vortex 2-D parameters <ul style="list-style-type: none"> surface velocity distribution 3-D parameters <ul style="list-style-type: none"> velocity field streamlines

2.3. Dimensional analysis

A dimensional analysis is performed to obtain a set of similarity parameters for the research phenomenon. This serves two purposes: to obtain conceptual-level insight regarding important quantities and relationships; and to provide a basis for choosing specific cases for empirical study, which enables efficient experimentation.

This section makes use of the parameterisation presented in Section 2.2. The *Buckingham Pi theorem* as explained by Anderson (2011, p. 36) is used to obtain a set of similarity parameters. Also, definitions for making time, velocity, displacement and Reynolds number non-dimensional will be presented. The similarity parameters which involve time will be re-written such they are explicitly dependent on non-dimensional time.

Assumptions

1. The flow over the wing is two-dimensional
2. The wing section is the *rounded flat plate* airfoil as presented in Figure 2.2.
3. The fluid behaves as a Newtonian fluid.
4. The airfoil makes a linear motion with constant acceleration.

Dimensions

It is assumed that the phenomenon can be described by the relations known in the field of fluid mechanics, excluding thermodynamic effects. This means that the ‘physical dimensions’ of the problem are those of the field of classical mechanics, namely: *mass* (m), *length* (l), and *time* (t).

Selection of parameters

The selection of parameters is based on – and biased by – common aerodynamic knowledge. The parameters ρ, μ, V are commonly used in dimensional analysis of aerodynamic phenomena, therefore they feature here as well. Seven parameters are selected in total. The selection is presented as follows. A summary is given in Table 2.3.

$P_1 \quad \rho$ **fluid density.** The density describes the inertia of the fluid (mass per unit volume). According to Newton's second law ($F = m \cdot a$) it is a proportionality between net force applied to and acceleration of a fluid particle. It is also a proportionality between the linear momentum and velocity of a fluid particle. The density is assumed to be constant and equal everywhere in the flow.

$P_2 \quad \mu$ **coefficient of dynamic viscosity.** The viscosity of the fluid relates shear stresses to velocity gradients. Assuming that the fluid is a Newtonian fluid, the viscosity coefficient relates shear stress to normal velocity gradient: $\sigma = \mu \cdot dV/dy$ where y is the distance from the wing surface.

$P_3 \quad R$ **radius of curvature of trailing edge.** Stream velocity is related to the local curvature of a body (Obert, 2009, p. 47) and the trailing edge is strongly curved; thus its contour has arguably a large effect on the flow-field, so the curvature of the trailing edge is included in the list of parameters. Since it is assumed that the airfoil is a rounded flat plate, this single parameter describes the whole trailing edge region.

$P_4 \quad V$ **velocity of airfoil w.r.t. free stream.** From potential flow theory it is known that velocity distributions around a body are linearly proportional to the free-stream velocity. Therefore this parameter is related to the magnitude of flow velocities in the domain in general, and therefore also to the magnitude of accelerations and stresses.

$P_5 \quad a$ **acceleration of airfoil w.r.t. free stream.** Since we are dealing with a transient phenomenon, it is expected that the timescale of the airfoil's motion has an effect on the evolution of the flow-field. The acceler-

ation, together with the velocity, represents this time, since acceleration is the time derivative of the velocity. It is assumed that the acceleration is constant, so the time is the ratio between velocity and acceleration: $V = at$.

P_6 c **chord length of airfoil**. From potential flow theory it is known that the spatial extent of the influence of a body on the fluid in the domain is related to the size of the body. Therefore this parameter represents the size of the region of flow influenced by the airfoil.

P_7 s_s **position of stagnation point**. This parameter indicates the tangential location of the stagnation point that is expected to exist on the suction side close to the trailing edge. This parameter is understood as being representative for the ‘status’ or ‘quality’ of the trailing edge flow condition (see Section 2.2, p. 36). This parameter is the ‘wanted’ parameter: it is not known beforehand and is assumed to depend on the other parameters.

Table 2.3: Summary of parameters, dimensions, and variables for use with the Buckingham Pi theorem. The variables for the set of repeating variables are indicated in bold face.

parameter indicator	P_1	P_2	P_3	P_4	P_5	P_6	P_7
parameter symbol	ρ	μ	R	V	a	c	s_s
units	$\frac{kg}{m^3}$	$Pa \cdot s$	m	$\frac{m}{s}$	$\frac{m}{s^2}$	m	m
dimensions	$\frac{m}{l^3}$	$\frac{m}{lt}$	l	$\frac{l}{t}$	$\frac{l}{t^2}$	l	l

Dependencies between parameters

The independent parameters of the problem are: ρ, μ, c, R, a . These are all constants. The dependent parameters are V and s_s (see also Table 2.2 on p. 38). The dependent and variable parameter V is related to the independent and constant parameter a by the relation $V = at$. This relation involves the parameter t (time) which is independent and variable. This parameter is not included in the set of parameters mentioned above to keep the dimensional analysis simple and to keep the parameter set similar to what is usual for steady-state flows. However, for the purpose of explicitly representing time-dependence in the dimensionless numbers, any dimensionless parameter group containing V or a can be rewritten as function of t using the relation $V = at$. This will be applied later in this Section.

Results of the Buckingham Pi theorem

The Buckingham Pi theorem as explained in (Anderson, 2011, p. 36) is used to obtain a set of non-dimensional parameter groups. The procedure requires that a set of “repeating variables” is selected in which all fundamental dimensions (m, l, t) are represented. The combination (ρ, V, c) is chosen. However, the choice of this set is somewhat arbitrary – multiple parameter combinations are actually possible.

Performing the procedure described by Anderson leads to four non-dimensional groups - which are also called Π -products, or similarity parameters - which are presented with explanation in Table 2.4. Equation (2.6) relates the Π -products to each-other. This means that, given two different cases in which the phenomenon occurs, called A and B , when the Pi-products Π_1, Π_2, Π_3 have equal values in A and B , then Π_4 will also have equal values in A and B . This knowledge enables efficient experimentation. For example, if we want to determine the relation between s_s/c and Π_1 we should devise an experiment in which we can measure s_s/c and choose the parameters of our experiment such that we can vary Π_1 while Π_2 and Π_3 remain unchanged.

$$\Pi_4 = f(\Pi_1, \Pi_2, \Pi_3) \quad (2.5)$$

$$\frac{s_s}{c} = f\left(\frac{\rho V c}{\mu}, \frac{R}{c}, \frac{c a}{V^2}, \frac{s}{c}\right) \quad (2.6)$$

Table 2.4: Non-dimensional parameter groups (or Π -products) resulting from application of the Buckingham-Pi procedure.

Π -product indicator	Π -product	meaning of Π -product
Π_1	$\frac{\rho \cdot V \cdot c}{\mu}$	the Reynolds number based on the airfoil's chord length, which is usually denoted by Re_c or Re .
Π_2	$\frac{R}{c}$	normalised trailing edge radius: the "relative sharpness" of the trailing edge.
Π_3	$\frac{c \cdot a}{V^2}$	a parameter which is related to the wing motion, because it only contains terms that are time-derivatives of distance
Π_4	$\frac{s_s}{c}$	normalised stagnation point location. The value of this parameter is wanted.

Re-writing similarity parameters to express time-dependence

To explicate the time-dependence of the similarity parameters it is useful to rewrite them in the form $\Pi_A = \Pi_B \cdot T$ where Π_A is the parameter originally resulting from the dimensional analysis (either Π_1 or Π_3 as listed in Table 2.4), Π_B is a dimensionless product, and T is non-dimensional time.

Non-dimensional time. In order to make t non-dimensional we divide it by a reference time t_{ref} such that $T = t / t_{\text{ref}}$. We construct the value of t_{ref} using (2.7) which describes the displacement of the airfoil as function of time. We define that $t_{\text{ref}} = 1$ when $s = R$ (2.8) from which follows an equation for t_{ref} (2.9). So the non-dimensional time is (2.10). The dimensional time can be written as $t = T \cdot t_{\text{ref}}$, see (2.11).

$$s = 1/2 \cdot a \cdot t^2 \quad (2.7)$$

$$R = 1/2 \cdot a \cdot t_{\text{ref}}^2 \rightarrow s = R, \quad t = t_{\text{ref}} \quad (2.8)$$

$$t_{\text{ref}} = \sqrt{\frac{2R}{a}} \quad (2.9)$$

$$T = t / t_{\text{ref}} = t / \sqrt{2R/a} \quad (2.10)$$

$$t = T \cdot t_{\text{ref}} = T \cdot \sqrt{2R/a} \quad (2.11)$$

Non-dimensional velocity. The reference time which has just been defined enables the definition of a reference velocity (2.12), which in turn leads to definition of a non-dimensional velocity (2.13). It turns out that the non-dimensional velocity V equals the non-dimensional time T (2.13). The dimensional velocity can be written as function of V by (2.14).

$$V_{\text{ref}} = a \cdot t_{\text{ref}} = \sqrt{2aR} \quad (2.12)$$

$$\tilde{V} = V/V_{\text{ref}} = V/\sqrt{2aR} = T \quad (2.13)$$

$$V = \tilde{V} \cdot V_{\text{ref}} = \tilde{V} \cdot \sqrt{2aR} = T \cdot \sqrt{2aR} \quad (2.14)$$

Time-dependent Reynolds number. The chord-based Reynolds number $Re_c = (\rho V c)/\mu$ is time-dependent due to the inclusion of parameter V . Using (2.14) the Reynolds number can be rewritten as product of a constant reference Reynolds number and non-dimensional time:

$$\frac{\rho \cdot (V) \cdot c}{\mu} = \frac{\rho \cdot (\tilde{V} \cdot V_{\text{ref}}) \cdot c}{\mu} = \frac{\rho \cdot V_{\text{ref}} \cdot c}{\mu} \cdot T = Re_{\text{ref}} \cdot T \quad (2.15)$$

Non-dimensional wing displacement. The similarity parameter $\Pi_3 = \frac{c \cdot a}{V^2}$ can be written as function of time using $V = at$ and then rewritten as product of some dimensionless number and dimensionless time using (2.11), see (2.16). Then using (2.7) it can be rewritten in terms of displacement; this is inverted and the constant 2 is removed for convenience, resulting in a ratio of wing displacement and chord length (2.17). The result s/c can be used instead of the original number $\Pi_3 = \frac{c \cdot a}{V^2}$. However, instead of rewriting Π_3 in terms of displacement, we may also rewrite (2.16) in terms of non-dimensional time using the relations $V = at$ and (2.11) resulting in (2.18). We can then rewrite it such that it becomes a function of $\Pi_2 = R/c$, resulting in (2.19). Note that R is present in this relation because T is defined in terms of R in (2.10).

$$\Pi_3 = \frac{c \cdot a}{V^2} = \frac{c \cdot a}{(at)^2} = \frac{c}{at^2} \quad (2.16)$$

$$\frac{c}{at^2} \propto \frac{c}{s} \rightarrow \Pi_{3,\text{new}} = \frac{s}{c} \quad (2.17)$$

$$\Pi_3 = \frac{c}{at^2} = \frac{c}{2r \cdot \frac{1}{T^2}} \quad (2.18)$$

$$\frac{c}{2R} \cdot \frac{1}{T^2} = \frac{1}{2R/c} \cdot \frac{1}{T^2} \propto \frac{1}{R/c} \cdot \frac{1}{T^2} \rightarrow \Pi_{3,\text{new},2} = \frac{R}{c} \cdot T^2 \quad (2.19)$$

Reduction of the governing equation. The relation between similarity parameters (2.6) is re-written using the time-dependent Reynolds number (2.15) and the time-dependent version of the displacement-related parameter (2.19) resulting in (2.20). This is the final result of this section. The original parameter set $[\rho, \mu, c, R, a, V, s_s]$ has been made non-dimensional and written as function of time, and related to each-other. We conclude that the stagnation point position s_s/c depends on the reference Reynolds number, the sharpness of the trailing edge, and the non-dimensional time via an unknown function f . Although the form of f is unknown, relation (2.20) allows to obtain some understanding of the dependence of s_s/c on the other parameters.

In order to determine f by experimental investigation one would like to be able to vary each term in (2.20), one factor at a time. However, note that only the second term can be varied (by varying R) without also varying other terms. Equation 2.21 shows s_s/c as function of c, R, a . Note that these parameters can relatively easily be changed during experimentation. In a CFD analysis or a detailed analytical analysis it is even possible to change the value of every independent parameter at will, however in an empirical study it is relatively difficult to change ρ or μ .

$$\frac{s_s}{c} = f\left(Re_{\text{ref}} \cdot T, \frac{R}{c}, \frac{R}{c} T^2\right) \quad (2.20)$$

$$\frac{s_s}{c} = f\left(\frac{\rho a t c}{\mu}, \frac{R}{c}, \frac{a t^2}{c}\right) \quad (2.21)$$

2.4. Potential flow analysis

This section discusses a first estimation of the initial non-lifting flow-field using numerical potential flow analysis. This serves three purposes. First, it will give an estimation of the location of the upper-surface stagnation point which is expected to exist (see Figure 1.7 on p. 11). This location is important because it determines the extent of the field-of-view which is required in the experiment. Second, the potential flow analysis will provide an estimation of the magnitude of velocities in the vicinity of the trailing edge. This knowledge is particularly useful when tuning the velocity measurement equipment in the experimental setup such that accurate measurements will be obtained for the range of flow velocities that occur. Third, a comparison between different airfoils with rounded trailing edges will indicate the dependence of the flow in the vicinity of the trailing edge on the overall airfoil shape and on the trailing edge radius.

Potential flow theory assumes that the flow is incompressible and irrotational, and inviscid, so it remains irrotational. The description by Batchelor (1967, p. 278) of the initial phase of the flow around an object put in motion from rest explains that the effects of viscosity in that phase increase in strength from zero and are confined to a thin region around the body in the starting phase of the motion. Therefore we assume that there exists some small period of time during the start of the wing's motion in which the effects of viscosity on the flow-field around the body can be regarded as absent (compared to the effects of pressure). This justifies the use of potential flow methods for calculating the surface velocity distribution that is present on the body in the first phase of the transient flow although the flow is viscous.

When the airfoil is at rest, the circulation about the airfoil is zero, so the circulation will be very close to zero in the first phase of the wing's motion (Batchelor, 1967, p. 438). This means the flow-field at that moment can be determined by a potential flow calculation in which the circulation is forced to be zero. The first part of this section explains the implementation of a panel method which was made for this purpose. The second part of this section presents two airfoil shapes which will be analysed by the panel method.

Panel method implementation

A second order vortex panel method (which models an airfoil as a series of straight panels on which 'sheets' of vorticity having a linear distribution are placed, see Figure 2.6) was available and it was easily modified to incorporate the condition of zero total circulation. The vortex panel method is programmed in MATLAB, according to the suggestions presented in Kuethe and Chow (1998). The zero-circulation condition is implemented by modifying the main matrix equation of the method ($\mathbf{A_N} = \Gamma \cdot \mathbf{B}$). The $\mathbf{A_N}$ matrix represents the influence of the strength of the vorticity at the end point of each panel on the velocity in the normal direction of each panel. The \mathbf{B} matrix represents the influence of the uniform free-stream on the velocity in the normal direction of each panel. When the vorticity distribution has been obtained, the velocity distribution about the wing is calculated, and from that the pressure distribution is calculated. For more detailed information concerning the working of the panel method the reader is referred to Kuethe and Chow (1998) for more detailed information about the principles and implementation of this panel method.

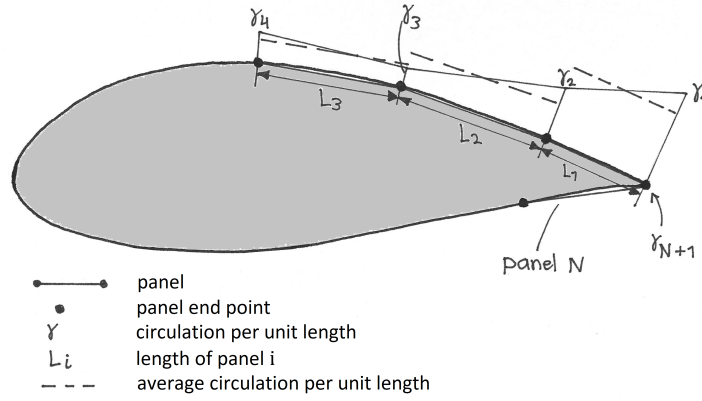


Figure 2.6: Illustration of the panel method discussed in this section. An airfoil is discretised using N straight panels over which the vorticity or circulation varies linearly.

Definition of the condition of zero circulation

The vorticity distribution, which varies linearly over each panel of the airfoil, is depicted on Figure 2.6. The strength of an element of the vorticity distribution equals the circulation of that element (Anderson, 2011, p. 327). The panel circulation Γ_i (where i denotes the i -th panel) is a simple average of the circulation value at the endpoints ($\gamma_{i,A}$ and $\gamma_{i,B}$) multiplied by the panel length L_i since the circulation is linearly distributed over each panel (2.22). See Figure 2.6 for an illustration. The total circulation of the airfoil Γ is calculated by summing the circulations Γ_i of each panel (2.23). It follows that the main matrix equation of the panel method ($A \cdot \Gamma = B$) can be modified according to (2.24) to determine a solution of vorticity distribution for which the integrated vorticity (i.e. the total circulation) over the airfoil surface is zero.

$$\Gamma_i = \frac{\gamma_{i,A} + \gamma_{i,B}}{2} \cdot L_i \quad (2.22)$$

$$\begin{aligned} \Gamma = \sum_{i=1}^N \Gamma_i &= \sum_{i=1}^N \frac{\gamma_{i,A} + \gamma_{i,B}}{2} \cdot L_i \\ &= \frac{\gamma_{1,A}}{2} \cdot L_1 + \frac{\gamma_{1,B}}{2} \cdot L_1 + \frac{\gamma_{2,A}}{2} \cdot L_2 + \frac{\gamma_{2,B}}{2} \cdot L_2 + \dots + \frac{\gamma_{N,A}}{2} \cdot L_N + \frac{\gamma_{N,B}}{2} \cdot L_N \\ &= \frac{\gamma_1}{2} \cdot L_1 + \frac{\gamma_2}{2} \cdot L_1 + \frac{\gamma_2}{2} \cdot L_2 + \frac{\gamma_3}{2} \cdot L_2 + \dots + \frac{\gamma_N}{2} \cdot L_N + \frac{\gamma_{N+1}}{2} \cdot L_N \\ &= \frac{\gamma_1}{2} \cdot L_1 + \sum_{i=2}^N \frac{\gamma_i}{2} \cdot (L_{i-1} + L_i) + \frac{\gamma_{N+1}}{2} \cdot L_N \end{aligned} \quad (2.23)$$

$$\begin{aligned} A_N(N+1, 1) &= L_1/2 \\ A_N(N+1, i) &= \frac{L_{i-1} + L_i}{2} \quad \text{for } i = 2 \text{ to } N \\ A_N(N+1, N+1) &= L_N/2 \\ B(N+1) &= 0 \end{aligned} \quad (2.24)$$

Flat plate with rounded edges

A very simple airfoil is created for the analysis of the trailing edge flow-field: a flat plate with rounded edges; see also Figure 2.2 on p. 35. The leading and trailing edges are formed by semi-circles. Figure 1 shows the contour of this ‘airfoil’, which is modelled by 100 panels on each of the flat upper and lower sides and 20 panels on each of the front and rear trailing edge arcs. The panelling in the trailing edge region is depicted on Figure 2.7. In the remainder of this report this airfoil shape will be called the ‘rounded flat plate’.

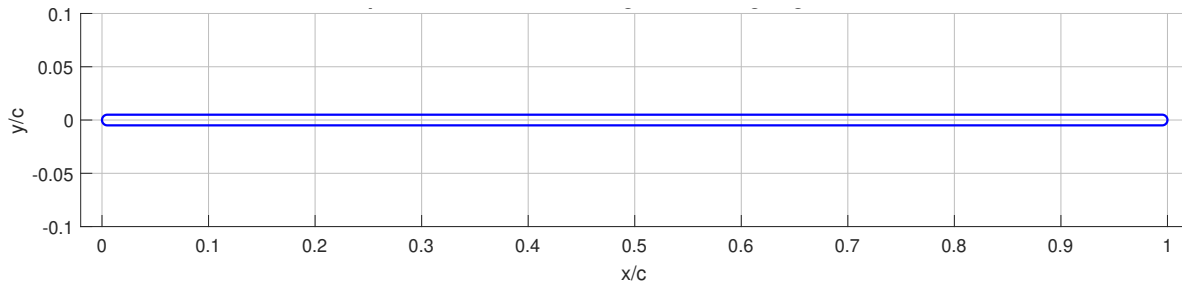


Figure 2.7: Contour of the rounded flat plate airfoil used for the potential flow analysis and the experimental investigation performed for the present research. The ratio of radius of curvature w.r.t. the chord length (R/c) equals 0.5%. This airfoil is modelled using 100 panels for the upper and lower sides (100 for each side) and 20 panels for the circular arc sections which form the leading- and trailing edges (20 for each).

Conventional airfoil with rounded trailing edge

In order to determine the dependence of the flow-field in the vicinity of the trailing edge of an airfoil on the overall airfoil shape, we will compare the trailing edge flow-field of the rounded flat plate with that of a conventional airfoil of which the trailing edge is rounded. We take the NACA-0012 airfoil as representative for a conventional airfoil.

Rounding of the trailing edge is performed by cutting the rear part from the airfoil and replacing it by a circular arc of given diameter which joins the upper- and lower sides smoothly (tangentially, so the contour has first-order continuity) as illustrated in Figures 2.8 and 2.9. This operation will reduce the chord. To make the chord length again equal to 1 the airfoil is stretched uniformly over its length. The circular arc is modelled by 20 panels.

In order to study the dependence of the trailing edge flow-field on the radius of curvature of the trailing edge, the procedure of rounding the trailing edge of the NACA 0012 is performed multiple times with varying degrees of rounding. The values used for the R/c parameter are: 0.25%, 0.5%, 1% and 2%. The value of $R/c = 0.5\%$ corresponds to the trailing edge of the rounded flat plate. The resulting airfoil shapes are presented on Figure 2.10.

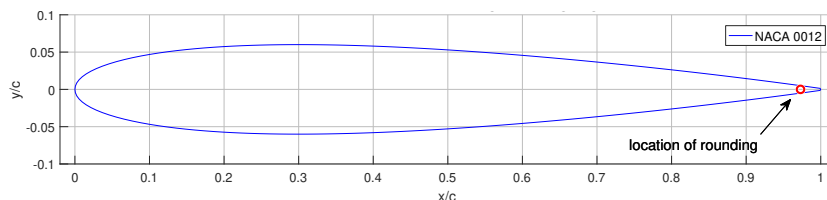


Figure 2.8: The location where the circle is fitted to the airfoil in the process of rounding the trailing edge: the chord-wise location where the airfoil thickness equals the desired diameter of the circular arc.

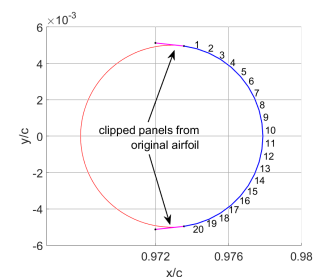


Figure 2.9: Detail of the panelling of the circular arc at the trailing edge. Twenty straight panels are used.

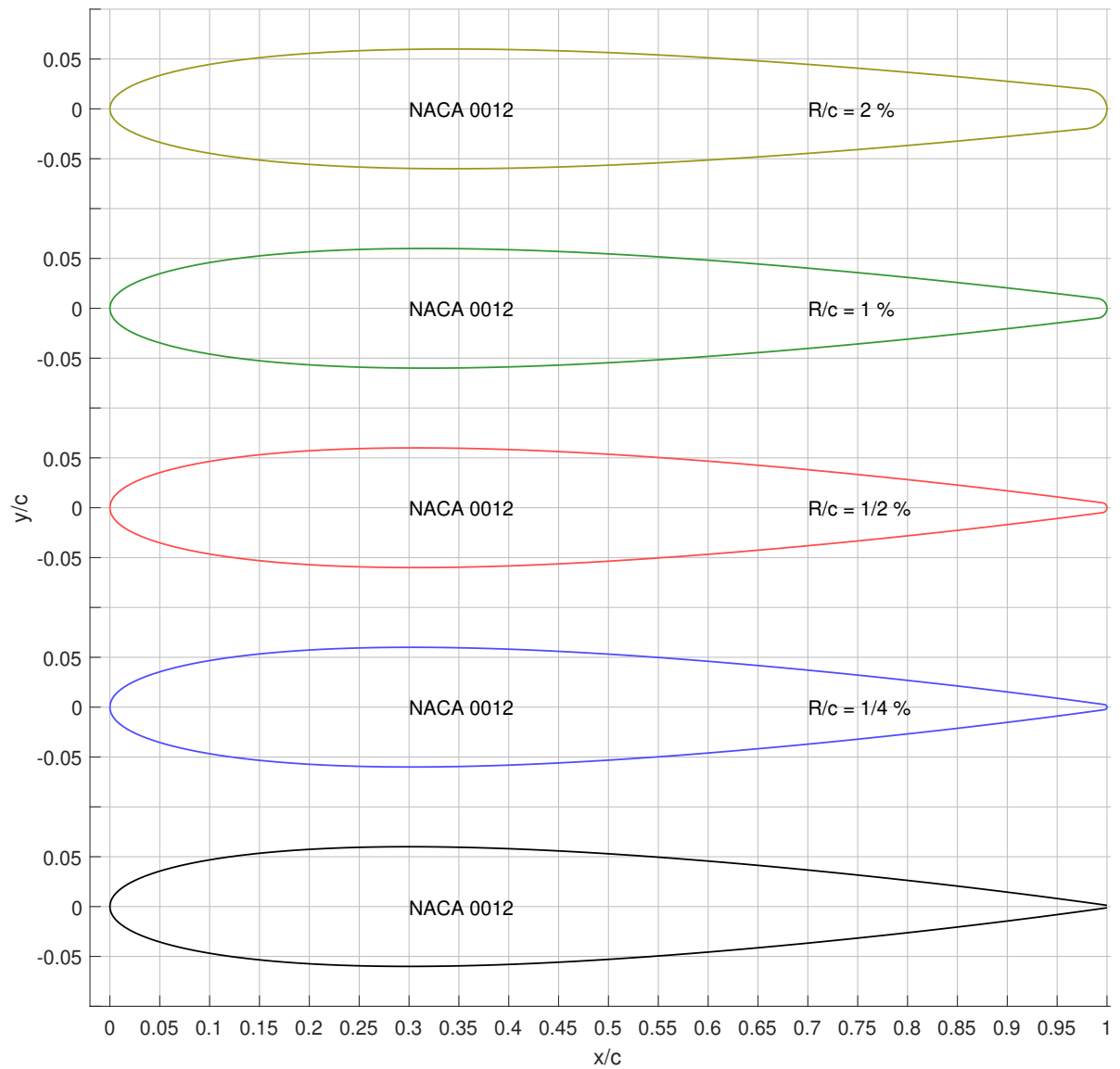


Figure 2.10: A series of NACA-0012 airfoils of which the trailing edge has been rounded with different radii. The airfoils have been stretched in chordwise direction after rounding of the trailing edge, to make the chord length equal to 1. The value of the ratio of curvature w.r.t. the chord length (R/c) is indicated for each airfoil.

2.5. Experiment

As made clear in the research definition (Section 1.7) we want to study the research phenomenon (i.e. the evolution of the flow of fluid in the region around the trailing edge of a wing when the wing is set in motion from rest) empirically. This section presents the design of the experiment that was devised to let the research phenomenon occur and to measure its properties. We start with explaining the selection of measurement technique (Section 2.5.1) and some conceptual design choices (Section 2.5.2) for the experimental setup. We will analyse the length- and time-scales in Section 2.5.3 which will give us some idea of the size of the setup and the required accuracies. Then we discuss some practicalities which constrain the design space in Section 2.5.4. Section 2.5.5 presents a short report of the proof-of-concept design which was performed to check the conceptual design. The conceptual and practical considerations are synthesised which leads to a conceptual design, presented in Section 2.5.6. The process of producing a detailed design is not described, but the result is presented in Section 2.5.7.

2.5.1. Choice of measurement technique

To take measurements of the phenomenon, the phenomenon has to be created and it has to be measured. The question of creation will be regarded later in this section; the question of measurement will be discussed as follows. We would like to obtain velocity field measurements in a plane, at multiple moments in time, such that both the spatial and temporal development of the flow field can be studied with enough detail. This implies that we need a “field measurement technique” which can take a “snapshot” of a velocity field or else a “point measurement technique” which can measure point velocities at different locations with such large acquisition speed that the flow can be assumed steady between the beginning and the end of the measurement of a velocity field. Intrusive measurement techniques (such as pressure measurement and Hot-Wire Anemometry) are not suitable because they disturb the flow because the equipment is large w.r.t. the size of the flow features to be studied. Intrusive measurement techniques are also not suitable for field measurement because this would require either very many (expensive) probes for simultaneous measurement or an impossibly quick automatic traverse system. From these quick considerations we dismiss intrusive measurement techniques. Regarding non-intrusive measurement techniques, we mention the following. Oil flow photography allows only qualitative studies at the surface of an object, so it is not suitable. LASER-Doppler Velocimetry is a “point measurement technique”, not a “field measurement technique”, so it is not suitable. Infrared thermography is not useful because no significant temperature differences will be present in the flow. Shadowgraphy and Schlieren photography are considered not suitable because it is expected that significant density changes do not occur. **Particle-Image Velocimetry** is suitable: it is a “field measurement technique” and it can be used in low-speed flows. A further reason for using this technique is the availability of specialised equipment and experience concerning this measurement technique at the TU Delft, namely at the Aerodynamics section of the faculty of Aerospace Engineering and at the Hydro/Aero-dynamic Laboratory of the faculty of Mechanical Engineering.

The Particle-Image Velocimetry (PIV) technique relies on the presence of particles in the flow which are illuminated by a special light source (often a LASER) and imaged using a special camera. The images (photographs) are compared to each other by a numerical procedure to determine the shift of particles between two time instants, from which the instantaneous flow velocity field is determined. See [Raffel et al. \(2018\)](#) for detailed information. The resulting flow velocity vector field can then be analysed to determine properties of interest, such as stagnation points and streamlines.

2.5.2. Preliminary conceptual design

The conceptual design of the experiment consists of the following parts: 1) wing model, 2) fluid, held in a certain domain, 3) a device to move wing and fluid w.r.t. each-other, 4) particles in the fluid, 5) PIV-equipment, 6) tools to extract velocity fields from PIV-images, 7) tools to determine properties of interest from the velocity fields.

Before going further with either the conceptual or the practical design of the experimental setup, we analyse the length- and time-scales of the phenomenon to obtain a more accurate understanding of the spatial and temporal requirements of the setup.

2.5.3. Analysis of length- and time scales

A simple experiment which produces visible flow separation from a sharp edge, such as moving a spoon in a cup of soup, will give an impression of the length- and time-scale of the phenomenon. A spoon is not the same as a typical wing, but it is supposed that the phenomenon of flow separation from a sharp edge is of such general character that it occurs in every case having the following ingredients: a viscous fluid, a sharp-edged object, and an abrupt change in the motion of the object through the fluid. This change of motion may be a change in velocity or a change in angle of attack (see also Section 1.3). From such an experiment we get the impression that the phenomenon is very local, both in space and time. It is difficult to see with the unaided human eye in case of trailing edge thicknesses of $O(1 \text{ mm})$ and airfoil chord lengths of $O(100 \text{ mm})$. From the theory presented in Section 1.4.2 we expect that it is important to measure the flow in the boundary layer (which is initially very thin after starting the motion) in order to follow and understand the development of the flow-field and not to miss important events that are causally linked to other events. With a trailing edge thickness of $O(1 \text{ mm})$ we may expect a boundary layer of $O(0.1 \text{ mm to } 1 \text{ mm})$ thickness, which gives a first impression of the length scale involved in measuring the phenomenon.

Although the length- and time-scales of the phenomenon are relatively small, it might be possible to make them of such magnitude as is practical for measurement by proper dimensioning of the experimental setup. Important dimensions are thought to be the chord length c and the trailing edge sharpness R/c . Furthermore it is important to have a proper size of the fluid domain w.r.t. the size of the airfoil. Note that the words ‘airfoil’ and ‘wing’ are used interchangeably; since we are studying 2-dimensional cases. For a qualitative analysis of the relation between the scales of the phenomenon and the geometrical parameters, a theoretical (dimensional) analysis must be done. But already now we can note that the scales of the phenomenon cannot be adjusted as we like without limits. For reasons of representativeness it is desirable that the trailing thickness and the chord length have a certain relation w.r.t. each other. The chord length must be of $O(200 \text{ mm})$ for practical reasons related to manufacturing and the available space for a test setup. So assume that we have the freedom to vary the trailing edge radius (assuming that the airfoil has a rounded trailing edge) between 0.1% and 1% of the chord length and that we can vary the chord length between 100 and 300 mm. The range of trailing edge radii is then 0.1 to 3 mm, which is approximately 1.5 orders of magnitude. Regarding the time-scale, we have an impression from simple experiments. The phenomenon seems to be executed so quickly that it cannot be studied with the unaided human eye, so the duration is of $O(0.1 \text{ s})$ at most. The research of [Zhu et al. \(2015\)](#) offers more precise information. They show that a trailing vortex is created and smooth flow off the upper- and lower sides of the trailing edge is present at 0.1 s.⁹ However, their work also mentions that important events and changes in the flow-field occur less than $\approx 0.01 \text{ s}$ after the motion is started. Figures 2.12 illustrate the time- and length scales just mentioned.

Let us assume that the measurement resolution should be one order of magnitude smaller than the scales of the phenomenon such that changes in the flow-field can be measured with enough precision. A likely trailing edge radius is 1 mm, from which we expect a flow-field length scale of 0.1 mm. The 0.01 s time-scale from the work of [Liu et al. \(2015\)](#) is used in this estimation. It follows that a spatial resolution of $O(0.01 \text{ mm or } 10 \mu\text{m})$ and a temporal resolution of $O(0.001 \text{ s or } 1 \text{ millisecond})$ are required. We conclude that measurement devices with “micro” and “high-speed” capabilities are needed.

⁹This data corresponds to their specific motion profile. In their experiment the wing was accelerated from rest with a motion profile described by $V=\sin(t)$ with V in m/s and t in s)

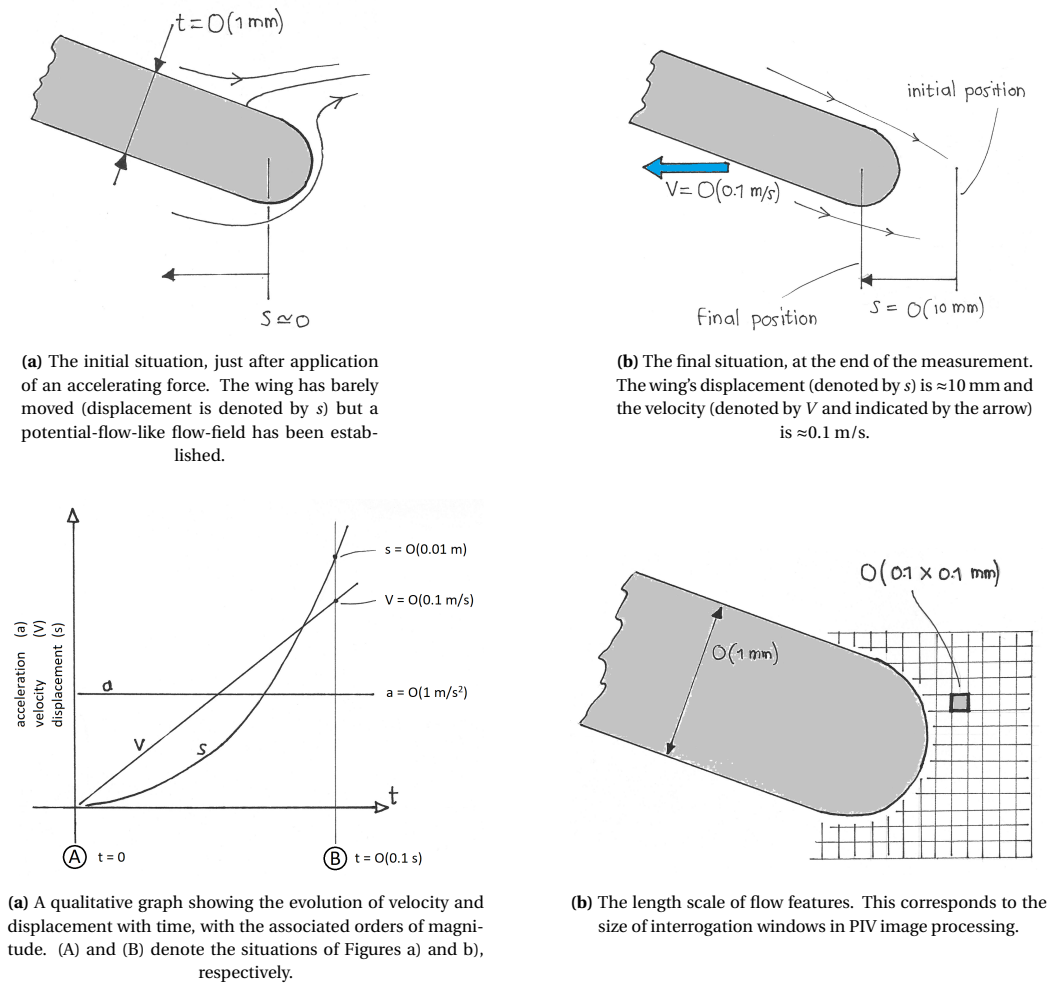


Figure 2.12: Sketches illustrating the time- and length scales of various aspects of the research phenomenon. Their magnitudes have a large bearing on the required measurement capabilities that are needed to record the phenomenon.

2.5.4. Practical design considerations

For a design of the experiment and corresponding experimental setup, choices have to be made regarding the following main points: 1) The medium used as fluid, 2) The wing/airfoil geometry, especially concerning the trailing edge, 3) The motion profile of the wing w.r.t. the fluid, 4) The size and shape of the fluid domain. These will be discussed in order in the following.

Choice of fluid medium. We can immediately make a distinction here, namely between liquids and gases. To keep the financial costs of the experiment small we will consider only fluids that are inexpensive and easy to obtain. This implies that the choice for gas means choosing for air. Regarding liquids, the obvious choice is water, or fluids that are based on water. When larger Reynolds numbers are desirable the advantage of water over air is that it has 15 times larger kinematic viscosity at room temperature (Kuethe and Chow, 1998), which means that a 15x larger Reynolds number can be attained for the same absolute geometrical size and velocity. Water can be made more viscous by adding glycerine.¹⁰ When PIV is used as measurement method, the use of water is strongly preferred over air, according to Veldhuis and Sciacchitano.¹¹

Choice of airfoil geometry. When considering the geometry of the airfoil to be used in our experiment, we naturally pay special attention to the geometry in the trailing edge region, since our phenomenon of interest occurs there. The shape of the rest of the wing is also important: it should be such that it does not give rise

¹⁰According to Veldhuis (private communication, August 2018)

¹¹Private communication, May 2018

to events in the flow domain that hinder us in our study of the trailing edge flow-field, such as a separation bubble somewhere on the wing.¹² In the design or selection of the airfoil the leading idea is that the trailing edge of a real wing has larger-than-zero thickness (Figure 2.13a). It is not infinitely sharp and thin (Figure 2.13d).¹³ So instead of the very edge being a point, it will actually be a curved line. This trailing edge contour line has some roundedness, which may vary from point to point (Figure 2.13b). It is expected, based on the theory of Section 1.4.2, that the location of sharpest rounding (smallest local radius of curvature) determines the point of flow separation. In order to study the flow separation process, we want to ‘magnify’ this region. Therefore we model the trailing edge contour line by a piece of arc which is tangentially connected to two pieces of straight line, according to the parameterisation presented in Section 2.2, depicted by Figure 2.13c. For the experimental part of this research we choose the same airfoil that is used for the theoretical analysis: the rounded flat plate, the parameterisation of which is defined on Figure 2.2. The precise shape is depicted on p. 45.

From the point of view of the practical relevance of the research it is desirable to select an airfoil that is representative for airfoils used in aviation. However, from practical considerations (concerning manufacturing of the model and resolution of measurements) it appears desirable to choose an geometry that has larger-than-usual trailing edge radius relative to the chord length. These aims are contradictory. We will choose the smallest possible R/c value which allows measurement of the flow-field with enough resolution, given the performance limitations of the available equipment for manufacturing of the wing and for measurement of the flow-field.

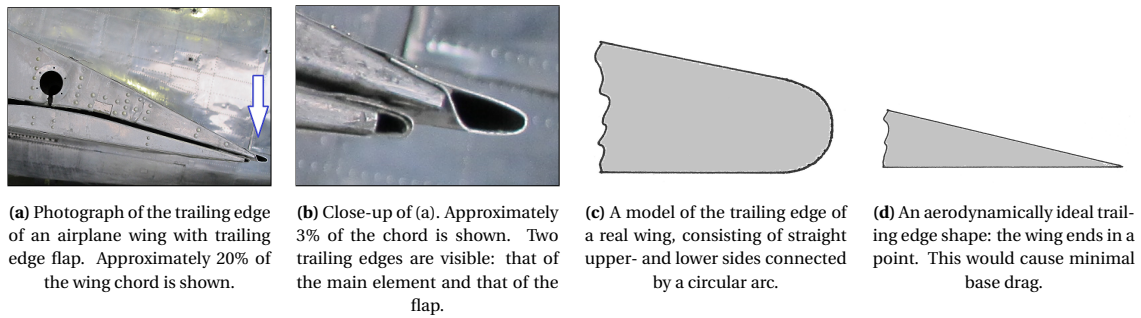


Figure 2.13: Illustrations of various forms of trailing edges. The form of (c) is closest to the shape that is used in the present research (cf. Figure 2.10).

Motion profile of wing w.r.t. fluid. In the initial state of the phenomenon the wing and fluid are initially at rest w.r.t. each other. We are interested to create relative motion between wing and fluid, which can be done in different ways: 1) move the wing and keep the fluid (that is, the general mass of fluid) at rest; 2) keep the wing at rest and move the fluid. A further option, although seemingly unnecessarily complicated, is to move the wing and fluid w.r.t. each other and their combination as a whole w.r.t. the inertial frame. Note that in this section we define motion as motion w.r.t. the inertial frame. This motion can have many possible forms. The motion profile can be described by defining a function of time: $s = f(t)$. We can also define a motion profile by defining a function of time for a higher-order derivative of position w.r.t. time, such as velocity or acceleration: $v = f(t)$ or $a = f(t)$. For selecting a motion profile we will keep in mind the following points of attention:

1. **Practical possibilities of achieving it in an experimental setup.** In order to minimise the cost of the experiment, we would like to have a motion profile that can be created by a simple actuator. The simplest actuator might be the force of gravity, which leads to a constant acceleration and thus a linear velocity profile (w.r.t. time).

¹²This is also discussed on p. 33.

¹³With a “real wing” is meant, for example, the wing of an aircraft, or any wing that is manufactured in reality, in contrast to wings of ideal shape which only exist as ideas.

2. **Representativeness for the case of an aircraft wing being put in motion.** We would like to bring forth the phenomenon in the same way as it is created at the wing of a real aircraft. Perhaps the only restriction is that the velocity is always increasing. It has to be remarked here that the acceleration of an aircraft usually starts slowly, such that the distance travelled by the aircraft before the Kutta condition is established might be quite large. The moment from which the Kutta condition is established might even not be uniquely defined when atmospheric turbulence is taken into account. We would like to study the phenomenon's development in a facility of limited size which will likely be on the order of 10 times the chord length; therefore we will try to 'compress' the motion profile of a real aircraft in time such that the travelled distance is in the order of magnitude of the chord length.
3. **Simplicity of its mathematical description.** For theoretical analysis it is advantageous when mathematical functions have simple descriptions. A simple motion profile would be a constant acceleration, which means a linearly increasing velocity w.r.t. time. Using such a profile will enable easy development of a theoretical model of the development of the trailing edge flow-field when the wing's velocity profile needs to be taken into account.

The simplest motion profile that fulfils these requirements is a constant acceleration, which is described mathematically by $s = 1/2at^2$ and $V = at$ where the displacement s , the velocity V and the time t are all zero until the motion begins.

2.5.5. Proof-of-concept experiment

A proof-of-concept experiment was performed to check the viability of observing the phenomenon with PIV equipment available at the university. From study of the image series it was concluded that the desired phenomenon can be produced and measured using available equipment and practical dimensions of wing model and setup. It was also concluded that a rounded trailing edge is needed with a "trailing edge sharpness" R/c of at least $O(1\%)$, otherwise the timescale and displacement of the wing during creation of the Kutta condition would be too small to be measured. Furthermore, automatic synchronisation of wing motion and image recording is desired to prevent generating large amounts of "empty data".

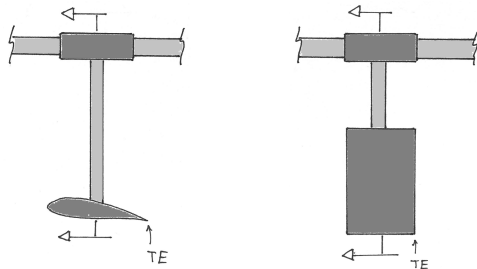


Figure 2.14: Two examples of the application of a sliding hinge to determine the motion of the wing in the experiment setup. The wing is mounted horizontally on the left and vertically on the right picture.

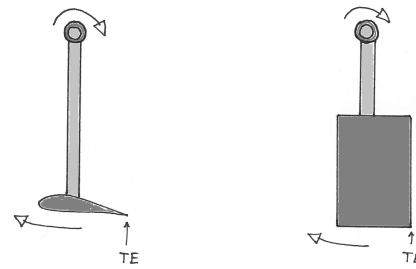


Figure 2.15: Two examples of the application of a rotating hinge to determine the motion of the wing in the experiment setup. The wing is mounted horizontally on the left and vertically on the right picture.

2.5.6. Synthesis of conceptual and practical considerations

Combining the conceptual design with the practical considerations resulted in an effective design. An illustration of it is presented on Figure 2.16. Water is selected as fluid. A fluid domain consisting of five sides is chosen, such that the water has one free surface. This free surface poses a disadvantage (which is discussed later) but it would be much more involved to confine the fluid to a six-sided domain. The wing is oriented vertically in the fluid domain such that the measurement plane, which is perpendicular to the wing's root-tip axis, is horizontal and thus parallel to the bottom of the domain. This minimises the effect of the free-surface motion on velocities in the measurement plane and it also prevents pressure gradients due to gravity in the

measurement plane. The wing, together with the mechanism to which it is attached, is positioned above the bottom of the fluid domain. The measurement plane coincides with the light sheet, which is thus also horizontal. A wing motion profile having a constant acceleration is chosen. This has two important advantages: firstly, the wing can be actuated by means of a simple falling weight, making use of gravity. Secondly, it allows straightforward calculation of the relations between acceleration, velocity, and displacement. Two types of hinges were considered: a sliding hinge (Figure 2.14) which would allow a pure translational motion of the wing, and a rotational hinge (Figure 2.15). The second option was selected because it is deemed practically simpler. The hinge location is $\approx 1\text{m}$ away from the measurement plane, such that the movement of the trailing edge can well be approximated by a pure translation. The tip of the wing is to be positioned closely to the bottom of the fluid domain such that leakage of fluid around the tip is minimal, see Figure 2.19. The camera is located beneath the fluid domain, looking upward. In this way the fluid boundary through which the camera ‘looks’ is flat. Viewing the water from above is problematic because the shape of the free-surface will distort the image of the object plane; so much that it cannot be corrected. The camera is to be positioned and oriented such that the lens axis is concentric with the wing’s trailing edge axis and the camera sensor is parallel to the measurement plane.

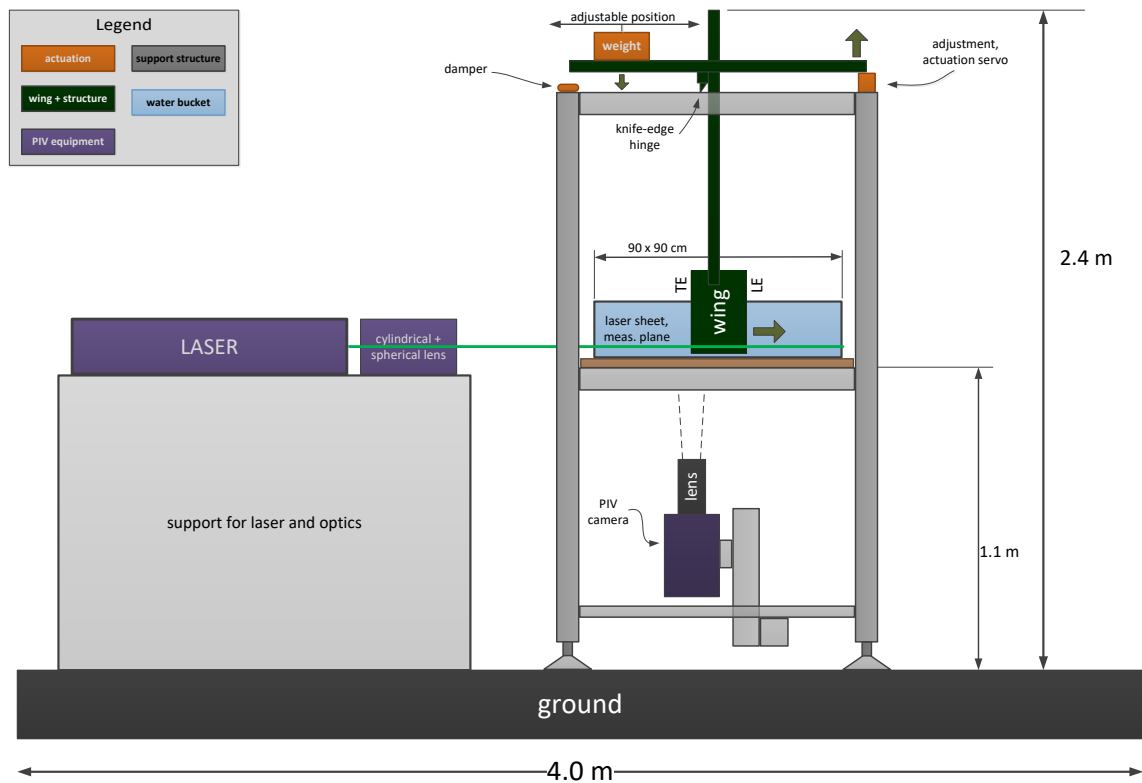


Figure 2.16: A sketch (to scale) of the experiment setup, shown in side-view. Note the knife-edge hinge on the top of the frame, which allows the wing to make a quasi-linear motion at the measurement plane, without play and almost friction-less.

2.5.7. Detailed design

A photograph of the experiment setup is depicted in Figure 2.21 which corresponds to the sketch of Figure 2.16. The main parts of the setup are described in order as follows.

Wing models. Three wing models were produced, each having a chord length $c = 200\text{mm}$ but with different thicknesses: $t = 1\text{mm}$, 2mm , and 4mm . This allows to investigate the phenomenon for three different “trailing edge sharpness” values, namely $R/c = 0.25\%$, 0.5% , and 1% . The span of the wing models is 300mm . Only $\approx 10\text{cm}$ of the span is immersed in the water. The tip clearance of the wing (i.e. the distance between the wing

tip and the bottom of the water tank) is ≈ 0.5 mm; see Figure 2.19.

The wings were produced from rectangular pieces of stock aluminium plate. These were cut by a robotic cutting machine. The pieces of plate were not perfectly flat, but flat enough for the purpose, having less than $\approx 0.025\%$ camber. The leading and trailing edges of the plate were squared by filing. Tubes of stainless steel or brass were glued to the leading and trailing edges of the plate by means of epoxy. The contour (i.e. the gap between the end of the plate and the tube) was smoothed by applying a paste of epoxy which was sanded with 600grit sandpaper after curing. When the contour was deemed smooth enough (inspection by eye) the wing models were spray-painted with matte black paint. The layer of paint was sanded with 1200grit sandpaper and painted again. The result was a wing model having the cross-section of a flat plate with rounded edges and an optically near-perfect smooth contour. Three holes were drilled at the wing root for attachment to a beam. Figure 2.17 presents a planform view of one of the wings and Figure 2.18 shows a cross-section view of the trailing edge.



Figure 2.17: Photograph of the wing model having 200mm chord, 300mm span and 2mm thickness (in planform view) that was produced for the experiment performed for the present research. Next to it is a 30cm ruler. The three holes on the top serve for mounting of the wing to the frame of the experimental setup.



Figure 2.18: A photograph of the wing model (which is also shown in Figure 2.17) showing a cross-sectional view, zoomed-in on the trailing edge part. The white particles on the wing surface are dust particles.

Water tank. The fluid domain is formed by the surfaces of a water tank having (inner) dimensions of $0.90 \times 0.90 \times 0.20$ m. This tank is formed by glass plates having a thickness of 10mm. The water tank was produced by the company *Aquariumhuis Romberg* in Delft, The Netherlands.

The length and width of the fluid domain is 4.5 times as large as the wing chord. Note that the wing is oriented vertically in the tank with the tip-root axis of the wing being oriented perpendicular to the bottom of the tank (see Figure 2.16). These dimensions are chosen such that, assuming a wing displacement of $O(10\text{mm})$ the effect of the walls of the tank on the velocity field around the wing is negligible.

The amount of water in the tank, in terms of the water height, was $\approx 8\text{cm}$; see Figure 2.19. This is not based on any calculations, it represents a guess of an optimum in which several parameters have a role. A smaller water height is preferred to reduce risks and to reduce the actuation force required to achieve a certain wing acceleration. However, at the same time, a larger water height is preferred such that the measurement plane

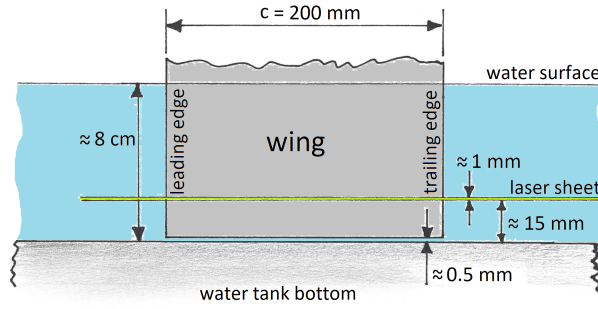


Figure 2.19: Sketch (not to scale) of the vertical positioning of the wing and laser sheet w.r.t. the bottom of the water tank.

can be further away from the bottom of the tank as well as from the free surface. A larger distance between tank bottom and measurement plane is preferred to reduce boundary layer effects in the measurement plane due to the bottom of the water tank. At the same time, a smaller distance between tank bottom and measurement plane (relative to the water height) is preferred to reduce out-of-plane velocities in the measurement plane due to vertical motion of the free surface.

Frame. The frame of the setup provides a stiff connection between the wing, the wing actuation system, the fluid domain, and the measurement equipment. The frame consists of aluminium beams produced by the company *Item Systems* in Delft, The Netherlands. Four beams of 2m length and 80x80mm rectangular cross-section are oriented vertically. Between these, three square rings are formed by horizontal beams. At ≈ 10 cm above the ground one ring provides mounting for the camera. At ≈ 1 m above the ground one ring supports the water tank. The highest ring, at ≈ 2 m above the ground, provides mounting for the wing motion system. The “main frame” just described can be levelled by means of adjustable legs. The frame has abundant strength and stiffness, which is required to prevent unwanted relative motion between the wing and the camera. Since magnification is large, a small frame deformation would result in relatively large image deformation.

The water tank is supported by a ≈ 4 cm thick wooden plate which in turn is supported by the middle set of four horizontal beams. A layer of foam blocks between the plate and the bottom of the tank provide some compliance such that the water tank is supported uniformly even when the wooden plate deforms under its load. The wooden plate has a ‘window’ of 30x30cm size located under the centre of the water tank, such that the fluid flow around the trailing edge of the wing can be observed by the camera from below.

The wing is attached to a set of beams which hinge on the main frame by a knife-edge hinge. This hinge fixes the position of the wing and allows rotational motion without play and with negligible friction. The wing rotates with an ≈ 1 m long arm, which, given the small rotation angle due to a wing displacement of ≈ 0.001 m, approximates a purely linear motion at the measurement plane. The wing can be fixed to the frame at a selectable angle of incidence by means of an adjustable clamp. The angle of incidence was set roughly to a desired value; its precise value is determined from the PIV images.

The wing motion is actuated by a set of steel weights of ≈ 5 kg which continuously apply a moment about the hinge line. When the setup is in standby-state the motion is prevented by a pin which holds the beams to which the wing is attached in place. When the operator desires to take a measurement he/she toggles a switch which, via the electronic control system, commands a servo to pull the pin such that the wing moves by the action of gravity.

The camera, which ‘looks’ upwards, is attached to the main frame by means of several beams which are connected to the lowest ring of horizontal beams. An adjustable clamp allows rotation of the camera about three axes. The camera is positioned and oriented such that the lens axis is concentric with the wing’s trailing edge axis.

PIV equipment. Images were taken by a LaVision Imager Pro HS 4M camera in combination with a Nikkor f=105mm D:2.8 lens. *Vestosint 2159* (which has $10\mu\text{m}$ particle diameter) was used as seeding material. A *MesaPIV* LASER was used for illuminating the seeding material. The camera and LASER were controlled using a LaVision Highspeed Controller (also called Programmable Timing Unit or PTU) and LaVision DAVIS software running on a PC. Images were acquired at a frequency of 2000 Hz. A spherical and cylindrical lens are used to transform the LASER light bundle into a light sheet. The light sheet is oriented horizontally, located $\approx 15\text{mm}$ above the bottom of the water tank. It is $\approx 10\text{cm}$ wide and $\approx 1\text{mm}$ thick at the trailing edge of the wing (see also Figure 2.19). A summary of data related to PIV is presented in Tables 2.5 and 2.6 on p. 56.

Synchronisation of motion and data acquisition. Synchronisation of the start of wing motion and the start of image acquisition was achieved by means of an electronic system which was developed specifically for this purpose. The system consists primarily of an *Arduino Leonardo* micro-controller, a switch, a servo, and a BNC connector. The Arduino “listens” continuously for toggling of the switch. When the switch is toggled, the servo is commanded to turn and unlock the wing. Also, a trigger signal is sent to the BNC connector, which is connected to the PTU via a coax cable. When this signal is received by the PTU the image acquisition is started. The relative timing between turning the servo and triggering the PTU can be adjusted such that the start of the wing motion is imaged while a minimum number of “empty” images is taken before the wing actually moves.

The electronic system also has functionality for reading an accelerometer. The purpose of this was to determine the acceleration of the wing, but this was abandoned during actual experimentation because of too large scatter in the acceleration data. The actuation-related components and the measurement related components of the electronic system have separate power supplies to prevent noise on sensor voltages due to current draw by the servo.

2.5.8. Measurement procedure

The procedure of taking an image-series of the research phenomenon is as follows. It is assumed that the apparatus, the camera, the LASER, and the PIV software has been set up. Figure 2.20 illustrates the data flow between the components of the experimental setup when the researcher performs a measurement.

1. Put the wing in its initial position. Lock the wing motion structure and arm the electronic system.
2. Stir the water in the vicinity of the trailing edge to get uniform seeding distribution. Remove seeding from the bottom of the water tank. The LASER is switched on during these tasks in order to inspect the seeding in the water around the trailing edge.
3. Switch off the LASER and wait for the water to come to rest ($\approx 1/2$ h).
4. Turn on the LASER and arm the camera. Turn off the room lights.
5. Activate the switch on the electronic system. This will unlock the wing motion structure and trigger the camera (see Figure 2.20).
6. Switch off the laser. Retrieve the images from the camera and store them on a hard disk.

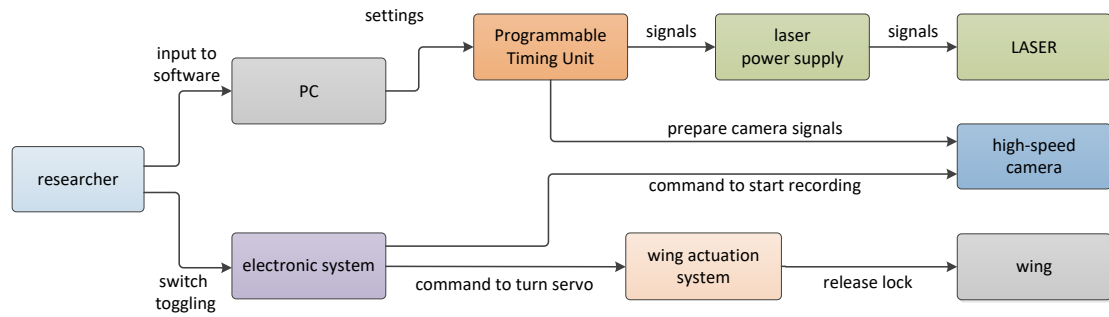


Figure 2.20: The data flow between the components of the experimental setup when the researcher performs a measurement. The researcher first executes steps 1-4 of the measurement procedure (see Section 2.5.8), then he/she operates the switch on the electronic system.

Table 2.5: Table of equipment related to Particle Image Velocimetry used in the experiment that was done for this research.

equipment	make/model
camera	LaVision ImagerPro HS 4M (PCO dimax)
seeding	Vestosint 2159
laser	MesaPIV
lens	Nikkor f=105mm

Table 2.6: Parameters related to PIV applied in the experiment that was done for this research.

parameter	symbol	quantity
particle diameter	d	10 μm
particle density	ρ_p	1000 kg/m^3
particle response time	τ_p	5.5 μs
imaging frequency	f	2000 Hz
time separation	Δt	0.5 ms
field of view	FOV	$\approx 40 \times 25$ mm
magnification	M	0.55
f-stop		≈ 12
laser sheet width		≈ 10 cm
laser sheet thickness		≈ 1 mm
sensor size		22x22 mm^2
sensor resolution		2016 x 2016 px cropped to 2016 px wide, 1200 px high
recording time		≈ 0.12 s
number of images per trial		≈ 250

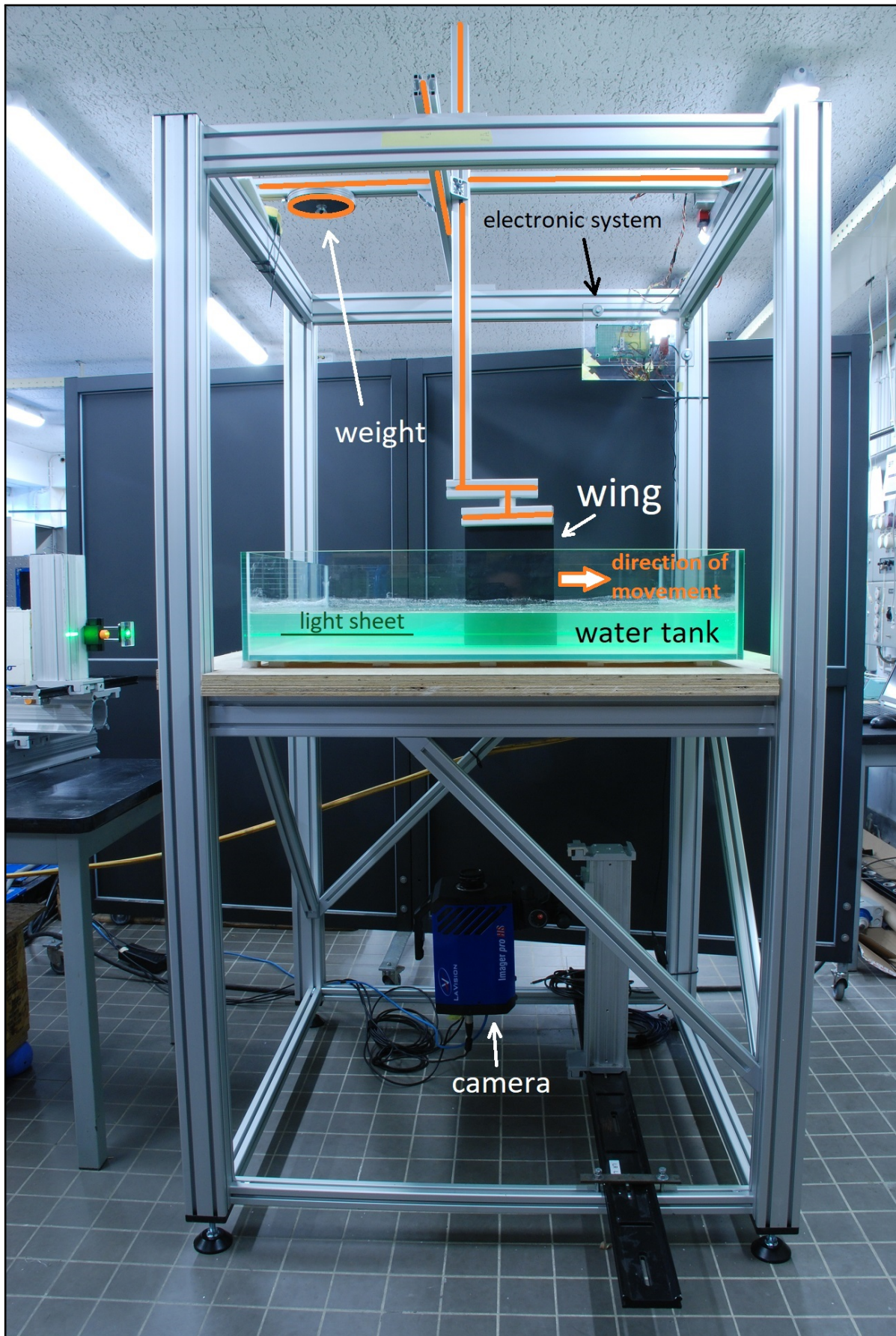


Figure 2.21: A photograph of the experiment setup used for the present research. The main parts of the setup are indicated by text. The orange-coloured beams constitute the moving part of the setup, to which the wing is attached.

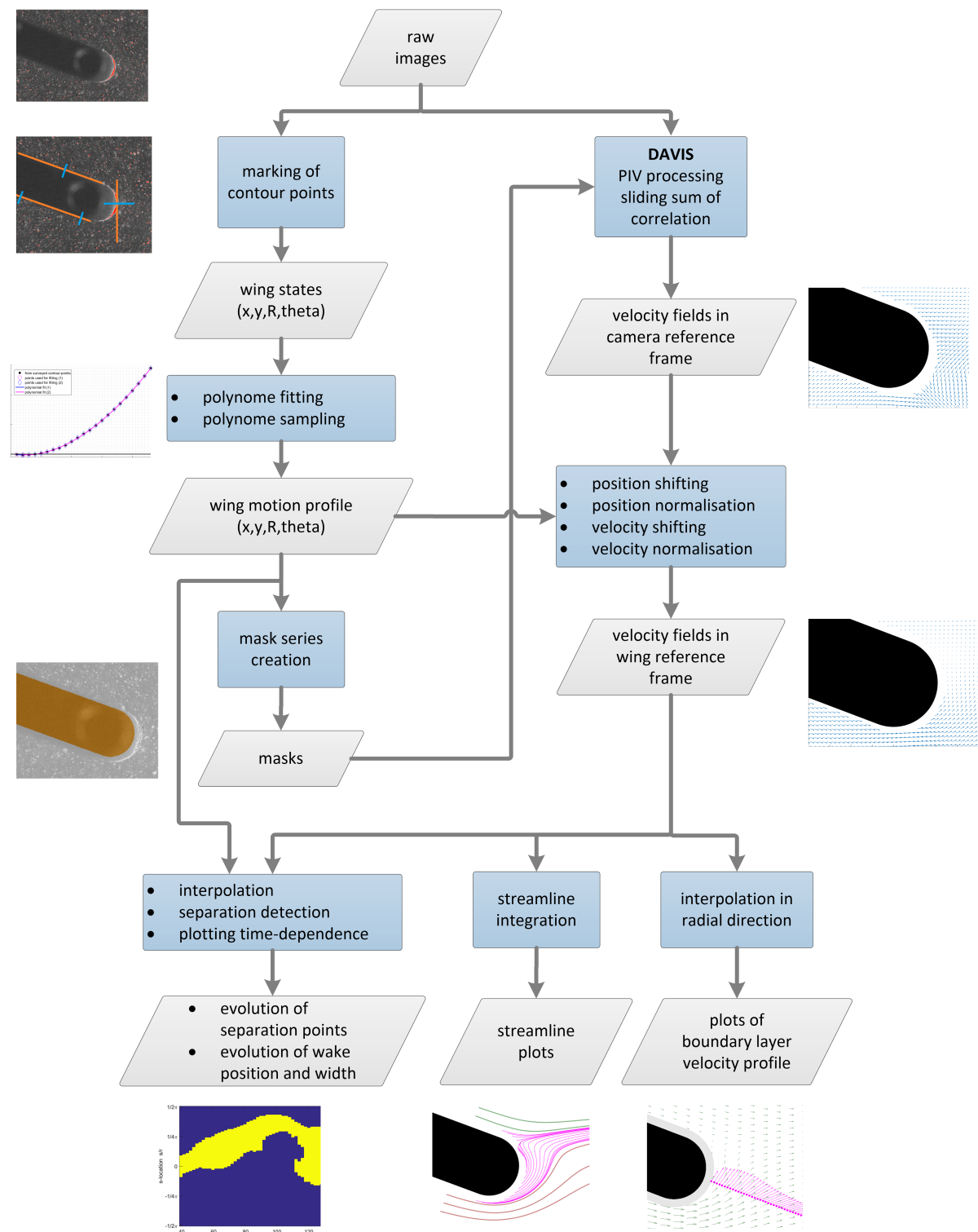


Figure 2.22: A diagram which illustrates how raw images are processed to flow visualisations. Dark-blue blocks represent processing steps. Light-blue blocks represent data, which are the inputs and outputs of processing steps. Some intermediate results are illustrated by images on the left and right sides of the diagram.

2.6. PIV processing methods and tools

The previous section discussed an experimental setup which is capable of producing images of particles. A number of data transformations are required before results are obtained which are suitable for answering the research questions. This section discusses the processing steps, the methods and the tools which serve to bridge the gap between PIV images and flow visualisations. A graphical overview is presented in Figure 2.22. All processing steps and intermediate results in that diagram are discussed in this section. The content of this section roughly complies to the data flow in the diagram. The reader is encouraged to have a look at the diagram first, because it will be helpful to understand the relations between the pieces of content of this section.

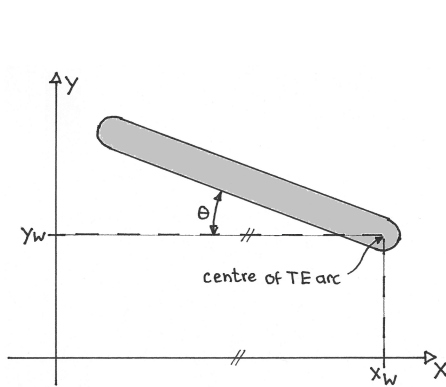


Figure 2.23: Definition of the wing's position and orientation w.r.t. the inertial reference frame; this is used in processing the PIV images recorded by the experiment setup. Since the displacement of the wing is important (not the absolute position) it does not matter where the origin is located.

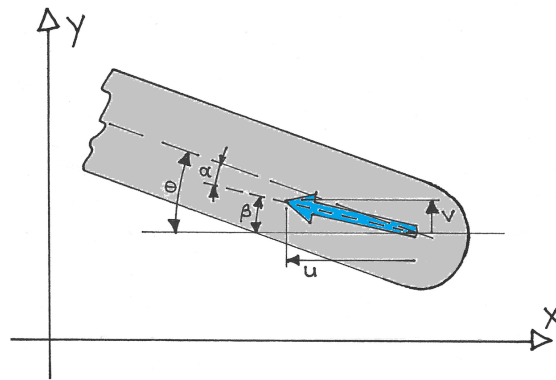


Figure 2.24: Definition of the wing's motion w.r.t. the inertial reference frame; this is used in processing the PIV images recorded by the experiment setup. Although a linear horizontal motion was envisaged during the design of the experimental setup, the actual motion involved both a horizontal and a vertical component, which are indicated by u and v . The blue arrow indicates the (instantaneous) direction of motion. The parameters α , β and θ denote angle of attack, flight path angle and incidence angle, respectively.

2.6.1. Measurement of wing motion

Knowledge of the position and orientation of the wing on each image is needed for two purposes: First, for producing a mask image that can be loaded in DAVIS (the software package used for processing the PIV-images in order to obtain velocity fields) to exclude the part of the image containing the wing from the processing; second, to determine the velocity and angle of attack of the wing.

Parameterisation. The position and orientation of the wing is described by three parameters. The position of the wing is defined by the position of the centre of the trailing edge arc. The orientation, or incidence angle, is defined as the angle between the horizon and the flat bottom part of the wing. One additional parameter is needed to determine the size of the wing on the image: the wing thickness, which is defined as the distance between the upper and lower flat parts of the wing, measured normal to the wing surface. For convenience we parameterise this dimension by the radius of the circular arc, which is equal to half the wing thickness. So there are four parameters to describe the position, orientation, and size of the wing: the horizontal position of the centre of the trailing edge arc x_W , the vertical position of that point y_W , the radius of the trailing edge arc R and the angle of incidence of the wing w.r.t. the horizon θ . This definition is illustrated in Figure 2.23.

Measurement of wing location on an image. A procedure was designed to determine the parameter set (x_W, y_W, R, θ) from four points marked on the contour of the wing. Figure 2.25 illustrates the markings: one point on the left-bottom, one point on the right-bottom (but still on the straight part), one point at the right-most part of the wing (touching the trailing edge arc) and one point on the top-middle of the wing. These points are found and marked manually on a raw image and their coordinates are noted. A computer script

was programmed to find the values of the (x_W, y_W, R, θ) parameters from the four contour points. Part of the algorithm is illustrated by Figure 2.26. Figure 2.27 shows how a wing at certain position, incidence angle, and thickness is fitted to the marked points.

Calibration. Pictures of a calibration plate were taken during the measurement campaign to facilitate the mapping of pixel coordinates to physical space. The calibration plate has an array of white points distributed uniformly with known spacing on a black background. The image of this plate is used to determine the ratio of physical length to pixel spacing. Although the calibration plate allows to correct for non-linear distortions, no such corrections are applied. This is justified by the assumption that image distortion is negligibly small because the camera axis is normal to the water tank and the field of view angle is small ($<5^\circ$).

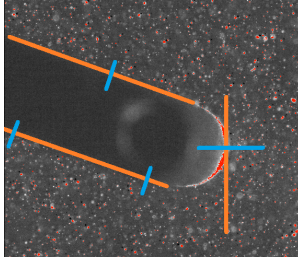


Figure 2.25: Markings on the wing contour on a raw PIV image. They were made by hand using Microsoft Paint.

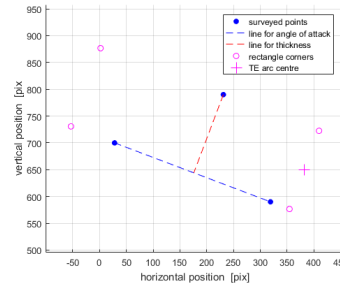


Figure 2.26: Illustration of lines used by the author's algorithm for determining the position and orientation of the wing from the marked contour points.

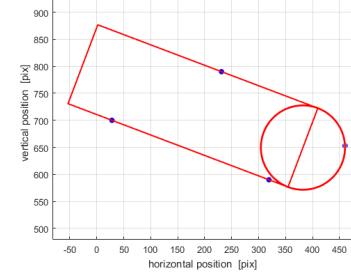


Figure 2.27: Illustration of how the wing contour (modelled by a rectangle and a circle) is fitted to the contour points marked on the raw PIV image.

Fitting of wing motion profile. Values of the (x_W, y_W, R, θ) parameters are wanted for each image in the time-series; that amounts to 250 sets of parameter values. This is achieved by determining the parameter values for every 10th image of the image-series, then fitting curves to the samples, and sampling this curve for each image of the complete series of images. Thus, 25 sets of parameter values serve as basis for 250 sets of parameter values. The x_W and y_W parameters are treated with 4th degree polynomials. The R and θ parameters are treated with 3rd degree polynomials. This process results in a set of precise (x_W, y_W, R, θ) values for each image of the image series. Figures 2.28 to 2.31 show the sets of (x_W, y_W, R, θ) parameters which are obtained for every 10th image and the lines fitted through them.

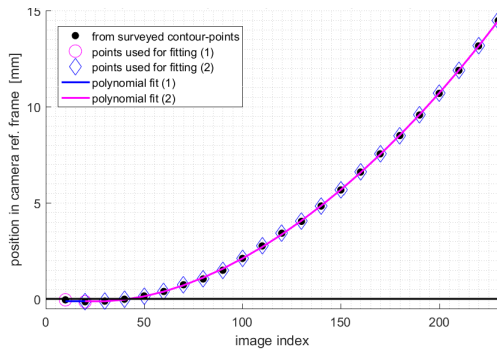


Figure 2.28: Fit of the horizontal position parameter x_W . Note that the beginning of the motion (represented by the first two data points) are treated by a linear fit while the remainder of the data points are fitted by a quartic. This is because the motion of the wing did not start at the first data-point but at a 'later' point. Standard deviations for the first fit, second fit, and overall fit are 0.071, 0.034 and 0.037 respectively.

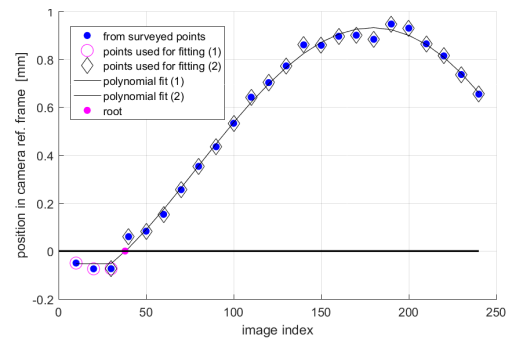


Figure 2.29: Fit of the horizontal position parameter y_W . The separation of fits mentioned for Figure 2.28 also applies here. Standard deviations for the first fit, second fit, and overall fit are 0.014, 0.022 and 0.021 respectively.

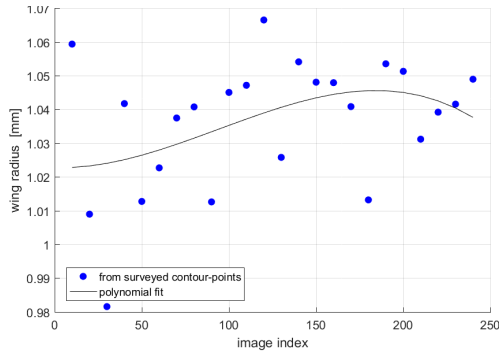


Figure 2.30: Fit of the radius parameter R . The points were fitted with a cubic, with a standard deviation of 0.018

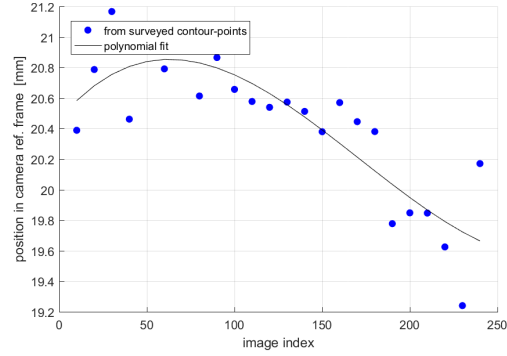


Figure 2.31: Fit of the incidence parameter θ . The points were fitted with a cubic, with a standard deviation of 0.23.

Determination of acceleration. The magnitude of the acceleration of the wing, which is wanted because it is supposedly an important factor for the evolution of the flow-field (see Sections 2.2 and 2.3), is determined by fitting a second-order polynomial to the measured horizontal wing positions. The wing is actuated by a falling weight, which moves due to the gravitational attraction, so the wing's acceleration is assumed to be constant. The proportion between the magnitude of the gravitational acceleration and the wing's acceleration depends on the proportion between the rotational inertia of the wing actuation system about the hinge axis and the inertia of the falling weight. MATLAB's `polyfit` function was used to fit a quadratic to the measured x_W data, as depicted in Figure 2.32. The magnitude of the horizontal acceleration is determined by rewriting the formula for the relation between position and time of a uniformly accelerated object (2.25), (where a is the acceleration and s is the displacement w.r.t. the location which the object had before the acceleration started), in the form of a quadratic equation (2.26). The result is (2.27) which gives the acceleration from the coefficients of the fitted quadratic. Note that since a pure uniformly accelerated motion is expected, the f and g coefficients of the fitted polynomial are neglected.

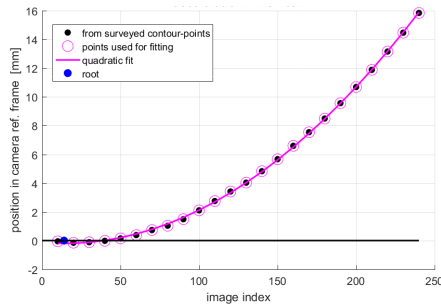


Figure 2.32: Fit of a quadratic to measured horizontal wing positions. The quadratic's coefficients are used to determine the wing's acceleration; see Equations 2.25-2.27.

$$s = 1/2 \cdot a \cdot t^2 \quad (2.25)$$

$$s = et^2 + ft + g \quad (2.26)$$

$$1/2 \cdot a \cdot t^2 = et^2 \quad \Rightarrow \quad a = 2e \quad (2.27)$$

Determination of velocity and angle of attack. Besides the need of values of the (x_W, y_W, R, θ) parameters for producing mask images, the position and orientation data is also used to determine the velocity and the angle of attack of the wing throughout the motion. The horizontal and vertical components of the velocity are obtained by numerical differentiation of the position as in (2.28). The flight path angle β of the wing is determined from the velocity components with (2.29). Subtracting the flight path angle from the incidence angle θ results in the angle of attack α (2.30).

$$u_W = \frac{\Delta c_x}{\Delta t} \quad v_W = \frac{\Delta c_y}{\Delta t} \quad (2.28)$$

$$\beta = \tan^{-1} \left(\frac{v_y}{v_x} \right) \quad (2.29)$$

$$\alpha = \theta - \beta \quad (2.30)$$

2.6.2. Masking of wing in PIV images

Using the ≈ 250 sets of (x_W, y_W, R, θ) values a wing mask image is made for each PIV-image. In this way a series of ≈ 250 mask images is made that covers the wing on the PIV images with a discrepancy of $O(10)$ pixels, which is $\approx 10\%$ of the wing thickness on the image. The masking was checked by semi-transparent overlaying of mask images and raw images (Figures 2.33 and 2.34).

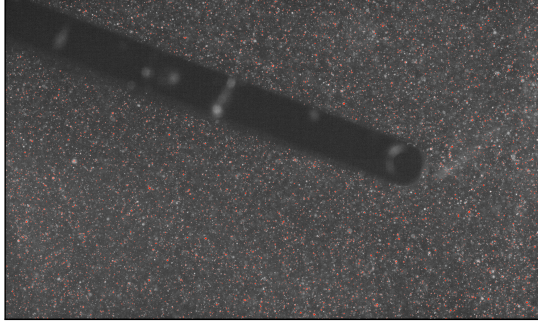


Figure 2.33: Example of a raw image acquired by the high-speed camera during the experiment. (The image corresponds to $I=50$ on the timeline on p. 77.)

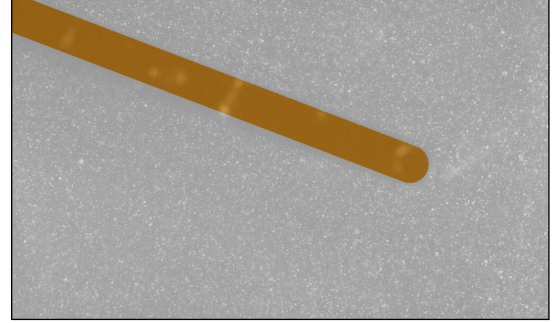


Figure 2.34: Overlay of a mask on its corresponding raw image (see Figure 2.33). Such overlays were used for checking the position, orientation, and size of the masks before using the masks in the calculation of velocity vector fields.

2.6.3. Calculation of velocity fields by PIV algorithm

The raw PIV images are pre-processed by a *Butterworth filter* to increase contrast between particles and everything else that is visible on the raw image. A *sliding sum-of-correlation* method is used to calculate velocity fields from the PIV images. According to [25], this method: “consolidates correlation peak height while averaging over random background correlation noise. Using sum-of-correlation on as few as two correlations can substantially improve peak to background noise ratios and displacement accuracies.” This method takes one image (I_A) at time t_A and another image (I_B) at time $t_B = t_A + N_{\Delta t} \cdot \Delta t$ where $N_{\Delta t}$ is an integer and Δt is the time separation between two sequential images in the time-series. Each image pair (I_A and I_B) produces a correlation map R_A . The correlation maps for successive image pairs are averaged, in the sense that the velocity field for image I_A at time t_A is determined from an average correlation map R which is the average of the correlation maps of an integer number N_R of image pairs, centered around I_A . The method is illustrated in Figure 2.35. A large value of $N_{\Delta t}$ is preferred because this increases sensitivity (and reduces uncertainty) of velocity measurement. At the same time, $N_{\Delta t}$ should not be so large that particles move out of an interrogation window between t_A and t_B because this will prevent the calculation of meaningful cross-correlation maps. This is most likely to occur at points in the flow-field where flow velocities are largest. So the value of $N_{\Delta t}$ is limited by the maximum flow velocity that is expected. In order to guarantee proper velocity measurement, $N_{\Delta t}$ is chosen such that a particle will not move more than 75% of the width of an interrogation window, so at least $\approx 25\%$ of the particles will remain in their interrogation window everywhere in the domain. It is suboptimal to use a fixed value of $N_{\Delta t}$ for the whole time-series because the flow velocity varies with approx. two orders of magnitude throughout the time-series. Therefore different values of $N_{\Delta t}$, ranging between 5 and 1, are used for different parts of the time-series. The range of images to be analysed with a specific value of $N_{\Delta t}$ is determined by solving (2.31) and (2.32). In these equations, $V_{f,\max}$ is the maximum velocity expected in the flow-field; s_{\max} is the maximum allowed displacement of a particle; w_{IR} is the physical width of an interrogation window; $V_{w(I)}$ is the wing velocity as function of image index where I denotes

the image index¹⁴; $\left(\frac{V_f}{V_w}\right)_{\max}$ is the maximum value of the ratio of flow velocity on the surface of the wing to wing velocity, which is determined from potential flow analysis.¹⁵ A summary of the processing operations performed on the PIV images is presented in Table 2.7.

$$V_{f,\max} = \frac{s_{\max}}{N_{\Delta t} \cdot \Delta t} = \frac{w_{\text{IR}} \cdot 0.75}{N_{\Delta t} \cdot \Delta t} \quad (2.31)$$

$$V_{f,\max}(I) = \frac{V_w(I)}{\left(\frac{V_f}{V_w}\right)_{\max}} \quad (2.32)$$

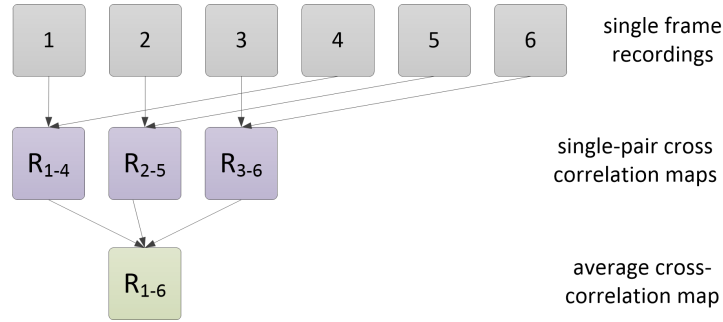


Figure 2.35: Illustration of the *sliding-sum-of-correlation* method. In this example, single images from the time-series are taken with a spacing of 3 images (i.e. $N_{\Delta t} = 3$) to produce single-pair correlation maps. Three of such correlation maps are averaged (i.e. $N_R = 3$). The resulting average correlation map (R_{1-6}) is in this example used to calculate the velocity field corresponding to image 2. The diagram is inspired by (Raffel et al., 2018, p. 188).

Table 2.7: Table of parameters for the calculation of vector fields from the PIV images taken in the experiment that was done for this research.

operation #	operation / parameter
operation 1	subtract minimum (Butterworth filter) filter length: 7
operation 2	apply mask from file
operation 3	sliding sum of correlation averaging length (N_R): 3 (I=1-46), 2 (I=47-240) correlation mode: cross-correlation correlation length ($N_{\Delta t}$): 5 (I=1-46), 3 (I=47-64), 2 (I=65-88), 1 (I=89-240) number of passes: 2 first pass: 128x128 px rectangular window, 50% overlap second and third pass: 32x32 px rectangular window, 75% overlap

¹⁴This follows from the wing motion profile; see Figure 3.6 on p. 75.

¹⁵The value of this parameter is taken as 3. See Figure 3.18 on p. 84 for an example surface velocity distribution.

2.6.4. Transformation of velocity fields to moving reference frame

The velocity vector fields calculated in DAVIS are transformed from the inertial (or camera) reference frame to the wing reference frame. The reference frames and coordinate systems that are involved are illustrated in Figures 2.3. The transformation of the velocity field is performed by execution of the following four operations: 1) The positions of the velocity vectors are shifted such that the origin of the velocity field is at the centre of the trailing edge arc of the wing, as in (2.33), where the subscript VF denotes the velocity field, W denotes the wing, RF denotes the wing reference frame, and IRF denotes the inertial reference frame. 2) The position coordinates are normalised by scaling them with the trailing edge radius of the wing, R , as in (2.34). 3) The velocity vectors are transformed from the inertial reference frame to the moving wing reference frame by subtracting the wing velocity, as in (2.35), where u and v are the horizontal and vertical components of the velocity, respectively. 4) The velocity vectors are normalised by scaling them with the magnitude of the wing velocity, V_w , as in (2.36). The wing velocity is calculated from the horizontal and vertical components of the velocity which have been determined earlier (Equation 2.28), as in (2.37). Figures 2.36 to 2.38 show exemplary velocity fields. The last two of these pictures clearly show the result of transformation of the vector field from the inertial/camera reference frame to the wing reference frame.

$$\begin{aligned} x_{VF} (WRF) &= x_{VF} (IRF) - x_w (IRF) \\ y_{VF} (WRF) &= y_{VF} (IRF) - y_w (IRF) \end{aligned} \quad (2.33)$$

$$\tilde{x}_{VF} = \frac{x_{VF}}{R} \quad \tilde{y}_{VF} = \frac{y_{VF}}{R} \quad (2.34)$$

$$\begin{aligned} u_{VF} (WRF) &= u_{VF} (IRF) - u_w (IRF) \\ v_{VF} (WRF) &= v_{VF} (IRF) - v_w (IRF) \end{aligned} \quad (2.35)$$

$$\tilde{u}_{VF} = \frac{u_{VF}}{V_w} \quad \tilde{v}_{VF} = \frac{v_{VF}}{V_w} \quad (2.36)$$

$$V_w = \sqrt{u_w^2 + v_w^2} \quad (2.37)$$

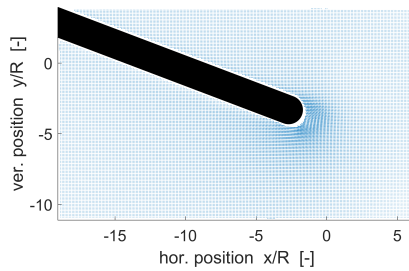


Figure 2.36: Velocity field in camera reference frame. The picture shows the complete extent of the measured field, which is a grid of 252 vectors wide and 150 high. Note that the origin is not at the centre of the trailing edge.

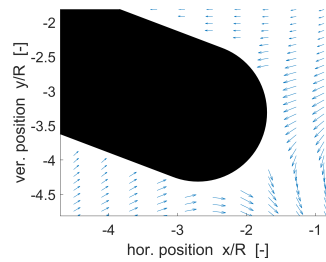


Figure 2.37: Velocity field in camera reference frame, close-up of the region around the trailing edge. Note that the vectors are not tangential to the wing contour.

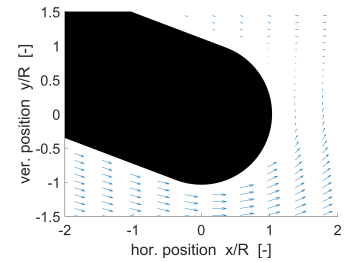


Figure 2.38: Velocity field in wing reference frame, close-up of the region around the trailing edge. The vector field has been transformed, note that the vectors are now tangential to the wing contour.

2.6.5. Interpolation of velocity fields for flow-field analysis

The velocity field in the wing reference frame is interpolated along several so-called “interrogation lines” for the purpose of determining the desired flow-field parameters. One type of interrogation line is tangential to the wing contour, at a fixed distance from the contour. This type is depicted in Figure 2.39. It is defined by three parameters: the distance from the contour r , and the end-point locations s_1 and s_2 . This type of interrogation line is used for determining the velocity distribution over the wing contour, as in the analysis of Section 3.3, and for determining the locations of separation points and the region of separated flow. A second type of interrogation line is the *radial interrogation line* which is perpendicular to the contour. This type is depicted in Figure 2.40. It is defined by three parameters: the distance along the contour s and the locations of the endpoints r_1 and r_2 . This type of interrogation line is used for determining the velocity profile in the boundary layer, for example as in Figure 3.12 on p. 80 and Figure 4.3 on p. 88.

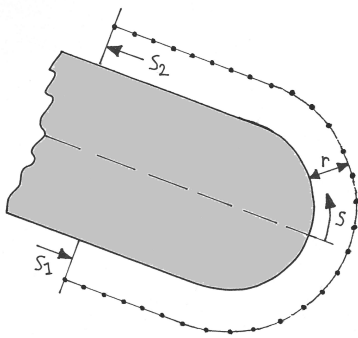


Figure 2.39: Definition of a “tangential interrogation line”. Here r is the distance of the interrogation line from the contour. s_1 and s_2 indicate the begin point and end point of the line on the contour. The arrow next to ‘s’ indicates that s_1 and s_2 are measured from the chord line, counter-clockwise positive.

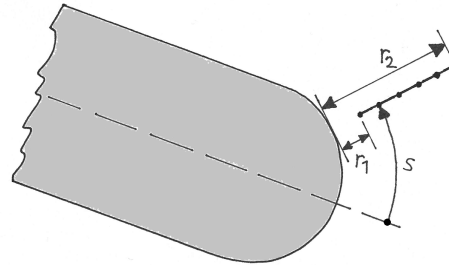


Figure 2.40: Definition of a “radial interrogation line”. Here s indicates the tangential position of the interrogation line. Although the arrow is drawn at a certain distance from the contour, this parameter is measured on the contour, from the chord line, positive in counter-clockwise direction, like in Figure 2.5 on p. 37.

2.6.6. Detection of flow separation

An important aspect of the flow-field which is studied in this research is the occurrence of (unsteady) flow separation. Usual ways of detecting a point of separation which work for steady flows (e.g. by finding the point on the surface of the body where the friction stress is zero) do not work for unsteady flows or require data which is not available in this research. As discussed in Section 1.4.5, the author has not found a method (and corresponding definition) for detection of flow separation in unsteady flow that uses only flow-field data outside the boundary layer.

So we develop a heuristic to detect flow separation. Batchelor (1967, p. 329) writes about flow separation (see Figure 2.41 for an illustration and Koromilas and Telionis (1980) for corresponding photographic evidence):

“In cases of separation from bodies of smooth geometrical form, the surface streamlines are observed to leave the surface more or less tangentially (...). If the streamline leaving the separation point S made an angle with the upstream wall less than 180° , it is readily shown that the external stream velocity, assuming it to be part of an irrotational flow, would be zero at S; there would thus be appreciable deceleration of the external stream before reaching S and, as has been seen, this would lead to back-flow and too great an accumulation of vorticity to be confined within a thin layer. In other words, tangential departure of the boundary-layer streamlines is the only self-consistent possibility in a steady flow.”

We can distinguish two parts in Batchelor’s statement: 1) the hypothesis of tangential streamline departure; and 2) the hypothetical explanation for this, which involves the mechanism of boundary layer stagnation. This last part corresponds to the explanatory theories described in Section 1.4. The first part presents one

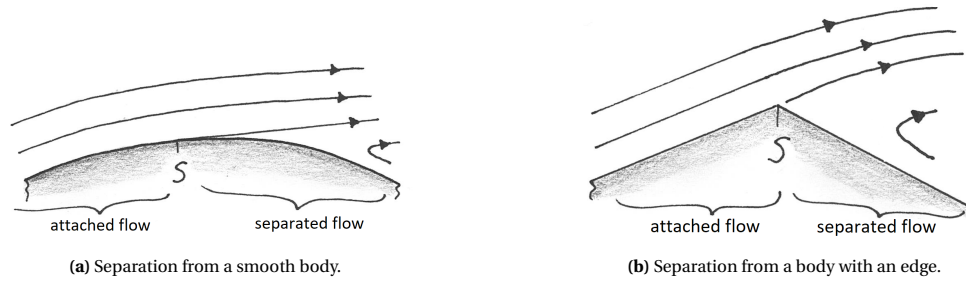


Figure 2.41: Illustration of the property that flow separates from a body in a direction which is tangential to the upstream surface. The point of separation, where a streamline bifurcates from the body, is indicated by 'S'.

Inspired by (Batchelor, 1967, p. 329).

feature useful for defining flow separation.

Preliminary definition of flow separation. I give here a preliminary definition of flow separation by mentioning some characteristics. This is the definition used in the Results and Discussion sections of this report. Note that flow separation contrasts with attached flow; see also Figures 1.10e and 1.10f on p. 18. In a situation of attached flow, the flow is parallel to the body contour, everywhere along the contour. We may define this somewhat more precisely by stating that fluid which is close to the body (say, at a distance of less than $1/10$ th of the local wall curvature or less than $1/10$ th of the length of the body) moves in a direction which is tangential to the local wall. We can then define flow separation as the existence of a region in the domain where this is not the case. In this finite region, flow is not parallel to the local wall. There must be some point or zone of transition between the regions of attached and separated flow. With respect to the region of separated flow the transition is located upstream (w.r.t. the main flow direction). Using this definition of flow separation, we can identify undesired flow separation. However, we cannot distinguish undesired flow separation from flow in the vicinity of a stagnation point (which may be attaching flow in the case of a front stagnation point or un-problematic separation in case of a rear stagnation point).

Finding separation point from streamfunction. In a potential flow case the following method can be used to determine the location of a stagnation point: the streamfunction Ψ is calculated for the domain and the points where $\Psi = 0$ are sought. Drawing a line through these points results in obtaining the dividing streamline, which runs from the stagnation point on the body into the domain (Anderson, 2011, p. 177, 255). Let us call this method the “streamfunction method”. The author tried this method but it does not give satisfactory results. It always results in one streamline (see Figure A.1), even in case a wake is present behind the body and two separation points are actually present (see Figure A.2). We may interpret the single streamline as representing the average location of the upper and lower separation points. However, we are interested to determine the location of the upper- and lower separation points. The distance between these points is related to the width of the wake. A different method is required to obtain this information. The reader is referred to Appendix A for illustrations and more information about the implementation of the streamfunction method.

Proposed method for determination of separation. The present author produced an algorithm which determines whether flow is separated or attached in a certain location based on the direction and magnitude of the velocity vector at that location. Let us call this the “direction and speed method”. The algorithm is quite simple and is computationally much cheaper compared to the methods mentioned in Section 1.4.5. Assume that we want to know whether flow is attached or separated at point P and assume that we possess a velocity field such that we can determine the direction and magnitude of velocity at P (see Figure 2.42c), and assume that we know the direction of the contour of the body which is present in the flow field.¹⁶ We determine a location on the body, called P_b , from which a line perpendicular to the body will intercept P (see Figure 2.42b). We then determine the direction of the body contour at P_b . The direction of flow and the direction of the

¹⁶Point P (see Figure 2.42a) should not be far away from the contour; it should lie within the ‘region of influence’ of the body, where streamlines are oriented parallel to the body in case of attached flow. As a rule of thumb we may assume that r should not be larger than $1/10$ th of the length of the body.

body at P_b are both measured w.r.t. the same line (e.g. the horizon) and are called θ_f and θ_b respectively. The difference in direction is calculated according to (2.38). The magnitude of the velocity at P , denoted by V_p , is also measured, and a velocity fraction, denoted by \tilde{V} , is calculated according to 2.39, where V_{ref} is a reference velocity which should be representative for the main stream velocity in the neighbourhood of P .

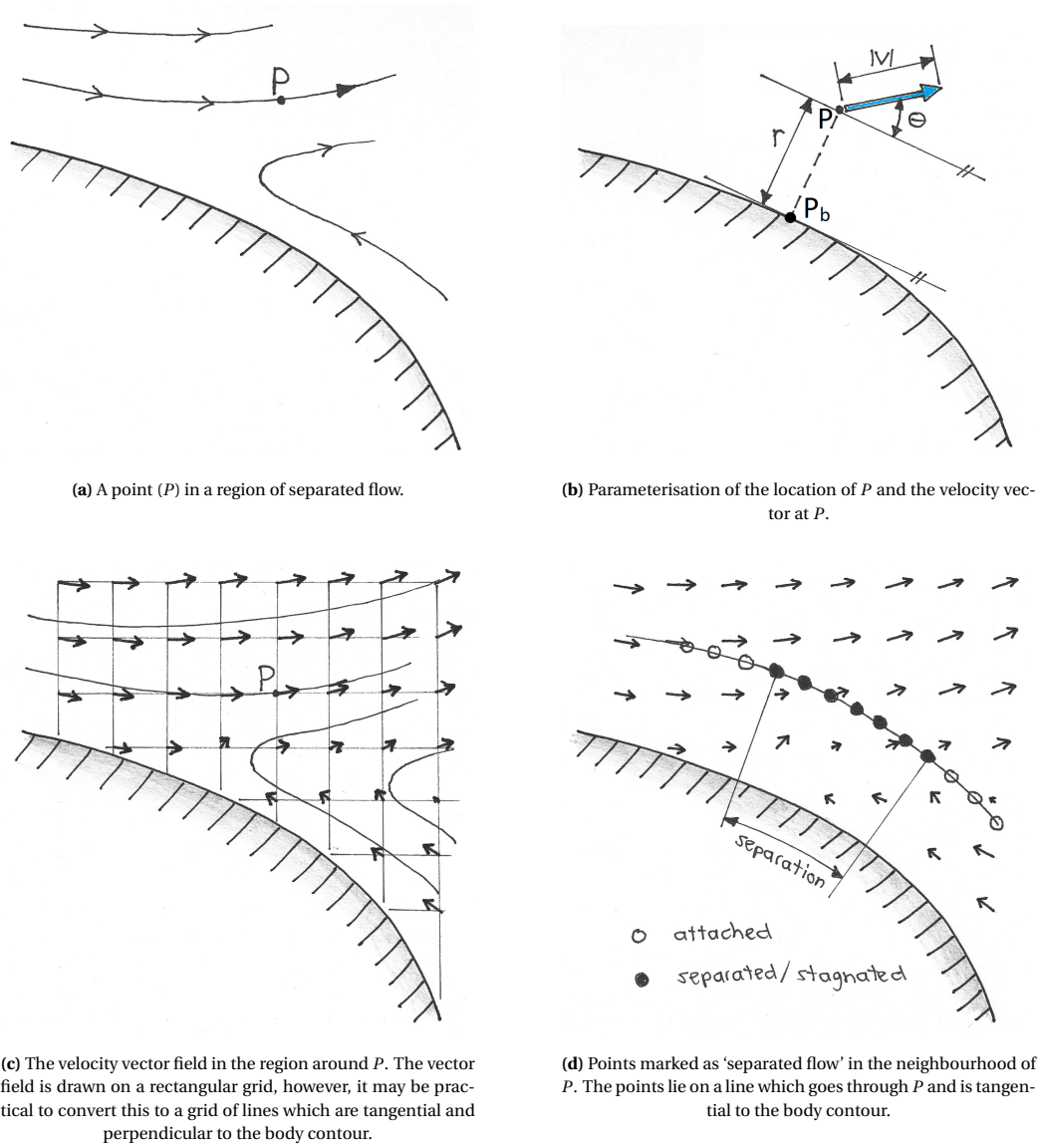


Figure 2.42: Illustration of the parameterisation corresponding to the proposed method for detection of flow separation.

$$\Delta\theta = |\theta_f - \theta_b| \quad (2.38)$$

$$\tilde{V} = \frac{V_P}{V_{\text{ref}}} \quad (2.39)$$

Determination of flow separation is based on two criteria: deviation of flow direction and reduced velocity¹⁷. We want a method which identifies the flow as separated when either the direction deviation surpasses a threshold value (denoted $\Delta\theta_{\text{max}}$) or when the velocity is below a threshold value (denoted by V_{min}) or in cases when the direction deviation and the velocity do not exceed their threshold values individually but are both close to the threshold values. The detection of reduced velocities is wanted to be able to detect a wake.

¹⁷It follows that point P should not lie in the boundary layer because this would lead to the flow being qualified as stagnated.

Such behaviour is represented by (2.40) and (2.41) and is graphed in Figures 2.43 and 2.44. The parameters S_a and S_v represent the ‘components’ of separation due to direction deviation and velocity, respectively. Their value is always between 0 (corresponding to attached flow) and 1 (corresponding to separated flow). The values of these parameters are combined according to (2.42) and (2.43) in order to produce a single separation parameter S . The value of S is also between 0 and 1. Since the final result of the determination should be binary (either attached or separated), some sort of rounding operation is necessary, according to (2.44). For threshold values $\Delta\theta_{\max} = 30^\circ$ and $\left(\frac{|V|}{V_{\text{ref}}}\right)_{\min} = 0.1$ and rounding threshold $p = 0.9$ the map shown on Figure 2.45 is produced which shows what combinations of flow angle deviation and velocity fraction are marked as separated flow.

Operations (2.40) to (2.44) can be applied to a series of points, for example points on a line which is tangential to the contour, close to the body (see Figure 2.42d). When this is applied in a region where a stagnation point is expected, the location of the stagnation point may be approximated by the “centre of mass” of the locations which are marked as separation.

$$S_a = \min\left(1, \frac{|\Delta\theta|}{\Delta\theta_{\max}}\right) \quad (2.40)$$

$$S_v = \min\left(1, \frac{V_{\min}}{|V|}\right) \quad (2.41)$$

$$A = A_a \cdot A_v \quad A_a = 1 - S_a \quad A_v = 1 - S_v \quad (2.42)$$

$$S = 1 - A$$

$$S = 1 - A_a \cdot A_v$$

$$S = 1 - (1 - S_a) \cdot (1 - S_v) \quad (2.43)$$

$$\begin{aligned} S_r &= 1 & \text{if} & & S &\geq p \\ S_r &= 0 & \text{if} & & S &< p \end{aligned} \quad (2.44)$$

Since in the present research the part of the velocity field that is closest to the wing is not obtained by PIV (due to practicalities and due to masking) the velocity field at a certain distance (denoted by r) from the contour is used for detecting flow separation. However, a sensitivity analysis proved that the method is insensitive to changes in r for $0.3 < r/R < 0.5$. The V_{\min} threshold is set at 10% of the mean velocity of the flow around the trailing edge. The $\Delta\theta_{\max}$ parameter is set at 30° , which is chosen such that the region marked as separated flow complies with the width of the wake as observed on streamline plots and on the movie of PIV images.

Validation. Validation of this method is required before its results can be relied upon. No extensive validation was done¹⁸, but three analysis were made which indicate that the results of the method are sensible. The first analysis is a comparison of the results of this method with results of the streamfunction method. The second analysis is an analysis of the sensitivity of the method w.r.t. values of the (threshold) parameters on which it depends. The third analysis is a comparison of results of the method with flow field features which are observed on PIV images. These analyses are presented in Appendix B.

¹⁸Note that validation of a method for identifying flow separation requires that definitions of ‘flow separation’ and ‘separation point’ in case of undesired flow separation are agreed upon first. Otherwise it is not possible to produce a reference case with known points of flow separation and known regions of separation against which the results of a method can be checked. Since apparently no universally accepted definition of those terms is present at this moment (which is mentioned in Section 1.4.5) an extensive validation may be challenging.

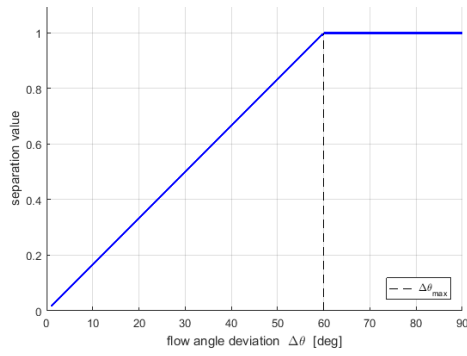


Figure 2.43: The influence of flow angle deviation on the identification of separation: the relation between S_a and $\Delta\theta$.
In this example $\Delta\theta_{\max} = 60^\circ$.

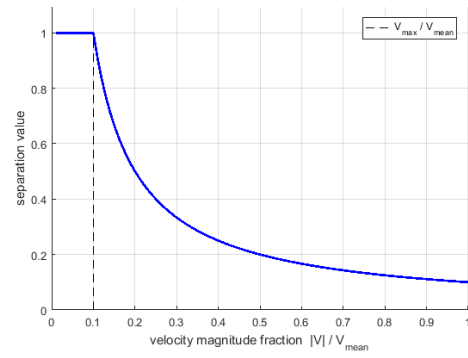


Figure 2.44: The influence of flow velocity magnitude on the identification of separation: the relation between S_v and V .
In this example $|V|_{\min} = 0.1 \cdot |V|_{\text{mean}}$.

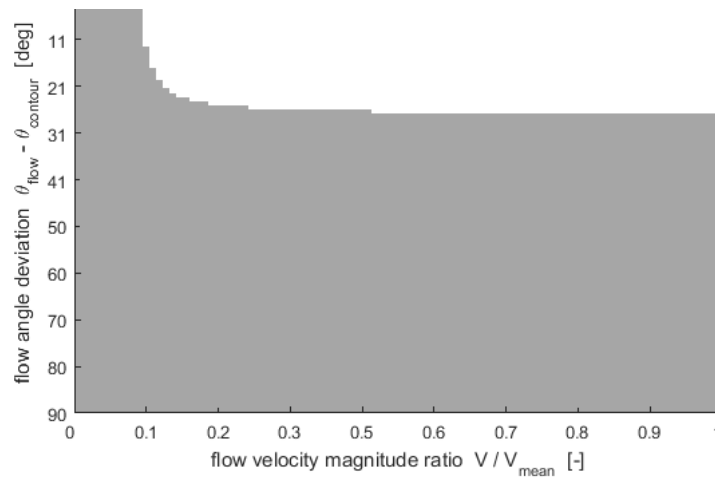


Figure 2.45: A map showing which combinations of values of flow angle deviation and velocity fraction are marked as separation. The dark area represents separation; the white area represents attached flow. The threshold values are set at: $\Delta\theta_{\max} = 30^\circ$, $|V|_{\min} = 0.1 \cdot |V|_{\text{mean}}$, $p = 0.9$.

2.6.7. Determination of streamline curvature

One of the properties of the steady-state Kutta condition flow-field is represented by the direction of flow which separates from the trailing edge along the upper and lower wing surfaces; as discussed in Section 1.3. We will check whether the flow-field exhibits ‘smooth flow-off’ by monitoring the curvature of streamlines above and below the trailing edge.

The radius of curvature of a streamline at a certain point is determined by taking two points (points A and B in Figure 2.46, the first point being at the location where the streamline curvature is desired), interpolating the velocity field at both points, and calculating the difference in direction of the interpolated velocity vectors. The locations of Points A and B are defined by the values of parameters Δr and d , as illustrated by Figure 2.46. The angles of the vectors w.r.t. the line going through A and B are denoted by θ_1 and θ_2 , see also Figure 2.47 and (2.45). The difference in angle, γ , is used to construct a triangle as depicted in Figure 2.48. In this picture the velocity vectors have been rotated towards the line going through A and B such that the vector at A is parallel to that line although the difference between the directions of the vectors remains the same. Lines perpendicular to the velocity vectors, going through A and B, will intersect at C if the velocity vectors are not parallel. The distance between the point of intersection and the line between A and B (measured normal to that line) is the radius of curvature (2.46). The radius of curvature of the streamline R_{str} is normalised w.r.t. the radius of curvature of the trailing edge R using (2.47)¹⁹ for convenience in graphing and interpretation. A value of $\tilde{R}_{str} = 0$ corresponds to a straight streamline (note that in that case $R_{str} = \infty$) and $\tilde{R}_{str} = 1$ corresponds to a streamline whose radius of curvature is equal to the distance between point A and the centre of the trailing edge, so a streamline which is concentric with the trailing edge.

$$\begin{aligned}\gamma &= \theta_2 - \theta_1 \\ &= \tan^{-1} \left(\frac{V_{B,y}}{V_{B,x}} \right) - \tan^{-1} \left(\frac{V_{A,y}}{V_{A,x}} \right)\end{aligned}\quad (2.45)$$

$$R_{str} = d \cdot \tan(1/2\pi - \gamma) \quad (2.46)$$

$$\tilde{R}_{str} = \frac{1 + \Delta r}{R_{str}} \quad (2.47)$$

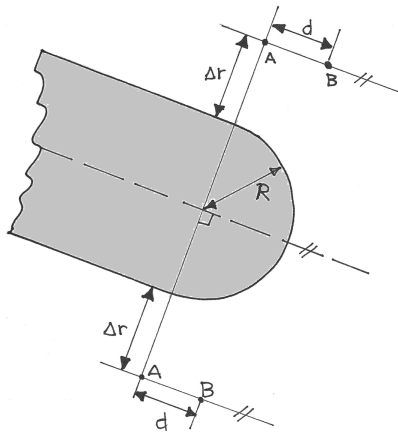


Figure 2.46: The definition of the location of velocity vectors which are used for determination of the local radius of curvature of streamlines at locations A, above and below the trailing edge.

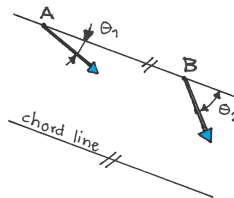


Figure 2.47: Measurement of the angles of the velocity vectors at A and B w.r.t. the chord line.

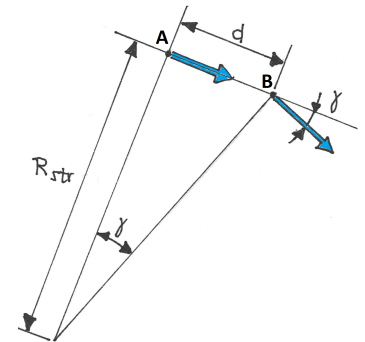


Figure 2.48: The geometry of the problem of determining the local radius of curvature of a streamline. Point A is the point of interest.

¹⁹Note that R is taken as 1 since all distances are normalised by the trailing edge radius in the PIV-processing calculations.

3

Results

This chapter presents results, which are divided in three parts. A roadmap of this chapter is presented in Figure 3.1. First, surface velocity distributions have been calculated for two airfoils and for various trailing edge radii, using the panel method, in order to determine the dependence of the trailing-edge flow-field on the overall airfoil shape and on the radius of curvature of the trailing edge. These results are presented in Section 1 of this chapter.

Second, the velocity fields measured using the experimental setup with PIV equipment have been processed in order to produce flow-field visualisations of various forms. These results show the transformation of the flow-field from an initial flow-field towards a steady flow. This is presented in Section 2.

The third section of this chapter presents a comparison between surface velocity distributions from the panel method calculation and ‘close-to-the-surface’ velocity distribution obtained from the empirical data. This will reveal whether the panel method is a suitable model for calculation of the initial trailing edge flow-field.

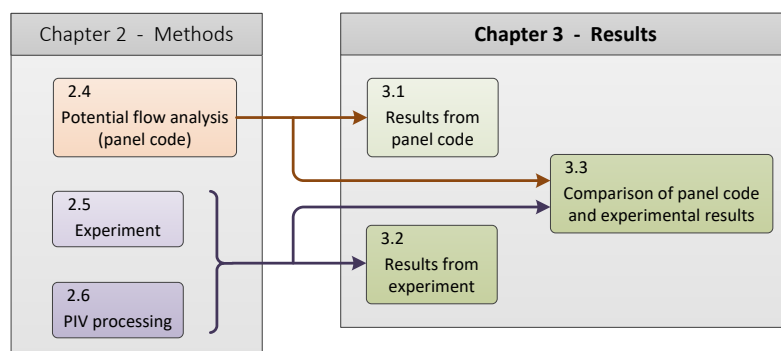


Figure 3.1: Roadmap showing how the sections of this chapter correspond to the sections of Chapter 2 of this report. The numbers indicate chapters/sections in this report.

3.1. Panel method results

The flows over the rounded flat plate and the NACA-0012 airfoil with rounded trailing edge presented on Figures 2.7 and 2.10 on pages 45 and 46 respectively are calculated using the panel method presented in Section 2.4. This method uses a boundary condition of zero total circulation. Both airfoils have a trailing edge radius of $R/c = 0.5\%$. The angle of attack for these calculations is 10.6° . The reason for choosing this value is clarified in Section 3.3. The situation is sketched in Figure 3.2. Graphs of the chordwise distribution of pressure coefficient¹ are shown in Figures 3.3 and 3.4. Note that for the rounded flat plate the C_p -distribution is symmetrical about the mid-chord position, which is expected because the airfoil geometry - and thus the boundary conditions of the problem - are symmetrical. The upper side has a suction peak at the leading edge and a stagnation point at the trailing edge. The lower side has a stagnation point at the leading edge and a suction peak at the trailing edge. The pressure distribution over the rounded airfoil is similar in shape. The leading edge suction peak is less tall and wider compared to that of the rounded flat plate. The pressure distributions in the trailing edge region are very similar in shape and also in magnitude. The stagnation point is located approximately at the point where the circular arc attaches to the upper flat part of the airfoil. The larger the angle of attack, the more close to the leading edge is the location of the stagnation point².

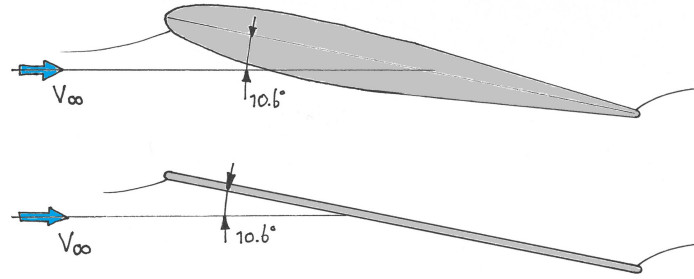


Figure 3.2: Sketch of the NACA 0012 with rounded trailing edge and the rounded flat plate at 10.6° angle of attack in a uniform free stream, corresponding to the analyses presented in this section. The free-stream direction is indicated by the arrows and denoted by V_∞ . The position of the front and rear stagnation points are indicated by the attaching streamline at the front and the separating streamline at the rear of the airfoils. The sketch is approximately to scale, in the sense that positions, thicknesses, and angles are representative; however, the airfoil and streamline shapes on this sketch should not be taken as reference.

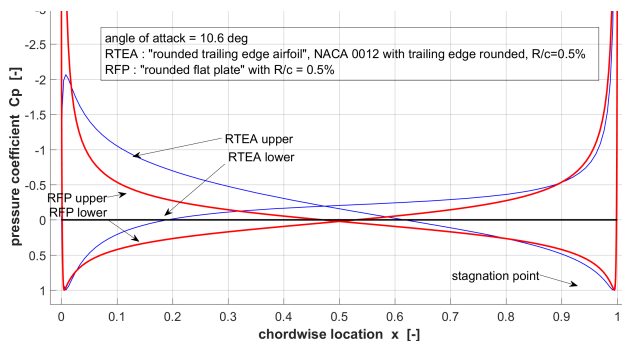


Figure 3.3: Pressure distributions over a rounded flat plate and a NACA-0012 with rounded trailing edge at 10.6° angle of attack in case of zero circulation, calculated by the panel method presented in Section 2.4. The trailing edge radius is 0.5% of the chord length for both airfoils. Note that the pressure distributions in the trailing edge region are very similar.

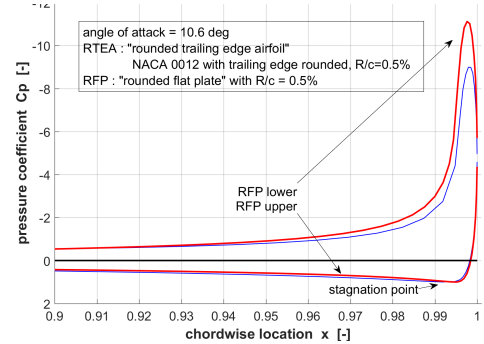


Figure 3.4: Detail of the pressure distribution of Figure 3.3 in the trailing edge region. The distributions are qualitatively the same, but the suction peak is $\approx 15\%$ larger on the rounded flat plate.

¹The distribution of pressure coefficient is also referred to as “ C_p distribution” or “pressure distribution”.

²See Figure 3.20 on p. 84 for a graph of this relationship.

Figure 3.5 presents the velocity distributions over the trailing edges of a set of NACA 0012 airfoils at an angle of attack of $\alpha = 9.1^\circ$.³ The trailing edges of the airfoils are rounded with different radii ($R/c = 1/4\%$, $1/2\%$, 1% , and 2%). The airfoils are depicted in Figure 2.10 on p. 46. The coordinate system used here is the (s, r) coordinate system shown on Figure 2.5 on p. 37. The velocity distributions are qualitatively similar. The magnitude of the velocity maximum differs by slightly less than a factor 2 between the cases of smallest and largest value of R/c ; its tangential position differs a little bit. The tangential location of the stagnation point varies, but that is because the s -coordinate depends on the radius of curvature. In terms of (x, y) coordinate the stagnation point location is more constant. We conclude that the main influence of increasing or decreasing the radius of curvature of the trailing edge is decreasing resp. increasing the magnitude of the velocity maximum.

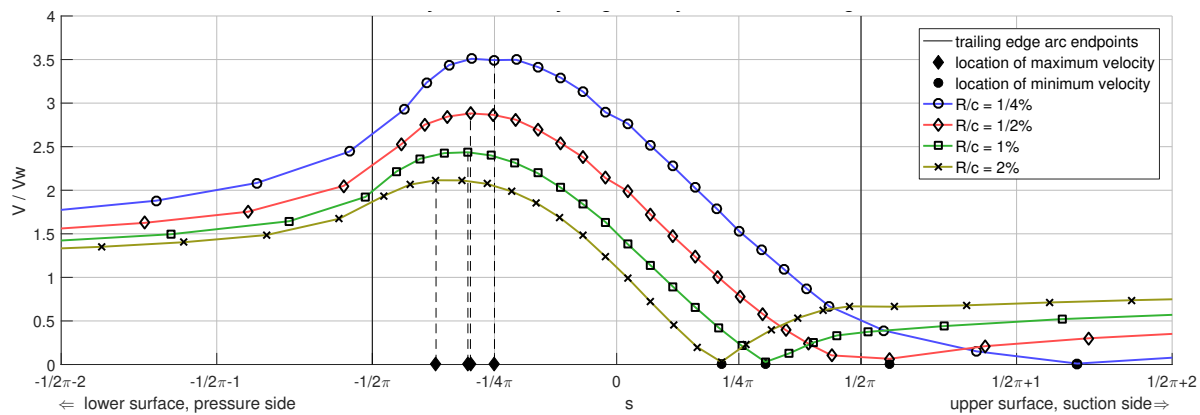


Figure 3.5: Calculated theoretical velocity distributions over the trailing edges of NACA 0012 airfoils which have been rounded with different radii, at 9.1° angle of attack, in case of zero circulation. The line colours correspond to those of the airfoils plotted in Figure 2.10 on p. 46.

³A thin, symmetric airfoil in potential flow with a Kutta condition applied has a lift-curve slope of $2\pi/\text{rad}$ (Anderson, 2011, p. 351); which corresponds to a lift coefficient of 1 at $\alpha = 9.1^\circ$.

3.2. Experimental results

This section presents visualisations of the time-wise development of the flow-field in the trailing edge region of a rounded flat plate which is put in motion from rest, which was measured experimentally. A brief summary of practicalities regarding the experiment is presented first. Then the measured wing motion profile is presented, which is important to understand the beginning of the development of the flow-field. A graphical and textual description of the development of the flow-field is given which points out specific patterns in the velocity field and changes in the flow topology. Finally, the evolution of the region of flow separation at the wing surface and the evolution of streamline curvatures at points above and below the trailing edge are presented.

3.2.1. Report of experiment

The experiment as described in Section 2.5 was executed during a two-week session. Approximately 20 trials were done of which ≈ 3 provided useful data (one trial means taking one PIV image series). Only one trial (#19) was used for the results presented in this section. Two fields of view were tried: $\approx 40 \times 25 \text{ mm}$ and $\approx 25 \times 15 \text{ mm}$. Two different angles of attack were tried: $\approx 10^\circ$ and $\approx 25^\circ$. Several different values of acceleration were tried. The following combination resulted in satisfactory image series: acceleration $a = 2.50 \text{ m/s}^2$, angle of incidence $\theta = \approx 20^\circ$, field of view $\text{FOV} = \approx 25 \times 15 \text{ mm}$, acquisition frequency $f = 2000 \text{ Hz}$. With this combination of settings, the research phenomenon could be imaged with sufficient spatial and temporal resolution and the trailing edge did not move out of view before the transient flow had occurred. The main reasons for disqualifying trials were: the water being not at rest before start of the trial and unsatisfactory image quality (for example due to agglomerated particles sticking to the bottom of the water tank and obstructing the view).

3.2.2. Wing motion profile

The experiment setup was meant to produce a purely linear wing motion, with constant acceleration and constant angle of attack. However, an unwanted lateral acceleration was also produced. This was presumably caused by an initially large lift force⁴ and lack of stiffness of the attachment of the wing to the frame of the experimental setup. The position, orientation, and motion profile of the wing are determined using the theory and methods explained in Section 2.6.1. Graphs of the wing motion are presented in Figures 3.6 and 3.7. The velocity is almost linearly increasing with time. The angle of attack is initially negative⁵ but increases towards a positive value of $\approx 25^\circ$. The angle of attack varies due to the varying lateral position of the wing (although the wing's incidence angle is constant).⁶ The velocity, flight path angle and angle of attack of the wing are calculated using Equations 2.29 and 2.30.

⁴Although initially the circulation around the wing is zero and there is no lift force of the form which is produced when a wing has a steady motion through a fluid (this lift force is usually related to the Kutta-Joukowski equation and Bernoulli's equation) there is a significant lift force – and also a drag force – produced by the wing when it is put in motion. This is related to the inertia (which is normally referred to by the density) of the fluid. The fluid is initially at rest and due to its inertia a force is required to accelerate the fluid. Note that when a wing is in steady motion w.r.t. inertial inviscid flow there is no drag force (Batchelor, 1967, p. 332) but the fluid is moving which indicates the presence of kinetic energy. This energy has to be put in the fluid at some moment. This occurs during the acceleration of the wing. See also the discussion of impulsive motion of a fluid by Batchelor (1967, p. 471).

⁵It is a curious result that the angle of attack is negative for $t < 23 \text{ ms}$ (corresponding to $I = 45$). The author is not certain how this can be explained. There is probably no error in the calculation of the angle of attack because the streamline plots shown on p. 78 correspond to the angle of attack evolution shown in Figure 3.7. Perhaps it is related to a slight asymmetry in the frame of the experimental setup which caused a small lateral displacement of the wing when the actuation force was applied.

⁶It is expected that the initially negative angle of attack causes the stagnation point to be closer to the chord line than expected from potential flow calculation between image 60 and 100 (see Figure 3.19 on p. 84) because friction stresses act for a longer time, which antedates flow separation w.r.t. a case in which the angle of attack is constant.

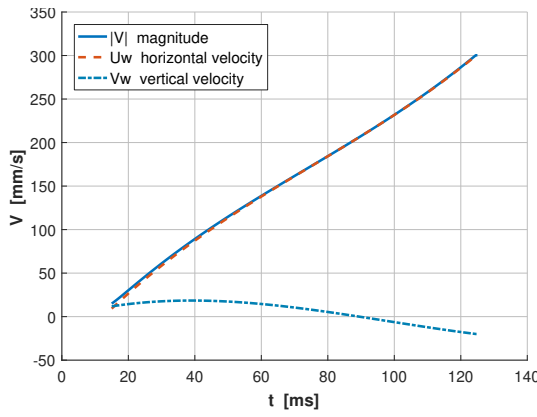


Figure 3.6: Velocity of the wing in the experiment. This data is obtained from an analysis of the wing's displacement through the PIV image series, as explained in Section 2.6.

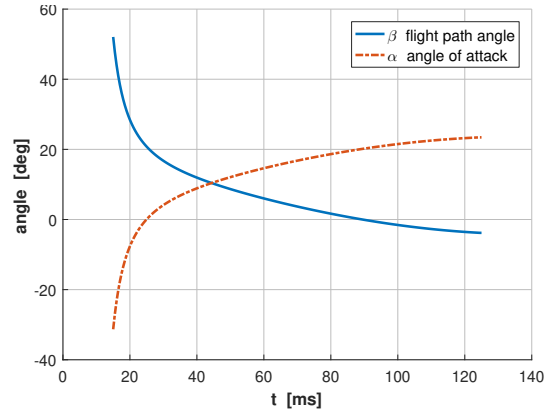


Figure 3.7: Variation of the wing's flight path angle and angle of attack vs time. The angle of attack is initially negative because the wing's motion direction vector was turned more upward than the wing's angle of incidence, due to the vertical velocity component.

3.2.3. Description of flow-field evolution

Figures 3.8 depict the evolution of the flow-field in the vicinity of the trailing edge of the wing in 8 stages. These sketches are based on observations of a movie of PIV-images and study of various forms of velocity field visualisations. The flow is from left to right. In the following description the radius of curvature of the trailing edge arc ($R=1.00$ mm) is used as reference length and the time $t_{\text{ref}} = \sqrt{2R/a} = 28$ ms is used as reference time, according to Equation (2.9) on p. 41. Important events which occur during the wing motion are marked on a time-line shown in Figure 3.9. The corresponding values of wing displacement, Reynolds number and image index (denoted by I in the following text) are also shown. The evolution of the flow-field from the beginning of the wing motion to the end of the data is presented in detail by Figures 3.10 which show instantaneous streamlines in the wing reference frame in the vicinity of the trailing edge at equi-spaced time intervals, and by Figures 3.11 which show the evolution of the vorticity field.

In the beginning ($I=50-90$), after the angle of attack has increased to positive values (Figure 3.8a) fluid moves from the leading edge of the wing (which is not depicted in these pictures) towards the trailing edge, along the straight pieces of both the upper and the lower side of the wing. At the same time fluid moves from the lower end of the trailing edge arc towards the upper end, along the arc. The flow is attached to the wing everywhere and the flow-field looks exactly like a potential flow-field such as sketched in Figure 3.2 on p. 72. In the trailing edge region there exists a single stagnation point which is located on the wing surface at $s \sim 1/4\pi$ (using the coordinate system presented in Figure 2.5) and a dividing streamline coming from the stagnation point and extending into the flow-field in mostly downstream and slightly upward direction. The dividing streamline is concave towards the trailing edge. This picture corresponds to Figures 3.13a and 3.12a.

The flow around the stagnation point decelerates and the region of nearly-stagnated velocity grows in size (Figure 3.8b). This growth occurs mainly below the dividing streamline, towards the lower end of the circular arc. The precise shape of this region can be observed on the velocity contours shown in Figure 3.13a. Flow separation will occur first in this region. The development of the velocity field between $I=90$ and $I=120$ can be studied in detail in Figure 3.12 and corresponding streamlines can be studied in Figure 3.13. At $I=95$ the stagnation point is at $s \sim 1/4\pi$. At $I=110$ we can see that the velocity vectors close to the wing in the segment between $s \sim 1/8\pi$ and $s \sim 1/4\pi$ have become very small. At $I=115$ fluid close to the wing (which is the part of the boundary layer that is closest to the wing) decelerates such that it starts flowing in the direction opposite to that of the fluid in the boundary layer further away from the wing (3.8c). This corresponds to the presence of a vortex pattern having a counter-clockwise direction of rotation. At this moment the wing's displacement is $\approx 3R$ and a time $T=1.7$ has elapsed since the beginning of the motion. After $I=115$ the centre of this vortex moves away from the wing. Figure 3.12f ($I=120$) shows the presence of the vortex as an approxi-

mately circular shape.

The diameter of the vortex increases and the centre of the vortex moves away from the wing, the distance between its centre and the circular arc now amounting to $\approx 1R-2R$. The core of the starting vortex is always higher than the centre of the circular arc (measured w.r.t. the horizon). Fluid coming from the region above the original location of the dividing streamline splits and goes in two directions: the bottom part of it goes between the wing surface and the vortex, the rest goes above the dividing streamline (Figure 3.8d). At this stage the original dividing streamline is not connected to the wing and the original stagnation point is not present anymore. Instead the stagnation point has moved away from the wing, into the flow domain; it is now located above the centre of the vortex. It moves away from the wing as time progresses, along with the vortex. On Figure 3.10 for $I > 140$ this can be seen as a region of zero velocity which is detached from the wing surface and located above the vortex centre.

As the vortex moves further away from the wing, fluid coming from along the upper surface of the wing moves downward along the trailing edge, underneath the vortex (Figure 3.8e). It curls round the vortex in counter-clockwise fashion and finally appears at the right hand side of the vortex, beneath the upper dividing streamline. Around $s = 0$ a new stagnation point and corresponding dividing streamline have appeared, which separates the flows coming from the upper and lower surfaces of the wing (Figure 3.8f).

As the starting vortex moves further away from the wing, the flow-field becomes more symmetrical about the chord-line and also about the remaining dividing streamline (Figure 3.8g). Fluid in the vicinity of the trailing edge arc and the dividing streamline decelerates. This is visible in Figure 3.10 for $I > 150$. A wake is formed and two separation points are created, one below and one above the chord line. They move away from the chord line, along the trailing edge contour, until they remain approximately at the ends of the circular arc (Figure 3.8h). The wake is now approximately symmetrical about the dividing streamline and has a triangular shape, extending in chordwise direction up to the point where the streamlines from the upper- and lower separation points merge, which is at a distance of $\approx 3R$ from the trailing edge arc. At this time the centre of the starting vortex is $\approx 10R$ away from the wing. The right end of the dividing streamline connects to the bottom of the starting vortex. The boundary layers from the upper and lower surfaces of the wing join behind the wake and are both rolled-up onto the starting vortex, on the lower side of it, as shown in Figure 3.11. This is similar to the photographs by Pullin and Perry (1980) and in Van Dyke (1982). Furthermore, the streamline plots for $I=180$ to $I=240$ hint at the creation of a Von Kármán vortex sheet behind the trailing edge.

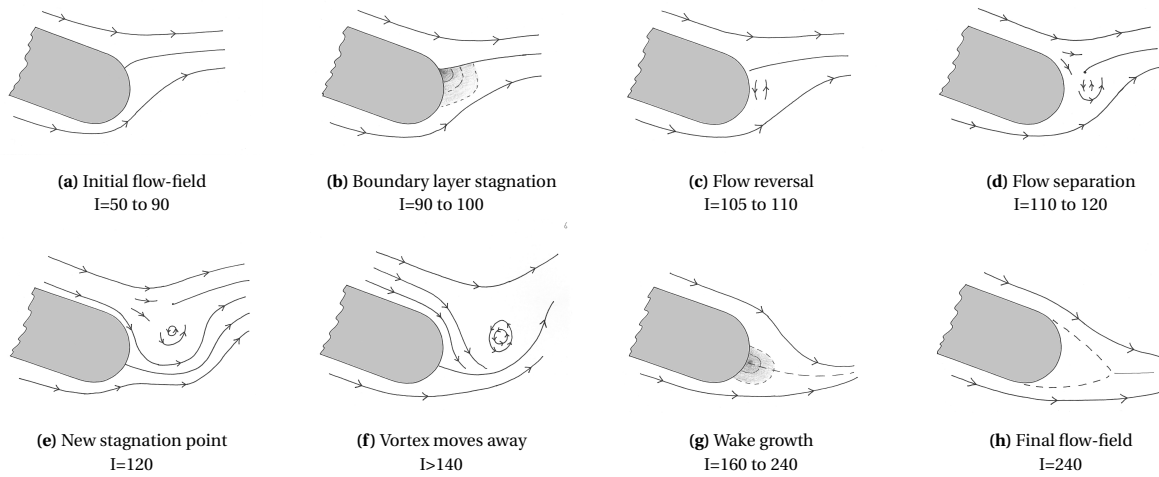


Figure 3.8: Sketches showing the development of the flow produced in the experimental setup in 8 stages. The sketches are approximately to scale and are based on the PIV data that was obtained in the experiment. The lines indicate streamlines in the wing reference frame. The shaded areas in b) and g) indicate regions of decelerated or stagnated flow. The dashed line in g) indicates the dividing streamline and in h) the boundary of the wake.

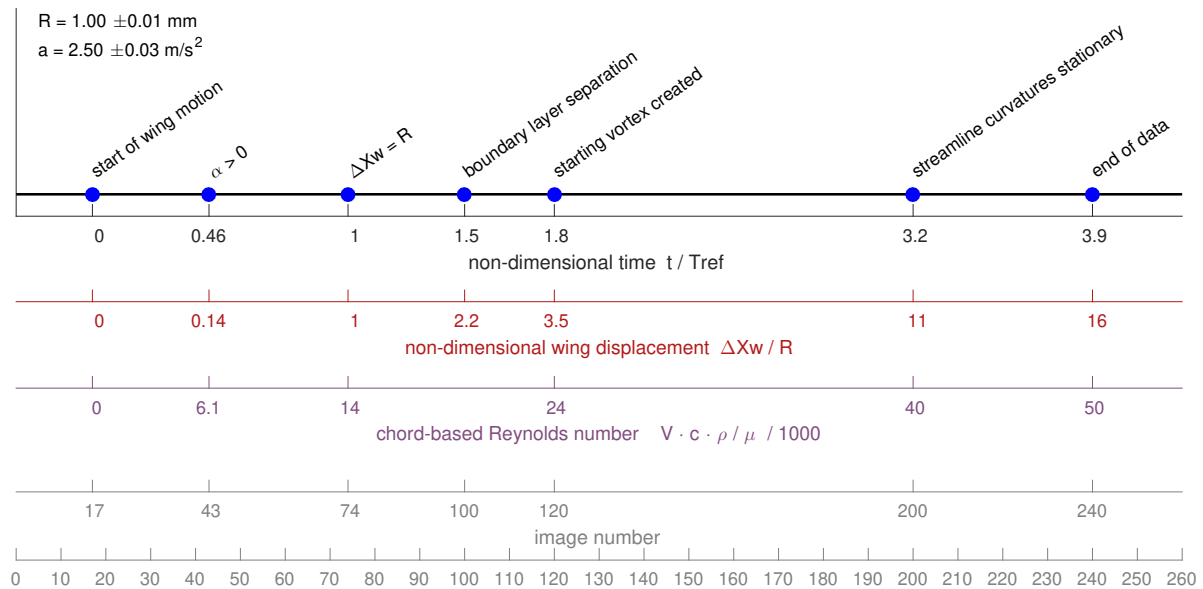


Figure 3.9: Timeline of important events during the wing's motion and development of the flow-field. Note that the non-dimensional time T is set to zero at the start of the wing motion, which is not equal to the beginning of the time-series. A non-dimensional wing displacement equal to 1 is reached when $T = 1$.

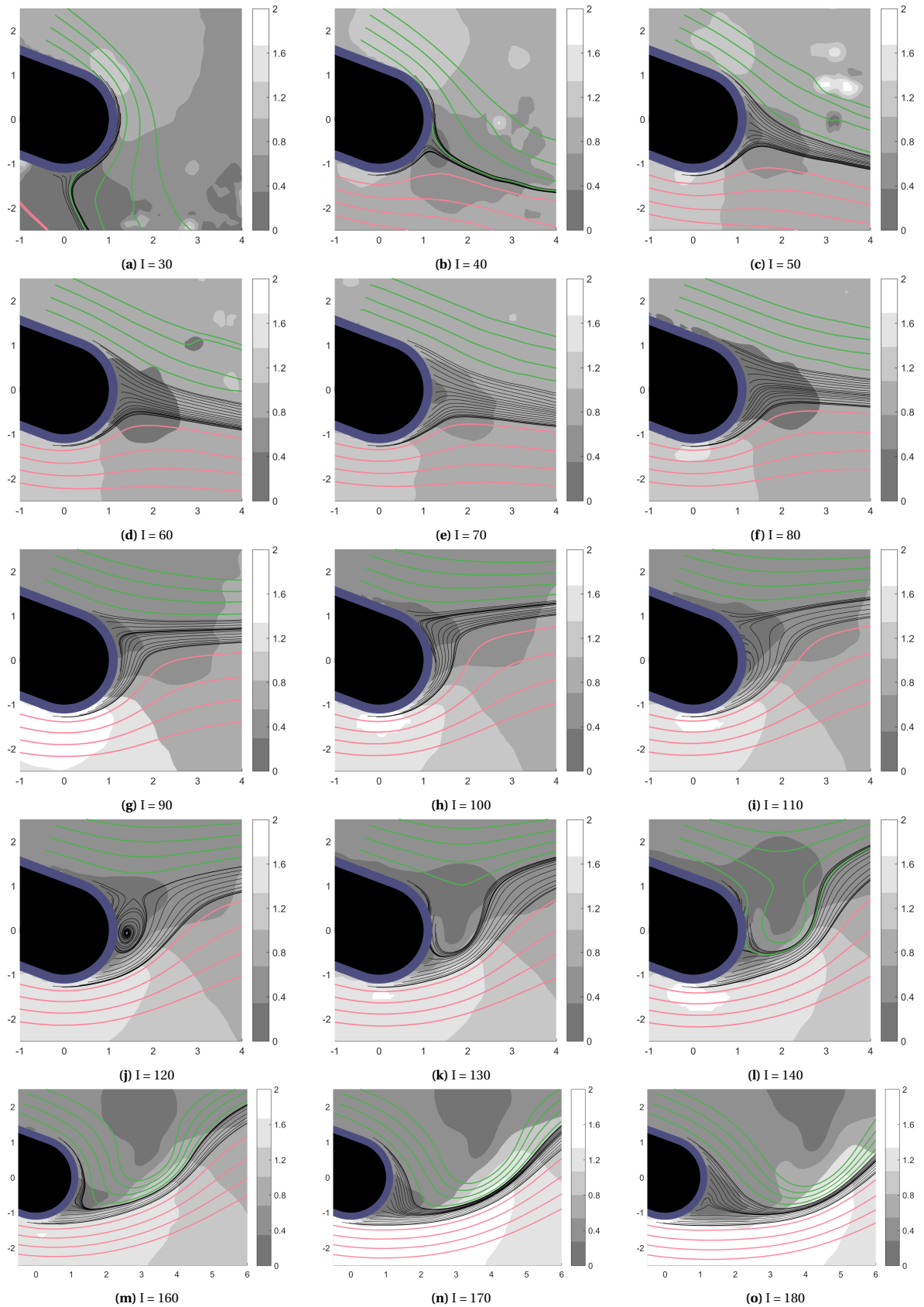


Figure 3.10: Instantaneous streamlines of the flow-field around the trailing edge in the wing reference frame, for a range of equi-spaced time values. Fluid flow is from left to right. The black area indicates the wing, the blue band around the wing indicates the region where no velocity data could be measured. Streamlines starting on the suction side (above the wing) have a green colour, streamlines coming from the pressure side (below the wing) have a red colour, streamlines starting at the circular part of the wing (at the outer edge of the gray band) have a black colour. The contours with varying darkness on the background of the images represent the magnitude of flow velocity, corresponding to the vertical colour bar on the right of each image. The velocity magnitudes are normalised by the wing velocity. The horizontal and vertical axes show horizontal and vertical position, respectively, with the origin at the centre of the trailing edge arc and distances normalised by the radius of the trailing edge. Please note that the Figure continues on the next page.

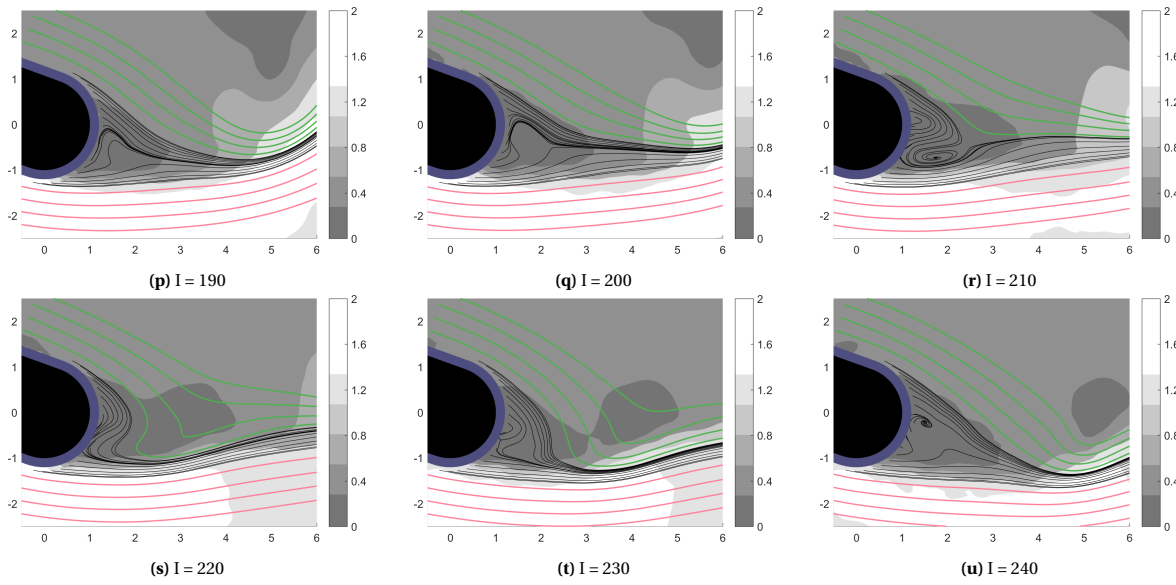


Figure 3.10: Instantaneous streamlines of the flow-field around the trailing edge in the wing reference frame, for a range of equi-spaced time values. Fluid flow is from left to right. The black area indicates the wing, the blue band around the wing indicates the region where no velocity data could be measured. Streamlines starting on the suction side (above the wing) have a green colour, streamlines coming from the pressure side (below the wing) have a red colour, streamlines starting at the circular part of the wing (at the outer edge of the gray band) have a black colour. The contours with varying darkness on the background of the images represent the magnitude of flow velocity, corresponding to the vertical colour bar on the right of each image. The velocity magnitudes are normalised by the wing velocity. The horizontal and vertical axes show horizontal and vertical position, respectively, with the origin at the centre of the trailing edge arc and distances normalised by the radius of the trailing edge.

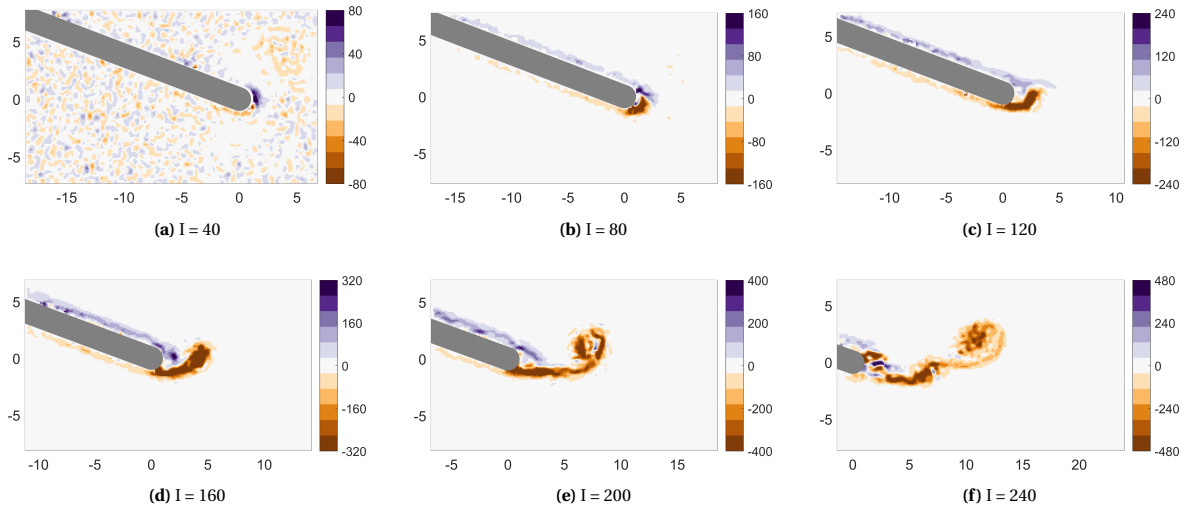


Figure 3.11: Evolution of the vorticity field around the wing, obtained from PIV data. A positive value (blue colour) denotes clockwise rotation, a negative value (red) denotes counter-clockwise rotation. (Note that the scale of the colourbar changes; the maxima are equal to $-2I$ and $2I$). Units are $1/s$. The horizontal and vertical axes show the horizontal and vertical position of the wing, respectively, with the origin at the centre of the trailing edge arc and distances normalised by the radius of the trailing edge.

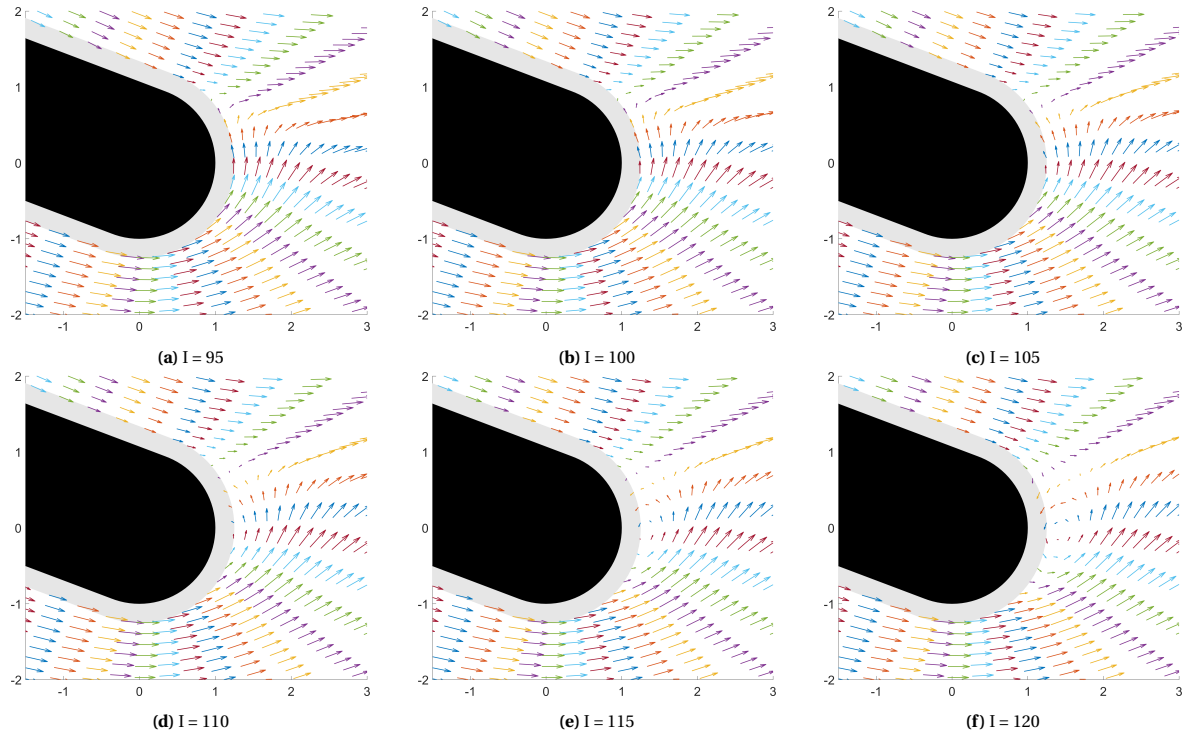


Figure 3.12: Velocity vectors in the wing reference frame, obtained by interpolating the velocity field at lines which are perpendicular to the wing contour, in the period of time in which boundary layer stagnation occurs. The horizontal and vertical axes show horizontal and vertical position, respectively, with the origin at the centre of the trailing edge arc and distances normalised by the radius of the trailing edge. These figures serve to show the process of boundary layer stagnation and separation of the starting vortex in detail. This is discussed in Section 3.2.3. A discussion of boundary layer velocity profiles is given in Section 4.2.2.

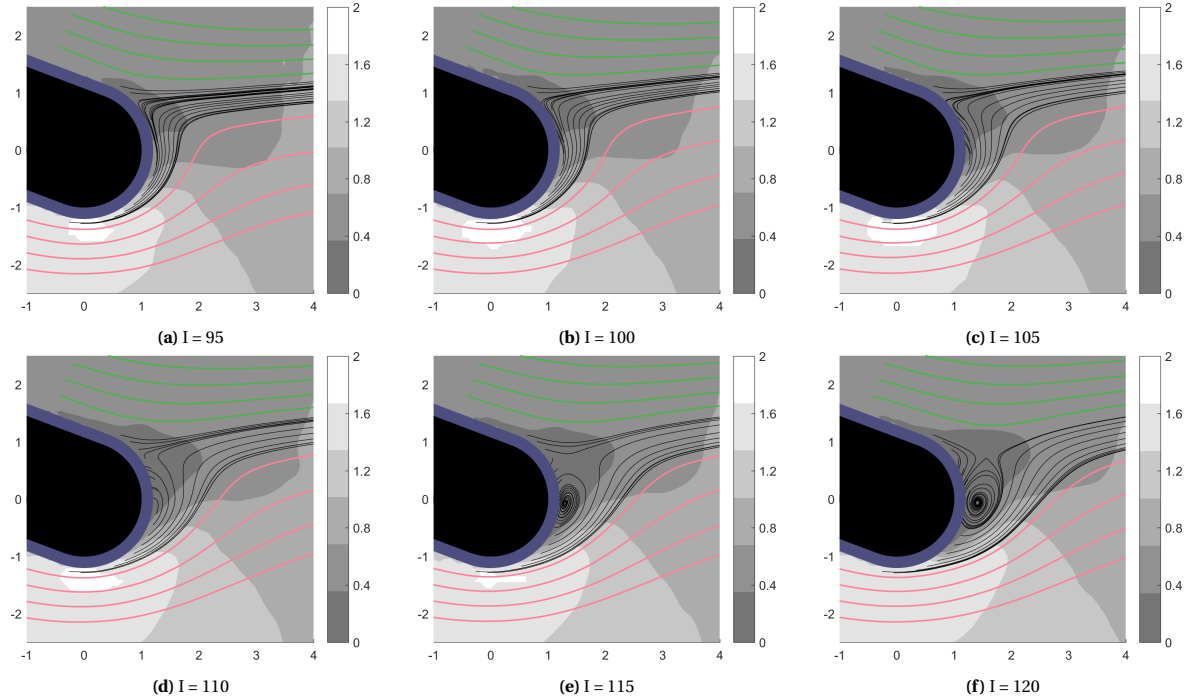


Figure 3.13: Instantaneous streamlines of the flow-field around the trailing edge in the wing reference frame for a range of equi-spaced time values, in the period of time in which boundary layer stagnation and the beginning of flow separation occurs (corresponding to Figure 3.12). See the caption of Figure 3.10 for further information regarding the plots. These figures serve to show the process of boundary layer stagnation and separation of the starting vortex in detail. This is discussed in Sections 3.2.3 and 4.2.2.

3.2.4. Evolution of region of flow separation

Figures 3.14 and 3.15 depict the evolution of the region of flow stagnation/separation through time. The “direction and speed method” for detection of flow separation, as discussed in Section 2.6.6, is used to identify flow separation with the following parameter values: $r=0.3$, $\Delta\theta_{\max} = 30^\circ$, $V_{\min}/V_{\text{mean}} = 0.1$. A tangential interrogation line (see Figure 2.39 on p. 65) with ≈ 100 points on the circular part of the trailing edge (see the right column of Figure B.3 in Appendix B for an example) is used to interpolate the velocity vector field and determine where flow separation occurs. The points marked as stagnated or separated flow are shown on Figure 3.14. The upper and lower ends of this region, as well as the tangential location of its centre-of-mass, are graphed on Figure 3.15.

Between the beginning of the motion and $I=100$ the region moves towards the suction side at a constant rate. Between $I=40$ and $I=100$ there is a single stagnation point whose location is represented by the middle line in Figure 3.15. After $I=105$ the region suddenly grows to a maximum size which occurs around $I=115$. The lower side of the region of separation ‘drops’ about 4 times as much as the upper side. This corresponds to the downward shifting of the stagnation point as described in Section 3.2.3. Between $I=120$ and $I=140$ the region of separated flow has constant size and position. Between $I=135$ and $I=145$ the region shrinks and drops slightly. After $I=150$ the region of separated flow grows and its centre-of-mass first goes up, then after $I=180$ starts to oscillate slightly. Two separation points exist now, which are represented by the upper and lower lines in Figure 3.15. They remain approximately on the upper and lower ends of the circular arc.

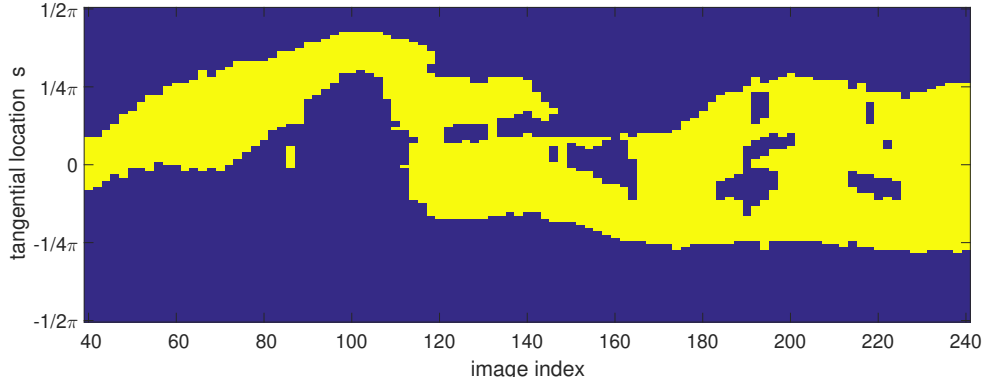


Figure 3.14: Time-wise evolution of the region of flow separation. Separated or stagnated flow is indicated by the light coloured part. The vertical axis corresponds to the (s,r) coordinate system presented on Figure 2.5 on p. 37. Before $I = 100$ a single stagnation point exists, although an area of finite height is marked as ‘separated flow’. After $I = 3.14$ two points of flow separation exist. The regions of attached flow within the wake at $I=160,190,220$ are due to vortical flow in which part of the flow is tangential to the airfoil surface.

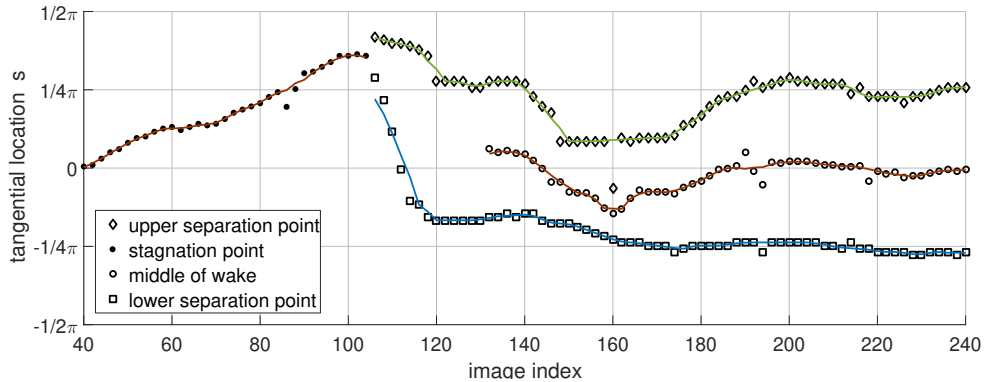


Figure 3.15: Evolution of the tangential locations of the upper and lower sides of the area of flow separation and its centre of mass with time. The upper and lower lines correspond to the upper and lower sides of the area shown in Figure 3.14. The lines represent smooth curves through the data points; obtained using a 5-point robust LOWESS filter. The vertical axis corresponds to the (s,r) coordinate system presented on Figure 2.5 on p. 37.

3.2.5. Evolution of streamline curvature

In Section 1.3 it was mentioned that the direction of streamlines above and below the trailing edge of an airfoil are in important indicator of the presence of the Kutta condition. The evolution though time of the radii of curvature of streamlines at points above and below the trailing edge is presented in Figure 3.17. The points where the curvature is determined are located according to the definition illustrated in Figure 2.46 in Section 2.6.7 with $\Delta r = 0.35$ and $d = 0.35$ (see Figure 3.16). A positive value of the normalised curvature (\tilde{R}_{str}) means that the streamline is curved in the same direction as the circular arc of the trailing edge. A value of $\tilde{R}_{str} = 0$ corresponds to a straight streamline (note that in that case $R_{str} = \infty$), and $\tilde{R}_{str} = 1$ corresponds to a streamline which is concentric with the trailing edge arc. The data shown here can be compared with the streamlines depicted on Figure 3.10 on p. 78.

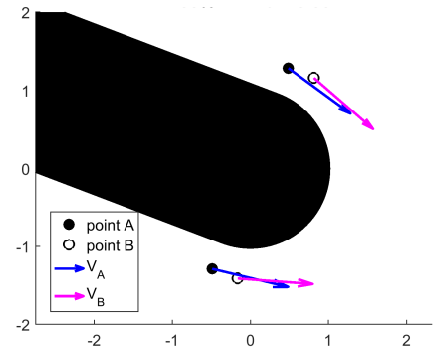


Figure 3.16: Illustration of location of points for interpolation of velocity field. The definition of the locations of points A and B is illustrated in Figure 2.46 on 70. In this case, $\Delta r = 0.35$ and $d = 0.35$.

In Figure 3.17 we observe that the lower streamline is always curved in counter-clockwise direction; its curvature is in the same direction as that of the trailing edge. However, the streamline is never concentric with the trailing edge, although this is expected for $I=40-100$, when the flow is attached. This may be explained by the fact that the curvature measurement is taken in the vicinity of the stagnation point; since streamlines tend to curve away from a body in the vicinity of a (rear) stagnation point. This mechanism also explains the negative values of the normalised curvature of the upper streamline between $I=80$ and $I=120$. Note that the upper streamline is almost concentric with the trailing edge arc around $I=160$, which can also be observed on Figure 3.10m. After $I=140$ both the upper and lower streamlines both gradually become more straight. At the end of the time-series their normalised curvature values are not yet stable, but vary around ≈ 0.2 . However, when taking the average curvature between $I=180$ and $I=240$ we can observe that the upper and lower streamlines have approximately the same average value, which indicates that the (separating) flow over the trailing edge is approximately symmetric. This data, together with the streamline plots for $I > 180$ given in Figure 3.10, suggests that the Kutta condition is present.

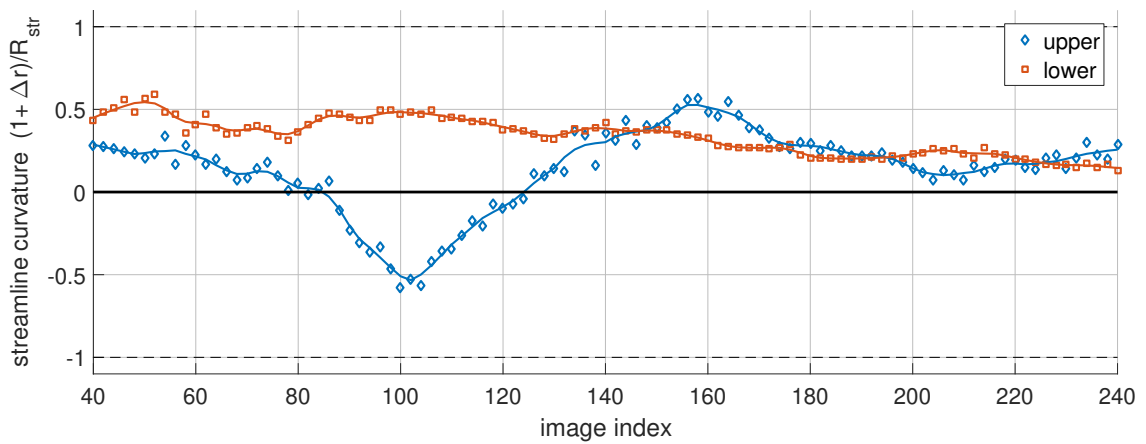


Figure 3.17: Time-wise evolution of streamline curvatures, obtained from PIV data. The vertical axis corresponds to the definition of normalised streamline curvature as given by (2.47) on p. 70. A value of 0 corresponds to a straight streamline; a value of 1 corresponds to a streamline which is concentric with the trailing edge. The lines represent smooth curves through the data points, made using a 7-point LOWESS filter.

3.3. Comparison of experimental and panel method results

Two completely different methods are used in this research to determine the trailing edge flow-field, namely a panel method, which is an implementation of potential flow theory, and PIV, which is an empirical method. In order to determine whether these methods produce corresponding results, it is interesting to compare the velocity distribution on the wing surface measured by PIV with what is predicted for the given airfoil and angle-of-attack by potential flow theory. This is done for one specific angle of attack – so one flow-field snapshot from the experimental data.

Selection of cases for comparison. From the experimental data the flow-field at $I = 90$ is selected because it represents some optimum between upward position of the stagnation point (which is more upward at larger angle of attack, thus at larger times) and small friction effects (which also increase with time). Although diffusion occurs (see the vorticity plots on p. 79) the flow is still attached to the surface, so it still resembles potential flow. It is assumed that this is sufficient for at least qualitative comparison of the results of the two methods. The angle of attack for this calculation follows from the data of Figure 3.7 and equals 10.6° , which is input for the panel method. Calculations are done for a NACA-0012 airfoil with rounded trailing edge and for a rounded flat plate which is equal to the airfoil used in the experiment. These geometries are presented in Figures 2.10 and 2.7 in Section 2.4 (p. 46). They have the same trailing edge rounding: $R/c = 0.5\%$. The NACA-0012 airfoil and the rounded flat plate are compared in order to determine whether the overall airfoil shape and the radius of curvature of the rounded trailing edge influence the velocity distribution in the vicinity of the trailing edge. The theoretical velocity distribution for the rounded flat plate is compared with the measured velocity distribution for the same airfoil in order to compare the theoretical and experimental methods. The reader is reminded that the panel method is implemented with a boundary condition of zero total circulation. Results are presented in Figure 3.18.⁷

Correction for off-the-surface probing of PIV data. The velocity data from the panel method correspond to control points located on the panels – so on the wing surface - while the PIV data correspond to locations being at a distance $r=0.5R$ away from the wing surface.⁸ To correct for this, the velocity distribution from the PIV data is multiplied by a factor 1.5. The rationale for this correction is that the flow-field in the vicinity of the trailing edge can be approximated by an irrotational vortex whose centre is at the centre of the trailing edge arc. For such a vortex the velocity at $r=1.5R$ would be 1.5 times as small as the velocity at $r=R$ because the distribution of tangential velocity of such a vortex is described by $V_t \propto \Gamma/r$ according to (Anderson, 2011, p. 263). This correction is very rough, not in the least because the actual flow is viscous and thus rotational. That notwithstanding, it enables rough quantitative comparison of the PIV and panel method results.

Comparison for specific angle of attack. On Figure 3.18 we see that the tangential locations of the points of maximum velocity match closely. The velocity peaks are similar in magnitude. The locations of the points of minimum velocity (stagnation points) are in the same region, namely about $s = 1/2\pi$, but do not match as well as the points of maximum velocity. The stagnation point on the rounded flat plate in the PIV data is at $s = 1/4\pi$ and at $s = 1/2\pi$ in the theoretical data; the stagnation point on the rounded NACA-0012 is at $s \sim 1/2\pi + 0.5$ (theoretical data). The velocity in the region outside $[-1/2\pi, +1/2\pi]$ is larger in the PIV data compared to the panel method results. Despite the quantitative differences, it is obvious that the shapes of the velocity profiles are qualitatively very similar. The PIV results clearly show a point of maximum velocity and also a point of minimum velocity, even though this data is interpolated at some distance away from the wing surface. Further discussion and conclusions regarding this comparison are given in Section 4.2.1.

Comparison for evolution through time. The determination of the locations of velocity maxima and minima from the PIV data and from the panel method predictions is performed for multiple time instances in the range $I = 50$ to $I = 100$, which is the period between the moment when the angle of attack becomes larger than

⁷The theoretical velocity distributions correspond to the pressure distributions shown in Figures 3.3 and 3.4 on p. 72.

⁸Velocity data closer than $r=0.25R$ to the wing surface cannot be obtained due to limitations of the PIV technique. The distance of $r=0.5R$ is chosen to be away from the part of the boundary layer in which friction effects are most prominent while still being relatively close to the wing surface.

zero and the moment when boundary layer separation occurs.⁹ This results in Figure 3.19, which shows the predicted locations according to the panel method and the locations obtained from PIV data. This graph was made by combining the data of Figure 3.7 and Figure 3.20. We see that the tangential locations of maximum velocity agree well over the whole time-range. Regarding the location of minimum velocity there is agreement initially, and the data series have the same trend, but a discrepancy grows with time. The dependence of the location of the trailing-edge stagnation point on angle of attack in case of potential flow is shown in Figure 3.20.

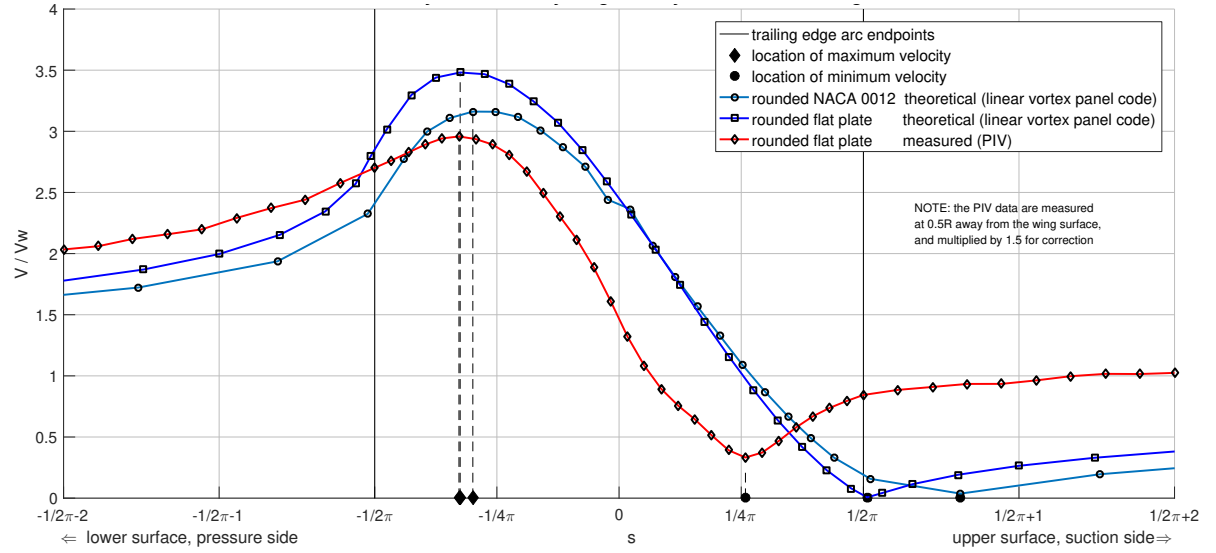


Figure 3.18: Distribution of the magnitude of flow velocity along the trailing edge. The horizontal axis shows the tangential location along the wing contour, using the s -ordinate as defined on Figure 2.5 on p. 37. The velocity distribution taken from the experiment is the absolute value of the magnitude of velocity vectors interpolated from the measured velocity field of image #90. The corresponding angle of attack is 10.6° .

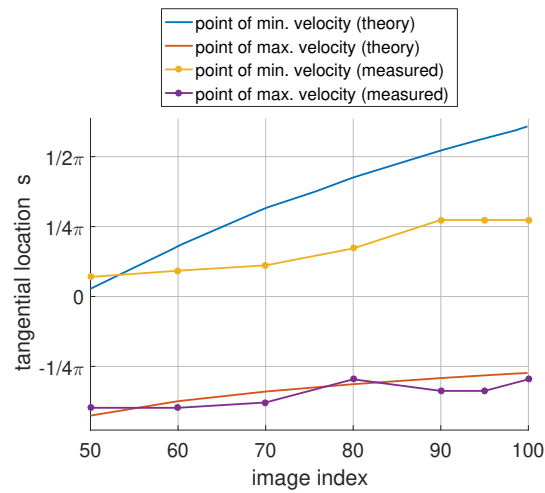


Figure 3.19: Comparison of predictions (by panel method) and measurement (by PIV) of tangential locations of minimum and maximum velocity in the surface velocity distribution around the trailing edge. The vertical axis shows the s -ordinate as defined on Figure 2.5 on p. 37.

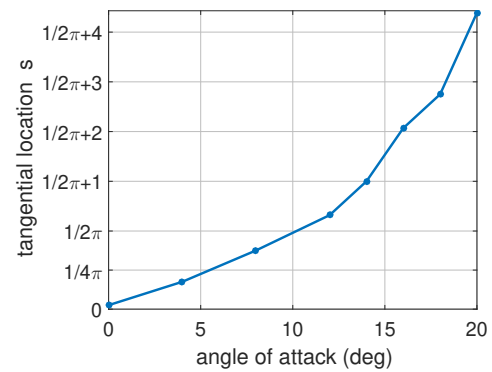


Figure 3.20: Tangential location of the stagnation point (point of minimum velocity) in the surface velocity around the trailing edge vs angle of attack, in case of potential flow around a rounded flat plate with $R/c = 0.5\%$, according to the panel method. The vertical axis shows the s -ordinate as defined on Figure 2.5 on p. 37.

⁹After flow separation has occurred no unique point of minimum velocity exists anymore.

4

Discussion

This chapter offers interpretations of - and conclusions from the results presented in the previous chapter. Figure 4.1 shows a roadmap, which clarifies how the sections of this chapter correspond to the sections of the previous chapter.

Section 4.1 presents discussion and conclusions regarding the results from panel method calculations. Section 4.2 discusses the results of the empirical work, with special attention to the observation of the effects of viscosity, and comparison with other works. Section 4.3 explicitly answers the research questions and checks the hypotheses.

The last two sections are not related to the results of any calculation or testing, but offer some theoretical ideas concerning the question which was the original motivation for this project: *is viscosity required for lift production?* Section 4.4 presents an argumentation for the necessity of viscosity for the creation of the Kutta condition in a flow. It is not complete nor perfectly watertight, yet it contributes to the discussions found in literature by using a more rigorous and more detailed argument. Section 4.5 presents an alternative mechanism which could theoretically produce a ‘Kutta-condition-like’ flow-field; which may be a counter-example for the statement that lift cannot be produced in absence of viscosity.

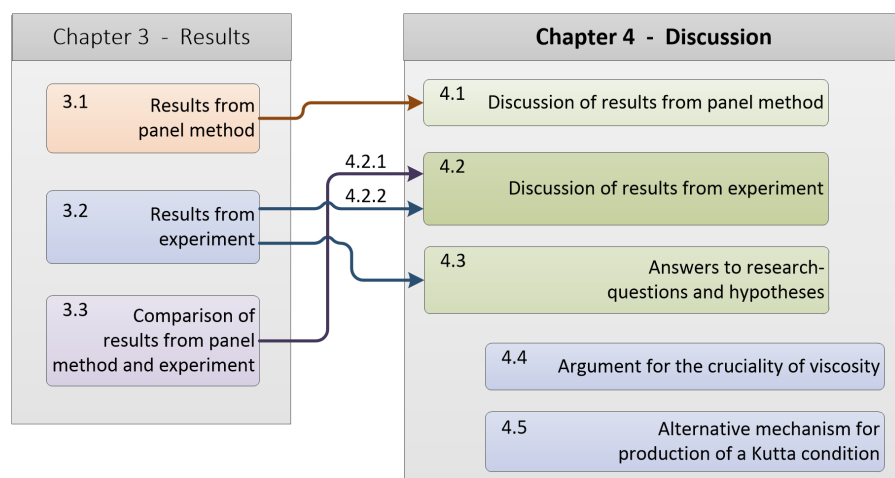


Figure 4.1: Roadmap for this chapter, showing how the sections of this chapter correspond to the sections of chapter 3 of this report. The numbers indicate chapters/sections in this report.

4.1. Discussion of results from panel method

This section presents discussion and conclusions regarding the results of the panel method which are presented in Section 3.1.

Comparison of pressure distributions on airfoil with rounded trailing edge and rounded flat plate. The difference in height and width of the suction peaks shown on Figure 3.3 on p. 72 is explained by the difference in curvature in the forward part of the airfoil: the contour of the rounded flat plate bends over 180 degrees in the most forward 1% of the chord while this curvature is ‘spread’ over the first 3/10th of the chord in the NACA-0012. The similarity of the pressure distribution in the trailing edge region is expected because the geometry in this region is almost the same. The only geometrical difference is that the upper and lower surfaces are parallel in the rounded flat plate while they make an angle of 16 degrees in the rear part of the NACA-0012. This geometrical difference might be related to the difference in magnitude of the suction peak on the lower surface of the trailing edge, which is larger by $\approx 15\%$ on the rounded flat plate.

Independence of sharpness of the trailing edge. The ‘sharpness’ of the trailing edge is denoted by the parameter R/c which is the radius of curvature of the trailing edge relative to the chord length of the airfoil. This parameter is indicative for the magnitude of the surface velocities that can be expected in the vicinity of the trailing edge. This can be understood from the relation between velocity and curvature in a flow: the more strongly a body is curved, the larger the local flow velocity (Obert, 2009, p. 47). This is proven by Figure 3.5 (p. 73). This data shows that indeed the magnitude of velocities increases when R/c is reduced. However, the *shape* of the velocity distribution around the circular-arc-shaped trailing edge of an airfoil does not depend on R/c .

Flow-field partition and independence of overall airfoil geometry. From the agreement between the calculated velocity distributions on the rounded NACA-0012 airfoil and the rounded flat plate (represented by Figures 3.4 on p. 72 and 3.18 on p. 84) we conclude that the velocity distribution on a rounded trailing edge is a local phenomenon, being almost independent from the shape of the front part of the airfoil. This independence becomes more clear when the radius of curvature is decreased relative to the chord length. When the trailing edge diameter is small enough, in the order of a percent of the chord length, we can consider the trailing edge region apart from the rest of the airfoil, because the flow-field in the trailing edge region is then so localised that it will not influence the global flow-field, and, vice versa, the global flow-field will not significantly affect the flow in the vicinity of the trailing edge (assuming potential flow).

Generality of results. Since the geometrical properties of the airfoils analysed here (i.e. a smooth contour, with the trailing edge formed by a circular arc of certain radius which tangentially joins the upper and lower airfoil sides) are representative for roughly every airfoil we can assume that every specific airfoil when rounded at the trailing edge with a diameter that is sufficiently small compared to the chord length will exhibit a pressure/velocity distribution in the vicinity of the trailing edge that is similar to that shown in Figures 3.4 and 3.18. Vice versa, we conclude that the shape of the velocity distribution calculated for the rounded flat plate is representative for the velocity distribution about the trailing edge of roughly any airfoil with rounded trailing edge in potential flow.

4.2. Discussion of results from experiment

This section discusses the experimental results of the present research which have been presented in Section 3.2. First, the comparison between the surface velocity distribution from potential flow analysis and from PIV data is discussed. Then, a large part of this section is devoted to observations concerning the effects of viscosity in the experimentally obtained flow-fields. The third part of this section discusses the oscillatory behaviour of the flow at the end of the wing's motion. The fourth and last part of this section compares the results of the present research with that of a number of works in literature.

4.2.1. Comparison of measured surface velocity with predictions by panel method

The difference in tangential location of the stagnation point between the theoretical and measured velocity distributions about the rounded flat plate (Figure 3.18 on p. 84) can be attributed to the effect of friction. It is expected that the period of the motion in which the angle of attack is negative, which precedes the moment from which the surface velocity is taken, causes the stagnation point to be closer to the chord line than expected from potential flow calculation between image 60 and 100 (see Figure 3.19 on p. 84) because friction stresses act for a longer time. This supposedly causes the real flow to 'lag behind' (i.e. the stagnation point and the associated flow in its vicinity are not as far towards the leading edge) w.r.t. potential flow, and antedates flow separation w.r.t. a case in which the angle of attack is constant. There are also some other quantitative differences. However, despite the differences we can conclude from the clearly apparent qualitative similarity that the panel code is a suitable method for predicting the velocity distribution in the trailing edge region of an airfoil in attached flow without circulation, at least in a qualitative way. We can also conclude that early authors (see Section 1.4) were right in stating that the velocity field in the initial part of the wing motion¹ corresponds to what is predicted by potential flow models, specifically regarding the existence of a stagnation point on the wing's upper surface close to the trailing edge.

4.2.2. The effects of viscosity

Questioning the significance of viscosity in the process of the creation of the Kutta condition flow-field was the original motivation for the present study, so we would like to address whether we observe effects that may (or must) be attributed to viscosity. How can we prove that the flow-field observations presented in Section 3.2 are the result of viscous effects? The presence of viscous stress cannot be proven directly because viscous stresses were not measured in the experiment.

The theories presented in Section 1.4 refer to the effect of viscosity to explain the flow separation which occurs. Truckenbrodt and Batchelor explicitly use the term 'boundary layer' and talk about separation of the boundary layer. This means that certain effects which are known from the analysis of boundary layer flows are expected to occur in the velocity field, such as reduced velocity near the wing surface. This effect is known to have a causal relation to the presence of viscosity, which is accepted with general consensus. So, let us assume that the effects of viscosity have a driving influence on the flow-field development if we observe boundary-layer-like properties in the velocity field. To that end, we will compare the measured velocity distribution in a part of the flow-field with a well-known basic boundary layer velocity distribution: the velocity profile determined by Blasius.

¹The phrase 'the initial part of the wing motion' indicates the period in which the wing has been put in motion, so an initial flow-field has been established, but no (viscous) effects have occurred which produce a qualitative transformation of the flow-field. This corresponds to the flow-field in the period between $I = 30$ and $I = 90$.

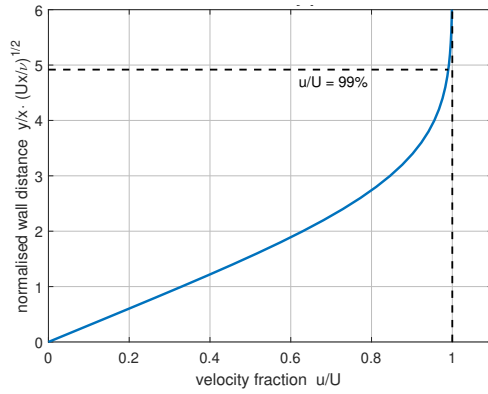


Figure 4.2: Theoretical velocity profile of a laminar boundary layer over a flat plate in steady motion according to Blasius. The horizontal axis corresponds to the magnitude of velocity as fraction of the velocity of the free stream which is far away from the surface. The distance from the wall (the vertical-axis) is normalised.

Data source: (Howarth, 1938).

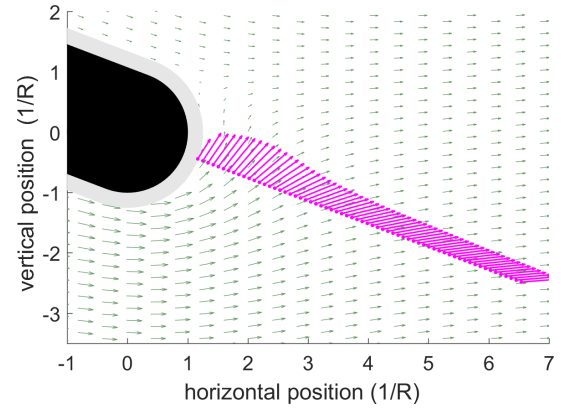


Figure 4.3: Velocity distribution behind the trailing edge, obtained by PIV, interpolated along a radial line for $I = 90$ at $s = 0$, from $r = 0.3$ to $r = 6$, corresponding to the (s, r) coordinate system presented on p. 37. Note that the velocity field shown in the background has a 3 times smaller resolution than the PIV data.

Comparison of measured velocity profile with Blasius' solution. The velocity profile of a laminar boundary layer according to Blasius is shown in Figure 4.2. This curve is the theoretical solution for the problem in which a Newtonian fluid moves steadily over a flat plate while there is a no-slip condition between the plate and the adjacent fluid. In practical situations the velocity profile of a boundary layer may look differently due to various factors, but nevertheless Blasius' solution displays the basic effect of shear stresses and the general shape of the resulting velocity profile in a qualitative manner.

Regarding the results of the present research, the velocity field behind the trailing edge for $I = 90$, at tangential location $s = 0$ (i.e. at the chord line), is interpolated as indicated by Figure 4.3. This selection may appear arbitrary, but actually the velocity field displayed in Figure 4.3 is not just a unique occurrence but occurs at many tangential locations in the flow-field at various times; which can be observed on Figure 3.12 on p. 80. The magnitudes of the interpolated velocity vectors are plotted versus distance from the wing, which results in the velocity distribution presented in Figure 4.4.

Note that in the PIV data no clearly defined “edge velocity” is present so the extent of the boundary layer cannot be determined according to the usual definition. There is a point of largest velocity in the radial velocity profile; we denote its distance from the wing contour by $r_{V_{\max}}$. Note that the velocity distribution of the flow in the region $r > r_{V_{\max}}$ (which we may call the ‘outer’ flow) as shown in Figure 4.4 has the shape of the velocity distribution of an irrational vortex. This may be expected because the flow is concentric with the centre of the trailing edge in a sector which is larger than 1/4th of a circle; see also Figure 3.10g on p. 78.

Figures 4.3 and 4.4 show that in the region between $r = 0$ and $r = r_{V_{\max}}$ the velocity monotonically decreases towards $r = 0$. Blasius' velocity profile (see Figure 4.2) is roughly fitted to that part of the velocity graph. The Blasius velocity profile is valid for a boundary layer over a flat plate in steady flow, which is quite different from the situation considered here; which explains the quantitative mismatch of the fit. Nevertheless, it is clearly visible that a “boundary-layer-like” velocity profile exists close to the wing in a conceptual sense. In all plots of Figure 3.12 the radial velocity profiles behind the trailing edge clearly show reduced velocities in the region closest to the wing.

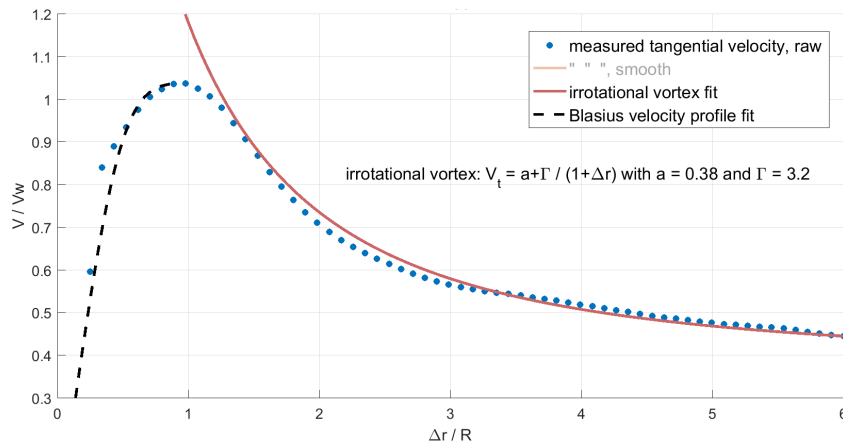


Figure 4.4: Graph of the velocity distribution along a radial line at $s = 0$, from $r=0.3$ to $r=6$ (corresponding to Fig. 4.3) with fits of velocity profiles of Blasius' boundary layer solution and an irrotational vortex. Both fits are applied visually. It is unknown why the constant a of the vortex fit is non-zero.

Events that may be attributed to viscosity. Several events (or flow patterns) occur whose occurrence may be attributed chiefly to the effect of viscosity:

1. The presence of vorticity in the flow close to the wing surface (see Figure 3.11).
2. The decrease of velocities, stagnation, and backflow below the dividing streamline at the beginning of the wing motion; see Figure 3.13 on p. 80. This behaviour is discussed in detail in Section 3.2.3 and corresponds to known behaviour of viscous flow (Chang, 1970).
3. It is observed that, after the starting vortex has become detached from the wing surface, fluid between the trailing edge and the starting vortex moves downward. This may be partly explained by the effect of viscous stress due to the downward motion of the left-side of the vortex, which applies a downward shear stress on the fluid between the wing and the vortex. This corresponds to the appearance of attached flow on the upper side of the circular arc around $I=160$; see Figure 3.10m on p. 78.
4. After the occurrence of attached flow at $I=160$, the 'upper separation line' (called such because it is at the upper side of the wake which now exists behind the lower part of the trailing edge) which starts at the chord line moves upward until it reaches $s = 0.5\pi$ at $I = 180$. This occurs possibly due to boundary layer separation of fluid which comes from the suction side and flows downward along the circular arc.

From these observations we may conclude that viscosity indeed has a major role in the flow-field development. This confirms theoretical descriptions of the transient flow which produces the Kutta condition flow-field (which were discussed in Section 1.4).

4.2.3. Oscillations in the final flow-field

In Section 1.3 it was mentioned that the Kutta condition is a stable phenomenon. Furthermore, it was suggested that the Kutta condition flow-field is a steady state which results from a transient flow. However, the data obtained from the experiment in this research suggests that the final flow-field is not steady. We will shortly discuss the unsteadiness observed in the flow and whether this presents a problem w.r.t. the expected steadiness of the Kutta condition flow-field.

The author suspects that after the moment where the data series ends the flow-field downstream of the circular arc oscillates up and down and forms a Von Kàrmàn vortex street. This has been observed by eye during the experimentations but it is not clearly visible on the PIV data. It has been observed in other experiments (Lugt and Haussling, 1974), (Zhu et al., 2015) and it is a phenomenon that is known to occur behind blunt objects in certain conditions. The streamline plots shown in Figure 3.10 for $I > 150$ suggest that a train of vortices is created of which the starting vortex is the first one. The evolution of flow separation (Figure 3.15) as well as the evolution of streamline curvatures (Figure 3.17) hint at the occurrence of oscillations for $I > 150$. In Figure 3.14 on p. 81 we can see three 'holes' in the region of separated flow (at $I = 160, 190$, and 220). We can also see a slight upward and downward displacement of the region of separated flow at $I = 200$ and $I = 230$ respectively. This supposedly corresponds to the first half period of a series of oscillations. The separation is 30 images. Given an acquisition frequency of 2000 Hz the half-period time is $30/2000 = 0.015$ s; thus the period of the oscillations would be 0.030 s, which corresponds to a frequency of 33 Hz. We will determine the Strouhal number of the oscillations using the thickness of the wing as characteristic length (because the vortex shedding behind the wing goes up-and-down) and the velocity of the wing w.r.t. the inertial reference frame as characteristic velocity (because this velocity equals the velocity of the flow w.r.t. the body). The wing thickness is 2.00 mm. The wing velocity is obtained from Figure 3.6. We will take the wing velocity at $I = 220$ (half-way of the first period of the oscillation). This occurs at $t = 220/2000 = 0.11$ s, which corresponds to a velocity of 260 mm/s. The value of the Strouhal number follows from (4.1). The chord-based Reynolds number at the corresponding moment is 45k, according to Figure 3.9; the thickness-based Reynolds number equals 450.

According to (Chang, 1970, p. 342) the Strouhal number of subsonic flow over a cylinder with a diameter-based Reynolds number of 450 is 0.205, which is in the same order of magnitude as the value obtained here, but $\approx 20\%$ smaller. This correspondence is probably caused by the fact that the trailing edge is a circular arc, so the geometry where vortex shedding occurs is the same as the rear side of a cylinder. The difference in magnitude might be attributed to the geometry of the front part of the wing section, which is much longer than the front half of a cylinder.

$$Str = \frac{f \cdot L}{U} = \frac{33 \text{ Hz} \cdot 2.0 \text{ mm}}{260 \text{ mm/s}} = 0.25 \quad (4.1)$$

Lugt and Haussling (1974) write the following about the steady state solution of their simulation of an ellipse at 45° incidence: *"At about $Re=45$ the steady state becomes unstable, and the flow changes to a stable mode in the form of the Kàrmàn vortex street. Although the critical Reynolds number of 45 is verified for circular cylinders only, indications are that this number might be valid for any blunt body or flat plate at an angle of attack beyond stall."* This implies for the case of the present research that the flow-field never becomes fully stationary. We conclude that the flow-field is not statically stable, but it is dynamically stable, at least when viewed on the scale of the trailing edge thickness.

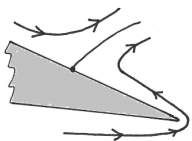
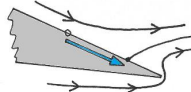
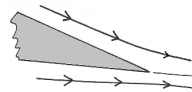
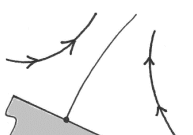
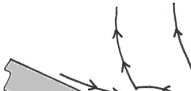
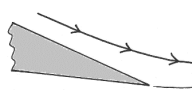
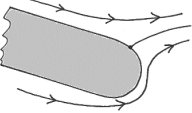
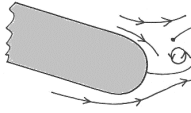
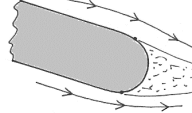
It is expected that the magnitude of the oscillations is proportional to the thickness of the trailing edge. This means that when the flow-field is viewed on the scale of the chord length, and when $R = O(0.001)$ or even smaller, the flow about an airfoil with rounded trailing edge with Kutta condition present can be regarded as virtually steady. We conclude that the final flow observed in the present research does comply with the Kutta condition's property of steadiness which is mentioned in literature.

4.2.4. Comparison of measured flow-field topology with that of other works

It is interesting to consider that the development of the flow field around the trailing edge differs in some aspects from the “classical” theoretical descriptions discussed in Section 1.4 and also from the results of the CFD experimentation presented by [Zhu et al. \(2015\)](#). The following paragraphs discuss some differences, which are summarised and illustrated in Table 4.1.

Magnitude of distance between initial stagnation point and trailing edge. Sketches given in literature such as ([von Kármán and Burgers, 1935](#)) and ([Batchelor, 1967](#)) to illustrate the creation of the Kutta condition show that a point of flow separation exists on the upper surface of an airfoil in the initial flow-field (see also Figure 1.7 on p. 11). This point is the stagnation point which corresponds to non-lifting potential flow around the airfoil; it is located at some distance away from the trailing edge. However, the precise magnitude of this distance is not indicated in these sketches nor explained in the corresponding theories. The theoretical data presented in Figure 3.20 on p. 84 indicate that even for the relatively large angle of attack of 20° the stagnation point on an airfoil, which has a trailing edge rounding of $R/c = 0.5\%$, is located at $4R$ away from the point where the flat upper surface joins the circular arc. This location is $2.5\%c$ from the rear of the airfoil, or $97.5\%c$ from the leading edge. This implies that the qualitative sketches given in literature such as ([von Kármán and Burgers, 1935](#)) and ([Batchelor, 1967](#)) are misrepresenting the location of the rear stagnation point, because such sketches suggest that it is in the order of $10\%c$ or $15\%c$ away from the trailing edge. Regarding this aspect, there is a significant quantitative difference between the present work and the “classical” sketches.

Table 4.1: Comparison of flow topology between that suggested by literature and that observed in the present research.

Source	First part of the motion	Transition	Last part of the motion
Classical theory (Section 1.4.5)	One stagnation point which is located on the suction side. 	Boundary layer stagnates, stagnation point moves towards edge. 	One stagnation point at the edge. Smooth flow-off. 
CFD investigation by Zhu et. al. (2015)	One stagnation point corresponding to potential flow and a separation bubble. 	Merger of separation points. 	One separation point at the edge. Smooth flow-off. Starting vortex shed. 
Observed in experiment (Section 3.2.3)	One stagnation point on the upper end of the circular arc, attached flow around edge. 	Boundary layer stagnates, starting vortex shed, new separation points created. 	Two separation points. Wake behind the edge. 

Results of Zhu et al. The investigation of [Zhu et al. \(2015\)](#) involves an extremely sharp trailing edge; ending in a point, without any radius of curvature. Some flow-field images of that study are given in Appendix D. In their numerical simulation, flow separation occurs at two locations; namely one at the zero-circulation potential-flow stagnation point location (although they do not call this a stagnation point but a semi-saddle) and another at the very edge, which forms due to boundary layer separation at the trailing edge. The latter causes a separation bubble on the upper side, which grows towards the leading edge. Two associated regions of separated flow grow in size and merge when they meet. The saddle point then moves upward in the domain and one separation point remains on the airfoil, located at the trailing edge. Such flow topology was also

observed by Koromilas and Telionis (1980, Fig. 48b). However, in the present research, part of the boundary layer was not captured by the PIV equipment. As a consequence, it is difficult to see whether this flow topology also occurs in the present research.

The investigation by Zhu et al. has the flow-field-transforming process occurring entirely on the suction side of the airfoil. With regard to that aspect it differs from the present research, where the flow-field transformation occurs mainly behind the trailing edge.

Levels of realism. The researchers mentioned in Section 1.4 and Zhu et al. considered airfoils with a strictly sharp trailing edge in which the upper- and lower lines of the airfoil contour meet each-other in a point. In mathematics it is possible to define an “infinitely sharp” trailing edge but in reality a wing will have a trailing edge of some thickness. This is true for aircraft wings and also for wing-models used in an experimental setup - even if they are produced carefully to minimise the trailing edge thickness. In a sense the cases considered by aforementioned researchers (pointed trailing edge in viscous flow) are “halfway” between the classical mathematical description of an airfoil in potential flow and a real airfoil in a real flow. The researchers have considered viscosity, which is one step from the ideal mathematical picture towards reality, but they have kept the “unrealness” of the pointed trailing edge.

Figure 4.5 illustrates the problem. It shows four hypothetical cases which represent several combinations of the properties of the Kutta condition flow-field on a real airfoil. When combining the realism of the presence of a wake shown in (a) with the realism concerning lift-production shown in (b) and (c), and the realism of a trailing edge of finite thickness shown in (a) and (c), case (d) is obtained which corresponds to the flow development observed in the present research. This case has all the required properties: a body with finite thickness in a lifting flow and the presence of a Kutta condition and the presence of a wake behind the trailing edge. This is the only case which realistically represents the creation of trailing edge flow-field on a lifting airfoil. See also Table 1.1 on p. 14.

It is concluded that the theoretical descriptions of the transient flow which produces the Kutta condition flow-field given in Section 1.4 correctly describe the transient flow, but they are not entirely realistic, because they omit the presence of a trailing edge of finite thickness and its associated effects. When the flow about an airfoil is viewed on the scale of the chord length, and when $R = O(0.001 c)$ or even smaller, the wake behind the trailing edge is practically invisible. However, in this research we are specifically concerned with the development of the trailing edge flow-field, which necessarily has a “zoomed-in” view on the trailing edge, which should show an edge of finite thickness in case of a practical airfoil.

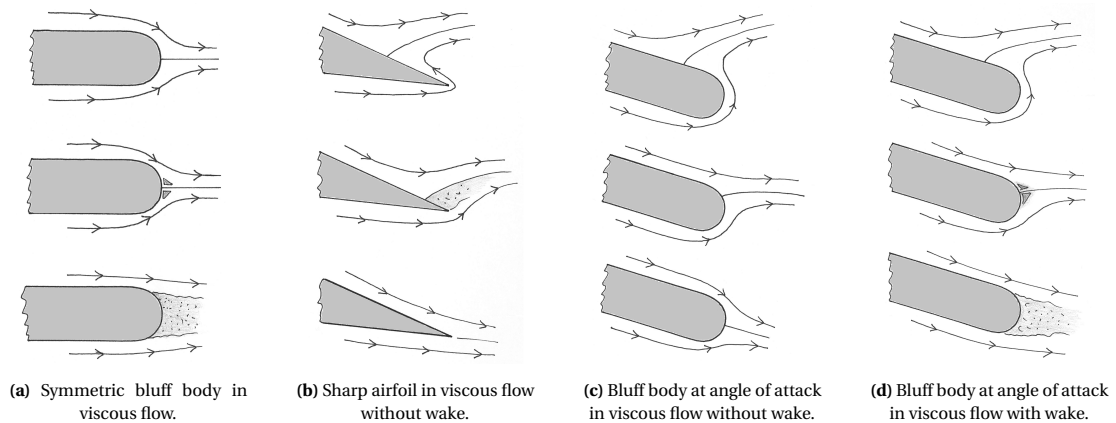


Figure 4.5: Four sketches of hypothetical cases in which the flow-field behind a body in a flow develops from rest. (a) is realistic, but does not represent a lifting flow; (b) corresponds to theories mentioned in the text and is not representative for real airfoils, because a real airfoil has a trailing edge with finite thickness; (c) is a mix of (a) and (b), it results in a Kutta condition flow-field but without a wake, which is also not realistic; (d) is most realistic and most representative for the phenomenon that is investigated in this study.

4.3. Answers to research questions and hypotheses

This section presents direct and concise answers to the research questions and hypotheses that were defined in the Research Definition (Section 1.7).

Answers to research questions

The main research question is: **How is the Kutta condition flow-field created at the trailing edge of a wing which is accelerated from rest?**

This is shown in detail in Section 3.2.3. In summary: Initially there is attached flow everywhere on the airfoil surface in the vicinity of the trailing edge (except for the one stagnation point where fluid leaves the wing). A boundary layer is formed. The flow decelerates close to the body. After flow-reversal has occurred in the part of the boundary layer which is close to the body, a vortex is formed which moves away from the wing, together with the original stagnation point. Two new separation points are formed on the trailing edge, which move towards the endpoints of the circular arc. The final flow-field is characterised by two separation points and a wake in between; this is symmetrical about the chord line. It appears that oscillations occur after the symmetrical flow-field has been formed, however this is not clearly visible in the data.

Q 1) What is the topology of the flow-field immediately after the wing has been set in motion?

Initially there is attached flow everywhere on the airfoil surface in the vicinity of the trailing edge. There is one point where flow stagnation occurs; around which flow leaves the wing. A dividing streamline attaches to this point. Unfortunately, due to deficiencies of the experimental setup, the angle of attack was initially negative in the experiment; as a result the stagnation point was located on the bottom of the trailing edge (which is consistent with the negative angle of attack) while it was expected to be on the top.

Q 1.1) Is there a single point or multiple points or a single zone or multiple zones of flow separation?

There is a single point of separation, see Figures 3.8a and 3.10a-3.10h on pp. 77 and 78.

Q 1.2) What is/are the location(s) of the points/zones where flow separation occurs?

As mentioned in Answer 1, the point of flow separation was originally located on the lower part of the trailing edge arc, see Figure 3.10a on p. 78. (Later it moved upward when the angle of attack increased.)

Q 1.3) Is that location coincident with what is predicted by potential flow theory? If not, what is the magnitude of the deviation?

Yes, as discussed in Section 3.3 and shown in Figure 3.19 on p. 84, the location of the separation point corresponds to what is predicted by the panel code for the given angle of attack.

Q 2. How does the topology of the flow-field evolve during the transient flow?

A boundary layer is formed. After the initial flow-field is set up (and after the angle of attack has increased to positive values and the separation point has moved upward), the flow decelerates close to the body. After flow-reversal has occurred in the part of the boundary layer which is close to the body, a vortex is formed which moves away from the wing, together with the original stagnation point. Two new separation points are formed on the trailing edge, which move towards the endpoints of the circular arc.

Q 2.1. What is/are the location(s) of the points/zones where flow separation occurs? and how does this evolve with time?

This is discussed in Section 3.2.4 and shown in Figures 3.14 and 3.15 on p. 81. Actually, the spatial resolution of the experimental data and the lack of data in the inner part of the boundary layer does not permit to accurately identify the locations where the original stagnation point detaches from the wing and where new stagnation points are formed. However, Figure 3.14 does give a useful indication of the size and location of the wake (which can be called a 'zone' of flow separation) which exists between the two final separation points.

Q 2.2. How does the position of the stagnation/separation point (zone) on the suction side evolve as function of the displacement of the airfoil w.r.t. its initial location?

To answer this question, the middle line of Figure 3.15 is taken and plotted versus the non-dimensional displacement. The result is shown in Figure 4.6 (see below).

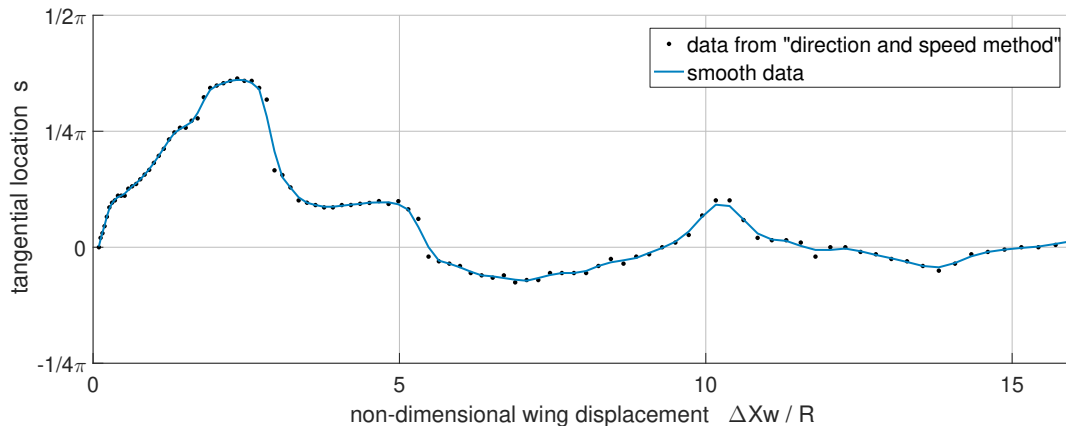


Figure 4.6: Graph of the tangential location of the stagnation point versus wing displacement. The data corresponds to the data of the middle line of Figure 3.15 (p. 81).

Q 2.3. What is the evolution of the streamlines which come along the upper and lower surfaces and pass the trailing edge?

The streamlines of the flow-field are shown in detail in Figures 3.10 on p. 78. The evolution of the radius of curvature of streamlines immediately above and below the trailing edge is discussed in Section 3.2.5 and shown in Figure 3.17 on p. 82. After $I=200$ the curvature values oscillate. The time-averaged values of the upper- and lower streamlines are approximately equal.

Q 3. What is the topology of the flow-field when the flow has become steady?

The final flow-field is characterised by two separation points and a wake in between; this is symmetrical about the chord line. It appears that oscillations occur after the symmetrical flow-field has been formed, however this is not clearly visible in the data.

Q 3.1. What is the position of the separation point when the flow has reached equilibrium?

Two points of flow separation exist, one on the lower and another one on the upper ends of the circular arc, see Figure 3.8h and 3.10u on pages 77 and 79 respectively.

Q 3.2. When is the final position of the separation point reached in terms of the displacement of the airfoil?

It is difficult to define when the flow has settled. The data do not reveal a perfectly steady state at the end of the time-series. The graphs of the evolution of the separation point position (Figure 3.15) and streamline curvatures (Figure 3.15) through time show that the values of these parameters proceed towards an asymptote (despite some unsteadiness or scattering in the data). A criterion like the position of a certain gradient in the graph is not helpful to pinpoint at what time the flow has reached steady state due to the lack of smoothness in the graph. Using our bare eyes, we can see that the flow is unsettled before $I = 140$ (looking at the evolution of separation points) or before $I = 200$ (looking at the evolution of streamline curvatures). Taking the largest of these values, it seems reasonable to put the settling time at $I = 200$ which corresponds to $T = 3.5$.

Q3.3. What is the direction of the streamlines directly above and below the trailing edge?

At the chord-wise location of the centre of the circular arc, the streamlines are concave towards the trailing edge and point in the direction of the point where these streamlines (almost) meet (at the end of the wake), see Figure 3.10u on p. 79.

Q 3.4. What travel distance/time is needed to obtain trailing edge confluence where the dividing streamline is in the direction of the trailing edge?

According to Figure 3.10 on p. 78, this occurs only at the end of the time-series, which corresponds to a non-dimensional displacement of approx. 16. Here the direction of the dividing streamline is taken as the average direction of the upper and lower streamlines which pass the ends of the circular arc.

Verification of hypotheses

The main hypothesis is: **When a wing is accelerated from rest, there will initially be a potential-flow-like flow-field with fluid moving from the pressure side along the trailing edge to the suction side, and a stagnation point on the suction side. As time progresses, this point will shift towards the trailing edge as result of friction stresses. Finally, fluid will leave the wing smoothly at the trailing edge.**

Yes, this occurs, however the flow transformation is more complicated than only a shift of the stagnation point.

H 1) Immediately after the wing has been set in motion the flow-field corresponds to potential flow.

Yes. Qualitative correspondence of the overall flow-field is shown by comparison of Figures 1.7a and 1.7b on p. 11 with Figure 3.10h on p. 78. Furthermore, correspondence between the predicted surface velocities according a panel method and PIV measurements is discussed in Section 3.3 and shown on Figure 3.18 on p. 84.

H 1.1) There will be a stagnation point on the suction side close to the trailing edge.

Yes, between $I = 50$ and $I = 100$ a single stagnation point exists on the suction side, see Figures 3.8a and 3.10a-3.10h on pp. 77 and 78.

H 1.2) Fluid moves from the pressure side around the trailing edge to the suction side.

Yes, this occurs when the angle of attack is maximum and before flow separation occurs, between $I = 90$ and $I = 100$, see Figures 3.10g-3.10h on p. 78.

H 2) Flow separation at the suction side can be attributed to stagnation of the boundary layer.

Yes, it very much appears to be so, although this is not shown with complete certainty. Effects of viscosity which can be observed are discussed in Section 4.4 on p. 97.

H 2.1) Flow stagnation in the boundary layer occurs.

Yes, this can clearly be observed in Figures 3.12 and 3.13 on p. 80. Flow in the region between the chord line and one radian upward along the circular arc exhibits flow reversal after $I=110$.

H 2.2) Flow separates from the wing after flow in the boundary layer has stagnated.

Yes, this can clearly be observed in Figures 3.12 and 3.13 on p. 80. The boundary layer on the circular arc between the chord line and the stagnation point separates from the wing.

H 3) Hypotheses regarding the steady-state flow-field.

H 3.1) When steady flow is reached, the flow leaves the trailing edge in the direction where the trailing edge points. The dividing streamline as well as the neighbouring streamlines from the upper- and lower surfaces have no sudden changes in speed or direction.

Partly. The upper and lower streamlines leave the wing more-or less in the direction of the chord line and there are no sudden changes in direction, as can be observed on Figure 3.10u on p. 79. However, the real flow-field picture is different from the hypothesised one which is sketched from Figure 1.7g on p. 11 because the real wing has a thick trailing edge – not a pointed one.

H 3.2) The separation point location is not on the most rearward point of the trailing edge but slightly upstream, on the suction side.

No, such behaviour is not observed. As shown on Figure 3.15 on p. 81, the final locations of the separation points located on the upper and lower ends of the circular arc are symmetric about the chord line.

H 3.3) A “dead-water region” or wake exists at the suction side close to the trailing edge just after the fluid has been set in motion.

Partly. Yes, a zone of separated flow exists, which is shown by Figure 3.14 on p. 81, however, it occurs not immediately after the flow has been set in motion but after the starting vortex is created, and it is not located on the suction side but on the circular-arc part of the wing.

4.4. Notes on the cruciality of viscosity

The original motivation for this thesis was to study whether viscosity is necessary for the production of a Kutta condition (and thus for the production of lift). This section presents a frame-work that can be used to prove the necessity of viscosity. Figure 4.7 presents an argument which is designed in order to argue that viscosity is required for lifting steady flow. It was inspired by the work of [Craig \(1959\)](#). The argument is complete when parts A, B, D, and F are proved. These parts are discussed shortly in the following sub-section. The last part of this section presents a proof of D. Note that this section does not aim to present a complete, watertight proof for the necessity of viscosity for the production of lift, but rather a proposal for a proof with some starting considerations.

We consider the case of an airfoil in two-dimensional flow. We assume that the airfoil has an angle of attack such that the lift would be produced in a potential flow if the Kutta condition is applied. Parts A and B of the proof consider the rear stagnation point on the airfoil.

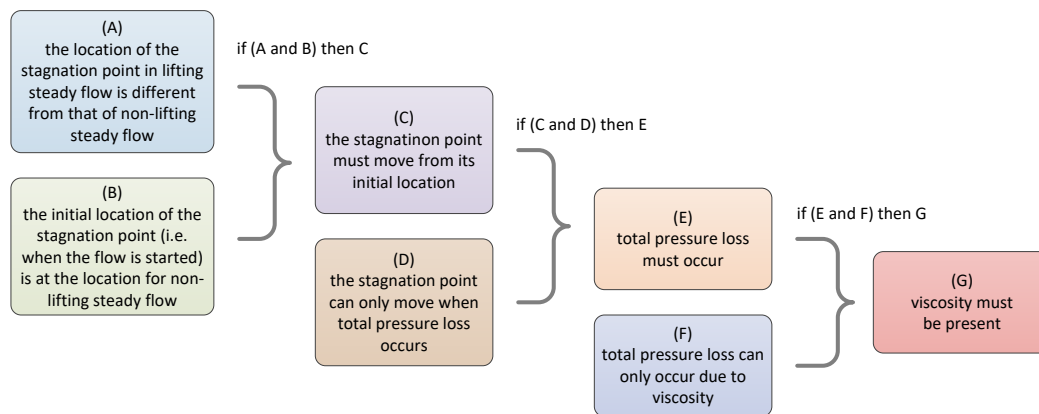


Figure 4.7: Logical structure of the proposed argument for the necessity of viscosity for the creation of lifting steady flow.

Parts of the proof

A (*the location of the stagnation point in lifting steady flow is different from that of non-lifting steady flow*) is shown by potential flow theory; see for example Figure 1.4 on p. 4. Note that we refer here to the one stagnation point present on the rear of the wing which is also a separation point. In viscous flow all points on the wing surface are stagnation points, but only one of them is a separation point. The dividing streamline (which is there regardless of viscous or inviscid flow) attaches to this point. See also Figures 1.10c and 1.10d on p. 18. Every value of the circulation (and thus the lift) corresponds to a unique location of the stagnation point, see Figure 1.4 on p. 4.

B (*the initial location of the stagnation point (i.e. when the flow is started) is at the location for non-lifting steady flow*). For this part to be true, it has to be proven that when the relative motion between airfoil and fluid starts, the initial location of the rear stagnation point cannot be anywhere else than the location for non-lifting steady flow. The present author feels that this might be true, and it is probably proven in literature, but it is not proven in this report. It has however been shown that the location can be determined by theoretical and empirical methods, see Section 3.3.

D (*the stagnation point can only move when total pressure loss occurs*) is proved by the argumentation presented in the next sub-section.

F (*total pressure loss can only occur due to viscosity*) is not proven yet. The most complete model of fluid flow is represented by the Navier-Stokes equations, but these are usually not in a form that is suitable for analysis of energy losses, since terms like total pressure or entropy are not present in the equations. But

there might be good starting points for proof. For example, consider Crocco's equation, which relates velocity and vorticity to entropy or total pressure. Crocco's equation, taken from Shapiro (1969), is shown in (4.2). This equation is valid for steady, incompressible (=divergence-free), inviscid flow. It shows that zero vorticity ($\omega = 0$) corresponds to zero loss of total pressure, so zero gradient in the total pressure field ($\nabla p = 0$).

$$\mathbf{V} \times \boldsymbol{\omega} = \frac{\nabla p}{\rho} \quad (4.2)$$

According to Kelvin's theorem, an irrotational potential flow will remain irrotational. When combined with Crocco's equation, this suggests that steady, incompressible, inviscid flows cannot produce changes in total pressure. In relation to this, Craig (1959, p. 42) comments: *"In fact, in the absence of dissipative forces the circulation cannot change, for no mechanism exists to change the system energy. Should a nondissipative system possess no circulation at a particular instant the circulation must remain zero at any succeeding time, and therefore the system can never show lift."* Similarly, Batchelor (1967, p. 332) states: *"No means of dissipating energy exists in an inviscid fluid, and no radiation of energy to infinity can occur by sound waves in an incompressible fluid or by gravity waves in the absence of density variations or a free surface to the fluid"*. However it is not impossible that there exist mechanisms that can cause pressure loss when the conditions of Crocco's equation do not apply.

Argument for necessity of total pressure loss for shift of stagnation point

Imagine an airfoil moving steadily through a fluid, as sketched in Figure 4.8. We assume that no heat transfer occurs and no work is applied, so the flow is homenergetic: the total enthalpy is equal and constant everywhere. The fluid is at rest at locations infinitely far away from the airfoil. We consider the flow around the airfoil in a reference frame which moves with the airfoil. The fluid located upstream of the airfoil, along line L in Figure 4.8, at infinite distance upstream of the airfoil is not affected by the presence of the airfoil; each point on line L has equal total pressure w.r.t. the moving reference frame.

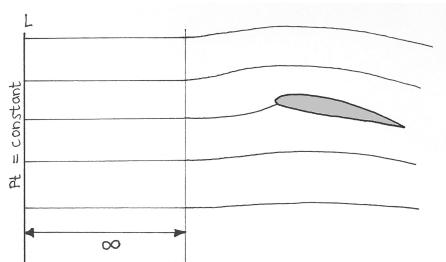


Figure 4.8: An airfoil moving steadily through a fluid. The total pressure is constant over line L which is located infinitely far upstream of the airfoil.

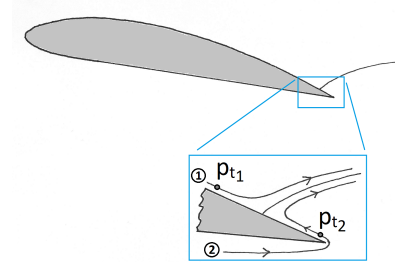


Figure 4.9: Qualitative sketch of the potential flow-field around a non-lifting airfoil. Note that the rear stagnation point is not at the trailing edge. Two streamlines are shown, one per side of the stagnation point. p_t indicates the total pressure of each streamline.

Imagine that the flow-field is like that sketched Figure 4.9. We focus on the flow in the vicinity of the trailing edge. There exists a stagnation point (SP) on the suction side just ahead of the trailing edge. No lift is produced in this situation. This corresponds to potential flow with zero circulation. The flow in the vicinity of the SP is characterised by the stagnation point, at which the flow is stagnated (has zero velocity), a so-called 'dividing streamline' which touches the body at the SP, and a stream on each side of the dividing streamline. Stream 1 comes from the upper side and stream 2 comes from the lower side of the airfoil. Close to the wing surface there will be flow tangent to the surface on both sides of the SP. Fluid will move towards the SP at both sides. In a parcel of fluid moving along the streamlines towards the SP, the velocity decreases and static pressure increases, until the velocity is zero and the static pressure equals the total pressure (= stagnation pressure) when it arrives at the SP; see Figure 4.10. When no loss of energy occurs, both streamlines have the same total pressure, so fluid parcels coming from both sides of the SP towards the SP will have the same static pressure when they have arrived at the SP.

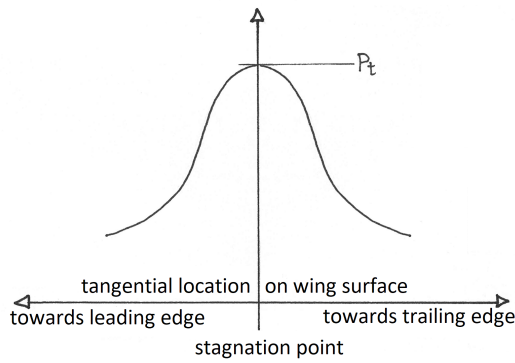


Figure 4.10: Graph of static pressure vs distance from stagnation point in case of inviscid flow. The streamlines approaching the stagnation point over the airfoil's surface (see Figure 4.9) have equal total pressure.

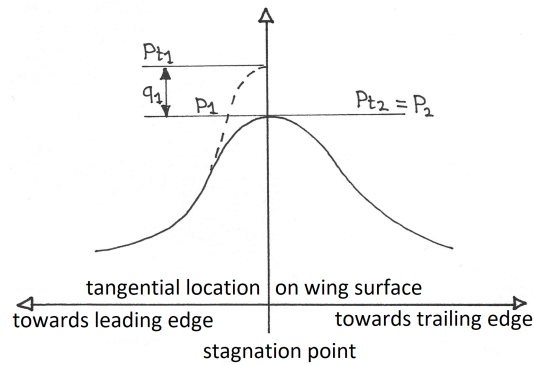


Figure 4.11: The same graph as Figure 4.10, but now the total pressures of streamlines 1 and 2 are not equal. The static pressures are equal at the stagnation point but the left side (streamline 1) has larger total pressure.

If energy loss would occur close to the wing surface between line L and the stagnation point, streamlines (1) and (2) might not have the same total pressure when they come in the vicinity of the stagnation point. Consider that $p_{t1} > p_{t2}$ (Figure 4.11). We can continue to think on two lines. When they have stagnated, their static pressure would be equal to the total pressure for each streamline, but these static pressures would not be equal. As a consequence, fluid that is located at the stagnation point will experience a pressure gradient and start to move towards the side of lowest static pressure, which is the side of lowest total pressure. Alternatively, when streamline (2) stagnates, and streamline (1) would reach the same static pressure as streamline (2), streamline (1) would have residual velocity. This would cause a movement of the “stagnation point” towards the right.² If streamlines (1) and (2) have equal total pressure the stagnation point will not move because there is no pressure gradient in the direction along the wall. It is thus argued that, when no energy is added or subtracted to the flow, a pressure-loss-producing process occurring close to the wall of the body is required in order to produce a shift in the location of the stagnation point.

²The two suggested lines of reasoning are stated in an extreme fashion to indicate the principle that a difference in total pressure will produce a shift of the stagnation point. In reality there will not be such large differences in total pressure as sketched in Figure 4.11. There would be a smooth variation of total pressure with position. Pressure gradients will be balanced by a combination of momentum gradients and viscous stress. The flow-field will be continuously adjusted instead of in discrete fashion as suggested by the reasoning in the text.

4.5. An alternative mechanism for production of the Kutta condition

A mechanism for production of a Kutta condition alternative to viscosity might be compressibility. This property applies to gases, not to liquids. A simple argument is given as follows. Consider an airfoil moving through potential flow without circulation, at an angle of attack which corresponds to lift production if the Kutta condition would be present, like Figures 4.8 and 4.9. Suppose that the flow around a trailing edge is modelled by an irrotational vortex whose tangential velocity distribution is described by (4.5) where Γ is a constant and r is the distance from the centre; see Figures 4.12 and 4.13. Now suppose that the flow is compressible. Also consider the relation between velocity and pressure which is described by Bernoulli's law (4.6), where p_t is the total pressure of the flow, which is equal and constant in the domain when dissipative mechanisms are absent. When the vortex velocity distribution is combined with Bernoulli's law we see that the static pressure will be smaller with decreasing r .³ It might happen that the pressure has decreased to zero at some limiting value of r which we will denote by r_L . If that happens, the flow cannot reach the region of $r < r_L$ because there is no pressure difference which can force it there.⁴ This means that flow will separate from the body if the radius of a trailing edge R is smaller than r_L .

$$V_t = \frac{\Gamma}{r} \quad (4.5)$$

$$p_t - p = 1/2 \rho V^2 \quad (4.6)$$

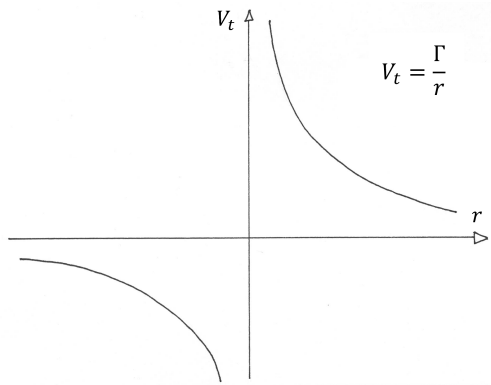


Figure 4.12: Theoretical velocity distribution of an irrotational vortex.

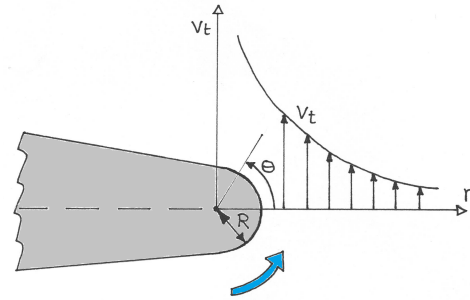


Figure 4.13: The irrotational vortex velocity distribution (see Figure 4.12) located at the centre of a rounded trailing edge. It is drawn at a line which is inline with the chord but it may also be drawn at another line emanating from the centre of the circular arc, which is indicated by θ . The radius of the rounded trailing edge of a wing is denoted by R . The blue arrow indicates the direction of motion of the flow about the edge.

McLean (2013, p. 481) gives the following elaborate thought about the hypothetical cause of the Kutta condition due to effects related to compressibility (note that he supposes a pointed trailing edge):

“In an otherwise subsonic flow governed by the Euler equations, attached flow around a sharp convex corner cannot produce infinite velocity, as it would in incompressible flow. It would, however,

³When the ideal-gas law (4.3) and the isentropic relation between pressure and density (4.4) are also considered we see that the density will decrease when pressure decreases. This defeats the applicability of the equation for the irrotational vortex because this is a result of potential flow theory which assumes that density is constant. Nevertheless, the considerations are valid for explaining the principle of decreasing pressure towards the core of a vortex.

$$p = \rho RT \quad (4.3)$$

$$\frac{p}{p_t} = \left(\frac{\rho}{\rho_t} \right)^\gamma \quad (4.4)$$

⁴A similar idea is discussed by Emrich and Reichenbach (1969).

cause an acceleration to a sonic condition at the corner, with a Prandtl-Meyer expansion fan (...) centered at the corner, producing a jump to supersonic speed on the downstream side. The corner would thus have a singularity with infinite acceleration, not infinite velocity, and downstream of the corner the supersonic flow would be terminated by a shock. This kind of attached-flows solution can exist only if the turning angle of the corner does not exceed the maximum Prandtl-Meyer turning angle of 130.5 degrees. For typical airfoil shapes with sharp trailing edges, the turning angle around the trailing edge is too large (typically in excess of 170 degrees), and the zero-lift flow pattern (...) is therefore impossible. This raises the interesting theoretical possibility that even an inviscid airfoil flow, provided it is compressible, would still have to satisfy the Kutta condition (...) And even if the turning angle is less than 130.5 degrees, the existence of an attached-flow solution is not guaranteed. It would depend on how much additional subsonic pressure recovery the flow faces downstream of the shock. If the shock terminating the supersonic bubble is strong enough, the resulting total-pressure deficit downstream could make it impossible for the flow to negotiate the rest of the pressure recovery. Finally, even when an attached-flow solution with a fan and a shock exists, it is only a theoretical possibility. In the real, viscous world, the boundary layer will either effectively fair over the corner, if it is shallow enough, or separate, eliminating the need for acceleration to supersonic flow."

McLean proposes the theoretical possibilities of the presence of an expansion fan and a shock at the trailing edge in steady flow. The transient process leading to such a situation, assuming that the flow develops from a situation of complete rest, is challenging to think about. The analysis of flow acceleration to supersonic velocity over a sharp convex corner such as presented in (Prandtl, 1965) assumes a situation of pure vacuum on the downstream side of the corner. Such a situation is distinctly different from the case of an airfoil which is immersed in fluid and finite pressure exists at both sides of the trailing edge. A hypothetical process is presented as follows, along with Figure 4.14.

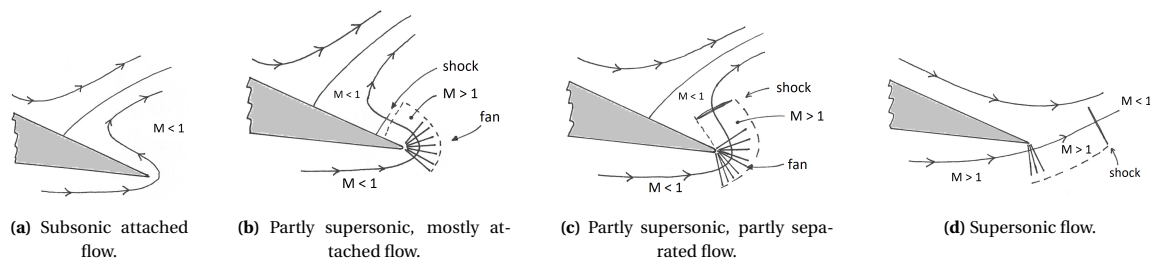


Figure 4.14: Sketch of the hypothetical development of supersonic flow about the trailing edge of an airfoil which is started from rest in a compressible flow.

When the airfoil is accelerated from rest there will initially be rough equivalence of pressure at the suction side and pressure side regions (Figure 4.14a), both in terms of total pressure and static pressure. An expansion fan through which the fluid coming from the pressure side is accelerated to supersonic velocity when going towards the suction side will be created if the static pressure at the trailing edge falls below the critical pressure (Figure 4.14b). It might be that the fan begins small in terms of radial distance from the trailing edge. A shock might be created between the expansion fan and the dividing streamline attached to the initial potential-flow stagnation point on the suction side. When the airfoil continues to be accelerated and the flow velocities continue to increase, the fan might grow in size, as well as the shock, and a larger region experiences supersonic flow (Figure 4.14c). Loss of total pressure through the shock will lead to displacement of the stagnation point and the corresponding dividing streamline towards the trailing edge. Once flow separation occurs at the trailing edge due to the static pressure reaching zero at some point along the corner, the flow will separate and turn over a smaller angle when passing around the sharp edge. After it exits the expansion fan, it will not be parallel to the upper surface of the airfoil. The (subsonic) flow above the dividing streamline will comply and alter the static pressure downstream of the shock (Figure 4.14d). This will in turn alter the geometry of the fan & shock.

Note that this is a complex process and just using “mental fluid dynamics” is an uncertain way of determining how it works. Nevertheless, it is an interesting theoretical possibility.

Following the previous citation, [McLean \(2013, p. 482\)](#) remarks about the appearance of inviscid separation from convex corners in numerical simulations of the Euler equations: *“In 3D numerical simulations of the Euler equations, a sharp convex corner can produce separation of the open, free-shear layer type. An example would be the leading and trailing edges of a sharp-edged delta wing. In these situations, numerical dissipation has the same qualitative effect that real viscosity would have in bringing about the separation and enforcing a kind of de-facto Kutta condition.”*. The present author has seen separation occurring in inviscid transonic flow over a sharp corner in CFD experimentation. A critical remark can be made about McLean's remark: Although there might be numerical dissipation in a simulation, this does not mean that every case of inviscid flow separation observed in numerical simulations should be attributed to numerical dissipation. Further investigation of this problem is outside the scope of the present work. The mathematically able reader is referred to [Ruban and Turkyilmaz \(2000\)](#) for further reading.

5

Conclusions and Recommendations

5.1. Conclusions

This work considers the time-wise evolution of the flow-field around the trailing edge of a generic wing model which is started from rest in a fluid and uniformly accelerated. This phenomenon is a transformative process which modifies the initial flow-field which exists when the wing is put in motion in such a way that the resulting flow-field is a lift-producing flow-field. Considered from an empiricist's perspective, this phenomenon is a key aspect of the generation of fluid-dynamic lift. Previous works studying the production of fluid-dynamic lift considered situations in which a steady trailing edge flow is present. This steady trailing-edge flow-field is usually modelled in potential-flow analysis by a mathematical boundary condition which is referred to as the “Kutta condition”. When considering the whole phenomenon of lift production as an initial situation without any movement, followed by a transient process, resulting in a steady trailing edge flow-field, we can point out the added value of the present research. Modelling fluid-dynamic lift by potential flow theory is only possible when it is assumed that the modelled situation has a steady trailing-edge flow-field with certain properties. However, the transient process from which that steady flow-field results in a real flow has historically gotten little attention in the study of fluid-dynamic lift.

The transient process transforming the initial situation into a final steady flow-field has been described theoretically in literature, at the earliest around 1935. A synthesis of theoretical descriptions by various authors is given in this report. In short, it is supposed that in case of a wing which is put in motion from rest in viscous fluid, fluid initially moves from the pressure side, along the trailing edge, towards the suction side. The circulation is initially zero and a stagnation point is present on the suction side, close to the trailing edge. Due to the presence of viscosity, a boundary layer is created, which stagnates on the suction side. Consequentially the stagnation point shifts from its original location towards the trailing edge. In the final flow-field, streamlines above and below the trailing edge are smooth and approximately linear. This theory has gotten little verification. Some analysis using Computational Fluid Dynamics (CFD) is presented in 2015 (namely by Zhu et al.) which confirmed the theoretical descriptions, however empirical verification was still lacking. The present research aims to fill that gap.

Methods

In the present research, results are obtained from three sources of information: literature, a panel method, and empirical research. The last one comprised the largest part of the project.

Literature. Approximately 150 pieces of literature, dating from 1900 to 2015, were scanned for relevance. Approximately 1/3rd of it turned out to be useful because the discussed the Kutta condition as main issue or side issue. Most of these works had a mathematical or theoretical character. The literature study revealed that the importance of the Kutta condition in airfoil theory is clear in fluid dynamics, but there is still confusion about what it means. Distinguishing between the mathematician's and the empiricist's perspective is useful in a discussion. The Kutta condition flow-field can be regarded as a steady-state equilibrium. In order to understand its origin in a real flow, the preceding transient flow needs to be studied. There has been consensus about a theoretical description of how the Kutta condition is produced in a real flow, but that description is somewhat superficial and had not been validated by empirical research. The literature study lead to the conclusion that an empirical verification of those long-standing theories is welcome, as mentioned in the introduction to this section.

Panel (potential flow) method. A panel method was implemented in a computer program to determine the theoretical velocity distribution over the wing surface. A summed total circulation amounting to zero was implemented as boundary condition. The first airfoil that is analysed is a 'rounded flat plate' or in other words, a rectangle with semi-circles added to the front and rear, such that a symmetric flat airfoil with rounded leading edge and trailing edge results. Furthermore, NACA-0012 airfoils of which the trailing edge is rounded with different radii of curvature are analysed. The velocity distribution that is predicted by this method for the case of an airfoil at positive angle of attack corresponds to classical textual descriptions and sketches; specifically regarding the aspects of the presence of a stagnation point on the upper surface close to the trailing edge, and a region of increased velocity between the upper- and lower sides of the trailing edge. From the similarity between the velocity distributions on the trailing edges of a conventional airfoil (i.e. the NACA 0012) with rounded trailing edges of various radii of curvature and on that of a rounded flat plate we conclude that the surface velocity distribution in the trailing-edge region has a generic shape which is virtually independent of the overall airfoil shape and the radius of curvature of the edge. These conclusions provide ground for significant generalisation of observations from specific experimental recordings of the transient flow-field around the trailing-edge of a real airfoil in a real flow. Also, they enable cross-verification of the panel method results and the experimental results.

Experimental setup. An experimental apparatus has been designed and constructed to record the Kutta-condition-producing transient flow around the trailing edge of a wing model. The setup consists of a wing model which is oriented vertically in a bucket of water (0.9x0.9 m). The wing is oriented perpendicular to the bottom, with ≈ 0.5 mm tip clearance, to produce two-dimensional flow at the measurement plane. The wing section is a rounded flat plate: the same as is analysed using the panel method. The radius of curvature of the trailing edge R is 0.5% of the chord length c , which is 200 mm. The wing is uniformly accelerated at 2.50 m/s^2 using a weight. A high-speed camera is used to record images of seeding particles in the flow. The images are taken in a region around the wing's trailing edge; the field of view being 25mm wide and 15mm large. The images are processed into velocity vectors fields using Particle Image Velocimetry (PIV) techniques. The velocity fields are further processed and analysed using custom-made computer scripts. Special attention was paid to the development of an electronic system which serves to synchronise the wing's motion and the recording of images by a high-speed PIV camera. The whole apparatus works effectively and consistently. Good spatial (0.1 mm) and temporal (0.5 ms) resolution is obtained.

Results from empirical investigation

The recorded flow-field is analysed in a reference frame which is fixed to the wing, and is visualised mainly using a series of streamline plots and a series of velocity vector plots. They show that the transformation of the flow field is as follows. The first visible flow-field resembles potential flow. A boundary layer is formed on

the wing surface. The existence of a stagnation point with corresponding dividing streamline on the upper side (i.e. the suction side) of the airfoil is superseded by stagnation of the inner part of the boundary layer on lower parts of the trailing arc. When time progresses, fluid close to the wing decelerates and flow reversal occurs. Fluid at larger distance from the wing shows this behaviour less strongly. A vortex-like pattern appears, which is recognised as a starting vortex. As time progresses, this vortex moves away from the wing in mainly horizontal direction, while its centre remains slightly above the chord line. Together with the movement of the starting vortex, the stagnation point which initially was on the suction side detaches from the airfoil and moves into the main flow, remaining on top of the starting vortex. After the starting vortex has detached from the wing, two points of flow separation are present on the wing contour, one being below the centre of the starting vortex where it originally was created, and the other being slightly above the chord line, but both on the circular part of the airfoil's rear end. A wake (i.e. a region in which flow velocity magnitudes are small) appears between the points of flow separation and as time progresses the separation points move toward the upper and lower ends of the circular arc. The result is a wake which is approximately symmetric about the chord line. Analysis of the evolution the region of separated flow and of the evolution of streamline curvatures about the trailing edge suggests that the flow-field starts to oscillate but this cannot be certainly stated due to lack of data for later times.

From the correspondence between the properties of the Kutta condition flow-field and properties of the final state of the flow-field observed in the experimental data (namely smooth-flow off and a symmetric flow-field about the chord line) we conclude that the transient flow which is studied in the present investigation is indeed the process which produces the Kutta condition in real flows. This means that the observations of the transforming flow-field can be used to verify the classical theory of stagnation point shifting due to viscosity. All factual aspects of the flow-field predicted by the theory have been observed, the most important ones being: an initial stagnation point on the suction side, relatively large velocities in the trailing-edge region, a rearward shift of the stagnation point, and a final (average) stagnation point location at the very 'edge'. We conclude that the theory has been verified except for the differences caused by the difference between a sharp trailing edge and a 'thick' trailing edge.

An important question, which is related to the original motivation for the present research, is: can the observed sequence of individual events be related to each other by a working principle which involves viscosity? While trying to avoid stepping too quickly from correlation to causation, we can say that effects of viscosity are strongly implied by the clear observation of boundary layer velocity profiles. From the correspondence between a basic velocity profile predicted by boundary-layer theory and the measured velocity fields it is concluded that early authors were right in attributing the separation of the starting vortex to boundary-layer behaviour. Since the role of viscosity in boundary-layer theory is widely accepted, we conclude that viscosity is a major factor in the development of the transient flow-field; and thus the Kutta condition that was produced in the experiment has a major dependence on viscosity.

The velocity field at a certain moment in time, relatively early in the development, when the flow still looks like potential flow, is interpolated at a constant distance from the wing surface. This results in a surface velocity distribution that can be compared with a velocity distribution calculated by the panel method for the combination of airfoil shape and momentary angle of attack. It turns out that the two surface velocity distributions are qualitatively the same, clearly showing a velocity maximum and a velocity minimum (i.e. a stagnation point). They are quantitatively similar regarding the location and the height of the maximum. This cross-verifies the panel method and the experimental method regarding their ability to display the initial potential-flow-like flow-field (at least qualitatively).

A comparison between the methods and results of the present research with that of other research yields some qualitative differences but also qualitative similarities. Other research regarding the transient flow around the trailing edge of a starting wing has considered airfoil shapes with pointed (i.e. strictly sharp) trailing edges. However, in the present research the trailing edge has a finite thickness. This was deliberately chosen because a strictly pointed trailing edge – which can be considered in mathematical analysis – cannot be produced in reality. Because of the thickness of the trailing edge, the experimentally observed final

flow-field has two points of flow separation and a wake in between them, which is not present in the sketches of classical theoretical descriptions, nor in the CFD analysis by Zhu et al. The present research is considered more realistic. Apart from this aspect, the flow-field evolution which has been qualitatively described in theory since approximately 1935 is confirmed by the present empirical observations. Concerning the development of streamline topology, the merger of two regions of flow separation which is observed in the results of Zhu et al. might also have occurred in the experimental flow of the present research but this cannot be verified because the inner part of the boundary layer is not resolved.

5.1.1. Accomplishment of research objective and implications

To the best of the author's knowledge, this research presents for the first time *an empirical study of the transient flow which produces the Kutta condition flow-field*. The research objective has been achieved: a parametric description of the spatial and temporal development of the 2D flow-field in the trailing edge region of an airfoil which is accelerated from rest has been made, based on empirical data. This has been used to verify existing theories regarding the creation of the Kutta condition flow-field. The research questions have been answered satisfactorily. The empirical research case has all of the qualitative properties of the general case in the theoretical description. The observed flow corresponds to the events predicted by the theoretical description. A methodology has been proposed for generalising the results of the empirical work. On that basis, the theory under consideration may be regarded as generally valid for cases in which a smooth airfoil with rounded trailing edge at non-zero angle of attack is accelerated from rest towards a final chord-based Reynolds number of at least $O(1k)$ while the wing section is completely immersed in viscous inertial flow.

The implication is that more ground is available for making statements about the Kutta condition and the associated role of viscosity. From the perspective of empirical aerodynamics this research may be appreciated as a valuable contribution to the knowledge of the *Genesis of the Kutta condition*. In a broader scope, this may be appreciated as a relevant and significant contribution to the knowledge of fluid-dynamic lift.

5.2. Recommendations

To elaborate on the present research, the following directions of research and points of attention are recommended:

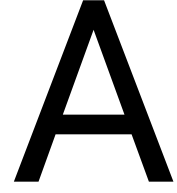
1. In order to display the process of flow separation more clearly, it is recommended that pathline flow visualisations are made. The importance of pathlines for detecting the location of flow separation in unsteady flows is suggested by the discussion in Section 1.4.5.
2. In order to obtain better understanding of the evolution of the streamline topology it is recommended that visualisations of the form of Figure 48b in Koromilas and Telionis (1980) are made.
3. In the present investigation, the angle of attack of the wing was not constant throughout the motion. For further experimentation with the experimental setup it is recommended to increase the stiffness of the frame to which the wing is attached, such that the wing makes a purely linear motion with constant angle of attack, even when it is loaded by a lift force. This would result in better resemblance between the wing motion in the empirical investigation and that assumed by theoretical predictions. As a consequence, the relations between the (non-dimensional parameterisation of the) wing motion and the flow-field development will be more useful for comparison with other research.
4. In order to obtain better understanding of the transient flow, it is recommended that more experiments are done to obtain knowledge of the dependence of the flow-field development on the similarity parameters (angle of attack, reference Reynolds number and trailing edge sharpness). It is easy to vary the angle of attack and the acceleration in the experiment setup. The aim here is to determine the function f in Equation 2.20 on p. 42.
5. In order to clarify the (time-dependent) relation between the development of the transient flow-field and the development of lift by an accelerating wing, it is recommended to repeat the measurements done for the present research and to measure the flow-field around the whole airfoil as well. A PIV recording of that would enable to determine the circulation about the airfoil. Also, applying a two-component force sensor between the wing and the frame which moves the wing enables to measure the evolution of lift and drag forces. Simultaneous application of these techniques would enable the determination of the evolution of circulation-dependent lift and ‘dynamic lift’ separately.
6. It is recommended that the relation between the appreciation of the Kutta condition in the mathematical and the empirical perspectives is studied more extensively. This will involve more than aerodynamics, because a good understanding of the character of science is needed. Therefore such a study will have a science-philosophical character.
7. In order to construct a solid proof for the necessity of viscosity, it is recommended that the parts (mainly parts D and F) of the argumentation for the necessity of viscosity for lift production presented in Section 4.4 are researched more extensively.
8. It is recommended that the “direction and speed” method for detection of flow stagnation and separation is tried on more cases and validated more extensively. The method is promising due to its computational efficiency. The method of Serra et al. (2018) may be useful for comparison of the location of the separation point that is detected on a body.

Bibliography

- [1] J. A. D. Ackroyd, B. P. Axcell, and A. I. Ruban. *Early developments of modern aerodynamics*. Butterworth-Heinemann, Oxford, UK, 2001.
- [2] John D. Anderson. *Fundamentals of Aerodynamics*. McGraw-Hill, New-York, USA, 5th edition, 2011.
- [3] L. Anton. *Ausbildung eines Wirbels an der Kante einer Platte*. PhD thesis, Göttinger Dissertation, Ingenieur-Archiv, Vol. X, 1939.
- [4] H.M. Badr, S.C.R. Dennis, and Serpil Kocabiyik. Numerical simulation of the unsteady flow over an elliptic cylinder at different orientations. *International Journal of Numerical Methods in Fluids*, 37:905–931, 2001.
- [5] P. Bassanini, C. M. Casciola, M. R. Lancia, and R. Piva. Edge singularities and Kutta condition in 3d aerodynamics. *Meccanica*, 34:199–229, 1999.
- [6] G.K. Batchelor. *An introduction to fluid dynamics*. Cambridge University Press, Cambridge, UK, 1967.
- [7] David Bloor. *The Enigma of the Aerofoil*. The University of Chicago Press, London, UK, 2011.
- [8] Paul K. Chang. *Separation of Flow*. Pergamon Press, 1970.
- [9] Paul P. Craig. *Observations of perfect potential flow and critical velocities in superfluid helium II*. PhD thesis, California Institute of Technology, 1959.
- [10] David G. Crighton. The Kutta condition in unsteady flow. *Annual Reviews of Fluid Mechanics*, 17:411–445, 1985.
- [11] Mark Drela. XFOIL: an analysis and design system for low Reynolds number airfoils. In *Low Reynolds Number Aerodynamics*, volume 54 of *Lecture Notes in Engineering*. Springer-Verlag, 1989.
- [12] R. J. Emrich and H. Reichenbach. Photographic study of early stages of vortex formation behind an edge. In I.I. Glass, editor, *Proceedings of the 7th International Shock Tube Symposium held at University of Toronto, Canada*, page 740. University of Toronto Press, Toronto, Canada, 1969.
- [13] R. A. Evans and M. I. G. Bloor. The starting mechanism of wave-induced flow through a sharp-edged orifice. *Journal of Fluid Mechanics*, 82(1):115–128, 1977.
- [14] Herman Glauert. *Elements of aerofoil and airscrew theory*. Cambridge: Cambridge Science Classics (reprint of 1983), 2nd edition, 1947.
- [15] Sydney Goldstein. *Modern Developments in Fluid Dynamics*. Dover Publications, London, UK, 2nd edition, 1965.
- [16] J. P. Gostelow. Trailing edge flow over turbomachine blades and the Kutta-Joukowski condition, 1975. ASME Paper 75-GT-94 (March 1975).
- [17] George Haller. Exact theory of unsteady separation for two-dimensional flows. *Journal of Fluid Mechanics*, 512:257–311, 2004.
- [18] H. Honji. Starting flows past spheres and elliptic cylinders. *Research Institute for Applied Mechanics, Kyushu University*, 19(65), 1972.

- [19] L. Howarth. On the solution of the laminar boundary layer equations. *Proceedings of the Royal Society of London*, A164(919):547 – 579, 1938.
- [20] K. Karamcheti. *Principles of Ideal-Fluid Aerodynamics*. John Wiley & Sons, 1966.
- [21] Joseph Katz and Allen Plotkin. *Low-Speed Aerodynamics*. Cambridge University Press, New York, USA, 2nd edition, 2001.
- [22] Felix Klein. Über die Bildung von Wirbeln in reibungslosen Flüssigkeiten. *Zeitschrift für Mathematik und Physik*, (58):259–262, 1910.
- [23] C. A. Koromilas and D. P. Telionis. Unsteady laminar separation: An experimental study. *Journal of Fluid Mechanics*, 97 part 2:347–384, 1980.
- [24] Arnold M. Kuether and Chuen-Yen Chow. *Foundations of Aerodynamics*. John Wiley & Sons, Inc, New York, USA, 5th edition, 1998.
- [25] LaVision. Flowmaster time-resolved particle image velocimetry systems, 2018. URL www.lavision.de/en/products/flowmaster/time-resolved-piv.
- [26] T. S. Liu, J. Z. Wu, J. Y. Zhu, S. F. Zou, and L. Q. Liu. The origin of lift revisited: I. A complete physical theory. In *45th AIAA Fluid Dynamics Conference*, 2015.
- [27] H.J. Lugt and H.J. Haussling. Laminar flow past an abruptly accelerated elliptic cylinder at 45° incidence. *Journal of Fluid Mechanics*, 65 part 4:711–734, 1974.
- [28] Doug McLean. *Understanding Aerodynamics: Arguing from the real physics*. John Wiley & Sons Ltd., Chichester, UK, 2013.
- [29] Unmeel B. Mehta and Zalman Lavan. Starting vortex, separation bubbles and stall: a numerical study of laminar unsteady flow around an airfoil. *Journal of Fluid Mechanics*, 67 part II:227–256, 1975.
- [30] L. Morino. Helmholtz decomposition revisited: vorticity generation and trailing edge condition. Part 1: Incompressible flows. *Computational Mechanics*, (1):65–90, 1986.
- [31] E. Obert. *Aerodynamic design of transport aircraft*. IOS Press, 2009.
- [32] Ludwig Prandtl. *Führer durch die Strömungslehre*. Friedr. Vieweg & Sohn, Braunschweig, Germany, 1965.
- [33] D. I. Pullin and A. E. Perry. Some flow visualization experiments on the starting vortex. *Journal of Fluid Mechanics*, 97(2):239–255, 1980.
- [34] Samir F. Radwan. Critical review of the trailing edge condition in steady and unsteady flow. Master's thesis, Lehigh University, 1981.
- [35] Markus Raffel et al. *Particle Image Velocimetry*. Springer, 2018.
- [36] A. Robinson and J.A. Laurmann. *Wing Theory*. Cambridge University Press, 1956.
- [37] A. I. Ruban and I. Turkyilmaz. On laminar separation at a corner point in transonic flow. *Journal of Fluid Mechanics*, 423:345–380, 2000.
- [38] H. Schlichting and E. Truckenbrodt. *Aerodynamik des Flugzeuges, part. 1*. Springer-Verlag, 1967.
- [39] W. R. Sears and D. P. Telionis. Boundary-layer separation in unsteady flow. *SIAM Journal on Applied Mathematics*, 28(1):215–235, 1975.
- [40] Mattia Serra, Jérôme Vétel, and George Haller. Exact theory of material spike formation in flow separation. *Journal of Fluid Mechanics*, 845:51–92, 2018.

- [41] Ascher H. Shapiro. Film notes for vorticity, 1969. URL web.mit.edu/hml/ncfmf/09V0R.pdf.
- [42] S. Taneda. The development of the lift of an impulsively started elliptic cylinder at incidence. *Journal of the Physical Society of Japan*, 33, 1972.
- [43] I. Tani. The wing section theory of Kutta and Zhukovski. In U. Müller, K. G. Roesner, and B. Schmidt, editors, *Recent developments in theoretical and experimental fluid mechanics*. Springer-Verlag, Berlin, 1979.
- [44] O. Tietjens and L. Prandtl. *Hydro- und Aeromechanik, part 2*. Julius Springer, Berlin, Germany, 1931.
- [45] E. Truckenbrodt. *Fluidmechanik, part 2*. Springer, Berlin, Germany, 4th edition, 1998.
- [46] M. Van Dyke. *An album of fluid motion*. The Parabolic Press, Stanford, California, USA, 1982.
- [47] P. van Pelt. *Literature study report of graduation project about the working principles of the Kutta condition*. TU Delft, 2018.
- [48] Th. von Kármán and J. M. Burgers. General aerodynamic theory - perfect fluids. In William Frederick Durand, editor, *Aerodynamic Theory*, volume II of *Aerodynamic Theory*. Julius Springer, 1935. Originally published by Julius Springer in 1935, republished in 1963 by Dover Publications.
- [49] H. Wagner. Über die Entstehung des dynamischen Auftriebes von Tragflügeln. *Zeitschrift für Angewandte Mathematik und Mechanik*, (5):17–35, 1925.
- [50] C. Witoszyński and M.J. Thompson. The theory of single burbling. In William Frederick Durand, editor, *Aerodynamic Theory*, volume III of *Aerodynamic Theory*. publisher unknown, 1934.
- [51] J. Y. Zhu, T. S. Liu, S. F. Zou, and J. Z. Wu. Causal mechanisms in airfoil-circulation formation. *Physics of Fluids*, 27(12), 2015.
- [52] J. Y. Zhu, S. F. Zou, L. Q. Liu, J. Z. Wu, and T. S. Liu. The origin of lift revisited: II. Physical processes of airfoil-circulation formation in starting flow. In *45th AIAA Fluid Dynamics Conference*, 2015.



Determination of stagnation point location by streamfunction method

In a potential flow situation the following procedure – which we will call the ‘streamfunction method’ - can be used to determine the location of a stagnation point.¹ We consider two-dimensional flow.

1. **The streamfunction Ψ is calculated for the domain.** The streamfunction is defined by (A.1) for an (x, y) coordinate system where A and B are two locations in the domain, u and v are the flow velocity components in the x and y directions, respectively, and where $\Delta\Psi$ represents the mass flux flowing through the streamtube which is bounded by streamlines which go through points A and B. Using the definition of Figure 2.5 on p. 37 we can rewrite this equation for the (s, r) coordinate system: (A.2), where V_s and V_r are velocity components in s and r directions, respectively.

A grid of iso-lines of s and r can be made where iso- s lines are perpendicular to the contour and iso- r lines are tangential to the contour. Since the streamfunction value is known at the airfoil contour (we set it to zero on the contour) we only have to integrate in the direction perpendicular to the contour in order to determine the value of the streamfunction in the domain. So we can implement (A.2) by a simple first-order numerical integration which starts at the contour ($r = 0$) and propagates away from the contour (towards $r = \infty$), see (A.3), where A is a certain point on the airfoil contour and Ψ_A is set to zero. This integration is started at different stations along the contour, so for different points on the line ($s, r = 0$).

$$\Delta\Psi = \int_A^B (u dy - v dx) \quad (\text{A.1})$$

$$\Delta\Psi = \int_A^B (V_s dr - V_r ds) \quad (\text{A.2})$$

$$\Psi(s_A, r) = \Psi_A + \sum_{r=0}^{r \rightarrow \infty} V_s \Delta r \quad (\text{A.3})$$

2. **The points where $\Psi = 0$ are determined.** In a computer implementation this amounts to finding the points where $|\Psi| < \Psi_{\text{ref}}$ where Ψ_{ref} is a threshold value (it is improbable that points where Ψ is exactly zero are found when a discrete solution method is used).
3. **A line is drawn through the points where $\Psi = 0$.** This results in obtaining the dividing streamline, which is also called the ‘stagnation streamline’ because it runs from the stagnation point on the contour into the domain (2, p. 255).

Unfortunately, due to limitations of the PIV technique, the velocity fields obtained in the present research lack data in a small band around the wing (in the region $0 < r < 0.25R$ where R is the trailing edge radius). This

¹Credits to Dr. Marc Gerritsma for mentioning this idea to the author.

has two important consequences. First, the mass flux in this region is unknown which causes error and uncertainty in the calculation of the streamfunction field. The presence of an error is implied by the fact that the iso-contour lines on the lower part of the circular arc in Figure A.1 do not match the streamlines in that region in Figure A.2. Also, the path of the ‘dividing streamline’ in the region without data is unknown so the stagnation streamline can be determined only up to a certain distance from the wing. The remaining distance towards the wing has to be bridged by means of extrapolation (see Figure A.1).

The author tried this method in order to determine the location of separation points, dividing streamlines, and wake widths in flow-fields obtained by PIV in the present research. However, it does not give satisfactory results. The method always results in a single streamline even in case a wake is present behind the body and two separation points (on the upper and lower side) are actually present (see Figure 3.14 on p. 81). The streamfunction method lacks the ability to find the width of the wake. This might be attributed to the fact that part of the velocity field in the boundary layer is unknown. We may interpret the single separation point on the wing which results from the streamfunction method as representing the average location of the upper and lower separation points which exists in the real flow.

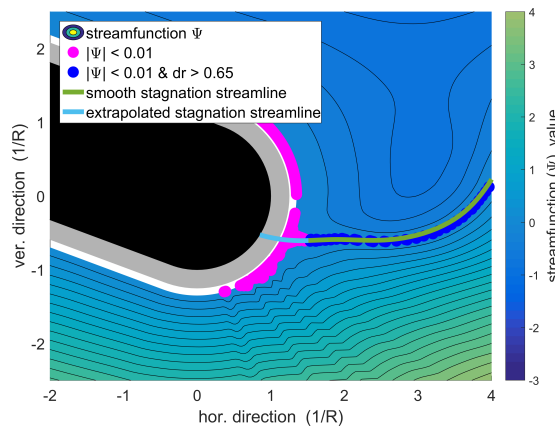


Figure A.1: Contourplot of the streamfunction value for image #150, with the locus of points where Ψ is close to zero, and extrapolation of that line towards the wing contour. The gray band represent the area where velocity data is absent.

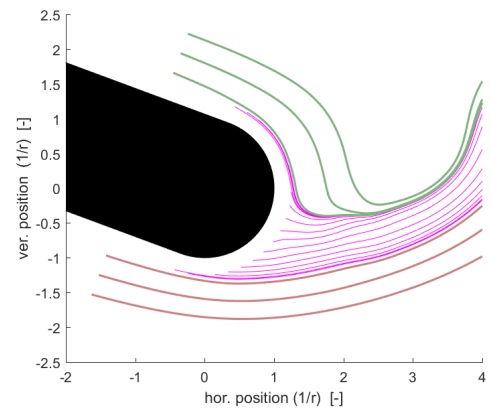


Figure A.2: Streamlines for the case of Figure A.1. Streamlines are determined by MATLAB's `streamline` method which integrates the velocity field step-wise.

B

Performance analysis of the “direction and speed method”

This appendix presents three analyses for assessment of the performance of the “direction and speed method” which is presented in Section 2.6.6 of this report. The first analysis is a comparison with the results of the streamfunction method which is described in Appendix A. The second analysis addresses the sensitivity of the method’s output to the values of the threshold parameters. The third analysis is a validation of the method’s results.

B.1. Comparison with streamfunction method

The performance of the “direction and speed method” and the streamfunction method for detection of flow separation is compared by comparing the stagnation point locations which are determined by both methods. This is done for three moments in the transient flow that was recorded for the present research (for $I=50$, $I=100$, and $I=150$ where I denotes the image number in a time-series of PIV images, see also the timeline on p. 77). The “direction and speed method” does not directly give a stagnation point location but identifies the flow as either separated or attached for a given set of points at known locations. When a series of points at fixed r but varying s ordinates is given, the tangential centre of mass of the points which are identified as ‘separated’ is taken as the stagnation point. The streamfunction method determines the s -location of the stagnation point by extrapolating the dividing streamline towards the contour, as explained in Appendix A. Results are presented in Figure B.3. The tangential location of the stagnation points determined by both methods match well for each of the three cases considered.

Also, the “direction and speed method” and the streamfunction method are both employed to determine the evolution of the location of the stagnation point through time for the flow-field evolution that was studied in this report (see Figures 3.10 on p. 78. The result is presented in Figure B.1. In the region of $I < 100$ the methods agree well, both in trend and in magnitude. In the region of $I > 100$ the results of the streamfunction method have much scatter due to sensitivity in the extrapolation of the dividing streamline towards the body, however, the trends of both methods are also the same in this region.

From observations of a video of raw PIV-images it is known that for $I > 100$ the motion of the stagnation point is not as much as implied by the scatter in the results of the streamfunction method so the “direction and velocity method” is more representative of the real flow. We conclude that the methods yield very similar results when a single-stagnation point location is used as parameter for comparison.

B.2. Sensitivity analysis

The sensitivity of the “direction and velocity method” to changes in the parameters r , $\Delta\theta_{\max}$, and V_{\min} is determined by choosing a baseline set of parameter values and changing the parameter values one at a time. This results in three combinations of parameter values, which are applied to three different moments in the evolution of the flow field, namely $I=50$, $I=100$ and $I=150$ (see also the evolution of the streamlines in the flow-field on Figure 3.10 on p. 77 and the corresponding timeline on p. 77). Results are presented in Figures B.4, B.5 and B.6. We see that the method is in general insensitive to the value of r . The method is sensitive to the value of $\Delta\theta_{\max}$ so a choice be made for selecting a value for that parameter. The method is only in one case ($I=100$) a little sensitive to the value of V_{\min} .

B.3. Validation

The “direction and speed method” was developed in the later stage of the author’s graduation project, therefore no extensive validation could be done, due to lack of time. However, some comparisons serving as preliminary validation are made. Figures B.2 show three cases in which the results of the “direction and speed” method are compared to data from other methods. Good agreement is found for the first two cases. The last case shows a quantitative error, but this can be reduced by adjusting the values of the threshold parameters of the “direction and speed method” (see the discussion of the method on p. 65).

B.4. Conclusions

There is uncertainty in size of the region of separated flow in absolute sense due to the sensitivity to $\Delta\theta_{\max}$. However, it is reasonable to assume that the error of the identification w.r.t. the real flow is similar for each flow-field picture. Therefore, the method is at least deemed suitable for analysis of relative changes, for example of the variation of the size of the region of flow separation and variation of the location of this region. In addition, if a suitable value of $\Delta\theta_{\max}$ can be determined by some calibration, the absolute magnitude of the results of the method also become reliable.

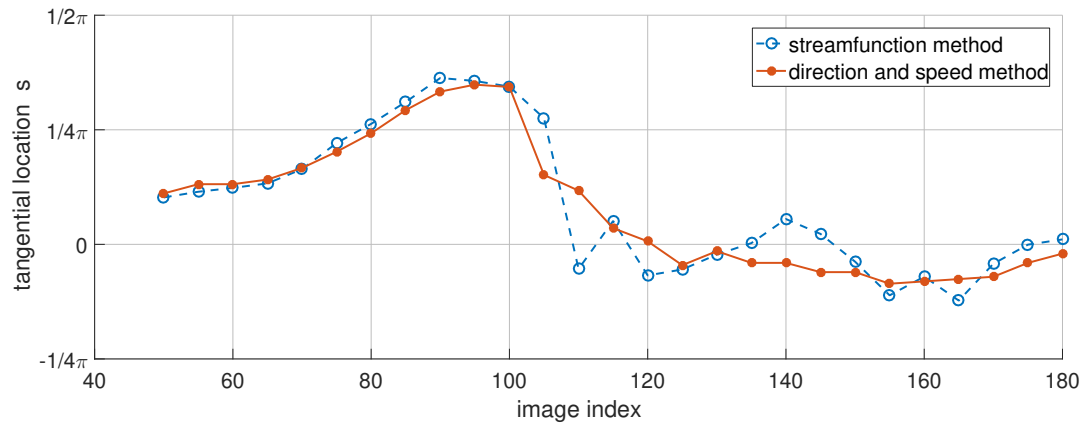
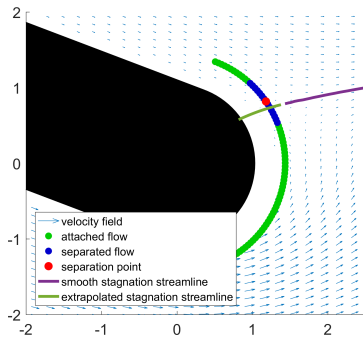
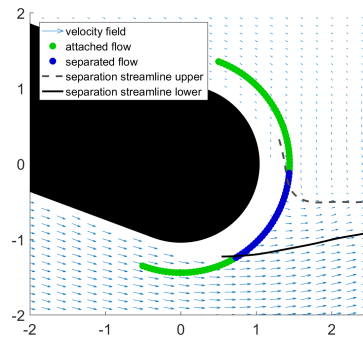


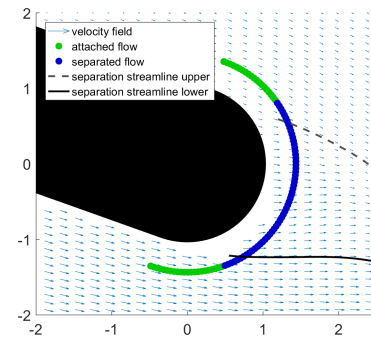
Figure B.1: Comparison of the time-wise evolution of the tangential locations of the stagnation point determined by the streamfunction method and the “direction and speed method”. The evolution of the flow-field can be viewed on Figures 3.10 on p. 78. The first method determines the location of the stagnation point on the body by taking the locus of points in the flow-field where the streamfunction value is zero and extrapolating that line towards the body. The second method determines the location of the tangential location of the stagnation point by taking the average tangential location of a series of points in the flow-field where the flow is marked as separated or stagnated.



(a) Validation of the location of the stagnation point. The red dot signifies that location as determined by the ‘direction and speed method’. It is the centre of mass of the blue points, along the line which is tangential to the wing contour. The green line connecting to the wing shows represents an extrapolation of the ‘zero streamline’ which results from streamfunction analysis. The point of intersection with the wing indicates the stagnation point according to the streamfunction method. The tangential stagnation point locations match very well.



(b) Validation of the region of separated flow determined by the ‘direction and speed method’. The gray lines represent streamlines which divide regions of attached and separated flow. The bottom streamline attaches to a separation point on the wing contour where the straight part and the circular arc connect. The position of these streamlines is obtained from studying a movie of PIV images. The lower streamline was located with certainty, however, the upper separation streamline could not be located with certainty, which is indicated by the dotted line. The region marked as separated flow by the ‘direction and speed method’ matches very well with that indicated by the separation streamlines.



(c) Like Figure (a), this figure shows another case of validation of the region of separated flow as determined by the ‘direction and speed’ method. Again, the location of the separation streamlines is obtained from studying a movie of PIV images. The region marked as separated is a bit too large, but it is symmetrically too large, which is beneficial, because this indicates that when adjusting the $\Delta\theta_{\max}$ or the $\frac{V_{\min}}{V_{\max}}$ parameters the region can be made to match both streamlines precisely.

Figure B.2: Comparison of the results of the ‘direction and speed method’ with results from other methods. Figure (a) shows a comparison with the streamfunction method which is described in Appendix A. Figures (b) and (c) show reference streamlines which are obtained from studying a movie of raw PIV images recorded in the experiment done for the present research.

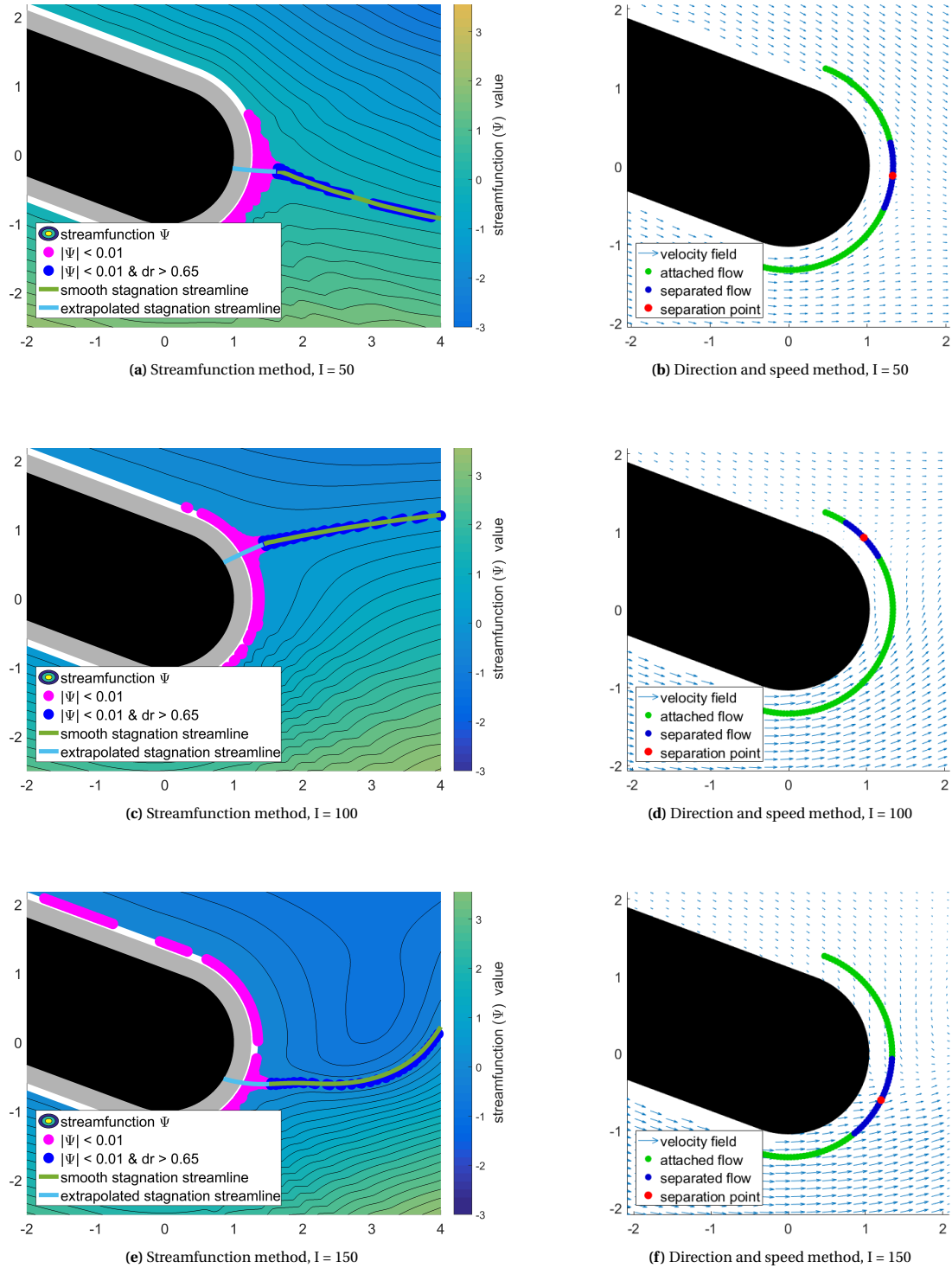
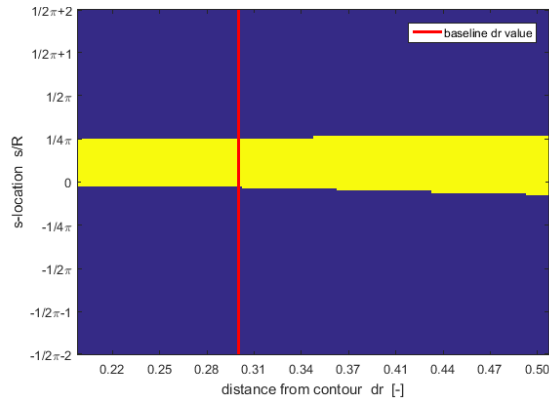
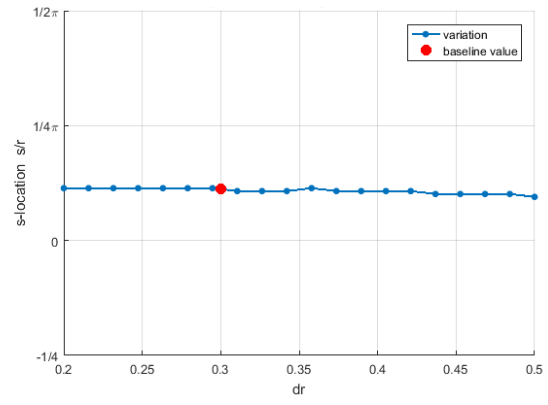


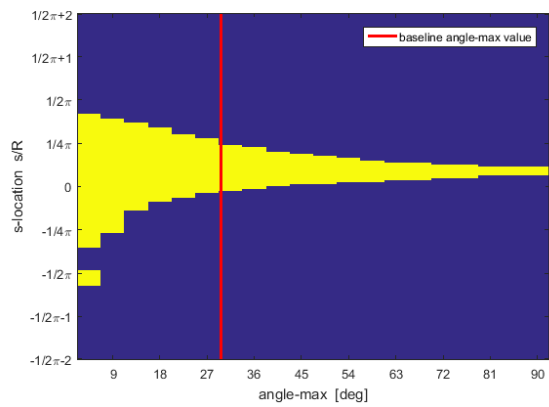
Figure B.3: Comparison of results of the streamfunction method (left column) and the “direction and velocity method” (right column) for determining the location of a stagnation point. In the left column the intersection of the blue streamline with the black body marks the stagnation point. In the right column the purple dot (which represents the average location of the points marked as separated flow, which are indicated by blue dots) marks the stagnation point. Results are shown for three different time instances in the evolution of the flow field. We see that the tangential stagnation point locations match well for each case. This is the case even though each flow-field is quite different: At $I=50$ (top row) the flow is attached except for the stagnation point. At $I=100$ (middle row) the flow is topologically the same as for $I=100$ but the stagnation point has moved towards the upper end of the circular arc. At $I=150$ (bottom row) the flow has almost reached steady state after a vortex has been shed. See also Figure 3.9 for more information regarding the evolution of the flow-field.



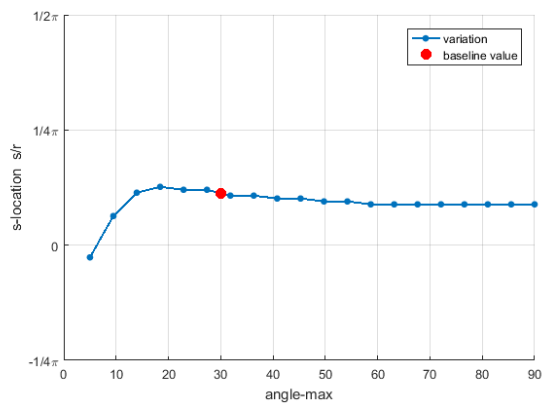
(a) Sensitivity of the region marked as separated flow to variation in r .



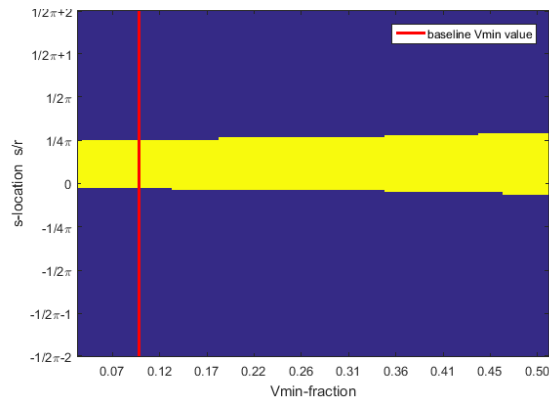
(b) Sensitivity of the tangential location of the stagnation point to variation in r .



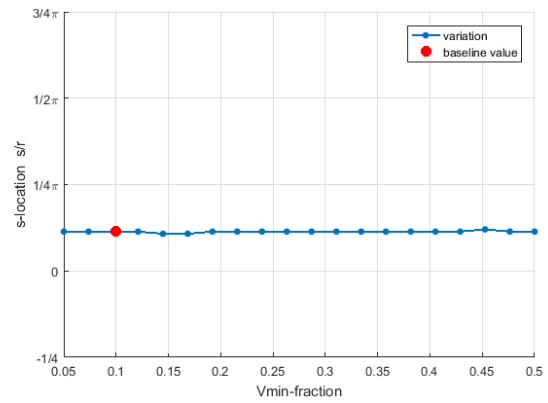
(c) Sensitivity of the region marked as separated flow to variation in $\Delta\theta_{\max}$.



(d) Sensitivity of the tangential location of the stagnation point to sensitivity in $\Delta\theta_{\max}$.



(e) Sensitivity of the region marked as separated flow to variation in V_{\min} .



(f) Sensitivity of the tangential location of the stagnation point to variation in V_{\min} .

Figure B.4: Sensitivity of the results of the “direction and velocity method” to changes in the parameters, for $l = 50$. Sensitivities to values of the parameters r , $\Delta\theta_{\max}$, V_{\min} are shown on the top, middle, and bottom rows, respectively. Baseline values of the parameters are 0.3, 30° , and 0.1, respectively. Parameters were changed one at a time. The horizontal axis of each image indicates the value of the parameter. The vertical axis shows the tangential location along the rounded trailing edge, according to the coordinate system shown in Figure 2.5. The left column shows the area which is marked as separated (in yellow). The right column shows the tangential location of the stagnation point. The baseline parameter values are indicated by red lines and red dots. Note that the method is insensitive to the value of r , sensitive to the value of $\Delta\theta_{\max}$ and insensitive to the value of V_{\min} .

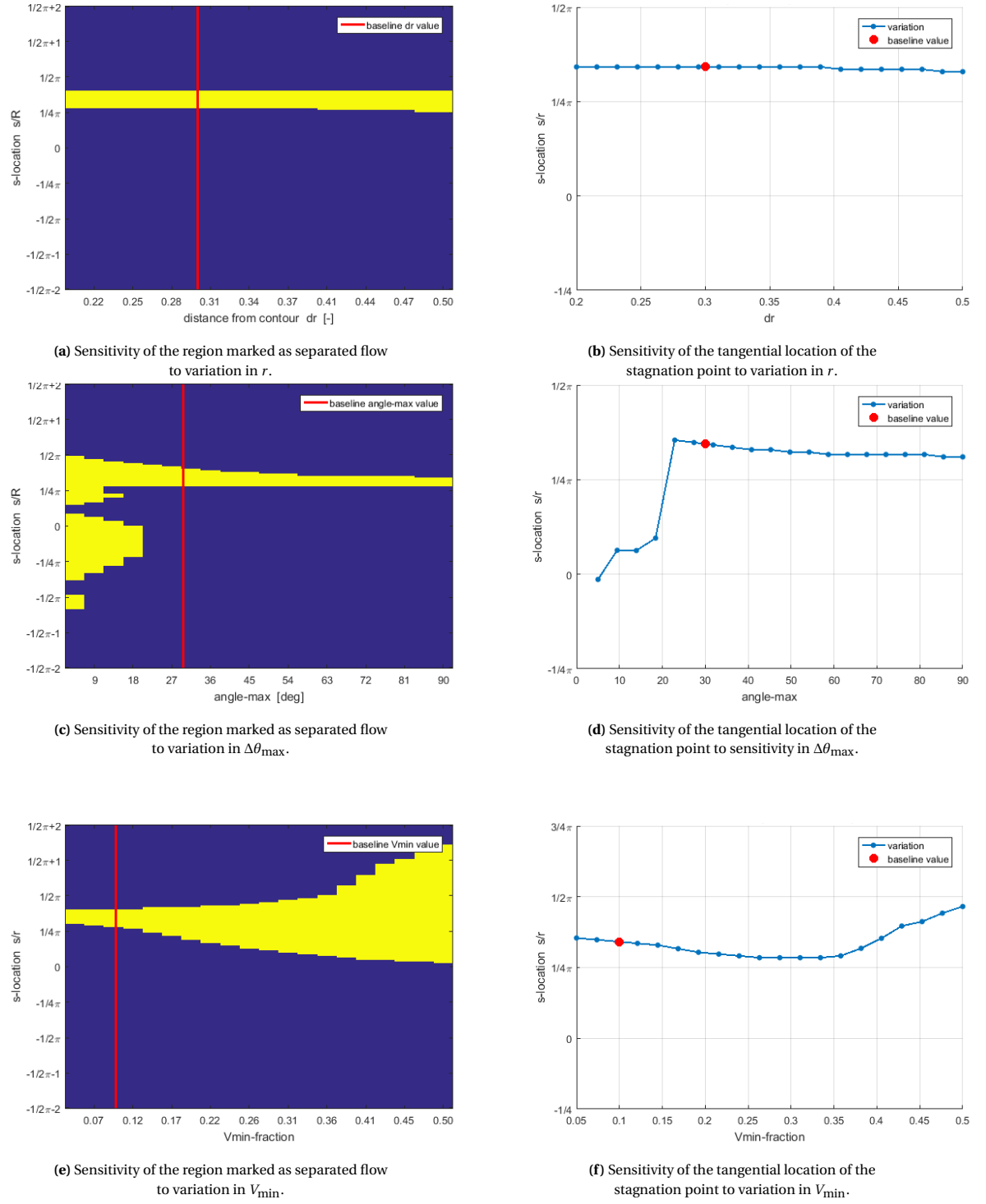
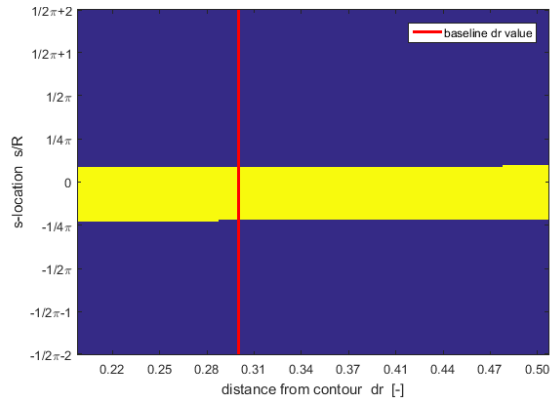
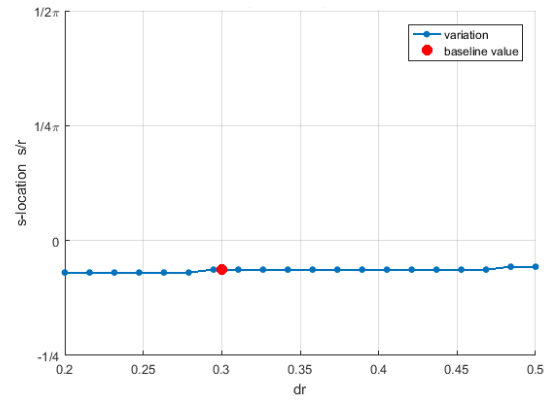


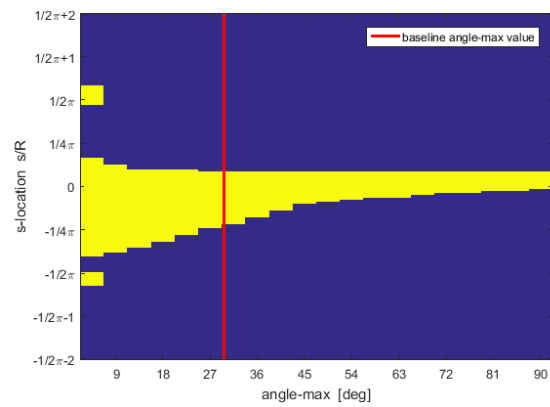
Figure B.5: Sensitivity of the results of the “direction and velocity method” to changes in the parameters, for $I = 100$. See the caption of Figure B.4 for more information. Note that the method is insensitive to the value of r , insensitive to the value of $\Delta\theta_{\max}$ if it is larger than ≈ 22 deg, and little sensitive to the value of V_{\min} if it is smaller than 0.35.



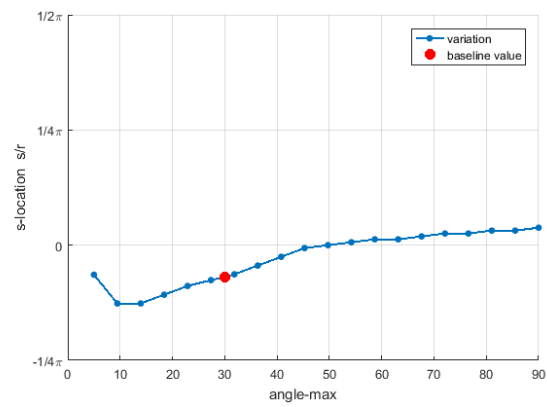
(a) Sensitivity of the region marked as separated flow to variation in r .



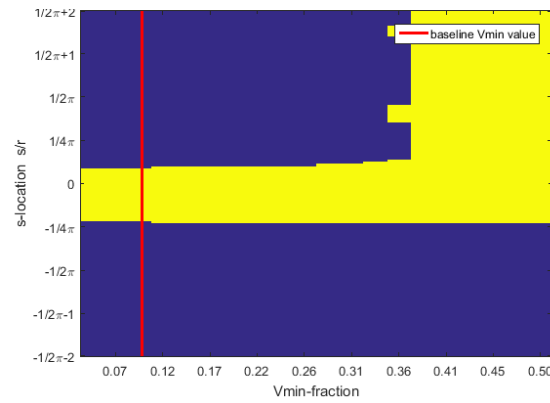
(b) Sensitivity of the tangential location of the stagnation point to variation in r .



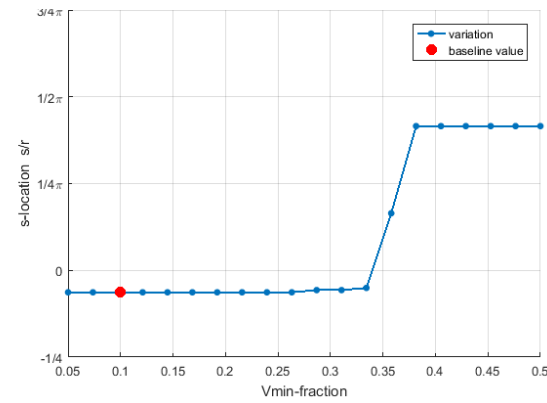
(c) Sensitivity of the region marked as separated flow to variation in $\Delta\theta_{\max}$.



(d) Sensitivity of the tangential location of the stagnation point to sensitivity in $\Delta\theta_{\max}$.



(e) Sensitivity of the region marked as separated flow to variation in V_{\min} .



(f) Sensitivity of the tangential location of the stagnation point to variation in V_{\min} .

Figure B.6: Sensitivity of the results of the “direction and velocity method” to changes in the parameters, for $l = 150$. See the caption of Figure B.4 for more information. Note that the method is insensitive to the value of r , sensitive to the value of $\Delta\theta_{\max}$, and insensitive to the value of V_{\min} if it is smaller than 0.34.

C

Photos of the flow-field around an airfoil starting from rest

This appendix presents a number of photographs depicting the flow about an airfoil which is started from rest. The photos are copied from (44, Abb. 42-50). Figure C.1 shows the flow-field development in 6 steps. Figure C.2 shows the development of the starting vortex.

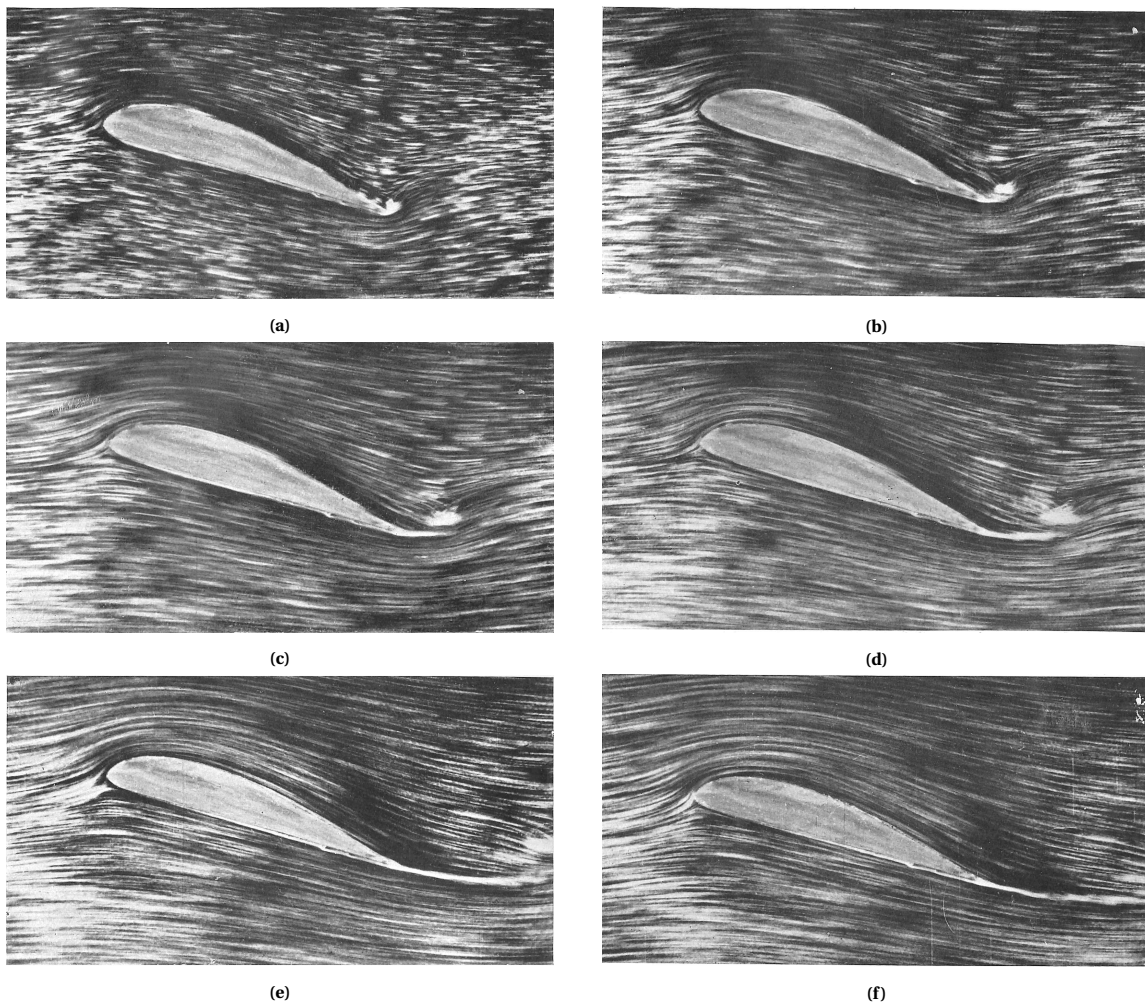
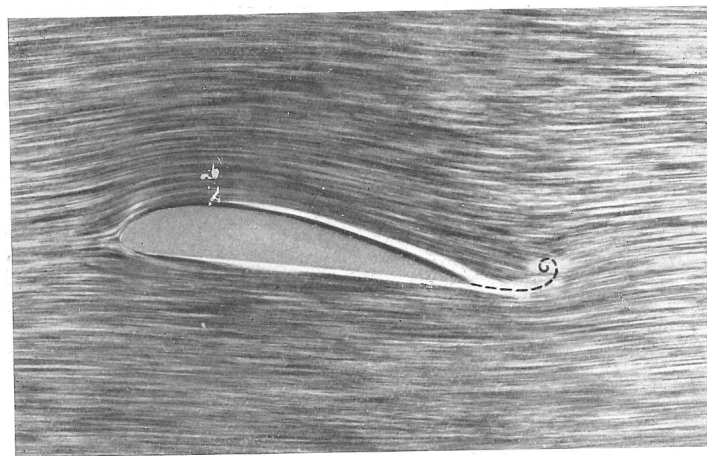


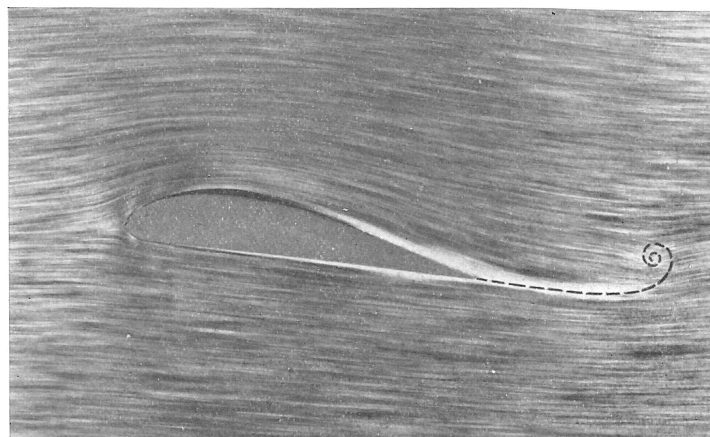
Figure C.1: Photographs of the development of the flow-field around and airfoil which is started from rest.
Figure (a) is the first of the time-series. Source: (44, Abb. 42-47)



(a)



(b)



(c)

Figure C.2: Photographs of the development of the flow-field around an airfoil which is started from rest, for the purpose of illustrating the development of the starting vortex. The dotted line indicates a path line of particles which come from the trailing edge and end up in the starting vortex. Figure (a) is the first of the time-series. Source: (44, Abb. 48-50)

D

Images of the transient trailing edge flow around an airfoil started from rest from numerical simulation

Figure D.1 displays results of a numerical simulation of starting flow over a NACA-0012 which is accelerated from rest, by [Zhu et al.](#), which is published in (51) and in (52).

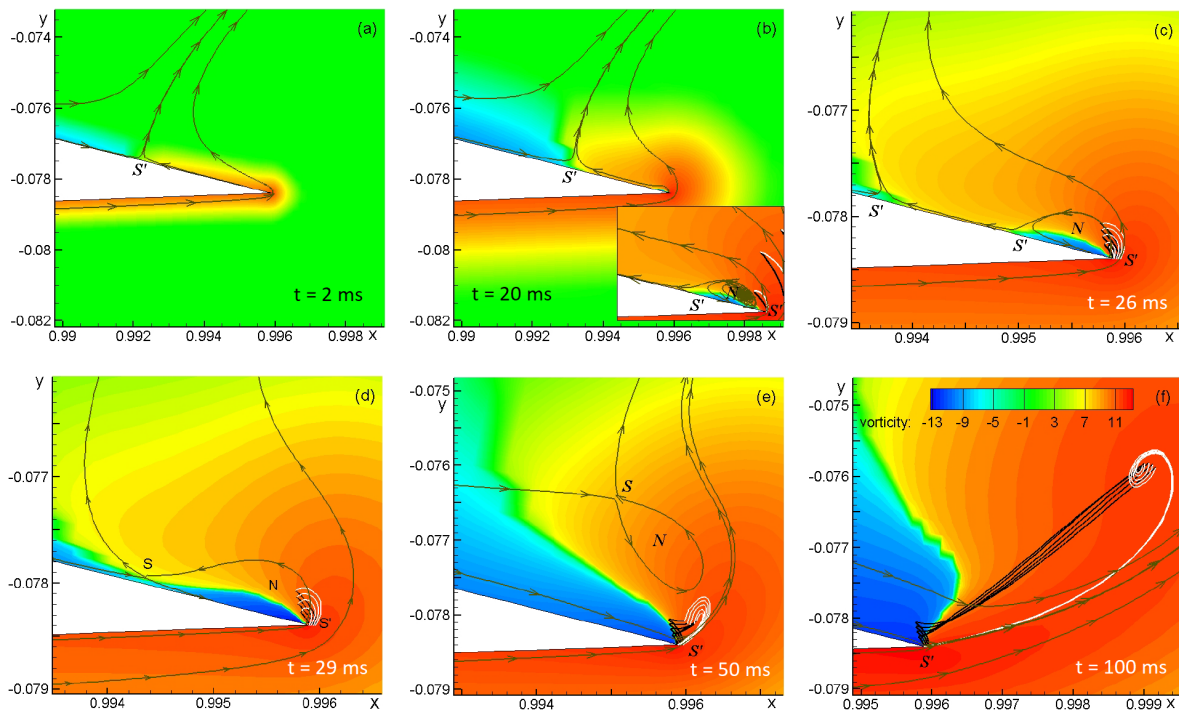


Figure D.1: Time variation of accelerated starting flow over a NACA-0012 airfoil at 6° angle of attack and a final chord-based Reynolds number of 10^5 when the flow becomes steady. Contours of vorticity with colourbar shown in (f), pathlines (black), streaklines (white), and streamlines (gray). Only the local flow-field near trailing edge is shown. (This caption is based on the caption of the figure in the original publication (52)). The 't = ' time indications in the figures were added by the present author.